School of Pharmacy

Development of a novel nanoparticulate carrier system for enhancement of bioactive molecule delivery into the brain

Naz Hasan Huda

This thesis is presented for the Degree of
Doctor of Philosophy
of
Curtin University

February 2017

Declaration

I declare that to the best of my knowledge and belief this thesis is my own account of my research and contains no material previously published by any other person except where due acknowledgment has been made. This thesis contains no material which has been accepted for the award of any other degree or diploma in any university.

Signature: Nazlinda

Date: 20-Feb-2017

Acknowledgement

Foremost, I would like to express my sincere gratitude to my supervisor, Dr Yan Chen for her advice, guidance, support, encouragement and patience throughout the course of study leading to this thesis. I am thankful to my co-supervisors Associate Professor Heather AE Benson and Dr Andrew Crowe for their conception of study and revision of manuscripts. It would be impossible to complete this thesis without their patience, motivation, enthusiasm and immense knowledge in the subject.

I express my sincere gratitude to the Curtin University for providing me with a Curtin Strategic International Research Scholarship (CSIRS) for undertaking the Doctor of Philosophy. I am grateful to Professor Kevin Batty, Head of School, School of Pharmacy, Professor Lynne Emmerton, Deputy Head, and Director of Research and Graduate Studies, School of Pharmacy, Professor Philip Newsholme, Head of School, School of Biomedical Sciences and Professor John Mamo, Director, CHIRI - Biosciences, for their efforts on developing a better academic atmosphere and creating an excellent research environment.

I would also like to thank Dr Alexander Richards for teaching me cell culture work, Giuseppe Luna and Michael Boddy for their elaborate training on the HPLC. I am grateful to Dr Hendra Gunosewoyo for helping me with laboratory reagents, chemical reactions, providing the freeze-drying facility and assisting me in interpreting NMR data. I would also like to thank Dr Madhu Page-Sharp for letting me try a few of her HPLC reagents and Dr Ganga Senarathna for advising on the transport study. I am grateful to Dr Ricky Lareu and Dr Simon Fox for organising the School's cell culture supply. I would also like to express my appreciation to Dr Joanna Kelly, Dr Rob Steuart, Dr Maïlys Vergnolle and Dr Connie Jackaman for maintaining superb cell culture facility. I would also like to extend my thanks to Dr Julia Koehn, Chee Wai Wong and Dr Vishal Chaturvedi for their assistance and expert advice on confocal microscopy. I would also like to thank Ms Elaine Miller for helping with the FESEM images, Dr Ching Goh for his guidance with the NMR and Dr Scott Bringans for helping with the mass spectroscopy analysis.

I would also like to express my appreciation to my fellow PhD students for their support: Sangeetha Mathavan for introducing Graphpad Prism and Chemdoodle to me, also Yan Jing Ng for introducing Google Drive and GPC to me. Thanks also go to Bhawna Gauri for proposing the correct stabiliser for the nanoparticle formulation and assisting in almost every step of the project. I am grateful to Behin Sundara Raj for helping with the MTT assay and Aparna Warrier for extending her kind assistance with overall cell culture procedure. I would also like to thank Omar Elaskalani for providing the protein analysis protocol and the reagent, also Adnan Mannan for providing the RIPA buffer and many other technical assistance regarding Graphpad, ImageJ and confocal microscope image processing. I would like to acknowledge Jorge Martinez and Sonia Jose for supplying all required reagents and technical assistance, and also Michael Stack, Joyce Thomas, Ausana Naidoo and Jennifer Ramsay for providing excellent administrative support. I would also like to extend my thanks to Angela Samec for supplying laboratory consumables and also for providing training on the freeze dryer. I very much appreciate the friendly assistance of Jenny Dolzadelli during my sessional teaching in the School of Pharmacy. Thanks a lot to Irene Cotte, Petra Behre and Debbie Stewart for providing general laboratory assistance. I thank Sam Siem and Charmaine D'Costa for giving me the best purchasing experience in my life. Additional thanks are given to all my fellow schoolmates Adnan Mannan, Aparna Warrier, Bhawna Gauri, Mohammad Shohel, Hilai Ahmadzai, Kevin Anderson, Remya Baker, Fatima Jahan, Mustafa Atee, Shamala Ayadurai, Gaewyn Ellison, Jully Gogoi Tiwari, Revathy Carnagarin and Malini Visweswaran for the tea, coffee, cake, bread, snacks, smile and shoulder when needed.

I sincerely thank my wife, Yeakuty Marzan Jhanker, for her love and understanding to ease my stress during the PhD journey. I also thank my children who sacrificed many of their fun time because of my extended hour work. Last but not least, I would like to thank my parents and other family members for supporting me throughout my life.

Dedication

I dedicate this thesis to my happy son, Raiyan Reeshan Huda and my loving daughter, Raina Neeshat Kongkon for making my life full of enjoyment.

Table of Content

List of Figures

List of Tables

Abbreviations

µg	Microgram
Å	Ångström
ABC	Adenosine triphosphate-binding cassette
ACh	Acetylcholine
AChE	Acetylcholinesterase
ACN	Acetonitrile
AD	Alzheimer's disease
ALS	Amyotrophic lateral sclerosis
AMT	Adsorptive-mediated transcytosis
ATP	Adenosine triphosphate
ATR	Attenuated total reflection
BBB	Blood-brain barrier
BCRP	Breast cancer resistance protein
bFGF	Basic fibroblast growth factor
Boc-DAB	N-boc-1,4-diaminobutane
BSA	Bovine serum albumin
BuChE	Butyrylcholinesterase
$CDCl_3$	Deuterated Chloroform
CHCA	α-cyano-4-hydroxycinnamic acid
CLSM	Confocal laser scanning microscopy
CMT	Cell-mediated transcytosis
CNS	Central nervous system
COOH	Carboxyl group
CPP	Cell-penetrating peptides
CSF	Cerebrospinal fluid
DAD	Diode-array detector
DAPI	4′,6-Diamidino-2-phenylindole dihydrochloride
DCC	Dicyclohexyl-carbodiimide
DCM	Dichloromethane
DCU	Dicyclohexylurea
DDS	Drug delivery system
DiD	1,1'-dioctadecyl-3,3,3',3'-tetramethylindodicarbocyanine
DL	Drug loading
DLS	Dynamic Light Scattering

DMEM	Dulbecco's Modified Eagle's Medium
DMF	Dimethylformamide
DMSO	Dimethyl sulfoxide
DMSO-D6	Deuterated dimethyl sulphoxide
DSC	Differential scanning calorimetry
DSPE-mPEG	1,2-distearoyl-sn-glycero-3-phosphoethanolamine-N-[methoxy polyethylene glycol-5000]
DSPE-PEG	Polyethylene glycol-distearoyl phosphatidylethanolamine
DSPE-PEG-NHS	1,2-dioleoyl-sn-glycero-3-phosphoetha-nolamine-n-[polyethyleneglycol]-hydroxysuccinamide
EBM-2	Endothelial Basal Medium-2
EE	Entrapment efficiency
EtAc	Ethyl acetate
FBS	Foetal bovine serum
FDA	Food and Drug Administration
FESEM	Field emission scanning electron microscope
FLD	Fluorescent detector
FTIR	Fourier transform infrared
GC-MS	Gas chromatography mass spectrometry
GPC	Gel permeation chromatography
H_2O_2	Hydrogen Peroxide
HBSS	Hanks' balanced salt solution
HBSS-F	HBSS containing 10% FBS
HBSS-P	HBSS containing 10mM HEPES and 20mM glucose
HCl	Hydrochloric acid
HD	Huntington's disease
HEPES	4-2-Hydroxyethylpiperazine-1-ethanesulfonic acid
HIV	Human immunodeficiency virus
HPLC	High-performance liquid chromatography
HSA	Human serum albumin
HTS	High-throughput screening
ICH	International conference on harmonisation
IV	Intravenous
JAM	Junctional adhesion molecule
LC-MS	Liquid chromatography-mass spectrometry
LDA	Laser doppler anemometry
LDV	Laser doppler velocimetry

LOD	Limit of detection
LOQ	Limit of quantification
MALDI-TOF-MS	Matrix-assisted laser desorption/ionisation time of flight mass spectrometry
mg	Milligram
mL	Millilitre
MRP	Multidrug resistance protein
MS	Mass spectrophotometer
MSDS	Material safety data sheet
MTT	Methyl thiazolyldiphenyl-tetrazolium bromide
MW	Molecular weight
MWCO	Molecular weight cut-off
NaOH	Sodium hydroxide
ND	Neurodegenerative diseases
NEAA	MEM non-essential amino acids solution
Neu5Ac	N-acetylneuraminic acid
ng	Nanogram
NHS	N-hydroxysuccinimide
NMR	Nuclear magnetic resonance
NP	Nanoparticle
NPs	Nanoparticles
NP-HPLC	Normal phase HPLC
O/W	Oil-in-water
ODA	Octadecylamine
PACA	Poly(alkyl cyanoacrylate)
PBS	Phosphate buffered saline
PC2	Physical containment level 2
PCS	Photon correlation spectroscopy
PD	Parkinson’s disease
PDI	Polydispersity index
PEG	Polyethylene glycol
PFA	Paraformaldehyde
P-gp	P-glycoproteins
Phalloidin-FITC	Fluorescein isothiocyanate labelled phalloidin
PLA	Poly(lactic acid)
PLGA	Poly(D,L-lactide-co-glycolide)

PLGA-DAB	Poly(DL-lactide-co-glycolide)-diaminobutane
PMMA	Poly(methyl methacrylate)
PVA	Polyvinyl alcohol
QLS	Quasi-Elastic Light Scattering
R^2	Coefficient of determination
RBF	Round bottom flask
RC	Regenerated cellulose
RES	Reticuloendothelial system
RHT	Rivastigmine hydrogen tartrate
RID	Refractive index detector
RMT	Receptor-mediated transcytosis
RP-HPLC	Reverse phase HPLC
RSD	Relative standard deviation
RT	Room temperature
RV	Rivastigmine base
SA	Sialic acid
SA-ODA	Sialic acid-octadecylamine
SDS	Sodium dodecyl sulphate
SESD	Spontaneous emulsion solvent diffusion
TAT	Trans-activating transcriptional activator
TDL	Theoretical drug loading
TEA	Triethylamine
TEER	Transendothelial electrical resistance
TEM	Transmission electron microscope
TFA	Trifluoroacetic acid
THF	Tetrahydrofuran
TJ	Tight junction
TMS	Tetramethylsilane
USP-NF	United States Pharmacopeia and National Formulary
Vitamin E-TPGS	d-α-tocopherol polyethylene glycol 1000 succinate
VWD	Variable wavelength detector
W/O	Water-in-oil
W/O/W	Water-in-oil-in-water
ZO	Zonula occludens

Abstract

Targeted drug delivery has always been used as an important strategy to overcome challenges presented by undesirable pharmacokinetics or biodistribution of drugs, especially when the targets of these drugs are inside the brain. There are examples including drugs for treating central nervous system (CNS) diseases such as Alzheimer's disease, Parkinson's disease, amyotrophic lateral sclerosis Huntington's disease, brain tumour and multiple sclerosis. Our brain is naturally protected by the blood-brain barrier (BBB) that restricts drug delivery into the brain tissue. Many drugs which have shown effectiveness *in vitro,* failed *in vivo* because of it.

Nanoparticulate drug delivery system (DDS) has been extensively researched as a promising formulation to deliver drugs into the brain because of its small size; capable of carrying hydrophilic and hydrophobic, large and small size of therapeutic agents; feasibility in surface modification to allow the attachment of targeting ligands; and relatively easier of providing controlled drug release. Recent progress in understanding the BBB and brain made possible to design better ligands to target the BBB and the brain. The aim of this project was to develop a novel type of poly(D,L-lactide-co-glycolide) (PLGA) based nanoparticulate DDS, with dual ligands to enhance the delivery of a model drug, rivastigmine hydrogen tartrate (RHT, a drug for treatment of mild AD) across the BBB into the brain. The dual ligand nanoparticles (NP) were surface modified with two hydrophilic ligands – (1) a BBB targeting ligand for higher brain penetration capability, and (2) a neurone targeting ligand for longer NPs residence time in the brain parenchyma.

These hydrophilic ligands were conjugated with hydrophobic moieties for the ease of their incorporation to the NPs formulation. The BBB targeting ligand, trans-activating transcriptional activator (TAT) peptide was conjugated with DSPE-PEG whereas the neurone targeting ligand, sialic acid (SA) was chemically attached with octadecylamine (ODA) to form conjugates. Both reaction schemes were developed and optimised concerning the reaction temperature, time and purification procedures. Several analytical methods (NMR, HPLC, MS, FTIR) were developed and optimised for the analysis of the final products.

The TAT conjugate was prepared by a nucleophilic substitution reaction and purified by dialysis. The reaction time was optimised using HPLC analysis and found to be 72 hours at which point a maximum reaction yield of about 83% w/w was achieved. The SA conjugate was synthesised via carbodiimide cross-linking reaction and purified by dialysis. NMR analysis revealed that the ODA was 100% conjugated with SA and the product yield was about 100%. FTIR spectra showed the appearance of a new amide bond and disappearance of the SA carboxylic bond, confirming the formation of a new conjugate.

HPLC analysis of RHT for drug loading and drug release samples was developed, optimised and fully validated for its selectivity, accuracy, linearity, precision and ruggedness. Limit of detection (LOD) and limit of quantification (LOQ) of the assay were 60ng/mL and 201ng/mL, respectively. This HPLC method exhibited good linearity over the assayed concentration range and satisfactory accuracy and selectivity, good intra- and inter-day precision. The developed HPLC method was accurate and selective for RHT analysis with good detection and quantification limits and was suitable for its intended use.

The dual ligand PLGA NPs were prepared using the synthesised ligand-hydrophobic chain conjugates employing double emulsion solvent evaporation technique. RHT was loaded in the NPs as a model drug. Also, two independent lipophilic tracers were loaded separately for the simple fluorometric quantification in plate readers and detection under the fluorescence microscope for the purpose of cellular characterisation of the dual ligand NPs. The NPs formulation was optimised to achieve the particle size between 70nm and 200nm as well as to achieve highest possible drug loading in the NPs. The optimised NPs formulation was evaluated for *in vitro* characteristics including particle morphology, size, zeta potential, drug loading efficiency, release profile and stability studies. The RHT-loaded optimised PEGylated dual ligand NPs were found to have negative zeta potential (−24.3 ± 2.5mV) and narrow size distribution (139.5 ± 3.9nm) ideal for targeting the BBB. DSC thermograms indicated that RHT was dispersed as an amorphous state in PLGA NPs whereas FESEM studies revealed that the NPs were spherical.

In vitro release studies showed 57.9 ± 3.3% release from PLGA NPs in 24 hours. Our investigation suggests that the optimised NPs systems were stable for at least seven days at 4°C in terms of their particle size, zeta potential and drug leaching.

Extensive cellular investigation of the dual ligand NPs system was carried out including - (a) the cell viability studies in two cell lines upon exposure to the system, (b) cellular uptake studies of the NPs system, and (c) their transport across an *in vitro* BBB model. The immortalised human cerebral microvascular endothelial cell line (hCMEC/D3) and human colon carcinoma cell line (Caco-2) were found to be more than 90% viable at as high as 200µg/mL NPs concentration. The cell uptake of the optimised dual ligand PLGA NPs were found to be superior (3.4-fold increase) to that of NPs without any ligand ($p < 0.005$) thereby showed a clear correlation between the ligand incorporation and cellular uptake. This investigation also demonstrated that the TAT peptide facilitates cellular uptake of the NPs systems which was temperature, time and particle concentration dependent, indicating the major update mechanism is endocytosis. The confocal microscopic study revealed that the dual ligand nanoparticles were accumulated in the nucleus and its qualitative results correlated well with those observed using a quantitative fluorescent spectroscopic method. Likewise, the NPs conjugated to the TAT peptide displayed significantly higher cellular transport than the tracer solution (12.6-fold, $p < 0.001$) and RHT solution (1.2-fold, $p < 0.05$).

Thus, it can be concluded that, the novel dual ligand nanoparticulate DDS developed has shown promising results with ability to enhance the uptake by human brain capillary endothelial cells and transport in an *in vitro* BBB cell model while exhibiting the versatility in carrying molecules of interest and has biocompatibility (low toxicity), potential to be used as a platform technology for brain drug delivery.

Chapter 1 General Introduction

1.1 The Human Brain-A Challenge for CNS Drugs

The human brain is the major organ of the central nervous system (CNS) that controls almost all physical and mental activities including cognition, sensation, sensory perception, communication and metabolism. Even with today's modern and sophisticated technology, the complete functional understanding of the human brain is yet to be explored (Bassett & Gazzaniga, 2011; Roy & Dwivedi, 2017). The human brain is roughly divided into three parts, the cerebral hemispheres (the cerebrum), cerebellum and brainstem. It contains approximately 100 billion neurones, 100 billion glial cells (oligodendrocytes, astrocytes, microglia etc.) and thousands of blood vessels (Herculano-Houzel, 2009; Auffret *et al.*, 2017; Yang *et al.*, 2017). It is well protected by a strong skull, suspended in the cerebrospinal fluid (CSF), and separated from the circulatory system by the blood-brain barrier (BBB).

Apart from the risk of physical injuries and neurotoxicity, there are hundreds of known CNS disorders reported in the literature including stroke, brain tumours, Alzheimer's disease (AD), Huntington's disease (HD), Parkinson's disease (PD), Prions disease, Down syndrome, ataxia, multiple sclerosis, Creutzfeldt-Jacob disease, schizophrenia, tardive dyskinesia, amyotrophic lateral sclerosis (ALS), herpes encephalitis and cerebral toxoplasmosis (Azevedo *et al.*, 2009; Kovacic & Somanathan, 2012; Khanam *et al.*, 2016). Neurodegenerative diseases (ND) have received immense attention in scientific society because of their increased incidence, mainly associated with the increase in life expectancy. ND are conditions which affect normal brain function resulting from deterioration over time of neuronal cells or their myelin sheath in the brain and/or spinal cord. These cells are responsible for our day-to-day activities such as processing sensory information, making decisions, and controlling movement. Neurones are not easily regenerated; therefore their damage leads to age-related diseases such as AD, PD, HD, multiple sclerosis and ALS (Cannon & Greenamyre, 2011; Khanam *et al.*, 2016).

There are two main types of ND: (a) conditions related to dementia affecting cognition and memory and; (b) conditions causing problems with movement. AD is the most common form of dementia which causes a progressive decline in functionality including but not limited to loss of memory, rationality, intellectual abilities and social skills (Banks, 2012). It was the 2nd leading cause of death in Australia in 2015, because of its prevalence in people over 85 years, and is predicted to be the leading cause of death in Australia within a few years ("Causes of Death, Australia, 2015," 2016). About 47 million people worldwide were living with dementia in 2015 (Wimo *et al.*, 2017). It has been predicted that unless an appropriate medication is developed for the prevention or treatment of AD, it will affect 1 in 85 people globally by 2050 (Story, 2016; Ariga, 2017). PD, the second most common ND, produces one or more of three major symptoms: tremor, rigidity (stiffness of the muscles) and akinesia (abnormal movement) (Geng *et al.*, 2016; Vermeiren & De Deyn, 2017). It is estimated that there are about 100,000 people living with PD in Australia, with a worldwide occurrence of approximately four million people (~1 in 1000) or about 1% of the population over the age of 60 years. Researchers have predicted that the number of PD patients will double by 2030 (Hurelbrink & Lewis, 2011; Tan *et al.*, 2013; Hiorth, 2016).

These two examples clearly highlight the growing global burden of ND. The disorders are devastating and expensive, both on a personal and global level. Currently, there is no effective therapy to prevent, cease or reverse the progression of many types of the ND despite that limited treatments available in assisting the management of symptoms and delay the progression of the disease. For example, PD is most often treated by replacing the missing dopamine with levodopa. Extensive research is in progress that is reflected by hundreds of on-going clinical trials to test various drugs against ND (Frank *et al.*, 2016; Bachurin *et al.*, 2017; Reiman, 2017). The challenge, however, is not just in finding right molecules to combat CNS diseases, but also effectively delivering it into the brain. More than 98% of the promising known small-molecule drugs and almost 100% of macromolecular biopharmaceutical products cannot be delivered into the brain due to the presence of the BBB (Pardridge, 2007; James *et al.*, 2016). Thus, effective treatment of many CNS diseases such as AD, PD, brain tumours, multiple sclerosis is considerably impaired (Gao *et al.*, 2013; Patel & Patel, 2017).

The BBB (Figure 1.1) is the brain endothelial cell layer between the cerebrospinal fluid of the CNS and the circulating blood system. The works of Paul Ehrlich, the father of modern chemotherapy, in the late l9th century first raised the concept of this barrier (Ehrlich, 1906). He observed that coloured dyes injected into the blood circulation of animals failed to stain the brain which phenomenon was attributed to the characteristics of the brain tissues rather than the compartmentalization theory. Later, his student Edwin Goldmann confirmed the existence of the BBB by directly injecting the dye into the CSF of animals' brains. This experiment demonstrated that in this case, the brains did become stained, while the rest of the body did not (Goldmann, 1913; Feng & Chien, 2003). Thus, it was hypothesised that the main function of BBB is to guard the delicate nerve cells against foreign substances and microorganisms in the systemic circulation. However, the protective mechanisms of the BBB also hinder the transport of many drugs in the CNS.

In general, a drug is transported from the blood to brain by paracellular and transcellular pathways, transport proteins, receptor-mediated transcytosis (RMT), adsorptive-mediated transcytosis (AMT) and cell-mediated transcytosis (CMT) (Chen & Liu, 2012). BBB severely restricts all these transport routes because it contains a very limited number of transport vesicles, and there is no fenestration. Furthermore, there is a lack of the gap between adjacent endothelial cells in many regions of the brain and if present, it is tight junction (TJ) formed by the most intimate cell-to-cell connection. A number of proteins including junctional adhesion molecule (JAM) -1, occludin, claudin, zonula occludens (ZO) -1, 2 are involved in generating this structure (Gonzalez-Mariscal *et al.*, 2016; Greene & Campbell, 2016).

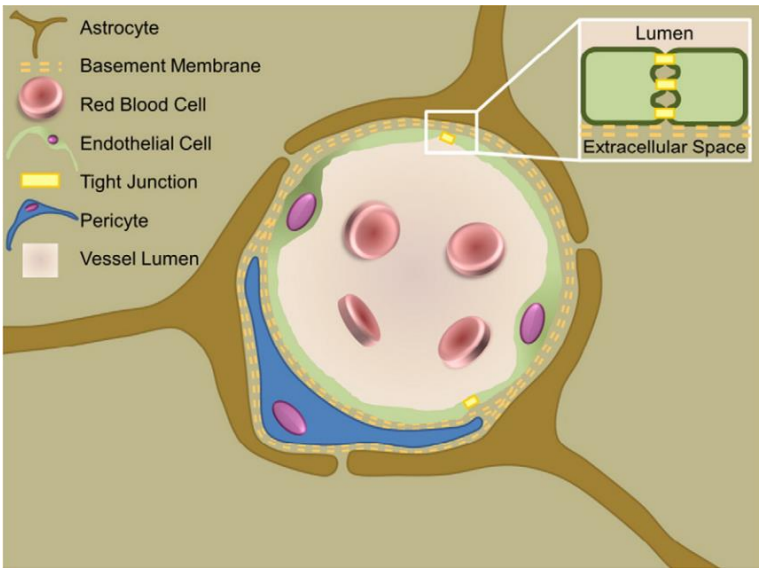

Figure 1.1. Biology of BBB that presents a major obstacle to drug delivery in the CNS (Timbie *et al.*, 2015).

The tightness of endothelial cells of BBB is upregulated by synergistic induction of pericytes, astrocytic end-feet, microglia, and a basement membrane made from structural proteins such as the extracellular matrix proteins collagen and laminin (Banerjee *et al.*, 2016; Erdo *et al.*, 2017). The resulting tight "neurovascular unit" only grants access about 2% of presently known small molecular weight drugs and very few of available large molecular weight drugs into the brain (Rautio *et al.*, 2008). As there is no lymphatic drainage, the BBB also restricts the passage of lymphocytes and other immune cells. Thus, it acts as a physical barrier, a transport barrier, an enzymatic barrier and an immunological barrier (Chen & Liu, 2012). This highly organised structure demonstrates a selective permeability for only the unionised compounds having a molecular weight (MW) of less than 500Da, lipophilicity (log P value close to 2) and less than ten hydrogen bonds (Pardridge, 2005a, 2005b). While the BBB performs the vital task of protecting the brain from harmful fluids, chemicals and toxins; it also poses a major challenge for brain drug development and delivery. This is considered to be the most important factor limiting the future growth of neurotherapeutics (Greene & Campbell, 2016; Erdo *et al.*, 2017). A better understanding of the existing BBB transport systems might assist the development of drug delivery system (DDS) with enhanced capability of delivering bioactive molecules into the brain.

1.2 Transport Mechanisms Across the BBB and DDS Development

Although human brain is well guarded by the BBB, several transport systems are in place to keep the brain functional (Chen & Liu, 2012; Patel & Patel, 2017). Biomolecules that are essential for the survival and proper functioning of the nervous system are transported in between blood and CSF via these transport facilities.

Very few small molecules can cross the BBB by simple diffusion due to their hydrophilic or lipophilic nature. Small water-soluble molecules, such as sodium and potassium ions, diffuse through the TJ utilising paracellular aqueous pathway. Small lipid-soluble molecules, such as alcohols and steroid hormones, use transcellular lipophilic pathways to get into the brain. Due to very strict rule present in this type of transport system, such as specific MW, charge, hydro- or lipophilicity, drug delivery into the brain exploiting passive diffusion did not get much attention (Upadhyay, 2014b; Rassu *et al.*, 2017; Wang & Wu, 2017).

The adenosine triphosphate-binding cassette (ABC) efflux transporter P-glycoproteins (P-gp), multidrug resistance protein (MRP) family and breast cancer resistance protein (BCRP) actively transport many lipophilic drugs (such as P-gp substrates) out of the brain through BBB. This transport mechanism plays a very important role in drug distribution to, and elimination from, the CNS. These active efflux transporters significantly minimise or completely eradicate the potential neurotoxic effects of many foreign materials, but also limit the CNS concentration of drugs that are potentially beneficial for the treatment of brain diseases. Suppressing P-gp at the BBB has been demonstrated to enhance drug accumulation in the CSF; therefore it appears to be an effective strategy to enhance drug delivery into the brain (Lingineni *et al.*, 2017; Sivak *et al.*, 2017; Tournier *et al.*, 2017).

Essential nutrients such as glucose, amino acids, hormones, bile salts and monocarboxylic acids are spontaneously transported into the brain by carrier-mediated transport systems. The process starts when these molecules bind to protein transporter on one side of the BBB, triggering a conformational change in the protein, resulting in the transport of the substance to the other side of the membrane. Usually, these systems solely work on the structural modification of the transport proteins without needing of any additional energy. However, in special situations, adenosine triphosphate (ATP) may provide energy to facilitate the process when compounds need to be moved against a concentration gradient (Pulicherla & Verma, 2015; Oberoi *et al.*, 2016).

Macromolecules like insulin, transferrin, and other endogenous peptides, are selectively transported through the BBB by RMT. Endothelial cells of BBB have specific receptors to bind and uptake these large biomolecules into the brain by vesicular trafficking technology. As soon as the ligands bind to their corresponding receptors on one side of the cell, the macromolecules are captured in vesicles, drawn across the cell and ejected on the other side of the cell. Unlike carrier-mediated transport systems, RMT is highly specific, works against the concentration gradient and can "ferry" high MW substances. This active transport system has much scope for developing drug delivery therapeutics and has been extensively studied for brain targeting (Kim *et al.*, 2015; Kuo & Chen, 2015). However, widespread expression of many receptors (such as transferrin receptors) on peripheral organs limits the capability of RMT for specific brain delivery. Also, the targeting ligand must compete with natural ligand present in the bloodstream to bind with the specific physiological receptor, thereby limiting the efficiency of the DDS (Jones & Shusta, 2007).

Another interesting transport system present in the BBB is AMT which does not rely on the receptors as the RMT (thus, less specific), however, is capable of transporting molecules at a higher rate. The driving force of the AMT is the electrostatic interaction between oppositely charged molecules. Peptide molecules with positive surface charge are usually transported upon binding with the negatively charged plasma membrane surface (Malhotra *et al.*, 2013; Sharma *et al.*, 2016a). Although AMT is not as specific as the RMT, this transport system has higher capacity and hence, attracts much attention for drug delivery. Furthermore, drastic alternations of the BBB receptor system have been reported earlier in many neurodegenerative disease conditions that may render the RMT based drug delivery system less efficient, if not completely useless (Weiss *et al.*, 2009). The AMT has been successfully used to deliver drugs in severe CNS disease conditions (such as tetanus) giving the indication that this transport system undergoes which insignificantly affects its drug transport capability (Hervé *et al.*, 2008). The targeting ligands, in this case, are either positively charged proteins or cell-penetrating peptides (CPP) such as trans-activating transcriptional activator (TAT) peptide (Qin *et al.*, 2011b; Milletti, 2012).

All transport mechanisms mentioned above permit only solute molecules, whereas CMT is capable of transporting whole cells. Monocytes, macrophages and other immune cells are transported into the brain via CMT (Pang *et al.*, 2017). The drug delivery approach exploiting CMT uses the physiological phagocytic cells (like monocytes) to load the desired drug or DDS and the drug-loaded cells traffic the desired molecule across the BBB. Advantages of this method include the possibility of high drug loading, elimination of the need for nano-sized carriers, the inclusion of magnetic guidance and possibility of treating brain under inflammation. Selectivity seems to be an issue with this drug transport system because a high percentage of administered dose was reported to be ended up in liver and spleen (Jain *et al.*, 2003). Although a relatively new concept, drug or nano-sized drug carriers loading via phagocytosis into monocytes, and then using the loaded monocytes to deliver the molecule of interest into the brain, seems to be a valid and promising approach (Tong *et al.*, 2016; Pang *et al.*, 2017).

The various physiological transport mechanisms present at the BBB are shown in Figure 1.2.

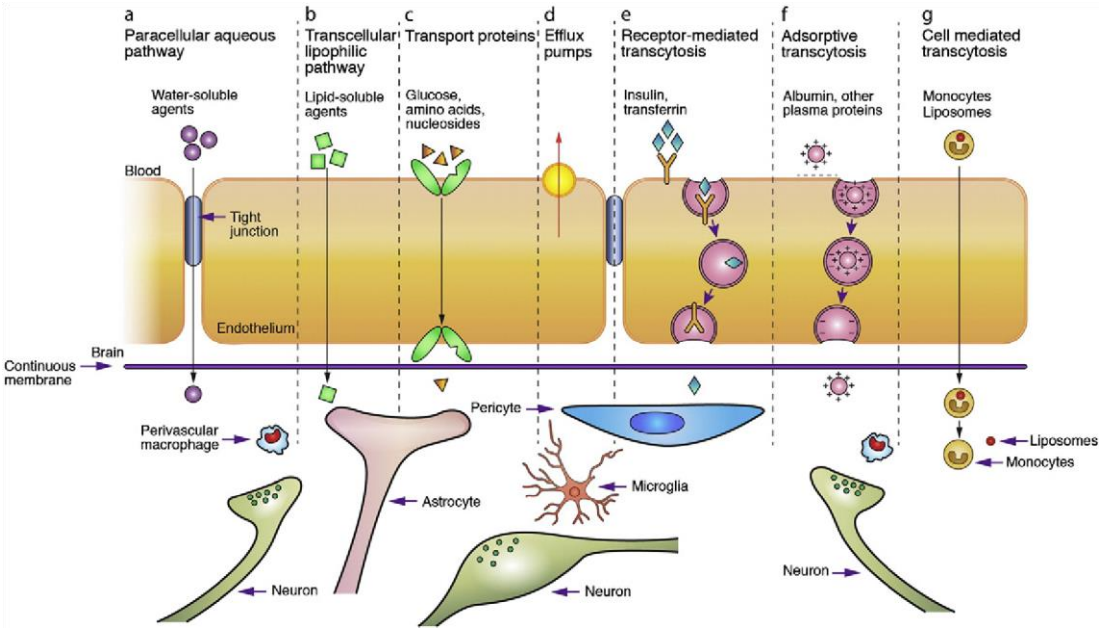

Figure 1.2. The various physiological transport mechanisms present at the BBB (Chen & Liu, 2012).

1.3 Strategies to Enhance CNS Drug Transport

As of 2017, there is no ideal DDS that can guarantee to deliver the majority dose of the loaded drug into the brain at an optimum concentration to exert their intended pharmacological activities (Patel & Patel, 2017). Research is going on continuously to overcome this problem – ranging from directly injecting the drug into the CSF (intrathecal injection) to incorporating the drug carrier into physiological cells to be trafficked via the BBB. In the former approach, the drug is injected into the spinal canal or the subarachnoid space so that it directly reaches the CSF without any loss. This method must be carried out by a specialist (such as a Neurosurgeon) in an appropriate clinic or hospital capable of handling the unwanted complications that may arise from the action. Consequently, direct intracerebral injection is only occasionally used, to avoid tissue destruction at the site of injection and the high risk of intracerebral infection. This approach is not patient-friendly, and the number of suitable drugs for intrathecal delivery is very limited (Pardridge, 1998). All other methods to enhance brain drug delivery can be roughly divided into three categories, namely-(1) bypassing the BBB, (2) non-carrier mediated drug delivery, and (3) carrier-mediated drug delivery. This section briefly discusses these strategies, their scope and limitations:

1.3.1 Bypassing the BBB

Alternative routes, like intranasal administration of drugs, offer the potential to completely avoid the BBB instead of crossing it. This approach can directly deliver lipid-soluble small molecules into olfactory lobe CSF, demonstrating a rapid onset of action. However, serious mucosal irritation and irreproducible absorption pattern due to nasal congestion are major drawbacks of this route that are yet to be addressed to make it clinically safe and successful. There is also a chance of partial degradation of the drug in the nasal mucosa, and frequent use of the intranasal route can result in mucosal damage (Nagpal *et al.*, 2013; Kaur *et al.*, 2016).

1.3.2 Non-carrier Mediated Drug Delivery

In non-carrier mediated drug delivery, either the drug is chemically modified to increase its BBB permeability or the target (BBB) is compromised to offer better penetrability to the drug. For example, in the lipophilic prodrug synthesis method, drug molecules that are normally unable to cross BBB are chemically altered into lipophilic prodrugs or active analogues to enhance their CNS absorption by passive diffusion. Heroin (diacetyl derivative of morphine), for example, exerts more than 30 times bioavailability in the brain compared to its original substance (Oldendorf *et al.*, 1972). Prerequisite for this tactic is a starting drug molecule with low MW, and even after the modification, the MW should be below the threshold of 500 Da. Unfortunately, many drug molecules discovered by high-throughput screening (HTS) have already significantly high MW making them unsuitable candidates for this approach. For example, doxorubicin (MW 543.5) is used for a wide range of cancer treatment except those in the brain because of its poor CNS distribution (Aryal *et al.*, 2015). However, this drug is not a suitable candidate for prodrug synthesis due to its high MW. The second problem with this method is that with increasing lipid solubility, plasma solubility of the substance becomes low with high albumin protein-binding resulting in higher drug distribution in non-target tissues. It is difficult to find an appropriate balance between optimum hydro- and lipo-philicity of the substance with ideal pharmacokinetics parameters which is in favour of brain drug delivery/targeting (Pardridge, 1998; Misra *et al.*, 2003).

Another way to increase the BBB permeability of a drug is to use cationization technique. The BBB surface is negatively charged; therefore cationic molecules have better chance to get adsorbed onto the surface of the BBB and to get absorbed inside eventually. An approach to chemically modifying a drug molecule into a positively charged molecule is one strategy to enhance its brain uptake. However, potential toxicity and non-specific distribution of the cationized molecule has hindered further development of this method (Witt *et al.*, 2001; Witt & Davis, 2006).

Since very few pharmacologically active molecules retain their desired activity after chemical alteration, BBB modifications by different techniques have been attempted. For example, administration of hyperosmolar mannitol or arabinose solutions into the carotid artery leads to a temporary reduction in BBB functionality by "cell shrinkage" of the endothelial cells. This 'osmotic opening' of the BBB ultimately opens the TJ for a period of about 20-30 minutes and thus enables the paracellular transport of the drug. However, these are non-specific openings of the BBB for all substances including toxins and neurotransmitters from the systemic circulation that can lead to brain cell damage and infections (Azad *et al.*, 2015; Garg *et al.*, 2015).

Histamine, bradykinin and bradykinin analogues are used for biochemically disrupting the function of the TJ. Organic solvents such as ethanol and dimethyl sulfoxide (DMSO) or emulsifiers, such as sodium dodecyl sulphate (SDS), polysorbate 80 and alkylglycerols have also been reported to open the TJ (Pardridge, 2005a; Escalona-Rayo *et al.*, 2017; Joseph & Saha, 2017). However, this approach is clinically unsafe and may cause permanent breakdown of brain's self-defense mechanism. Temporary disruption of the BBB can also be initiated via physical stimuli such as ultrasound, microwave, and electromagnetic field. Many proteins, peptides, mRNA and DDS such as liposomes or nanoparticles (NP) have been reported to be effectively delivered into the brain using this technique. However, existing technology is still unable to control the extent and duration of the BBB opening precisely, thus demands more research in this field.

Finally, inhibition of efflux pumps present in the BBB can enhance brain retention time of some drugs. These drugs are substrates to P-gp, which means active efflux transport by P-gp "kicks" the drug out of the brain as soon as they enter. This can be a devastating situation and major obstacle for getting high enough drug concentration inside the brain. To tackle this problem, either the drug can be modified chemically, or P-gp inhibitor can be administered alongside the drug (Kabanov *et al.*, 2002; Fang *et al.*, 2016). Efflux pump suppressors work by blocking the P-gp and other related proteins thereby retaining the drug inside the brain. Batrakova *et al.* (2015) showed that when Pluronic® P85 was co-administered with P-gp substrate drugs, a significantly higher amount of the drugs was found in the brain.

The approach of suppressing efflux pump is better suited only to acute diseases treatment where maximum drug concentration is desired for a relatively short period. Repeat administration of efflux pump suppressors for chronic disease treatments causes prolonged P-gp inhibition that may interfere with P-gp regulated homeostatic regulation. Obstructing efflux pumps in BBB may lead to a high drug concentration in the brain due to the reduction in drug elimination that can also result in serious neurotoxicity even at a much lower dose than well-tolerated doses (Silva *et al.*, 2015).

A very important criterion for the successful drug transport across the BBB, apart from its pharmacokinetic properties, is that the drug must be present at a high concentration in the circulatory system for prolonged period. This issue cannot be addressed with the non-carrier mediated drug transport system because their biological half-life can only be increased by altering their molecular structure. This approach is seldom practical due to the potential loss of the desired pharmacological properties of the drug molecules. Thus, an alternate method of drug delivery was sought that involves carrier(s) to fulfil the higher blood residence time of drug thereby increasing its chance of getting absorbed into the brain.

1.3.3 Carrier-mediated Drug Delivery

In the carrier-mediated drug delivery approach, an inert vehicle is usually employed to carry and deliver the drug(s) of interest to its site of action. Popular carriers for CNS drug delivery include liposomes and NPs. Liposomes are particles composed of a single or multilayer phospholipid bilayer outer membrane and an inner hydrophilic pocket, which can be loaded with various kinds of agents (Peng *et al.*, 2017). Phospholipids are the major component of the biological systems; therefore, they possess low toxicity and are biodegradable. Conventional liposomes are rapidly taken up by the reticuloendothelial system (RES) and thus have a very short plasma half-life (Schnyder & Huwyler, 2005). Sterically stabilised liposomes are formulated to overcome this problem by incorporating hydrophilic polyethylene glycol (PEG) chain on the surface, a process called PEGylation. This results in a significantly lower particles uptake in the RES and offers them longer blood circulation time (She *et al.*, 2014). These modified liposomes are commercially available as a drug carrier (Hau *et al.*, 2004; Wibroe *et al.*, 2016), such as in Caelyx® (Essex Pharma GmbH, Munich, Germany), a liposomal doxorubicin formulation for the treatment of glioblastoma.

Particulate carrier systems also include nanocrystals/nanosuspensions, polymeric NPs, solid lipid NPs and nanostructured lipid carriers. All systems can be adopted as drug carriers and have a size in the nanometer range (<1 micron). An ideal particulate carrier system should meet the following conditions:

- Controlled, sustained release in the target tissue
- Non-toxic, non-immunogenic
- Chemically and physically stable
- Biodegradable
- Sterile
- Cheap and simple production
- Tunable for targeted drug delivery

NPs based on poly(D,L-lactide-co-glycolide) (PLGA) satisfy many of the above requirements. They are simple and inexpensive to manufacture, have good storage stability, are readily biodegradable, non-immunogenic and do not show acute toxicity (Cheng *et al.*, 2011; Fonte *et al.*, 2012). There is the potential to achieve controlled release, and specific ligands can be attached to the surface to direct the NPs to target tissue (Cheng *et al.*, 2007; Sahana *et al.*, 2008; Zhou *et al.*). NPs are spherical, solid, colloidal particles, having a size in the range between 10 and 1000 nm (De Jong & Borm, 2008). Their small size allows easy intravenous (IV) application because the smallest capillaries of the human body have an average diameter of 3 - 8 microns (Singh & Lillard, 2009). NPs for drug delivery can be prepared from biocompatible synthetic or natural polymers or lipids. There are many NPs manufacturing procedures developed and described. The main production processes are desolvation, ionic gelation, salting out, nanoprecipitation and solvent evaporation. The most common types of the polymers used for developing nanoparticulate DDS include human serum albumin (HSA), gelatin, chitosan, poly(methyl methacrylate) (PMMA), poly(lactic acid) (PLA), PLGA and poly(alkyl cyanoacrylate) (PACA) (Norakankorn *et al.*, 2007; Valente *et al.*, 2013; Azimi *et al.*, 2014; Langiu *et al.*, 2014; Zhang *et al.*, 2014; Sulheim *et al.*, 2016; El-Hammadi *et al.*, 2017).

Nanoparticulate DDS offer several benefits over IV administration of a drug solution:

- ♣ protect the drug from degradation,
- ♣ the possibility of drug targeting,
- ♣ reduced adverse drug reactions and
- ♣ a sustained release

The advantages of NPs over liposomes are the low cost in production, uncomplicated preparation techniques and their great physical stability (Olivier, 2005). The drug may be: (a) adsorbed to the surface, (b) included in the solid, *i.e.*, dispersed into the polymer matrix, (c) encapsulated by the polymer, or (d) covalently bound to the matrix (Singh & Lillard, 2009; Mahapatro & Singh, 2011). Drug loading inside the NPs may occur during or after its production, but former is more common (Lu *et al.*, 2011). Covalent binding of the drug to polymer matrix is often carried out with the help of covalent bonding between the polymer and drug. Since the only free drug is pharmacologically active, it should be noted that bond between drug and polymer must be designed to be cleaved at the target site. An example of the drug-polymer conjugate (paclitaxel-albumin) containing nanoparticulate finished product is Abraxane®, manufactured and commercialised in the United States by Abraxis BioScience (Los Angeles, USA). An up-to-date list of albumin-based systems in clinical trials and marketed products can be found in the literature (Larsen *et al.*, 2016).

The real beauty of the nanoparticulate DDS resides in its capability of targeted delivery of the biomolecule to its intended site of action. At the end of the 18th century, Paul Ehrlich developed the concept of targeted drug therapy. He proposed to develop a "magic bullet" that could specifically recognise diseased cells and kill without harming the healthy cells (Ehrlich, 1902). The usage of NPs as a drug carrier for the site or disease specific pharmacological activity has been investigated for several decades with reports of selective enhancement of drug delivery in the target tissue (Huang *et al.*, 2014; Kim *et al.*, 2015). After IV administration, bare lipophilic NPs are rapidly coated with lipoproteins of blood, opsonized and absorbed by various organs (liver, spleen and lungs) and cells of the RES. This concept was reported to be highly beneficial for the delivery of antivirals, such as azidothymidine, to macrophages (Lobenberg & Kreuter, 1996). The distribution of the NPs within the body is based only on their physicochemical properties, therefore this kind of drug targeting is referred to as '*passive targeting'*.

One way to change this primary distribution pattern of the NPs is to modify their surface. For example, hydrophilic PEG chains can be grafted on the NPs surface to increase the overall particle hydrophilicity thereby minimising their chance of inclusion within the phagocytic system. Almost all the recent particulate DDS designed for IV administration, have been reported to include PEG either as an independent chain or as conjugated with the core polymer (Chen *et al.*, 2016; Jenkins *et al.*, 2016; Mogoşanu *et al.*, 2016; Liang *et al.*, 2017). PEG is considered as the current gold standard to "hide" NPs from macrophages and other organs of the RES. Likewise, NPs can also be coated with polysorbate 80, poloxamer 188 or other surfactants to increase their surface hydrophilicity thereby increasing their capability to escape the RES (Wilson *et al.*, 2008; Kreuter, 2014). NPs with a reduced chance of getting engulfed by the RES are termed "Stealth NP" (Brigger *et al.*, 2004). Furthermore, targeted accumulation of the NPs in brain cells can be accomplished by the binding of BBB-specific molecules to the particle surface. Significantly higher brain selectivity can be achieved by including a neuron-specific ligand to the NPs surface. Tosi *et al.* (2010) demonstrated that PLGA NPs, which bear on their surface a BBB-penetrating peptide (similopioid peptide) for BBB crossing and also a sialic acid (SA) to interact with brain receptors, exhibit enhanced accumulation in brain cells. This changed body distribution due to the modified NPs structure is called '*active targeting'*.

PLGA based NPs are a promising approach especially for the biodegradability, biocompatibility and non-immunogenic properties of the polymer. Unlike many other polymers, PLGA is approved by the US Food and Drug Administration (FDA) as a safe polymer to be used on patients (El-Hammadi *et al.*, 2017). With the help of PLGA NPs, it is possible to modify the biodistribution of drug molecules. As a result, optimum concentrations of pharmacologically active ingredients can be achieved at the desired organ and at the same time side effects in the other organs are reduced (Bondioli *et al.*, 2010; Danhier *et al.*, 2012). Since unmodified PLGA NPs, like all other lipophilic NPs, are taken up by non-phagocytic eukaryotic cells, macrophages and dendritic cells, they can be used for targeting the liver, spleen, kidney and lung (Alexis *et al.*, 2008). However, the ability of surface-modified PLGA NPs to transport drugs across the BBB is particularly interesting for drug delivery into the brain (Cheng *et al.*, 2007).

Many promising targeted PLGA nanoparticulate drug delivery systems have been reported so far using d-α-tocopherol polyethylene glycol 1000 succinate (vitamin E-TPGS) as an emulsifier. Most of these studies were based on the pioneering works of Feng's group those can undoubtedly considered as a major contribution in this area. A substantial amount of work has been carried out to develop and optimise nanoparticulate formulation of paclitaxel, a popular anticancer drug including their in-depth *in vitro* and *in vivo* characterisations. (Mu & Feng, 2003; Feng *et al.*, 2004; Dong & Feng, 2006).

In theory, nanoparticulate DDS seems to be very promising with the possibility of both passive and active drug targeting capabilities. Practically, a very limited number of nanoparticulate dosage forms are available commercially demonstrating that pharmaceutical manufacturers are not fully convinced about the potential of this technology or are struggling to turn it into commercial reality. Problems that contribute to this slow development of nanoformulations are related to their stability, toxicity, challenges in providing adequate quality assurance and batch-to-batch variation (Duncan & Gaspar, 2011; Wicki *et al.*, 2015). For hydrophilic drugs, in particular, drug loading in the NPs is a challenging task and is critical regarding dose determination and practical implication of the final formulation.

1.4 PLGA NPs for Brain Drug Delivery

The concept of using PLGA polymer as controlled drug release was introduced back in the 1980s (Sanders *et al.*, 1984; Fong *et al.*, 1986; Schakenraad *et al.*, 1988). Since then numerous investigations proved its biological safely and drug release efficacy. Hence, PLGA NPs have been employed by many research groups to deliver biomolecules to various organs including the brain (Amass *et al.*, 1998; Feng, 2006; Win & Feng, 2006). In this section, we will first briefly discuss typical formulation approaches for PLGA NPs preparation, and then, different approaches that have been developed to enhance brain drug delivery using PLGA NPs will be discussed.

1.4.1 Preparation Techniques for PLGA NPs

Many research groups have formulated PLGA NPs by several techniques including emulsion solvent evaporation, membrane emulsification, nanoprecipitation, salting-out, microfluidic technology and flow focusing methods. They are discussed here:

In the oil-in-water (O/W) emulsion solvent evaporation method, PLGA and drug solution in the organic phase is emulsified in an aqueous phase containing stabiliser; and the organic solvent is removed by evaporation leading to the formation of PLGA NPs via emulsion droplet solidification. A high-energy device (such as probe sonicator or high-speed homogenizer) capable of producing high shear stress is generally employed for the emulsification procedure (Bhardwaj *et al.*, 2009; Özcan *et al.*, 2013). Commonly used stabilisers are polyvinyl alcohol (PVA), polysorbate, poloxamer, PEG, SDS and vitamin E-TPGS. The size, surface charge, drug entrapment efficiency (EE), drug release, pharmacokinetics and cellular interaction of NPs varies depending on the type and concentration of the stabiliser used. The stabiliser should be selected keeping the final usage of the NPs in mind (Mu & Feng, 2002; Win & Feng, 2005; Kulkarni & Feng, 2013). The organic solvent may either be evaporated by continuous stirring at room temperature (RT) and ambient pressure or if the formulation allows, can be accelerated under vacuum or elevated temperature. Dichloromethane (DCM) or ethyl acetate (EtAc) have been used as the organic solvent for this technique. Hydrophobic drugs have been reported to be encapsulated into PLGA NPs using this NPs preparation method (Mainardes & Evangelista, 2005; Kuo & Yu, 2011).

Water-in-oil-in-water (W/O/W) emulsion solvent evaporation method is a modification of O/W solvent evaporation method and is employed to encapsulate hydrophilic drugs into PLGA NPs. The inner aqueous phase containing hydrophilic drug is emulsified in the water-immiscible organic solvent containing PLGA. The resulting primary water-in-oil (W/O) emulsion is emulsified again in a stabiliser-containing external aqueous phase, forming the final double emulsion (W/O/W). The organic solvent is removed either slowly by continuous stirring at RT and ambient pressure, or quickly under vacuum and/or elevated temperature to produce PLGA NPs. The escaping tendency of the hydrophilic drug into the external aqueous phase during the NPs preparation may result in poor drug EE (Zhang *et al.*, 2011). To address this issue, some researchers modified the aqueous solvent systems by incorporating electrolytes and/or adjusting the pH (Astete & Sabliov, 2006; Misra *et al.*, 2009).

In the O/W salting-out, nanoprecipitation or solvent displacement technique, a water-miscible organic solvent (*e.g.*, acetone) containing PLGA and drug is emulsified into an electrolyte-saturated aqueous solution by a low-energy mixing device such as the magnetic stirrer. Either solvent system can be added to the other, either in a drop-wise fashion or all at once. When the organic solvent and a large amount of water mix together, the organic solvent diffuses out of the emulsion droplets into the aqueous phase (salting-out), thereby lost its ability to dissolve PLGA and PLGA NPs are produced holding the drug in their matrix. Several electrolytes have been used in this process, such as sodium chloride, magnesium chloride, magnesium acetate, and calcium chloride. Acetone is the most preferred organic solvent for this technique. Other solvents such as DMSO, acetonitrile (ACN), dimethylformamide (DMF), PEG and tetrahydrofuran (THF) are also employed (Govender *et al.*, 1999; Karve *et al.*, 2011; Sah & Sah, 2015). This NPs preparation technique does not use halogenated solvents or high-energy devices for the emulsification. However, the method has limitation in encapsulating hydrophilic drugs due to the usage of a high amount of water during the NPs preparation (Konan *et al.*, 2002). Chen *et al.* (2008b) showed that the incorporation of an ionic additives (dextran sulphate) with the hydrophilic peptide drug (dalargin) can offer significant increment in the drug loading in PLGA NPs.

The nanoprecipitation method has been modified to prepare PLGA NPs by spontaneous emulsion solvent diffusion (SESD) technique. A solvent mixture composed of two miscible solvents (such as DCM-acetone) is used as the organic phase where one of the solvents is water-immiscible (DCM) while the other one is water-miscible (acetone). The interfacial tension between water-immiscible solvent and water is lowered by the water-miscible solvent during the emulsification procedure. Additionally, the rapid diffusion of water-miscible solvent from emulsion droplets to water results in nanosized droplets. Solid PLGA NPs is produced when the water-immiscible solvent is evaporated from the nanoemulsion (Niwa *et al.*, 1993; Murakami *et al.*, 1999; Ibrahim *et al.*, 2013).

There are some other NPs preparation techniques employed by different research groups throughout the globe in order to increase the loading efficiency of hydrophilic drugs into PLGA NPs. For example, membrane emulsification technique, hydrophobic ion pairing technique, reverse micelle-hybridized O/W emulsion technique and microfluidic technology platforms (Sah & Sah, 2015). Some of the methods even achieved 100% EE and very narrow particle size distribution. However, the reported particle size of the NPs produced by these methods ranged from 200 to 500nm which is not suitable for brain drug delivery. Win and Feng (2005) conducted their cell uptake study in caco-2 cell line and found that ideal particle size for targeting BBB is about 100nm but further increase in particle size could render the DDS less efficient.

1.4.2 PLGA NPs Surface Modification for CNS Drug Delivery

Many approaches have been investigated over the last few decades to tailor PLGA NPs for brain-specific drug delivery. These approaches can be classified into three major categories - (1) enhancement of systemic circulation time, (2) enhancement of NP-BBB interactions and (3) enhancement of NPs-brain cell interactions.

Enhanced/optimum systemic circulation time for the NPs has been achieved by adjusting the particle size and surface hydrophilicity of the PLGA NPs. *Firstly*, NPs with diameters of 70-200 nm show the best results for *in vivo* applications (Owens & Peppas, 2006). Any NPs smaller or larger than this have been reported to be either excreted from the blood very quickly or are captured by the liver or spleen.

Controlling the size of the PLGA NPs is critical to ensure maximum blood circulation time. The desired particle size can be achieved by adjusting the method of NPs synthesis, polymer type and concentration, stabiliser type and concentration, drug-polymer ratio and type of organic solvent (Astete & Sabliov, 2006; Khare *et al.*, 2014). After achieving the target particle size, the next challenge is to prolong the systemic circulation time of the PLGA NPs. These NPs are hydrophobic in nature and hence undergo extensive removal by the RES.

Hence, *Secondly*, the PLGA NPs have been coated with hydrophilic molecules to overcome this problem. Many long chain hydrophilic molecules are helpful to resolve this issue, such as PEG, human serum albumin (HSA), poloxamers, polysorbate, TPGS and polysaccharides (Dinarvand *et al.*, 2011; Cai *et al.*, 2016). PEG is the most commonly used molecule, which is either physically mixed with the PLGA during the NPs manufacturing process or chemically conjugated with PLGA prior to NPs preparation (Chen *et al.*, 2008b; Tehrani *et al.*). Some researchers also reported that inclusion of a second hydrophilic molecule along with the PEG may be advantageous. Chen *et al.* (2013) clearly demonstrated that when PLGA NPs are PEGylated, they can escape/delay RES removal, offering significantly higher systemic circulation time. Therefore, these NPs were reported to have superior antinociceptive properties compared to the non-PEGylated NPs. HSA, a human protein, also has received special interest hydrophilicity-imparting agent for the PLGA NPs and demonstrated success as an NPs surface grafting molecule (Kratz, 2008; Wohlfart *et al.*, 2011).

Enhanced NPs-BBB interaction can be achieved by modifying the NPs surface with CPP, receptor-mediated endocytosis ligands or adsorptive-mediated endocytosis ligands (Kreuter, 2013, 2014). There are several reports of the incorporation of CPP on NPs surface for improved biomolecule delivery across the BBB for treatment of CNS diseases. Most commonly used CPP are TAT peptide, angiopep, penetratin, rabies virus glycoprotein, prion peptide and SynB. The TAT peptide is an arginine-rich CPP first isolated from human immunodeficiency virus (HIV)-1 protein, that can now be custom synthesised following the amino acid template (Margus *et al.*, 2012; Raucher & Ryu, 2015).

On the other hand, the receptor-mediated endocytosis ligands target highly expressed BBB receptors including low-density lipoprotein receptor, leptin receptor, transferrin receptor, insulin receptor, insulin-like growth factor receptor, diphtheria toxin receptor, nicotinic acetylcholine receptor and scavenger receptor class B type (Cai *et al.*, 2016; Gao, 2016b). When appropriate ligands are attached, these receptors can be exploited to transport drug loaded PLGA NPs across the BBB. For example, Tosi *et al.* (2010) successfully used the opioid peptide like structure named as g7 (NH_2-Gly-L-Phe-D-Thr-Gly-L-Phe-L-Leu-L-Ser(O-β-D-Glucose)-COOH) to efficiently deliver an antinociceptive drug (loperamide) into the CNS. In the later years, applicability of this glycopeptide has been further investigated by different research groups and g7 demonstrated superior BBB targeting efficiency (Tosi *et al.*, 2014; Salvalaio *et al.*, 2016). Active transport systems present in the BBB (such as amino acid, hexose, and monocarboxylate transporters) can also be used for brain-targeted delivery. Lastly, positively charged PLGA NPs can assist its interaction with the negatively charged BBB surface. As a consequence, the NPs have been reported to experience higher absorption rate in the brain through adsorption-mediated endocytosis (Hervé *et al.*, 2008). Thus, molecules that can render a positive surface charge to the NPs (like chitosan, polyethylene imine, poly(b-amino ester), poly-L-lysine and polymethacrylates) have been used to improve PLGA NPs interaction with BBB resulting in better transcytosis (Bilensoy, 2010; Jaruszewski *et al.*, 2012).

Finally, after crossing the BBB, the residence period of the PLGA NPs in the brain is extended by enhancing NPs-brain cell interactions. This is achieved by modifying NPs surface with the ligand capable of interacting with brain cells. It should be noted that the surface ligand type depends on the specific disease. For example, brain tumour cells often overexpress several receptors, including transferrin receptor, low-density lipoprotein receptor, interleukin-13 receptor, epidermal growth factor receptor, matrix metalloproteinase-2, integrins and nucleolin (Maletinska *et al.*, 2000; Hovanessian *et al.*, 2010; Zhan & Lu, 2012). Hence, scientists have focused on these receptors for brain tumour-targeted DDS. For example, Cui *et al.* (2013) coated their PLGA NPs with transferrin that demonstrated prolonged brain residence time and consequently, strong anti-glioma effect on the brain tumour. *In vitro* cellular study also reported the high absorption of the transferrin-coated PLGA NPs over the unmodified NPs (Chang *et al.*, 2009).

Similarly, PLGA NPs were functionalized with Pep-1, another ligand which targets interleukin-13 receptor (Wang *et al.*, 2014a). The DDS exhibited a significantly enhanced cellular association (2.2 fold) in rat glioma cells and able to suppress tumour effectively compared to the non-targeting NPs. Researchers used SA as neurone targeting ligand on PLGA NPs which demonstrated their significantly better brain distribution than the unmodified NPs for up to 24 hrs (Tosi *et al.*, 2010).

The selection of brain targeting ligands on the nanoparticulate DDS mainly depends on the target physiological BBB transport mechanism. Because of their demonstrated potentiality, here we will only focus on the CPP for targeting the BBB and SA for targeting at brain receptors:

AMT is believed to be a well-characterised physiological BBB transport mechanism to exploit for brain drug delivery and has been reported to show promising results (Section 1.2 above). The polyethylene glycol-distearoyl phosphatidylethanolamine (DSPE-PEG) coupled with the CPP peptide (Gly-Leu-Pro-Arg-Arg-Arg-Arg-Arg-Arg-Arg-Arg-Arg) has been used as a ligand on liposome surface that significantly improved BBB trafficking of the drug using AMT (Yang *et al.*, 2013). However, a much shorter TAT peptide (RKKRRQRRR) can be used for brain targeting with an added advantage of smaller NPs (Vogel *et al.*, 1993).

SA is another ligand that we found interesting due to its capability of increasing the brain resident time of the NPs. This physiological acid is an essential nutrient for brain development and has been reported to successfully interact with brain receptors when grafted on the particulate DDS (Bondioli *et al.*, 2010; Tosi *et al.*, 2010). The SA family includes 43 derivatives of the neuraminic acid, but, in this thesis we will be using the N-acetylneuraminic acid (Neu5Ac) (Figure 1.3) and for simplicity, will call it SA.

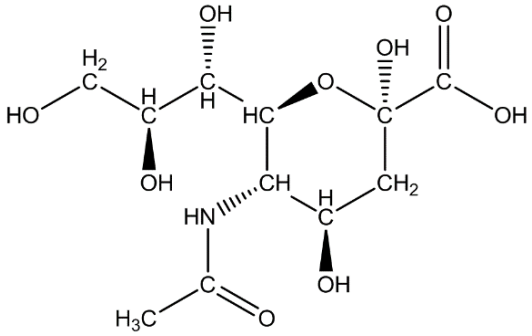

Figure 1.3. The molecular structure of sialic acid.

1.5 Dual Ligand Targeting for Brain Drug Delivery

Targeting the brain using more than one ligand for drug delivery is relatively new concept, however, being a very promising approach, research has been carried out by many groups within short period (Kibria *et al.*, 2011; Miao *et al.*, 2014; Doolittle *et al.*, 2015; Gao, 2016b; Gao, 2016a; Gao *et al.*, 2016). Main focus of these investigations, however, was to target cancer cells using dual ligand decorated liposomes and polymer micelles. Several studies have been conducted to deliver antinociceptive drug into the brain using CNS-targeted dual ligand NPs (Tosi *et al.*, 2010; Tosi *et al.*, 2014). The authors found that the dual ligand nanoparticulate system was able to deliver and retain the model drug inside the brain parenchyma over 24 hours compared to the single ligand system that was capable of retaining the drug only for 5 hours. As yet, no research has been conducted for efficient CNS delivery of RHT employing SA and TAT peptide as targeting ligands for nanoparticulate DDS. Thus, in this thesis, we will focus on RHT delivery in the brain using NPs surface modified with dual ligands (SA and TAT peptide) as a better targeting approach.

1.6 Characterisation of NPs

To produce reliable, good quality and reproducible biological data, it is mandatory to properly characterise nanoparticulate DDS *in vitro*. This section briefly describes the commonly used techniques used for quality control of NPs except *in vivo* characterisation which is beyond the scope of this thesis, hence excluded.

1.6.1 Dynamic Light Scattering (DLS)

Once administered intravenously, the size of the NPs plays the most important role on determining the fate of the NPs. DLS, also known as photon correlation spectroscopy (PCS) or Quasi-Elastic Light Scattering (QLS) is the most commonly used method for determining the size of NPs (Brar & Verma, 2011). The measurement method is based on the light scattering property of colloidal suspensions. When a monochromatic light beam (usually, laser) passes through a colloidal suspension, scattering light perpendicular to the laser beam can be observed. Now, micro- or submicron particles suspended in a liquid undergo Brownian motion which is inversely proportional to the size of the particle (Xu, 2015; Bhattacharjee, 2016). The intensity and fluctuation of the scattered light as a function of time can be used to monitor the velocity of Brownian motion (*i.e.*, translational diffusion coefficient) and ultimately for determining the size of the colloids. Theoretically, the size of particles of low specific gravity in the range of 3nm-3µm is measurable, however, the DLS is commonly used in the particle size range of < 1 µm (Brar & Verma, 2011).

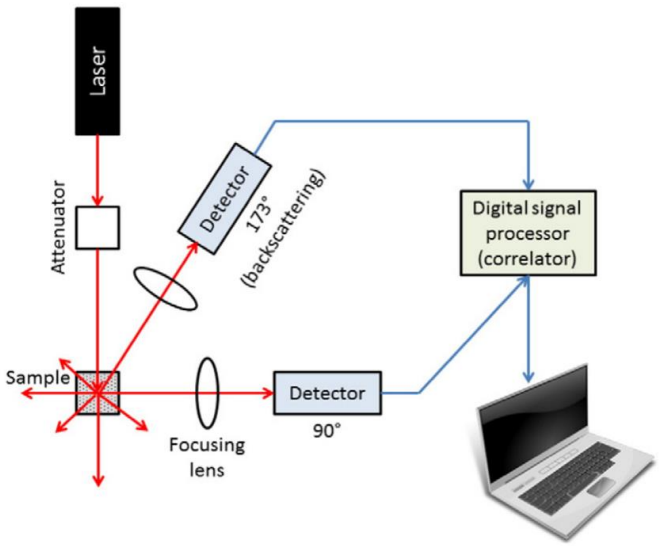

Figure 1.4. Schematic diagram of DLS instrumentation (Bhattacharjee, 2016).

1.6.2 Zeta Potential (ζ-potential)

The surface charge of NPs in suspension is called the Nernst potential or Stern potential (ψ_δ) and is often controlled by the surface groups present on the NPs. The zeta potential (ζ) rather Nernst potential is often used to describe the surface charge of particles as the former can be easily determined. In most cases, zeta potential is proportional to the Nernst potential. The zeta potential is the electrical potential of a charged particle at its shearing plane. A charged particle in suspension will attract its counterion in solution and any surface-active molecules to its surface resulting in the formation of the electric double layer (Attwood, 2013). The shear plane is the interface between the fixed and diffused portion of the electric-double layer (Sinko, 2011). The magnitude of zeta potential, which is determined by the electrophoretic mobility of the NPs under the influence of applied electric field, is the most important factor that determines the stability of a colloidal dispersion. Therefore, measurement of zeta potential will not only provide an indication of the charge nature of the NPs (*i.e.*, positive or negative) but also the likelihood of the stability of the colloids.

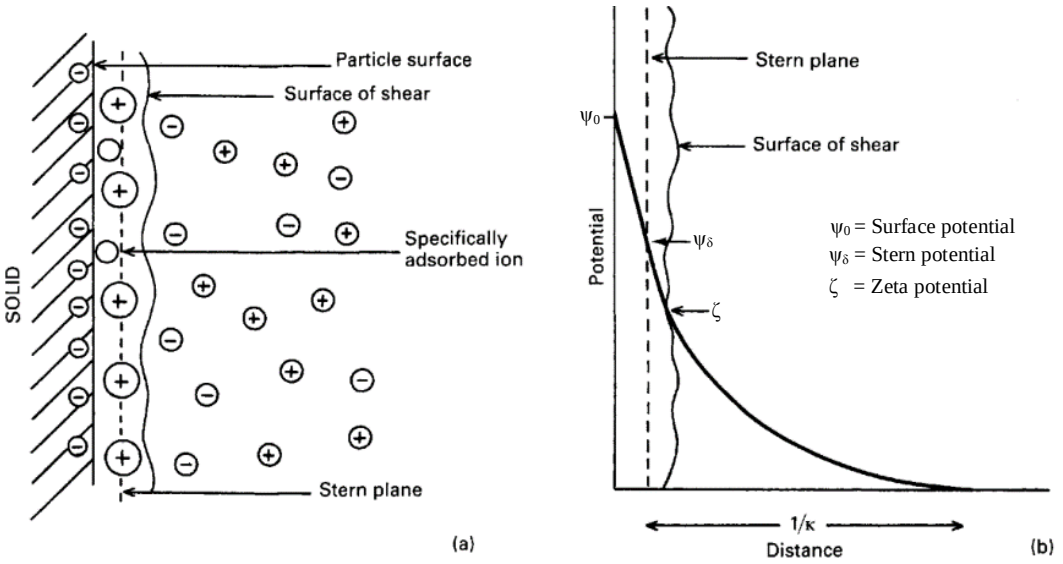

Figure 1.5. Illustration of (a) the electric double layer on a negatively charged particle in a dispersion medium, and (b) changes in potential with distance from the particle surface showing surface, stern and zeta potentials (Attwood, 2013).

1.6.3 Entrapment Efficiency (EE)

The EE of an NPs formulation is calculated from the ratio of nanoparticulate-bound drug to the total amount of drug used at the start of the formulation procedure (Guo *et al.*, 2017). Determination of EE is generally carried out indirectly by determining the amount of free, *i.e.*, unbound drug. For this purpose, the supernatant containing free drug is separated from the NP suspension by centrifugation, filtration or other suitable methods, and the supernatant is analysed for unbound drug determined. The amount of bound drug is calculated from the total amount of the drug minus the free drug. The formula for calculating the EE is :

$$EE\ (\%) = \frac{Initial\ amount\ of\ drug\ (mg) - amount\ of\ free\ drug\ (mg)}{Initial\ amount\ of\ drug\ (mg)} \times 100$$

Knowing the EE of NPs formulation is important to evaluate the formulation technique that offers minimum drug wastage and has a higher potential for scaling up. However, it is worth mentioning that the EE can be very much influenced by the added amount of the drug at the start and the drug: polymer ratio. Thus, a high EE may be obtained due to the fact that initial amount of the drug used was small and it may not reflect an optimum formulation because the final NPs can still be associated with a low drug loading (*i.e.*, low payload of NPs).

1.6.4 Drug Loading (DL)

DL is often reported as the percentage of the nanoparticulate-associated drug compared to the total weight of the NPs (Guo *et al.*, 2017). It is also determined indirectly following the same method mentioned above. However, it should be noted that the 'drug loading' indicates the actual amount of drug entrapped inside and/or associated with the NPs reflecting drug dose carried by them. The 'entrapment efficiency', on the other hand, indicates how efficient the nanoparticles production procedure. The formula for calculating the DL is:

$$DL\ (\%) = \frac{Amount\ of\ drug\ in\ NP\ (mg)}{Amount\ of\ Polymer\ and\ additives\ (mg) + \ Amount\ of\ drug\ in\ NP\ (mg)} \times 100$$

Knowing the NPs DL is of great importance and the information is critical to check the reproducibility of the manufacturing process and to calculate the drug dose that a nanoparticle formulation carry. In this work, DL was used as one of the criteria for assessing the optimum formulation.

1.6.5 Drug Release Study

A drug release assay is a powerful tool in dosage form development that gives an indication of the active pharmaceutical ingredient release from NPs polymeric matrix. It is an essential evaluation technique during the initial development stage of any dosage form despite the route of administration. The *in vitro* drug release study involves exposure of the dosage forms to a set of conditions that will induce drug release and subsequently, quantification of the amount of drug release. During the study, an *in vitro* setup is selected to simulate *in vivo* parameters, and more importantly, all batches under investigation are tested under the same state. This important experiment not only provides information about the total amount/percentage drug release from a dosage form but also evaluates the potentiality to employ it as controlled/sustained release formulation (Gupta & Mohanty, 2017).

Several *in vitro* drug release study methods have been reported including dialysis bag, reverse dialysis bag, microdialysis and different USP dissolution apparatus techniques. Among them, the dialysis bag technique is employed extensively to determine drug release from nanoparticulate systems due to simplicity and satisfactory reproducibility of the method (de Andrade *et al.*, 2015). This method offers convenience in drug sampling and replacement of release medium. A sealed dialysis bag containing the final NPs formulation is placed inside the release medium; usually, phosphate buffered saline (PBS) pH 7.4, under a sink condition, at a temperate of 37°C under agitation to simulate physiological conditions (Seidlitz *et al.*, 2011). Samples collected periodically are analysed to produce drug release pattern from the NPs. Different types of dialysis devices are commercially available to make the job easier (such as Float-A-Lyzer®), however, release studies with simple dialysis bag method have been reported to produce consistent data with small inter-study variation (Badran *et al.*, 2017; Hu *et al.*, 2017).

1.6.6 Morphological Study of NPs by Microscopic Method

Light microscopic methods are not suitable for visual characterisation of nanoparticulate dosage forms because of their limited resolution due to the wavelength of visible light (400-800 nm). Electron beams have a much higher resolution since they have a much smaller wavelength than visible light. The resolution in the transmission electron microscope (TEM) is less than 1 nm and less than 5 nm in the field emission scanning electron microscope (FESEM) (Pawley, 1997; Havrdova *et al.*, 2014).

FESEM provides a very large depth of field as well as superb digital image processing capability. These features made FESEM a major visual characterisation tool in the field of nanoscience. The principle of FESEM is well known - when the metal-coated NPs are irradiated with a high energy electron beam, interactions between the specimen electrons and incident electrons produce various signals including secondary electrons and back-scattered electrons (Klang *et al.*, 2013). These different types of signals are then detected, converted into electric signals and finally amplified to feed into the display unit. High-resolution topographical information of the sample surface can be obtained by scanning a beam of the electron across the sample and forming the complete image point-by-point (Chang *et al.*, 2014; Postek *et al.*, 2016).

As discussed, FESEM works with scattered electrons, however, TEM is based on transmitted electrons. Instead of focusing to a fine point and scanning line by line, TEM uses a broad static beam to provide the details about nanoparticle's internal composition. Samples in TEM must be cut thinner to enable it to provide valuable information such as morphology, crystallisation, atomic arrangement in material or even magnetic domains. Although TEM has much higher resolution than SEM, it only provides two-dimensional pictures, unlike SEM that is able to provide three-dimensional images (Yaghmur & Glatter, 2009).

1.6.7 Cell Study

Once the NPs formulations are optimised and deemed to have sufficient drug loading, final sets of *in vitro* experiments are carried out with cell lines before performing relatively expensive *in vivo* (animal) studies. There are hundreds of cell lines available for different types of research and, the ultimate therapeutic goals of the NPs should be considered for selecting appropriate experimental cell lines. For example, NPs designed for delivering drugs into the brain need a cell line capable of producing TJ mimicking physiological characteristics of BBB (Weksler *et al.*, 2013).

Cytotoxicity or cell viability assay is designed to determine the mortality rate of the cells under experiments upon exposure to the drug and its carrier, such as NPs. The result is reported as percent viability compared to the untreated/control group of cells. Researchers whose goal is to target specific cells and destroy them (like, cancer research), a high cell morbidity is expected. However, where the goal is to cure the cells or to deliver a particular agent to the cells (such as diabetes research), a cell viability near 100% is desirable. MTT assay is a well-established method for determining cell viability and is used extensively in all types of research (Zhang *et al.*, 2014; Ciappellano *et al.*, 2016).

The investigation of NPs uptake in the right cell line can provide useful information about the efficiency of the DDS at the early stage of the development process. During this cell uptake study, the NPs are cultured with the cells for a predetermined time. The amount of drug (with NP) absorbed by the cells can be determined by (usually) rupturing the cells and analysing the drug content with high-performance liquid chromatography (HPLC). The result is often reported as the nanogram (ng) of drug uptake or as microgram (µg) of NPs uptake per milligram (mg) of cell protein (Kooijmans *et al.*, 2012). The advantage of such chemical analysis method is that any active form of the drug will be quantified and any potential metabolites caused by the cellular enzymes will also be picked up. However, due to the usage of relatively high number of replicates in the cell culture works, incorporating HPLC analysis can sometimes be uneconomical and very time consuming for the cell uptake study. To address this issue, multimode plate reader can be an excellent choice for drug content analysis that can perform the quantification in a matter of seconds. However, they do not offer the capability of separating the drug from possible degraded products.

Many cell uptake studies have been conducted with fluorescence molecule loaded NPs for both qualitative (*e.g.*, immunofluorescence assay) and quantitative (*e.g.*, flow cytometry assay) determination of NPs uptake (Liu *et al.*, 2016a). Although quantitative assays provide accurate numerical data, most of the times qualitative findings is desirable to support the analytical results. Moreover, a picture can tell a thousand words, and thus, visual confirmation/representation has always been welcomed by the scientific community. The modern, sophisticated microscopic techniques are capable of capturing cellular images demonstrating the NPs internalisation and/or their perinuclear accumulation making them as valuable as the quantitative data.

Finally, the hypothesis of BBB penetration capability of the NPs can be validated by the cell transport study. Here the drug loaded NPs are challenged to pass through an intact cell monolayer that demonstrates high transendothelial electrical resistance (TEER) value, TJ characteristics of the BBB (Liu *et al.*, 2016b; Papadia *et al.*, 2016). Over a set time, the amount of drug passed through the cell layer is determined, and the pattern is analysed and compared to that of free drug to confirm or reject the hypothesis (Poller *et al.*, 2008).

1.6.8 Animal Study

Successful cellular studies are usually followed by animal studies to establish the *in vivo* effectiveness of the nanoparticulate DDS. These experiments help to understand the biodistribution pattern and toxicity profile of the DDS and provide vital information for the future human trials (Navarro *et al.*, 2016; Joseph & Saha, 2017). Initial animal studies involve small animals such as mouse, rat, guinea pig and may sometimes use higher mammals such as rabbit, monkey, dog. Depending on the type and intended application of the nanoparticulate DDS, healthy and/or disease-induced animals are employed (Martinez, 2011; Patravale *et al.*, 2012). A number of *in vivo* studies to investigate the efficiency of brain targeting capability of the nanoparticulate DDS have been conducted (Tosi *et al.*, 2010; Salvalaio *et al.*, 2016).

1.7 Alzheimer's Disease and Rivastigmine Hydrogen Tartrate

Being a vital organ of the human body, brain diseases hampering its functionality have a detrimental impact on human life including social negligence, financial burden and moreover higher mortality rate. The gradual increase in number of ND patients throughout the world is alarming. Presently, the most common brain disease among aged people is AD. Being a natural process, ageing cannot be stopped and neither the disease development. The increase in trend of AD development, thus, forces researchers to put a lot of attention on AD research, especially to find out novel treatments regimen to fight the disease. Generally, dementia cannot be cured with a single method or treatment. The mode of treatment is mainly determined by type and stage of dementia (Swerdlow, 2007; Zlokovic, 2008; Khachaturian *et al.*, 2011; Williams & Spencer, 2012; Anand *et al.*, 2013; Antoniou *et al.*, 2013). Three approaches are suggested: (1) treating the underlying causes of the disease (if found) – this may include tumour, drug, excess fluid, head injury, hormone deficiencies or imbalanced nutrition; (2) treating the symptoms to improve or control them – this may include music, aroma, art activities or occupational therapy. Environmental modification and socialisation and involvement in everyday activities like taking a walk or simple cooking may be also beneficial for the person with dementia by preserving their dignity and self-esteem; and (3) treating the disease with some available medications to slow down the progress of the disease. For example, rivastigmine hydrogen tartrate (RHT) is a widely-used drug for the treatment of early stage of AD (Winblad *et al.*, 2016).

RHT (Figure 1.6) is chemically known as (S)-N-Ethyl-3-[(1-dimethylamino)ethyl]-N-methylphenylcarbamate hydrogen tartrate (CAS No. 129101-54-8, MW 400.42). The aqueous solubility of RHT and rivastigmine free base is 8% w/v and 0.2% w/v, respectively. The drug has the pka of 8.85 and logP of 2.3. According to the supplier it is chemically stabile until exposed to alkaline substance or oxidising agents at high concentrations and/or for prolonged period.

FDA approved the drug for the treatment of AD on April 21, 2000 (Cherian & Gohil, 2015). RHT is a "cholinesterase inhibitor" that inhibits both acetyl cholinesterase (AChE) and butyryl cholinesterase (BuChE) responsible for the degradation of acetylcholine (ACh) into non-functional metabolite. Among the many chemical changes that the brain encounters during AD, depletion of ACh is one of the earliest and biggest changes. RHT increases central cholinergic function by enhancing ACh level in mild to moderate AD patients that ultimately slows down AD progression. Also, acetyl cholinesterase interacts with beta-amyloid to promote deposition of amyloid plaques in the brain of AD patient, which can also be slowed down with the RHT therapy (Grossberg, 2003; Greig *et al.*, 2005; Pohanka, 2014; Zemek *et al.*, 2014; Kumar *et al.*, 2015).

RHT has been reported to improve or maintain patients' performance *viz.* cognitive function, global function, behaviour and day-to-day activities (Birks *et al.*, 2015; Farlow *et al.*, 2015). This drug is commercially available as capsules, oral solution and patches. However, the current therapeutic regimen of RHT demands frequent dosing causing its cholinergic side effects. Like other CNS drugs, treatment efficacy is not threatened by drug potency but its ability to cross BBB, because RHT demonstrates restricted entry into the brain due to its hydrophilic nature (Wilson *et al.*, 2008).

First RHT-loaded NPs was developed by Wilson and his team back in 2008 (Wilson *et al.*, 2008). Further research was carried out by other research groups for improving the formulation strategy to make the delivery system safer and more efficient. Table 1.1 summarises some published papers that reported the use of polymeric NPs for RHT brain delivery.

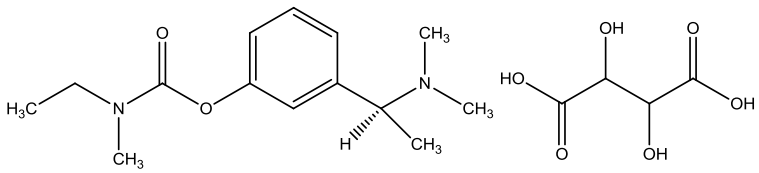

Figure 1.6. The molecular structure of Rivastigmine hydrogen tartrate.

Table 1.1. Summary of published brain targeted RHT-loaded polymeric NPs compositions with their *in vivo* investigation outcome.

Core polymer	**Coating material**	***In vivo* study result**	**Reference**
Poly(n-butyl cyanoacrylate)	Polysorbate-80	2.12-fold brain uptake	(Wilson *et al.*, 2008)
Chitosan	N/A	2.49-fold brain uptake	(Fazil *et al.*, 2012)
PLGA Poly(n-butyl cyanoacrylate)	N/A Polysorbate-80	Faster regain of memory loss (Morris Water Maze Test)	(Joshi *et al.*, 2010)
Chitosan	Tween-80	Increased neuroprotectant effect	(Nagpal *et al.*, 2013)
L-lactide-depsipeptide	N/A	Faster regain of memory loss in amnesic rat	(Pagar *et al.*, 2014)

There is scope to use many other targeting techniques to deliver RHT into the brain through BBB, such as using AMT. For example, polyethylene glycol-distearoyl phosphatidylethanolamine (DSPE-PEG) coupled with the CPP peptide (Gly-Leu-Pro-Arg-Arg-Arg-Arg-Arg-Arg-Arg-Arg-Arg) has been used as a ligand on RHT liposome surface that significantly improved BBB trafficking of the drug (Yang *et al.*, 2013). However, a much shorter TAT peptide (RKKRRQRRR) can be used for brain targeting with an added advantage of smaller NPs (Vogel *et al.*, 1993). The incorporation of this short TAT peptide on RHT loaded NPs is not investigated by anyone as of 2017, and the effectiveness of the DDS is yet to be evaluated. On the other hand, NPs made of SA functionalized PLGA has been reported to successfully interact with brain receptors (Bondioli *et al.*, 2010; Tosi *et al.*, 2010). No study has been carried out so far which incorporates both TAT peptide and SA on the same NPs system, which seems to be an interesting attempt at this stage. Currently available data suggests that TAT and SA, when grafted separately on the NPs, improved BBB permeability and brain residence time are achieved, respectively. Therefore, we hypothesise that incorporation of both TAT and SA ligand on the same NPs DDS will enhance its BBB permeability as well as the brain residence time.

1.8 Overall Objectives

The principle objective of this research was to develop, optimise and characterise a novel polymeric nanoparticulate delivery system with two surface ligands having BBB and neurone targeting capability for RHT delivery in the brain. The research objectives were sub-divided into following points:

- Design, optimisation and evaluation of the conjugation between hydrophilic TAT peptide and lipophilic DSPE-PEG chain to prepare the BBB targeting ligand (DSPE-PEG-TAT).
- Design, optimisation and evaluation of the conjugation between hydrophilic SA and lipophilic octadecylamine (ODA) chain to prepare the neurone targeting ligand, sialic acid-octadecylamine (SA-ODA) conjugate.
- Formulation development and optimisation of an RHT-loaded PEGylated PLGA based nanoparticulate DDS with dual ligands for targeting both BBB and neurone.
- Development, optimisation and validation of a simple, fast, economical and stability indicating HPLC method for RHT analysis.
- *In vitro* evaluation of the developed dual ligand NPs system by extensive cellular characterisation, including:
    - *cytotoxicity study* to assess the effect of NPs system on cell viability of hCMEC/D3 and Caco-2 cells.
    - *cellular uptake study* for quantitative and qualitative evaluation of enhancement of NPs uptake in the cell, and
    - *cellular transport study* to assess the transport enhancement potential of the NPs system across the *in vitro* BBB model.

1.9 Thesis Overview

We presented this study in four main chapters, each consisting of an introduction, method, results and discussion section. The main research chapters are followed by a general summary chapter that also includes limitation of the study and future research scope. The research work is presented chapter-wise as follows:

- **Ligand synthesis and analysis:** This chapter explains chemical conjugation/synthesis of the targeting ligands and their qualitative and quantitative evaluation via different analytical techniques including HPLC, Fourier transform infrared (FTIR) spectroscopy, Nuclear magnetic resonance (NMR) spectroscopy and Matrix assisted laser desorption ionization-time of flight- mass spectrometry (MALDI-TOF-MS). The synthesised ligands were used in later studies described in further chapters.
- **Development and validation of analytical methods:** The chapter addresses the development, optimisation and validation of a stability indicating HPLC analytical method for quantification of RHT.
- **Formulation development and characterisation:** This chapter describes the formulation development and optimisation methods for PLGA NPs preparation. The optimised, ligand attached PLGA NPs formulations were characterised for their physicochemical properties including particle morphology, size, charge, stability and drug release profile. Cellular studies were performed using the NPs systems which were described in further chapters.
- **Cellular characterisation of NPs:** This chapter focuses on the *in vitro* evaluation of the PLGA NPs formulations in two cell lines. The chapter comprises detailed evaluation of cytotoxicity, cellular uptake and cellular transport of the dual ligand NPs system.

Chapter 2 Ligand Synthesis and Analysis

2.1 Introduction/Overview

Targeted drug delivery can be achieved by grafting appropriate molecules on the NPs surface, called ligands. As the human circulatory system is aqueous-based, it is important that hydrophilic ligands are selected, and these ligands have been attached to or associated with NPs surface. Generally ligands can be incorporated into the NPs via various approaches including – (a) direct coupling with the hydrophilic end of core hydrophobic polymers; (b) chemically attaching the ligand to a hydrophobic molecule then mixing it with the core hydrophobic polymer while preparing the NP; and (c) coating the pre-formed NPs with targeting ligands by physical adsorption (She *et al.*, 2014; Son *et al.*, 2014; El-Hammadi *et al.*, 2017; Park *et al.*, 2017). Irrespective of the ligand incorporation method, it is important that the NPs formulation procedure ensures the targeting ligand(s) remain exposed in the aqueous phase.

The ultimate aim of this project was to formulate drug loaded, dual ligand containing NPs to selectively target – (a) the BBB to facilitate NPs entry into the brain, and b) the brain receptors to retain the NPs for a longer residence time inside the brain. Among the many targeting ligands discussed in Chapter 1, the TAT peptide was selected to target the BBB by enhancing NPs uptake into the brain via adsorptive-mediated endocytosis. On the other hand, as the brain is rich in SA receptors, the SA ligand was chosen due to its superior brain targeting capability and ease of incorporation in the NPs matrix (Tosi *et al.*, 2010; Yang *et al.*, 2013; Yin *et al.*, 2015; Nair *et al.*, 2016; Patel *et al.*, 2016). These ligand molecules are hydrophilic; therefore, incorporation into our lipophilic PLGA NPs core required conjugation with lipophilic molecules. We hypothesised that the lipophilic part of the resulting conjugate would be embedded into the PLGA matrix by physical bonding, while the hydrophilic parts (targeting ligands) would be exposed to the outer aqueous phase to act as targeting ligands.

In this thesis, initially, we attempted to conjugate the SA ligand with the PLGA core polymer via attaching amine group to the polymer carboxyl group (functionalization). However, the preliminary synthesis steps did not show satisfactory yield, and thus the scheme was discontinued. As an alternative, we attached SA ligand with another hydrophobic molecule (ODA) while TAT peptide to DSPE-PEG for dual targeting.

2.2 Materials

Acid terminated PLGA (Cat. # B6013-1, intrinsic viscosity 0.19 dL/g, number-average MW ~3.5 kDa), with a 50/50 ratio (PLA/PGA) was supplied as LACTEL Absorbable Polymers (Durect Corporation, Birmingham, USA). N-boc-1,4-diaminobutane (Boc-DAB, Cat. # 15404), fluorescamine (Cat. # F9015, ≥98%), dicyclohexyl-carbodiimide (DCC, Cat. # D80002, 99%), N-hydroxysuccinimide (NHS, Cat. # 130672, 98%), trifluoroacetic acid (TFA, Cat. # T6508, 99%), triethylamine (TEA, Cat. # 90337, ≥99.5%), SA (Cat. # A2388, ≥98%, MW 309.27), ODA (Cat. # 74750, ≥99%, MW 269.51), anhydrous DMF (Cat. # 227056, ≥99.8%) and mineral oil (Cat. # 330779, light) were purchased from Sigma-Aldrich (Castle Hill, Australia). ACN (A998-4, ≥99.9%), THF (Cat. # T425-4) and DCM (Cat. # D/1856/17) were obtained from Thermo Fisher Scientific (Scoresby, Australia).

Polystyrene standards with MW of 0.37, 3.7, 12.9, 51.2, 754 and 954kDa were supplied by Shodex® (Tokyo, Japan). Millex-HN Syringe-tip filters were from Merck Millipore (Bayswater, Australia). TAT peptide (RKKRRQRRR, Cat. # 378879, 98.4%, MW 1340) was purchased from GL Biochem Ltd. (Shanghai, China). 1,2-dioleoyl-sn-glycero-3-phosphoetha-nolamine-n-[poly(ethyleneglycol)]-hydroxysuccinamide (DSPE-PEG-NHS, Cat. # PG2-DSNS-2K, MW ~2000) was obtained from Nanocs Inc. (Boston, USA) supplied by Life technologies (Mulgrave, Australia). Deuterated chloroform ($CDCl_3$, Cat. # DLM-7TB-100S, 99.8% containing 0.05% v/v tetramethylsilane (TMS)) and deuterated dimethyl sulphoxide (DMSO-D6, Cat. # DLM-10TB-10, 99.9% containing 0.05% v/v TMS) were procured from Cambridge Isotope Laboratories, Inc. (Andover, USA). All other analytical reagents were of highest possible purities. All reagents were used as obtained without further purification.

2.3 Methods

2.3.1 Synthesis of PLGA-DAB

The synthesis of PLGA-diaminobutane (PLGA-DAB) conjugate was attempted via PLGA activation to functionalize the polymer so that the BBB targeting ligand (SA) can be attached to it in the subsequent steps. The PLGA-DAB synthesis was carried out in three major steps (Figure 2.1). Carbodiimide cross-linking method using DCC/NHS as the coupling reagents was employed to mediate the formation of an amide linkage between the terminal carboxylic group of PLGA and the free amine group of boc-DAB. The boc group was then removed to yield the final product, PLGA-DAB (Montalbetti & Falque, 2005; Khare *et al.*, 2014).

Step 1: acid terminated PLGA was activated, purified and degree of activation was analysed. Briefly, PLGA (175mg, 0.05 mmole), DCC (52mg, 0.25 mmole) and NHS (29mg, 0.25 mmole) were dissolved in 10mL ACN and stirred for 12 hrs at RT under nitrogen (N_2) environment. Completion of this reaction was determined by hydroxamate method via quantifying the conjugated NHS with PLGA (Section 2.3.1.1). The reaction mixture was filtered through a 0.45 µm syringe-tip PTFE filter (Merck Millipore, Bayswater, Australia) to remove insoluble by-product dicyclohexylurea (DCU). The activated PLGA was isolated by precipitation into 100mL cold methanol under vigorous stirring and collected by centrifugation at 2000g for 20 min. The precipitate was washed with methanol 3-4 times to remove unreacted DCC and NHS and then dried under reduced pressure at 30°C for 10 min. The purified product (PLGA-NHS) was used immediately for the next reaction steps.

Step 2: boc-DAB (15.5 µL, 0.08 mmole), was added dropwise to the solution containing activated PLGA (140mg, 0.04 mmole) and TEA (225 µL, 1.6 mmole) in 10mL ACN and kept on a stirrer for 24 hrs at RT under nitrogen environment. TEA acted as a catalyst to yield permanently bonded amide conjugate (Greenwald *et al.*, 2003). The reaction mixture was precipitated in diethyl ether under vigorous stirring and subsequently centrifuged at 2000g for 20 min to collect PLGA-boc-DAB conjugate. The resulting pellet was washed 2-3 times with cold diethyl ether to remove unreacted boc-DAB and TEA. The product was dried under vacuum at 30°C for 60 min. The percentage of boc-DAB conjugated to PLGA was determined by ^{1}H NMR spectroscopy.

To remove the boc group from PLGA-boc-DAB conjugate, 100mg of the solid was dissolved in 5mL of DCM, 500 molar equivalents of TFA (*i.e.* 1mL) was added to the solution and stirred in an ice bath for 2 hrs under nitrogen environment. DCM (boiling point 39.6°C) and TFA (boiling point 72.4°C) were removed under vacuum at 40°C in the rotary evaporator (Büchi Rotavapor R-200, Flawil, Switzerland). The solid mass was redissolved in DCM, and the solvent was again evaporated using similar settings. This procedure was repeated 8 to 9 times to completely remove the free TFA, which was evident by cessation of TFA fume production (bubbling) during the evaporation process. The resulting PLGA-DAB-TFA salt was treated with TEA for 2 hrs at RT at a salt:TEA molar ratio of 1:10 to produce PLGA-DAB. The mixture was diluted and placed in a standard semipermeable regenerated cellulose (RC) dialysis tube with a molecular weight cut-off (MWCO) of 1 kDa (Cat. # 132103, Spectra/por®-Spectrum Labs. Inc., Rancho Dominguez, USA) and dialysed for 12 hrs against Milli-Q water using a dynamic flow of 1mL/min to remove TEA. Finally, the content of the dialysis bag was frozen at −40°C and lyophilized for 48 hrs in a Dynavac FD3 freeze dryer (John Morris, Perth, Australia) to acquire a white solid product.

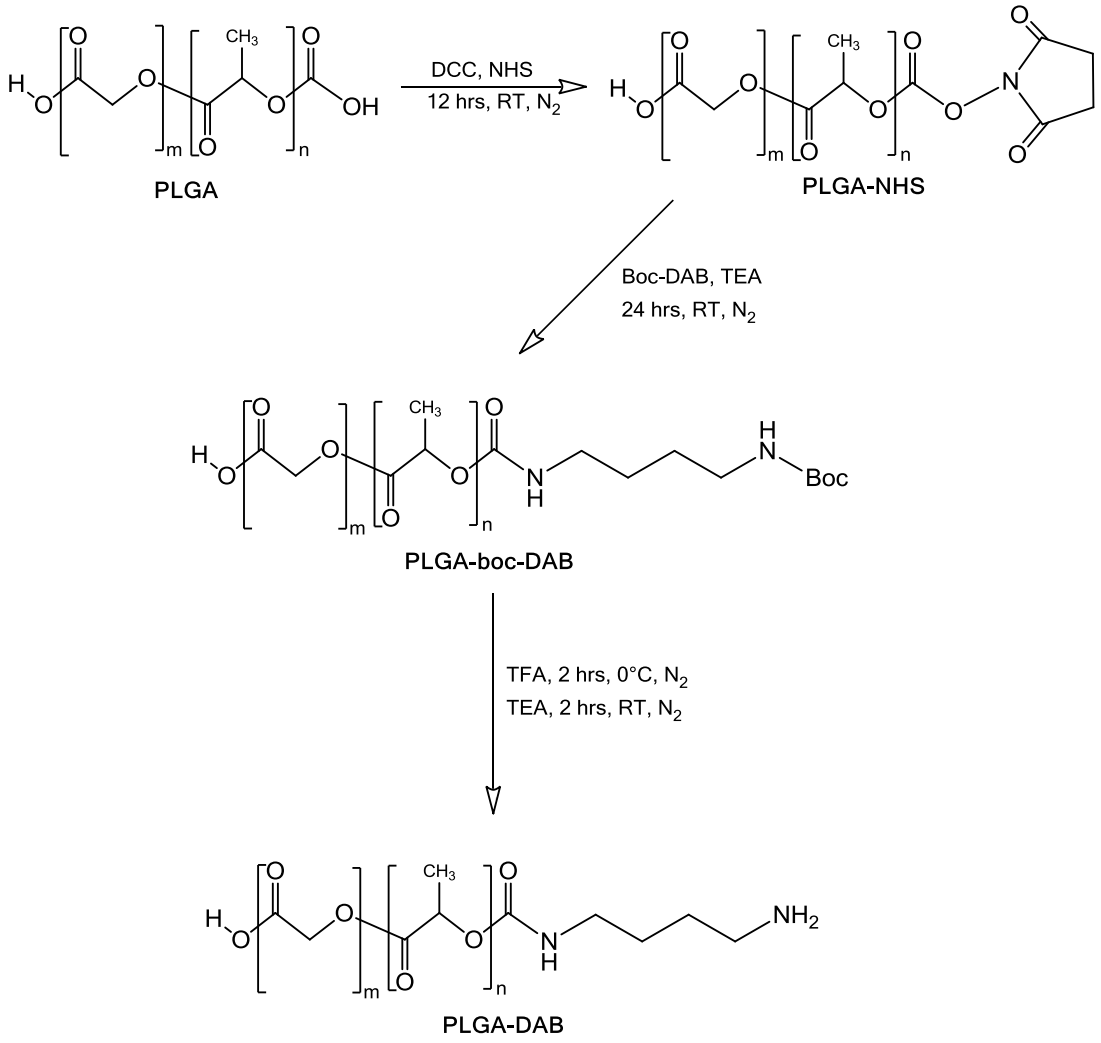

Figure 2.1. Scheme for conjugation of PLGA and DAB using DCC/NHS based coupling.

2.3.1.1 Determination of PLGA Activation Degree

Hydroxamate method was used to determine the degree of PLGA activation, as previously reported (Iwata *et al.*, 1998; Khare *et al.*, 2014). Briefly, 0.2mL of 2N sodium hydroxide (NaOH) was added to 1mL of PLGA-NHS solution (in between 1 and 10mM) to produce free NHS by breaking down the PLGA-NHS conjugate. The reaction mixture was placed in a water bath at 40°C. After 10 min, it was acidified by adding 1.5mL of 0.85N Hydrochloric acid (HCl) and centrifuged to remove precipitated polymer. 0.5mL developing solution (5% ferric chloride in 0.1N HCl) was mixed with 2mL of the supernatant to produce a brown colour. The intensity of the developed colour represented the degree of PLGA activation. To prepare a standard curve, five known concentrations of NHS (1mM to 10mM, 1mL each) were used in place of the sample and processed/analysed by the same procedures. A UV-vis spectrophotometer (Shimadzu UV mini-1240 series, Shimadzu Corporation, Japan) was used to measure absorbance at 500 nm wavelength. The unreacted NHS in PLGA-NHS solution was quantified directly without addition of NaOH by the same method.

2.3.1.2 NMR Analysis

^{1}H NMR spectra were recorded for both the starting materials (boc-DAB and PLGA) and PLGA-boc-DAB conjugate by NMR spectrometer (Bruker Ultrashield Plus Biospin GmbH Nuclear Magnetic Resonance Spectrometer, Avance III 400 MHz, NaNoBay, Bremen, Germany) using DMSO-D6 as the solvent and TMS as the internal standard.

2.3.1.3 Chromatographic Analysis

The starting material (Boc-DAB) and the final product (PLGA-DAB) were analysed by gel permeation chromatography (GPC), which is capable of separating and quantifying a molecule of interest from the polymer mixture. To accurately quantify PLGA-DAB, we coupled fluorescamine to PLGA-DAB and conducted analysis using GPC with a fluorescent detector (FLD) and refractive index detector (RID). Briefly, samples were derivatized with fluorescamine according to the method employed by Tan and Patsiga (1977) with minor modification. 1mL of boc-DAB or PLGA-DAB solution prepared in ACN (0.1 to 1.0µM) was mixed with 0.5mL TEA (70nM) and vortexed for 2 min to obtain a homogeneous basic solution. 1.5mL of 2mM fluorescamine solution was then added to the mixture and further vortexed for 23 min for the derivatization reaction to being completed. Both the derivatized solutions were visually clear.

Upon derivatization, samples were filtered through a 0.45 µm nylon syringe-tip filter after discarding the first 2mL of the filtrate to ensure that only soluble materials were being injected into the GPC column. The filtration step removed any potential particulate by-product or entangled polymer that might be present in the reaction mixture. Although we have checked that the filter did not adsorb any derivatized boc-DAB, we could not perform the same test for PLGA-DAB due to the unavailability of the standard. An Agilent 1200 system (Agilent Technologies Australia, Mulgrave) consisted of a degasser (G1379B), binary pump (G1312A), autosampler (G1329A) with a thermo-control unit (G1330B), thermostat controlled column compartment (G1316A), FLD (G1321A) and RID (G1362A) was used for the analysis. Acquired data were processed by Agilent ChemStation®, B.04.03 SP1 software. The GPC column used was a Jordi Gel DVB, 100-50000 Da MW range, 5µm particle size, 1000 Ångström (Å) pore size, 250mm X 4.6mm ID, with a Jordi 5µm mixed bed GPC guard column, 50mm X 4.6mm ID (Mansfield, USA). The mobile phase was 100% THF at a flow rate 0.5mL/min. Duplicate injections of 50µL with needle wash by the mobile phase was used to analyse all samples. The analysis was performed maintaining the column and RID temperature at 30°C at a flow rate of 0.5mL/min and FLD excitation/emission wavelengths of 390 and 473nm, respectively.

The same method was employed to analyse the crude reaction mixture. The reaction mixture in ACN was first derivatized, and then the clear solution was filtered and injected into GPC column for analysis. Calibration curves were obtained using 0.1, 0.2, 0.4, 0.6, 0.8 and 1.0µM boc-DAB standard solutions in ACN maintaining the basic pH with 70nM TEA. PLGA-DAB samples were prepared in ACN and analysed in the same fashion as boc-DAB.

2.3.2 Synthesis of Sialic acid-Octadecylamine Conjugate

The synthesis of SA-ODA conjugate was carried out by a scheme adopted from a recently published method (She *et al.*, 2014) using DCC/NHS as a coupling agent between SA and ODA in a molar ratio of 3:1 (Figure 2.2). Briefly, 5mL anhydrous DMF was taken out of the septum-closed original bottle with the help of a glass syringe and a 26G needle. The solvent was transferred into a 50mL 2-neck round bottom flask (RBF), which was already purged with nitrogen gas to ensure an inert atmosphere for the reactions. SA (50mg, 0.1617 mmole) and DCC (33.8mg, 0.1617 mmole) were added to the RBF containing the 5mL DMF quickly without compromising the inert atmosphere. The reaction mixture was kept under moderate stirring at RT for 15 minutes. NHS (37.2mg, 0.3232 mmole) was added to the reaction mixture and stirred for another 6 hrs at RT under a nitrogen atmosphere. The insoluble DCU (by-product) was filtered by a DMF resistant 0.45µm syringe-tip PTFE filter, and the filtrate was collected into another 50mL 3-neck RBF to conduct the next reaction step.

An additional 2mL DMF was used to rinse the first RBF and passed through the same filter to make sure that entire reaction mixture was properly transferred into the new container. ODA (14.5mg, 0.0538 mmole) was then added to the reaction mixture in the RBF under moderate stirring. Being an air sensitive material, ODA was handled inside the nitrogen inflated glove bag (108D X-17-17 HG) purchased from Glas-Col (IN, USA). Immediately after addition of ODA, the temperature of the reaction was raised gradually to 60°C in an oil bath using a hot plate magnetic stirrer. The temperature was maintained for 12 hrs under nitrogen gas for the reaction to be completed. The diagram of reaction setup is given in Figure 2.3.

After completion of the reaction, the reaction mixture was brought to RT. An excess amount of Milli-Q water at a ratio of 1:5 was used to dilute the reaction mixture and then fully dialysed against deionized water. Dialysis was performed using a standard RC dialysis tube with MWCO of 1 kDa (Cat. # 132103, Spectra/por®-Spectrum Labs. Inc., Rancho Dominguez, USA) under constant stirring in one litre of deionized water exchanged five times a day for two days. The retentate was aliquoted into 20mL glass vials with 5mL in each. The content was frozen and then lyophilized overnight using Coolsafe 55-4 Pro freeze dryer (Scanvac, Lynge, Denmark) equipped with a Vacuubrand pump (Wertheim, Germany) to yield the final dry product. Dried product was stored at −20°C in tightly closed, aluminium foil wrapped, nitrogen-filled containers until used. Final product (SA-ODA) quality was assessed by FTIR and ^{1}H NMR. The theoretical yield was calculated by multiplying the number of moles of the rate limiting compound (ODA) and the MW of the conjugate (SA-ODA). The actual product yield was calculated by the following equation (detailed calculations are given in Appendix II):

$$Yield\ (\%w/w) = \frac{Final\ product\ weight}{Theoretical\ yield\ (weight)} \times 100$$

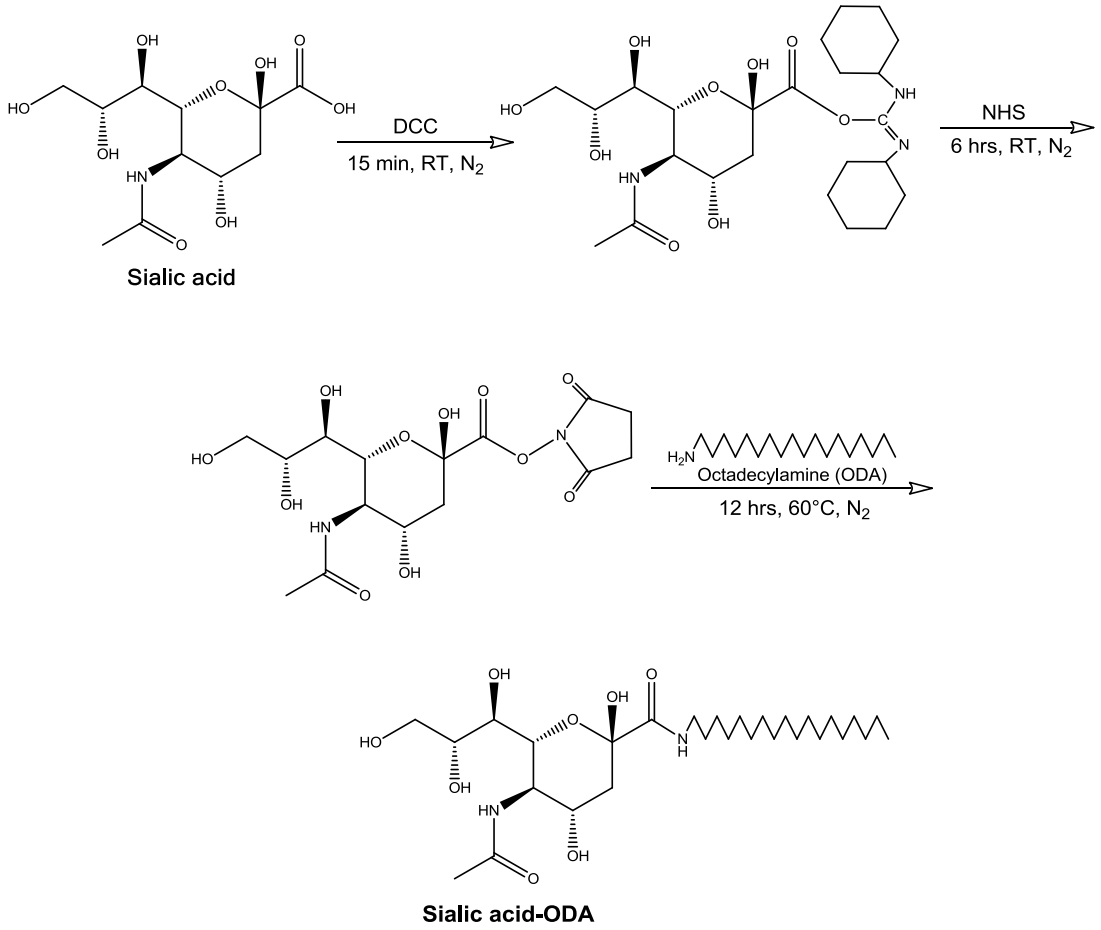

Figure 2.2. Synthesis of SA-ODA through carbodiimide couplings.

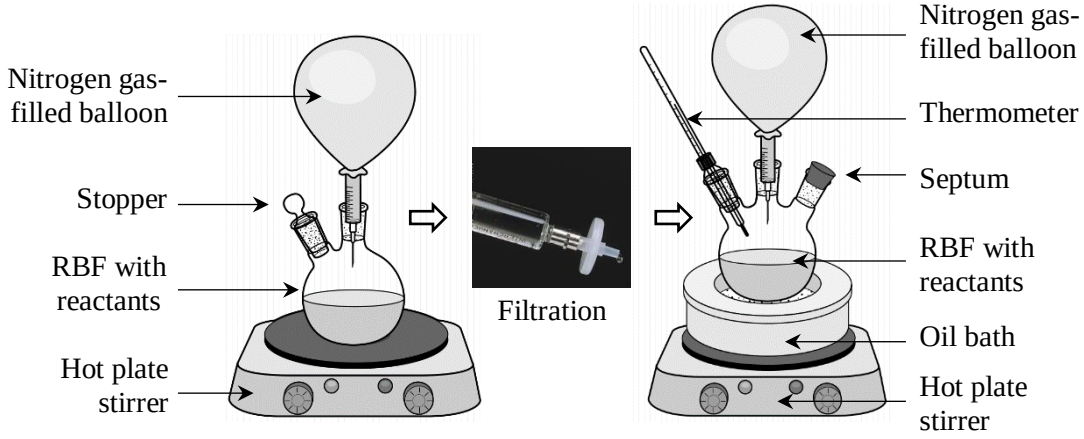

Figure 2.3. Reaction setup diagram for conjugation of SA and ODA.

2.3.2.1 NMR Analysis

The product (SA-ODA) was characterised by ^{1}H-NMR spectroscopy using a Bruker Ultrashield Plus Biospin GmbH Nuclear Magnetic Resonance Spectrometer (Avance III 400 MHz, NaNoBay, Bremen, Germany). A minute amount (6 to 20mg) of the solid sample was dissolved in DMSO-D6 employing 0.2% TMS as a reference. The data acquisition and analysis were carried out by TopSpin® software Version 3.1.

2.3.2.2 FTIR Analysis

FTIR spectra were acquired by FTIR spectrometer (Spectrum Two, Perkin-Elmer Corporation, Wellesley, USA) equipped with an attenuated total reflection (ATR) smart orbit accessory with diamond crystal. The sample holding plate with the crystal was cleaned effectively with acetone-wet Kimtech Kimwipes®. Upon complete drying of the acetone, the background spectrum was recorded and subtracted from the subsequent sample spectra. Approximately 2mg of the dry product (SA-ODA) was added to the sample plate ensuring that the sample entirely covered the diamond crystal. The arm was moved to lock over the crystal, and the metal tip was lowered to press the sample on the crystal. Force gauge reading was maintained between 100 and 120 to create a uniform disk of the sample. The sample was scanned with the number of accumulations at 10 and resolution at 4cm^{-1} to obtain a spectrum. The set scan range was 450 cm^{-1} to 4000cm^{-1}. Spectra were analysed by Perkin-Elmer Spectrum® software Version 10.4.00.

2.3.3 Synthesis of DSPE-PEG-TAT

Synthesis of DSPE-PEG-TAT conjugate was carried out following a published procedure with modification (Yang *et al.*, 2013) using DSPE-PEG-NHS and TAT peptide (Figure 2.4.). Briefly, 55mg TAT peptide (0.041mmole) was dissolved in 10mL anhydrous DMF in a 50mL RBF purged with nitrogen gas. 100mg DSPE-PEG-NHS (0.05mmole) was added to the RBF under stirring. A ratio of 1:1.2, mol/mol (TAT peptide: DSPE-PEG-NHS) was maintained to ensure that the reaction was fast and proceeded to the conjugate direction (Yang *et al.*, 2013; Wang *et al.*, 2016). A minute quantity (~30µL) of TEA was added to the reaction mixture to raise the pH to 8-9 to facilitate the coupling reaction. pH was monitored by testing 10µL of the reaction mixture on pre-wet pH test strips. Inert conditions were maintained by a constant nitrogen gas flow, and the reaction mixture was kept under stirring for 72 hrs at ambient temperature. A control reaction was carried out simultaneously without DSPE-PEG-NHS to demonstrate the stability of the TAT peptide during the reaction span. The diagram of reaction setup is given in Figure 2.5.

To remove unreacted materials and solvent, the RBF content was diluted with Milli-Q water at a ratio of 1:5 and fully dialysed against deionized water using a dialysis bag with MWCO of 1 kDa (Cat. # 132103, Spectra/por®-Spectrum Labs. Inc., Rancho Dominguez, USA) at RT. Lyophilisation of the residual content of the dialysis bag provided a dry white powder. The product was stored under inert conditions at −20°C away from light and moisture until used.

The theoretical yield was calculated by multiplying the number of moles of the rate limiting compound (TAT peptide) and the MW of the conjugate (DSPE-PEG-TAT). The actual product yield was calculated by the following equation (detailed calculations are given in Appendix III):

$$Yield\ (\%w/w)\ = \frac{Final\ product\ weight}{Theoretical\ yield\ (weight)} \times 100$$

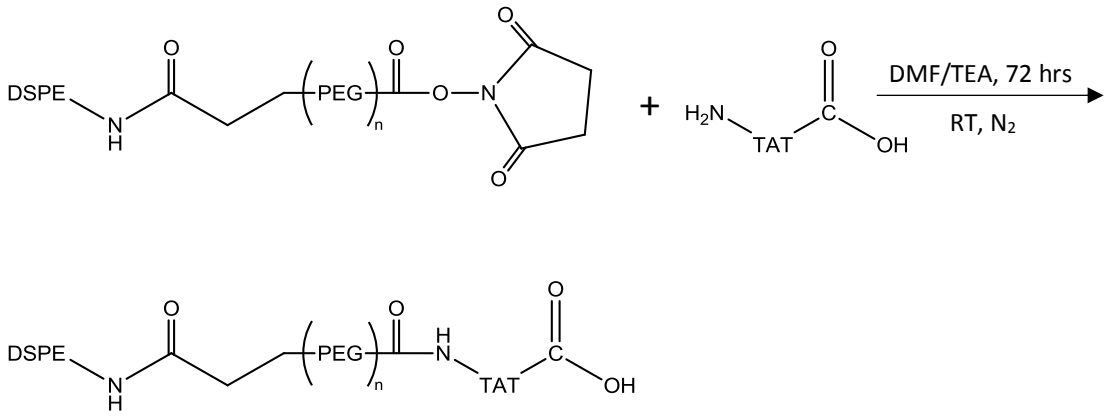

Figure 2.4. Scheme for conjugation of DSPE-PEG-NHS and TAT peptide to produce DSPE-PEG-TAT conjugate.

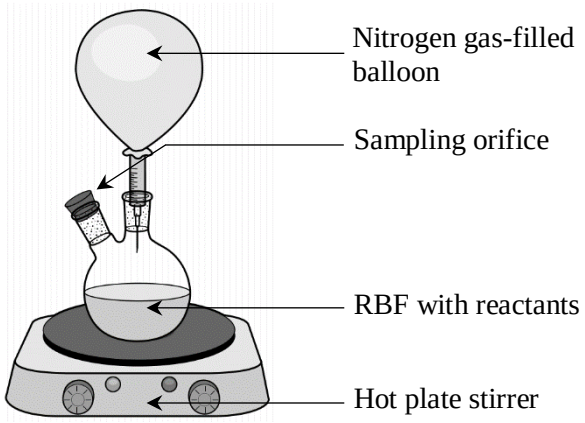

Figure 2.5. Reaction setup diagram for the synthesis of DSPE-PEG-TAT.

2.3.3.1 Reaction optimisation

Formation of product and reduction in starting material (TAT) were regularly monitored every 12 hrs via HPLC analysis to optimise the reaction time. Briefly, a 10µL reaction mixture was withdrawn using a syringe from the reaction vessel without compromising the inert reaction conditions. The samples were diluted 20 times with water containing 0.1% TFA and placed in small volume HPLC inserts. 10µL samples, in duplicate, were injected and analysed by the following HPLC method.

2.3.3.2 Chromatographic analysis

A gradient HPLC method was employed for the analysis of free TAT peptide remaining in the reaction mixture as well as the product, DSPE-PEG-TAT. Agilent 1200 system (Agilent Technologies Australia, Mulgrave) consisted of a degasser (G1379B), binary pump (G1312A), autosampler (G1329A) and variable wavelength detector (VWD, G1314B). Acquired data were processed by Agilent ChemStation®, B.04.03 SP1 software. The HPLC column was a Grace Apollo C_{18}, 5µm particle size, 150mm X 4.6mm (Grace Davidson Discovery Science, Baulkham Hills, Australia). A flow rate of the mobile phase through the gradient run was maintained at 1mL/min while the mobile phase composition was altered. A binary gradient mobile phase consisting of A) 0.1% v/v TFA in water and B) 0.1% v/v TFA in ACN was used. The HPLC gradient is shown in Table 2.1. TAT standards were prepared in DMF and diluted 20 times with water containing 0.1% TFA and used to prepare a calibration curve, which was used to analyse unreacted TAT in each reaction sample. The same HPLC assay method can also detect the peak of DSPE-PEG-TAT. The peak area of both TAT and DSPE-PEG-TAT were monitored to estimate the level of DSPE-PEG-TAT in the reaction mixture at a particular reaction time.

Table 2.1. Gradient flow for HPLC analysis of DSPE-PEG-TAT.

Time (min)	Flow (mL/min)	%A	%B
0	1.0	95	5
5	1.0	95	5
30	1.0	65	35
31	1.0	95	5
36	1.0	95	5

A: 0.1% TFA in water; B: 0.1% TFA in ACN.

2.3.3.3 Mass Analysis

The mass of the reaction product was determined by MALDI-TOF-MS using an AB SCIEX MALDI-TOF/TOF 5800 System (ABSciex, Framingham, USA) in reflector mode with a mass range of 400-8000 m/z and a laser intensity of 3200V. A small amount of the samples was dissolved in 40µL of 2% ACN, 0.1% TFA and spotted 1:1 with α-cyano-4-hydroxycinnamic acid (CHCA) matrix in the same solvent on an MALDI plate for mass analysis.

2.4 Results and Discussion

2.4.1 Synthesis of PLGA-DAB

Zero length cross-linkers, DCC and NHS were used for PLGA-DAB conjugate synthesis. It is a widely employed carboxylic group activation method, and the formed active esters are suitable for coupling with primary amines (Montalbetti & Falque, 2005). The method involves activation of PLGA terminal carboxylic acid by DCC and NHS, and the formed O-acyl derivative of carboxylic acid readily reacts with a nucleophile like the amine group of boc-DAB. These reactions lead to amide bond formation between boc-DAB and PLGA. Since boc-DAB has one end amine group protected and leaves the other end primary amine group free, this reaction using boc-DAB allows the specific amine group reaction and prevent any possibility of forming PLGA-DAB-PLGA or PLGA-DAB-DAB polymers.

Boc-protection was removed by the addition of excess TFA (Liu *et al.*, 2012). Unreacted TFA was removed by addition of DCM to form a positive azeotrope, which could be removed at a temperature much lower than the boiling point of TFA (72.4°C) (Chowdhury *et al.*, 2006). The process of addition of DCM was repeated multiple times for the thorough removal of TFA from the reaction mixture. The evidence of TFA fume production (bubbling) ensured the detection of its removal and cessation of fume production indicated completion of the process.

Later, the PLGA-DAB TFA salt was further treated with TEA to obtain free primary amine end group. Different salt: TEA ratio was tested and 1:10 ratio produced maximum conversion of the terminal TFA bound amine group to free amine group (Figure 2.6).

The activation of the starting molecule containing carboxyl group (-COOH) is a critical step in the carbodiimide reaction that mainly determines the final product yield. In this reaction step, the -COOH of the acid moiety forms a stable succinate ester that, upon addition of an amine compound, forms an amide. In the case of small molecules, this is a quick and straightforward reaction, however, in the case of large polymer molecules, it takes a longer time to be completed. We found that the degree of PLGA activation, as determined by hydroxamate method, was about 94% after 12 hrs of the reaction (Figure 2.7). There was no unreacted NHS present in the final PLGA-NHS product; therefore, we concluded that 12 hrs is the minimum reaction time required for the activation.

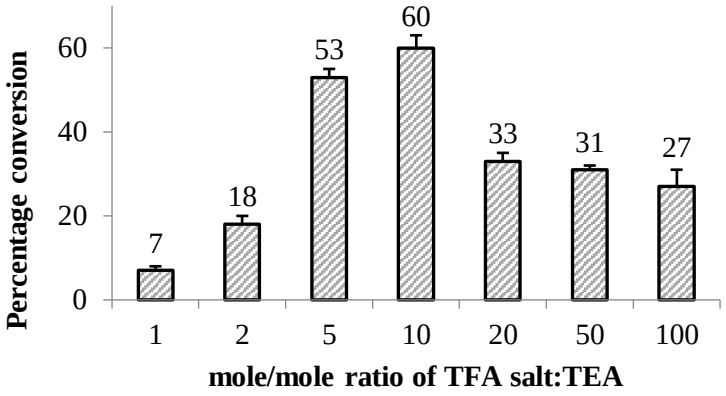

Figure 2.6. Effect of TEA on conversion of the PLGA-Boc-DAB TFA salt to free amine. Results are expressed as mean ± SD (n=3).

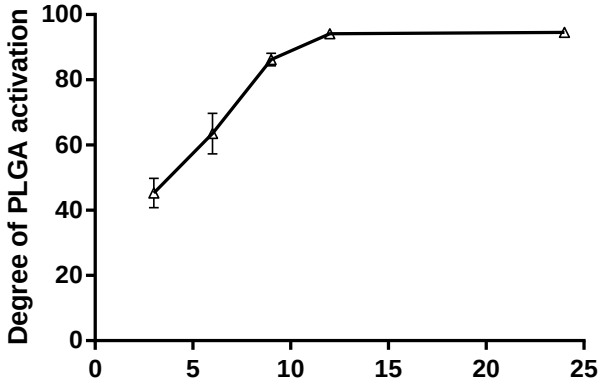

Figure 2.7. Effect of time on conversion of the PLGA to PLGA-NHS (n=3).

The conjugation of DAB to PLGA was confirmed by ^{1}H NMR spectroscopy. Figure 2.8, Figure 2.9 and Figure 2.10 show the NMR spectra of the starting materials, PLGA and boc-DAB as well as the PLGA-boc-DAB for the characterisation of the intermediate polymeric conjugate. PLGA-boc-DAB spectrum clearly shows the native PLGA peaks at 1.47, 4.91 and 5.20 ppm with the correct ratio (3:2:1), and also the largest peak from native boc-DAB ($3\times CH_3$) is present at 1.37 ppm.

The peak at 5.20 ppm is integrated as 26.0 to closely match the number of protons at position 'c' in PLGA as per the product information supplied by the manufacturer. Thus, the extent of conjugation was found to be 0.53 mol of boc-DAB/mol of PLGA based on the NMR analysis.

Figure 2.9 shows that the $-CH_2$ group nearest to the boc-protected amine group and the other $-CH_2$ group nearest to the free amine group in the boc-DAB produce peaks at 2.88 and 2.51ppm, respectively. However, in the conjugate NMR spectra (Figure 2.10), these peaks moved to 2.67 and 2.33ppm position indicating that a large molecule was chemically attached with boc-DAB.

Based on the NMR spectra we postulated that the PLGA polymer molecule was formed amide linkage with the boc-DAB molecule to form the polymer-small molecule conjugate, PLGA-boc-DAB. This conjugate formation was further confirmed by chromatographic analysis.

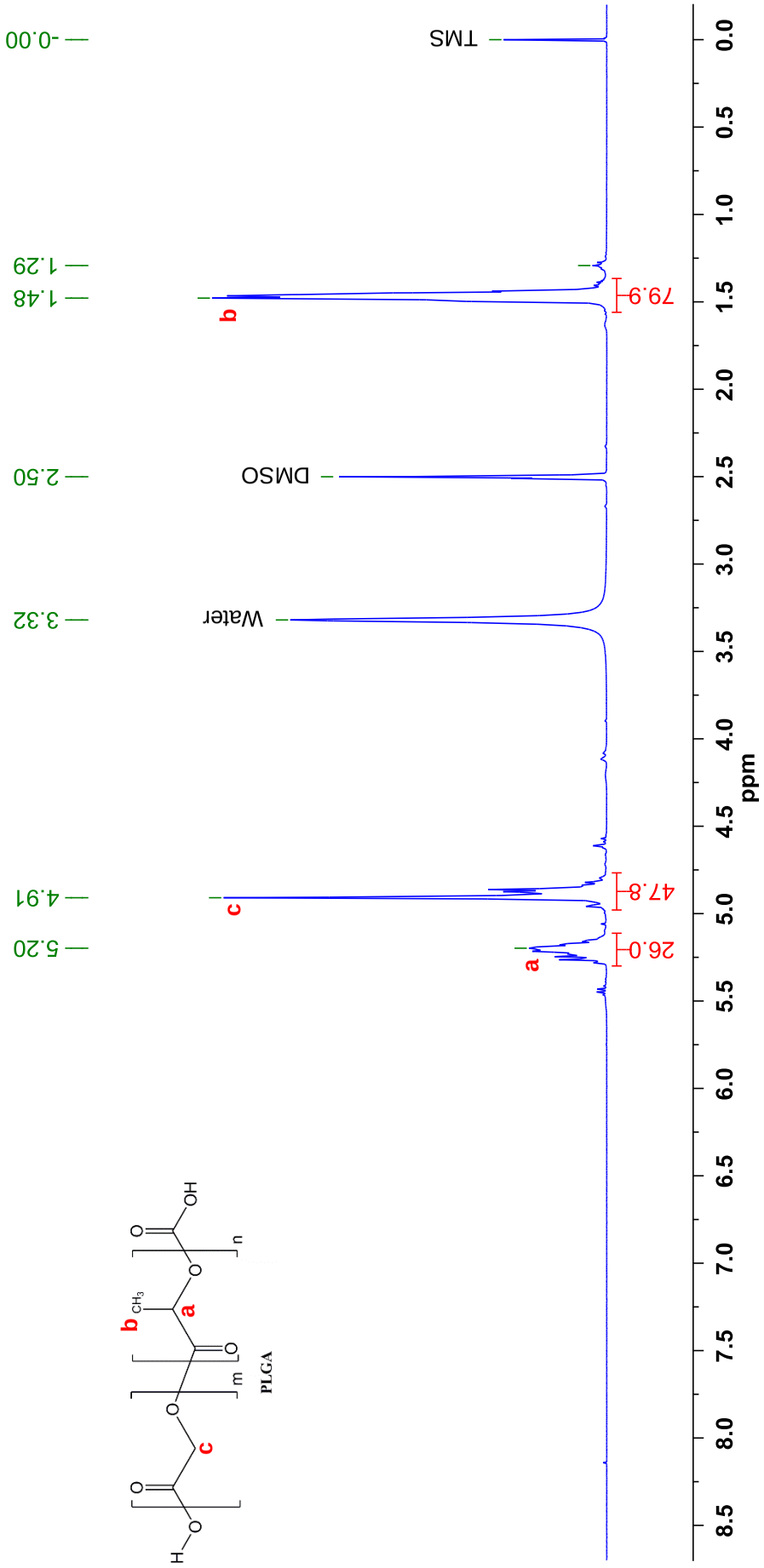

Figure 2.8. ^{1}H NMR (400 MHz) spectra of PLGA in DMSO-D6.

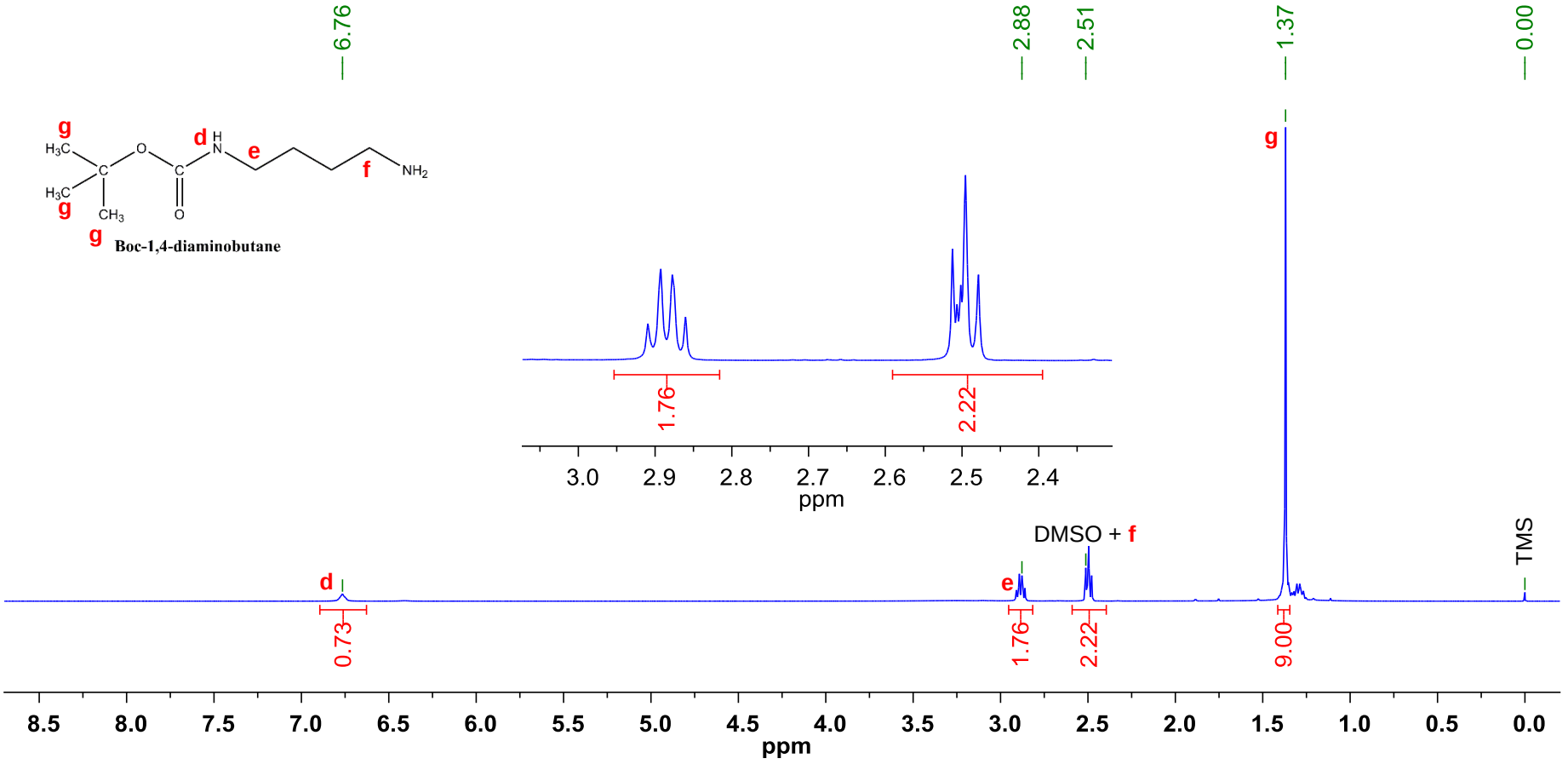

Figure 2.9. ^{1}H NMR (400 MHz) spectra of boc-DAB in DMSO-D6.

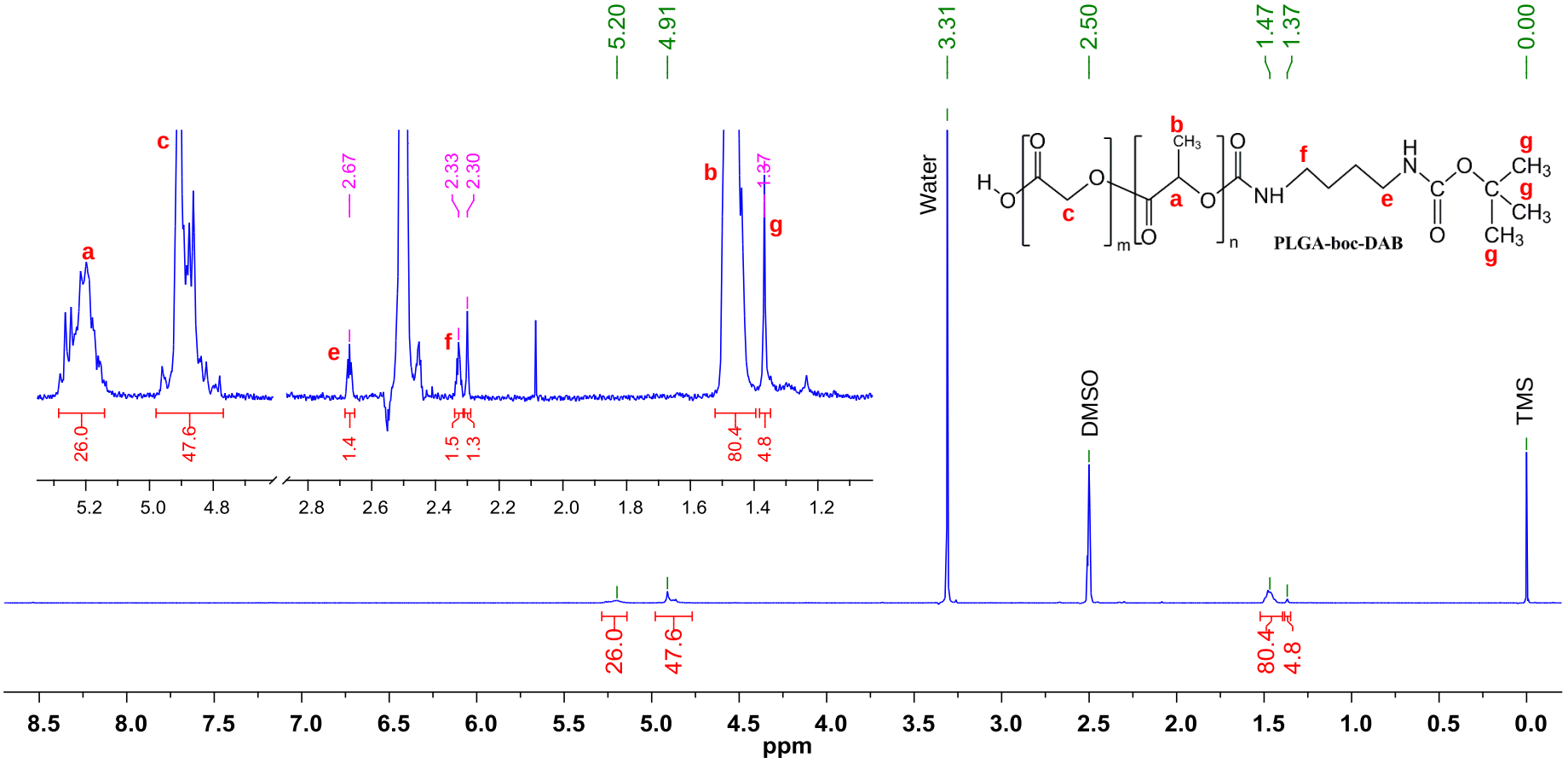

Figure 2.10. ^{1}H NMR (400 MHz) spectra of PLGA-boc-DAB conjugate in DMSO-D6.

Boc-DAB and PLGA-DAB fluorescence derivatives were analysed by refractive index and fluorescence detection using GPC coupled with both RID and FLD. The boc-DAB derivatives eluted without any interfering peaks at a retention time of 6.1 min. Retention times were 6.1 and 4.8 min (FLD) for fluorescamine derivatives of boc-DAB and PLGA-DAB, respectively. The RID confirmed that the peak at 4.8 min was a large polymer molecule. This chromatographic analysis confirmed that the conjugate of PLGA-DAB was formed in the reaction (Figure 2.11). All samples were analysed by GPC using injection volumes of 50 µL.

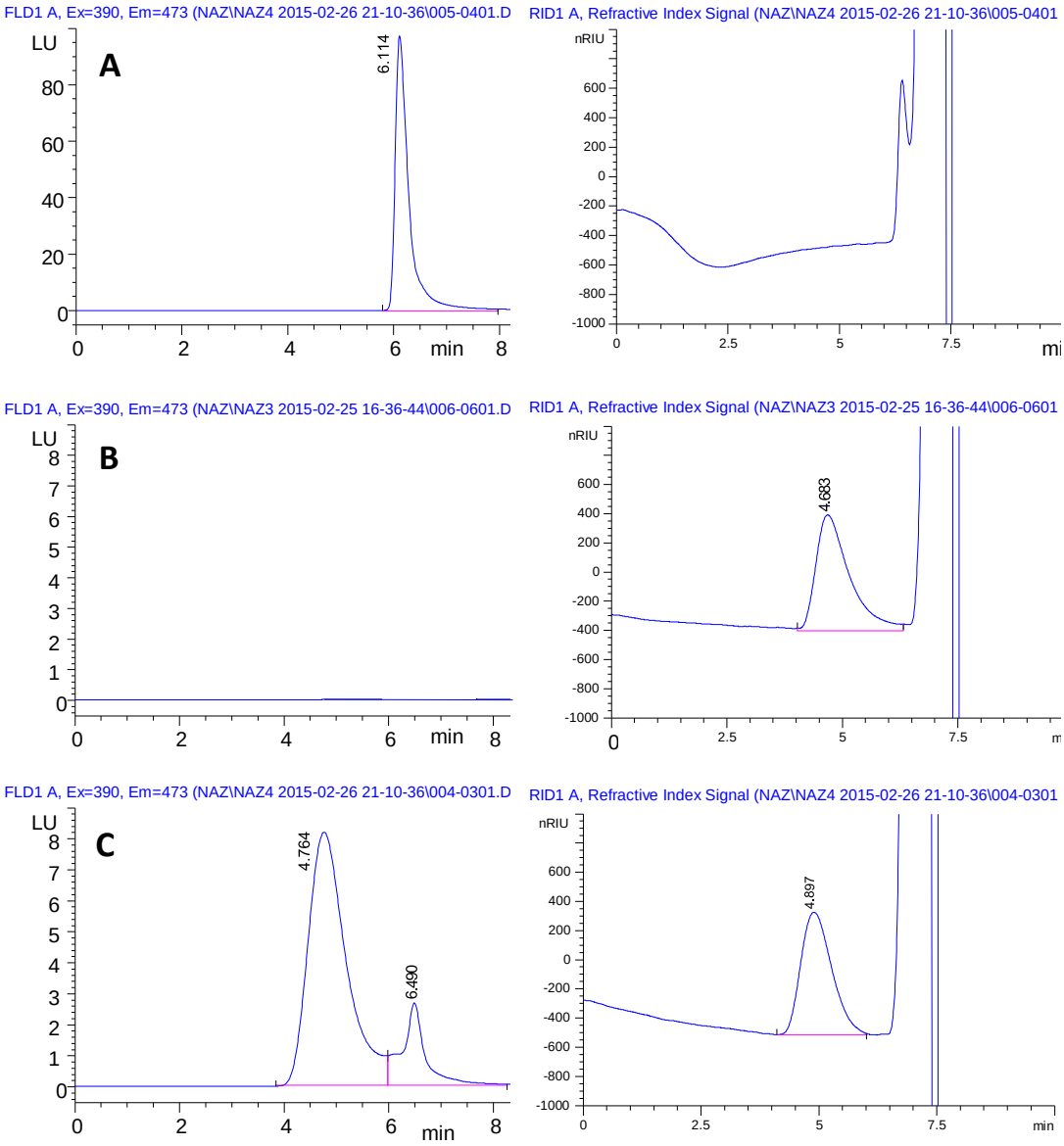

Figure 2.11. HPLC chromatogram of derivatized boc-DAB (A), PLGA (B) and derivatized PLGA-DAB (C). The left three spectra are fluorescence signals whereas the three spectra on the right are refractive index signals.

The combination of NMR and chromatographic analysis allows the accurate quantification and qualitative confirmation of the synthesised conjugate (Queiroz *et al.*, 2012). It is a challenge to conjugate PLGA to small molecules with bi-functional groups in a controlled manner and to accurately quantify polymer conjugates, especially from the crude reaction mixture (Patil *et al.*, 2009; Cook *et al.*, 2016). The use of boc-DAB solved this problem out and permitted the selective conjugation. This study also demonstrated GPC method that can simultaneously be used for monitoring the impact of reaction condition on the formation of PLGA-DAB as well as the analysis of final polymer-small molecule conjugates. Due to the lack of PLGA-DAB standard, the GPC method was used only for qualitative analysis and for monitoring the progress of the reaction. Quantitation of PLGA-DAB was achieved by the NMR spectra, which showed that in the final PLGA-DAB conjugate about 53.3% PLGA was attached with the DAB (mole/mole), which was satisfactory and much higher than earlier reports (Bhatnagar *et al.*, 2016). However, the total amount of the final product was small compared to the initial weight of the reactants. The reaction intermediate products were purified after every step to ensure that the impurities/unreacted reactants from the previous step do not interfere with the next step of the reaction. As there were multiple steps involved and each step resulted in a loss of a certain percentage of the materials, the final product yield (w/w) was only 3.4%. It may be possible to rectify the loss of materials by optimising each purification step. However, due to resource and time constraints, and the availability of a more efficient alternative, this reaction conjugate was not used for NPs preparation, and the scheme was discontinued.

2.4.2 Synthesis of Sialic Acid-Octadecylamine Conjugate

The SA-ODA conjugate was prepared by carbodiimide zero-length linking reagents – NHS and DCC following a method described in the literature (She *et al.*, 2014) with minor modifications. The purification of the crude product was achieved by dialysis against deionized water. The final product appeared as odourless off-white solid. The product structure was confirmed by both FTIR and ^{1}H-NMR spectroscopy and was found to be in agreement with the literature (She *et al.*, 2014).

The ^{1}H NMR spectra (Figure 2.12, Figure 2.13 and Figure 2.14) of the starting materials and the final conjugate show that characteristic peaks from both SA (-CH_3 peak at 1.85ppm) and ODA (-CH_3 peak at 0.85ppm and -CH_2 peak at 1.24ppm) were present. The spectra also show that in the final conjugate, the integral of $(-CH_2)_{16}$-peaks of the ODA remained similar in the pure ODA (Figure 2.13) and the conjugate (Figure 2.14), indicating the long carbon chain was still intact. The ratio between the -CH_3 groups of SA and ODA was very close to one indicating that all the ODA present in the sample was conjugated with the SA. FTIR analysis provided more information about the conjugation. A yield of close to 100% w/w of the final product (SA-ODA) was obtained indicating an efficient reaction scheme.

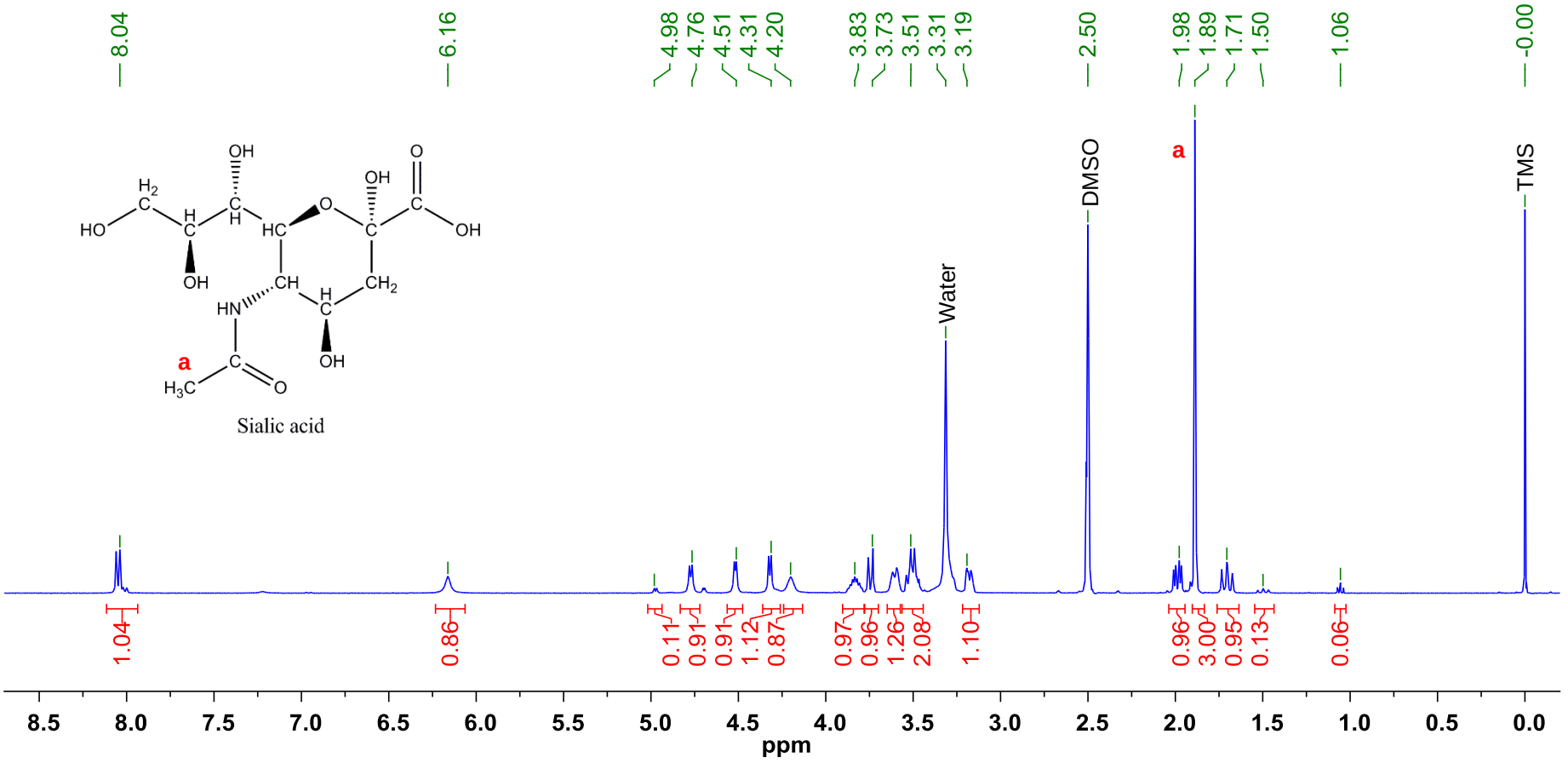

Figure 2.12. ^{1}H NMR (400 MHz) spectra of sialic acid in DMSO-D6.

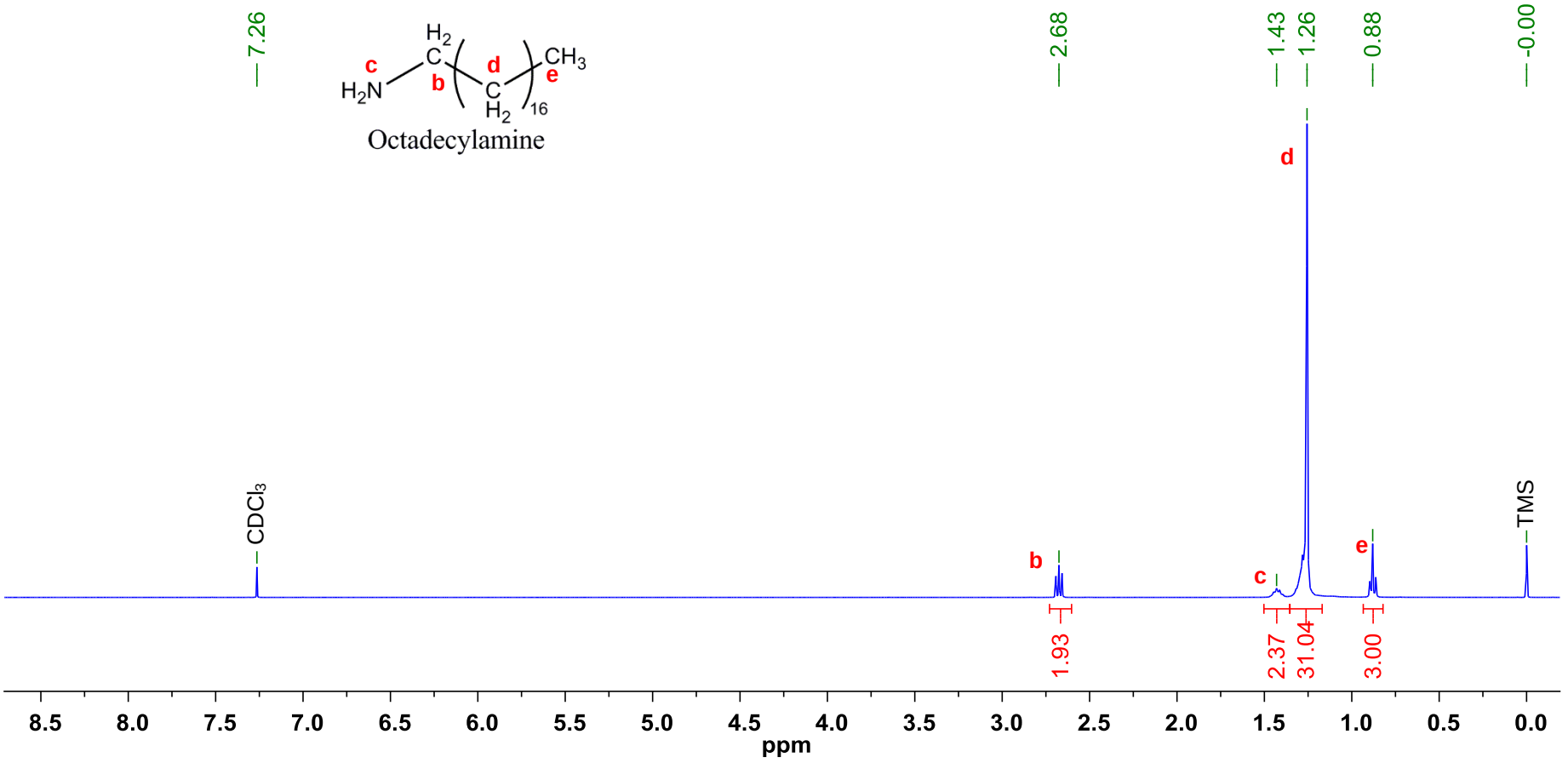

Figure 2.13. ^{1}H NMR (400 MHz) spectra of ODA in $CDCl_3$.

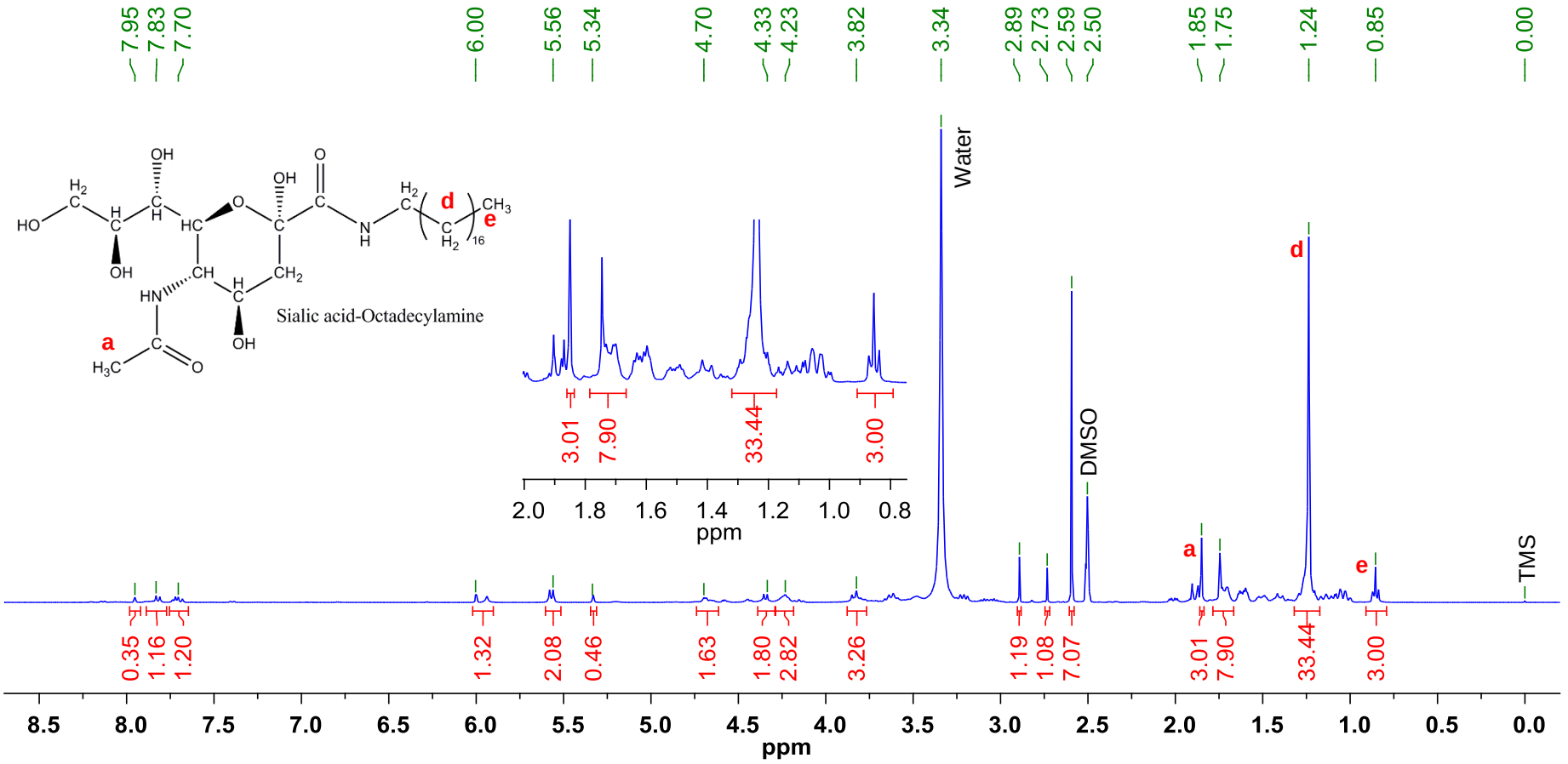

Figure 2.14. ^{1}H NMR (400 MHz) spectra of sialic acid-ODA conjugate in DMSO-D6.

FTIR is a useful tool for qualitative analysis as it can provide the fingerprints of materials to prove that the reaction actually took place as planned and a new compound has been synthesised. Here, we have discussed the spectra provided in the Figure 2.15 in light of the textbook (Field *et al.*, 2013) as well as literature (She *et al.*, 2014).

Figure 2.15-A shows the FTIR spectra of ODA clearly indicating the amine stretching in between 3100-3350cm^{-1}. Also, strong -C-H stretching bands near 2900cm^{-1} are evident. Figure 2.15-B is the FTIR spectra of SA which is a carboxylic acid that generally shows characteristic band at 1700-1725cm^{-1} because of the -C=O stretching (from free -COOH). Our spectrum of the sialic acid shows the peak at 1723cm^{-1} which is most probably the -C=O peak. The carboxylic acids also show a very strong and broad band covering a wide range between 2800 and 3500 cm^{-1} for the O-H stretch. However, alcohol groups (-OH) also appears as a strong, broad band covering the range of about 3000 - 3700 cm^{-1}. Sialic acid has several hydroxyl groups thereby masks the O-H stretch peak of the -COOH group. Furthermore, due to the ring opening, the -OH group nearest to the -COOH may form an aldehyde which may produced the band at 1723cm^{-1}. One of the bands at 1654 and 1528 cm^{-1} is generated by the amide group of the SA, however, we are unable to confirm which one.

The SA-ODA conjugate spectra (Figure 2.15C) shows that the -C=O stretching (from free -COOH) present in SA at 1723 cm^{-1} disappeared and a new band appeared at 1707cm^{-1} which could indicate the amide bond formation between SA and ODA. The physical mixture of SA and ODA (Figure 2.15D) shows all the bands from both SA and ODA with negligible alteration of the wavelengths. She *et al.* (2014) also verified the SA-ODA conjugation with FTIR. They assigned the 1723cm^{-1} band for carboxylic acid and claimed that the conjugation happened when the final product did not show this peak. From the FTIR spectra and above discussion, it can be speculated that the SA-ODA conjugate has formed indicated by disappearance of free -COOH peak (1723 cm^{-1}) and appearance of amide peak (1707cm^{-1}).

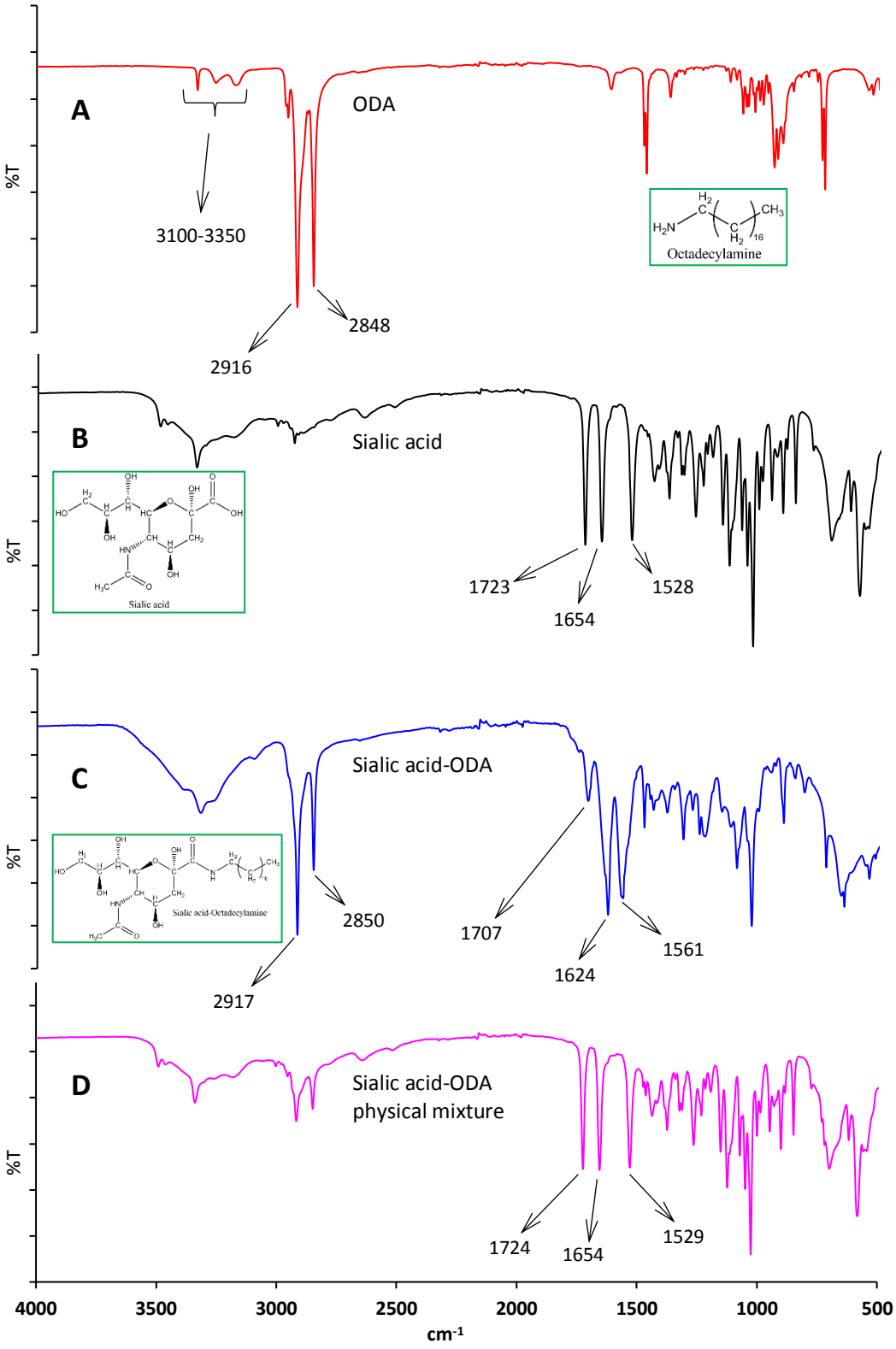

Figure 2.15. Characterisation of SA-ODA by FTIR: FTIR spectra of (A) ODA, (B) sialic acid, (C) sialic acid-ODA, and (D) a physical mixture of sialic acid and ODA.

2.4.3 Synthesis of DSPE-PEG-TAT

Following the method of Yang *et al.* (2013), DSPE-PEG-TAT was synthesised via a nucleophilic substitution reaction and purified by dialysis to get the final product as a white, odourless powder. We maintained strict 'no water' reaction environment and employed the pre-activated reagent (DSPE-PEG-NHS) as the lipid-PEG derivative to efficiently couple it with amine-group containing TAT peptide. Alkaline conditions were maintained to facilitate the reaction. The terminal amino group on TAT peptide attacked the carbonyl group of DSPE-PEG-NHS in anhydrous DMF and produced DSPE-PEG-TAT. The reaction time was optimised by monitoring completion of the reaction. The final product was confirmed to be DSPE-PEG-TAT conjugation by MALDI-TOF MS analysis result.

DSPE-PEG-TAT was separated and analysed by a gradient HPLC method. The TAT eluted without any interfering peaks at a retention time of 13.0 min, followed by the reaction product DSPE-PEG-TAT at a retention time of 14.4 min (Figure 2.16). The analysis time was optimised to 36 minutes that ensured all molecules were cleared from the system, including a few impurity peaks that were well resolved from the molecules of interest, but retained on the column much longer than them. The peaks of interest eluted within first 15 min of the run, however, the impurity from the TAT peptide and DSPE-PEG-NHS eluted after 29 min.

The final product yield was satisfactory (83.3%) calculated from the weight of the DSPE-PEG-TAT and the theoretical yield.

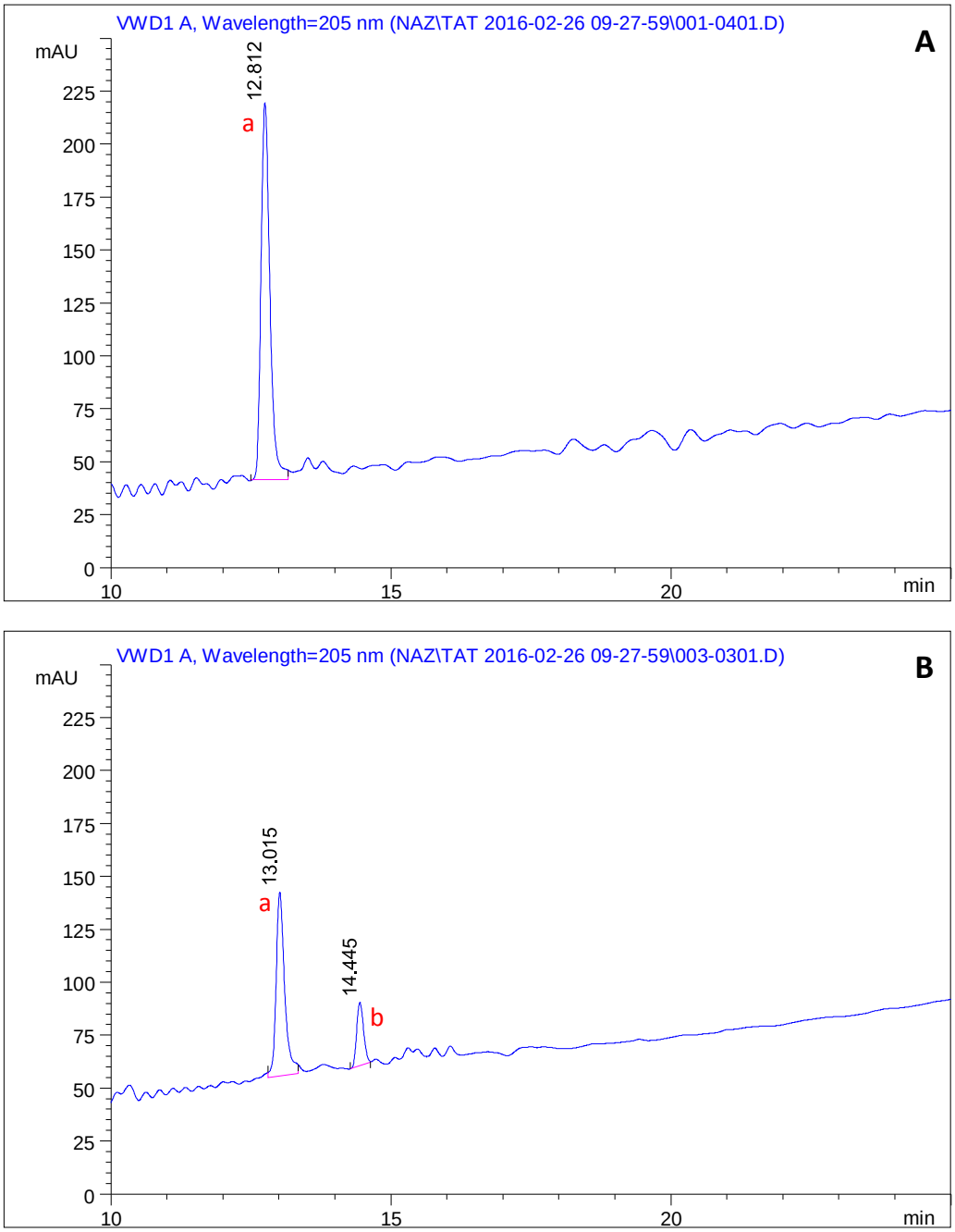

Figure 2.16. HPLC spectra of the reaction mixture at (A) zero hour and (B) 72 hrs. TAT peptide and DSPE-PEG-TAT peaks are indicated with (a) and (b), respectively.

HPLC analysis demonstrated that TAT continued to form the conjugate with DSPE-PEG-NHS until 72 hrs (three days), shown by depletion of the starting material. After three days, the product formation becomes very low thus demonstrating that reaction had attained its equilibrium. The reaction time, therefore, was optimised to run for three days to get the highest yield (83.3% w/w), similar to another research group who performed a similar type of reaction conjugating different peptide with DSPE-PEG-NHS (Xie *et al.,* 2015). The control reaction without any DSPE-PEG-NHS, showed negligible change in TAT peptide concentration confirming that reduction of TAT concentration in the reaction vessel was due to conjugation reaction and not due to degradation of TAT peptide (Table 2.2 and Figure 2.17). The TAT peptide concentrations at all the time points were calculated in comparison to day zero TAT peptide concentration that was taken as 100%.

Table 2.2. Change of the TAT concentration in the reaction and control vessel.

Days	**TAT in control vessel (%)**	**TAT in reaction vessel (%)**
0	100.0	100.0
0.5	99.3±3.2	66.2±3.3
1.0	98.4±2.3	43.6±2.9
1.5	99.1±1.6	33.4±1.3
2.0	98.6±3.1	29.4±0.9
2.5	96.1±1.6	25.9±2.1
3.0	97.6±3.9	24.1±1.3
3.5	96.2±2.3	22.8±2.4
4.0	96.8±1.3	22.1±3.1
5.0	95.8±1.2	21.9±1.9
6.0	94.2±1.9	22.2±1.2

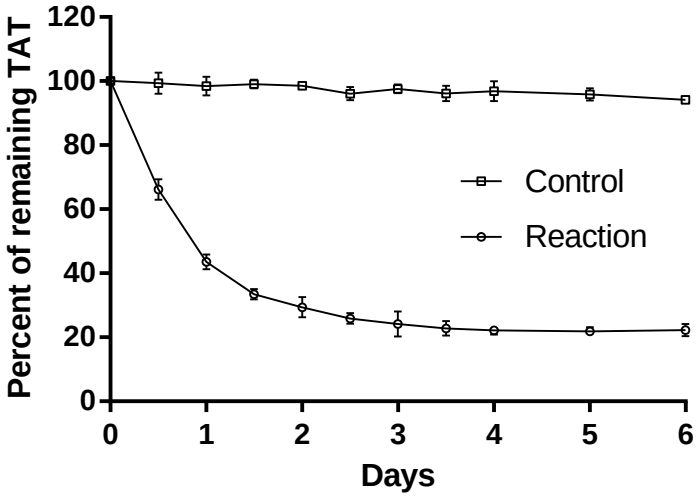

Figure 2.17. Percentage of remaining TAT peptide under control and reaction conditions. Results are expressed as mean ± SD (n=3).

To confirm the reaction product is DSPE-PEG-TAT, MALDI-TOF-MS analysis was performed. The MS spectra showed the MW of the resulting product was around 3348, which was in accordance with the theoretical MW of DSPE-PEG-TAT that can be calculated from the MW of TAT peptide (MW 1340 Da) and DSPE-PEG-NHS (MW 2009 Da) (Figure 2.18). Slight differences between the experimental and theoretical MW have also been reported by other researchers (Yang *et al.*, 2013) which is most probably due to the nature of polymer sample often present with a range of MW.

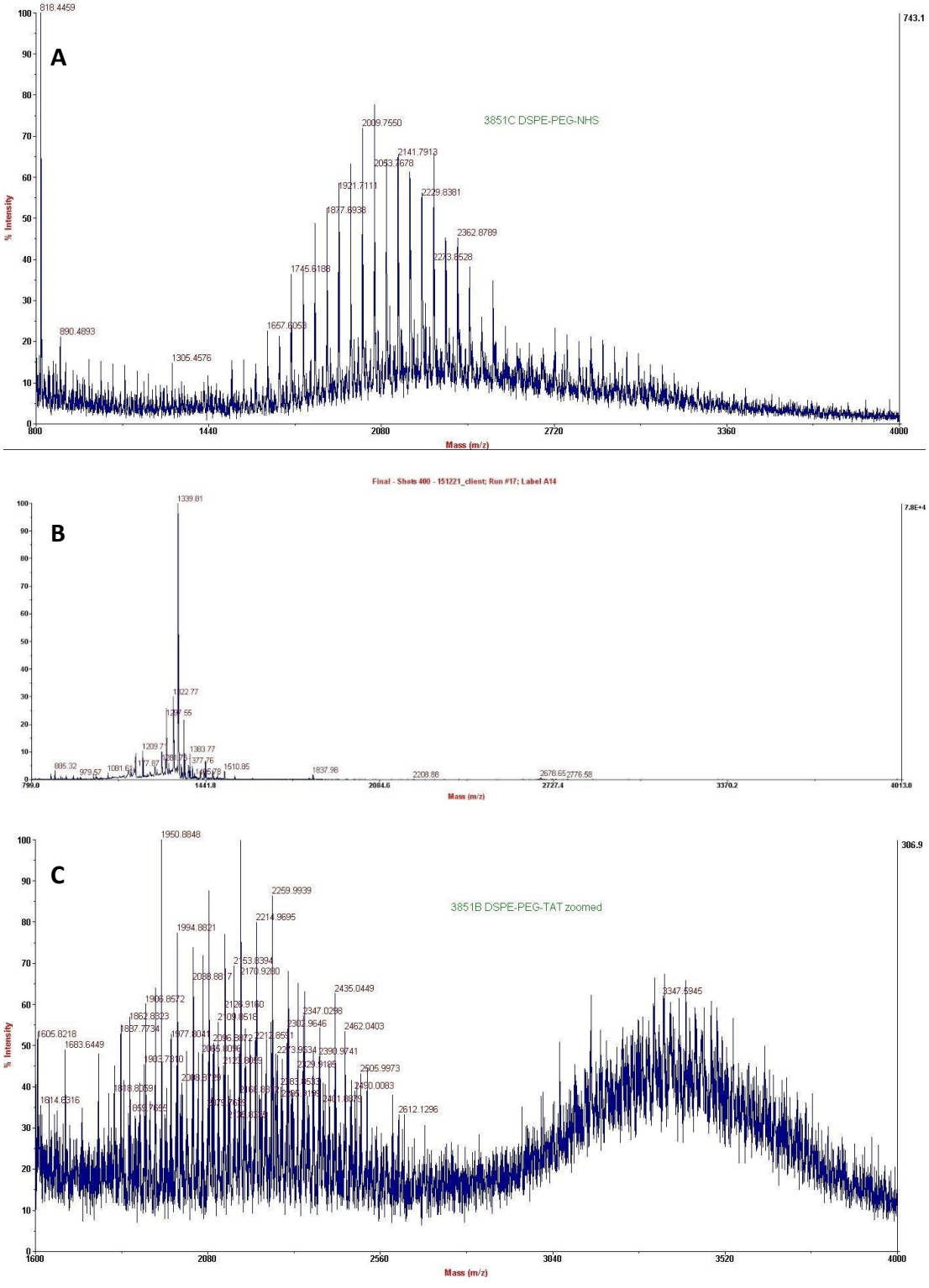

Figure 2.18. MALDI-TOF-MS spectra of (A) DSPE-PEG-NHS, (B) TAT peptide and (C) DSPE-PEG-TAT. The MW of DSPE-PEG-NHS, TAT peptide and DSPE-PEG-TAT were about 2009, 1340 and 3348, respectively.

2.5 Conclusions

PLGA was selected as the core polymer for NPs preparation due to favourable properties including biocompatibility, biodegradability, lack of toxicity and presence of functional carboxylic group for ease of ligand attachment. Functionalization of PLGA aimed to enable us to produce brain-specific NPs using ligands attached PLGA. Functionalization of the PLGA was carried out by chemically conjugating the polymer with DAB to facilitate the next step, where it would be conjugated with sialic acid. However, the yield was very low (about 3%), and thus the scheme was deemed too uneconomical to continue. Although this approach of incorporating the ligand directly onto the core polymer produced unsatisfactory yield, the ligands were effectively conjugated with PLGA molecules which introduced the -NH_2 functional groups to PLGA for future modification.

The alternative method of incorporating hydrophilic ligand into the NPs was conducted where both SA and the TAT peptide were conjugated separately with lipophilic molecules; SA with a relatively smaller molecule and TAT with a larger one. The SA ligand was successfully conjugated with ODA by carbodiimide reactions and produced satisfactory yield. The advantage of conjugating SA to ODA, in addition to it higher yield, is that it allows us to incorporate more SA ligand group into the NPs system due to the relative lower MW of SA-ODA. The TAT peptide ligand was also conjugated successfully with large commercially available lipid-PEG derivatives, DSPE-PEG-NHS, confirmed by MALDI-TOF-MS analysis.

It was expected that the lipophilic part of the conjugates would embed itself into the lipophilic core polymer matrix during NPs preparation exposing the hydrophilic ligand part into outer aqueous phase. As DSPE-PEG-TAT is a large amphiphilic molecule, so it is expected that TAT will be exposed on the NPs surface functioning as the first ligand, whereas, SA-ODA will be embedded deeper and serve as the second targeting ligand.

Chapter 3 Development and Validation of Analytical Methods for RHT

3.1 Introduction/Overview

The quantitative determination of RHT has been achieved using several analytical techniques such as spectrophotometry (Fazil *et al.*, 2012; Nagpal *et al.*, 2013), HPLC (Arumugam *et al.*, 2008; Arumugam *et al.*, 2011a; Yang *et al.*, 2013; Shah *et al.*, 2015), gas chromatography mass spectrometry (GC-MS) (Hossain *et al.*, 2002; Lee *et al.*, 2004; Sha *et al.*, 2004) and liquid chromatography-mass spectrometry (LC-MS) (Pommier & Frigola, 2003; Enz *et al.*, 2004; Frankfort *et al.*, 2006; Bhatt *et al.*, 2007; Arumugam *et al.*, 2011b).

Spectrophotometry is a simple quantitative analytical method that measures the light absorption capacity of the sample under analysis at different wavelengths. Fazil *et al.* (2012) determined the drug loading and encapsulation efficiency by measuring the amount of free RHT in the NPs supernatant using UV spectrophotometer. They used the same technique to quantify RHT in PBS in their *in vitro* permeability studies also. Nagpal *et al.* (2013) employed this method for measuring the DL, EE and RHT release from NPs in PBS. However, spectrophotometric method is not selective and cannot separate dosage form excipients, impurities or degradation products from the drug itself.

Mostly, RHT has been separated and quantified from various samples by HPLC, a powerful liquid chromatography technique that can simultaneously separate, identify and quantify compounds in a dissolved state (Arumugam *et al.*, 2008; Arumugam *et al.*, 2011a; Yang *et al.*, 2013; Shah *et al.*, 2015). The published HPLC methods so far used mobile phase pH ranging from 3 to 6 and different types of 250mm long column such as ODS, Kromasil C_8, XTerra RP18, $5C_{18}$-MS etc. Most researchers used a UV detector for detecting the drug except a few who used fluorescence detector in order to obtain enhanced sensitivity.

HPLC exploits the ionic and/or hydrophobic interaction of the analyte with the stationary phase (the column) and the mobile phase. The mobile phase is usually composed of a mixture of an aqueous phase (*e.g.* buffer) and one or more organic solvents with variable polarity. The column can be packed with either polar (normal phase HPLC or NP-HPLC) or non-polar material (reverse phase HPLC or RP-HPLC) depending on the polarity of the target analytes. RP-HPLC is generally the technique of choice when the analytes are less polar compounds (most drug molecules) (Watson, 2005). HPLC methods reported to date for separation and quantification of RHT in different sample matrices are summarised in Table 3.1.

Although a mass spectrophotometer (MS) can be coupled with either GC or HPLC to obtain a highly sensitive instrument, MS is expensive to procure and maintain. There are several reported methods (Sulochana *et al.*, 2014) for separation and quantification of RHT from both biological (rat, canine and human plasma, rat brain and urine) and pharmaceutical samples. However, for our present studies, a simple HPLC method was believed to be sufficient.

RHT is a basic drug molecule having an MW of 400.428g/mol and pKa of 8.85 (Canney, 2005). An acidic condition of at least two pH points lower than the compound pKa should be maintained to keep all RHT molecules positively charged. The initial analytical conditions were selected from the published methods and then modified to suit our purpose better. None of the published methods was found to be suitable for the available 150mm C_{18} column, hence, the objectives of the current study were set to develop and validate a simple, fast, sensitive, selective and accurate HPLC method using a commonly used column for *in vitro* RHT quantification and study its degradation behaviour under different stressed conditions.

Table 3.1. Summary of published HPLC conditions for RHT determinations.

Column	Sample Matrix	Mobile Phase	Flow Rate	Detection Technique	Reference
Waters Spherisorb, Silica	Human plasma	Acetonitrile-50mM aqueous sodium dihydrogen phosphate (17: 83 v/v, pH 3.1)	1.3mL/min	UV – 200nm	(Amini & Ahmadiani, 2010)
Inertsil ODS-3V, C_{18}	Rat plasma and brain	Ammonium acetate buffer (20mM, pH 4.5) and acetonitrile 74:26 (v/v)	1.0mL/min	Fluorescence detector, Ex/Em wavelength – 220/293nm	(Arumugam *et al.*, 2011a)
XTerra RP18, C_{18}	Raw material	10mM sodium-1-heptane sulphonate (pH 3.0) and acetonitrile 72:28 (v/v)	1.0mL/min	UV – 217nm	(Rao *et al.*, 2005)
Monomeric, C_{18}	Rat plasma	Acetonitrile and 20 mmol/L phosphate buffer pH 3.0 (25:75)	1.0mL/min	Fluorescence detector, Ex/Em wavelength – 220/293nm	(Karthik *et al.*, 2008)
$5C_{18}$-MS	Capsule	Methanol and water (90:10)	1.0mL/min	UV – 217nm	(Li *et al.*, 2011)
Kromasil C_8	Liposomes	20 mmol L^{-1} phosphate buffer pH 3.0 and acetonitrile (75:25 %, V/V)	1.0mL/min	UV – 210nm	(Arumugam *et al.*, 2008)
C_{18}	Solid lipid nanoparticles	Acetonitrile and potassium dihydrogen orthophosphate buffer pH 6.0 (20:80 v/v)	1.0mL/min	UV – 215nm	(Shah *et al.*, 2015)
ODS, C_{18}	Liposomes	Acetonitrile:water (20mM $NaH_2PO_4 \cdot 2H_2O$, 10mM $Na_2HPO_4 \cdot 12H_2O$) (25:75, v/v)	1.0mL/min	UV – 218nm	(Yang *et al.*, 2013)

3.2 Materials

RHT (Cat. # IC-CS-146-0-140108, ≥ 99.2%) was purchased from Innochem Technology Co., Ltd. (Beijing, China). HPLC grade ACN (Cat. # A998-4, ≥ 99.9%) was obtained from Thermo Fisher Scientific (Scoresby, Australia). TFA (Cat. # T6508, ≥ 99.0%) was procured from Sigma-Aldrich (Castle Hill, Australia). HCl (Cat. # 256, 32% w/v) and hydrogen peroxide (H_2O_2, Cat. # 260, 30% w/v) were obtained from Ajax Finechem Pty Ltd. (Taren Point, Australia). NaOH (Cat. # 104384F, ≥ 98.0) was obtained from BDH Laboratory supplies (Poole, England). Milli-Q water was generated using Milli-Q Ultrapure Water System (Merck Millipore, Bayswater, Australia).

3.3 Methods

3.3.1 Chromatographic Conditions and Optimisation

The HPLC system used for the method development and validation was an Agilent® 1200 instrument (Agilent Technologies Australia, Mulgrave) with a degasser (G1379B), binary pump (G1312A), autosampler (G1329A) with a thermo-control unit (G1330B) and VWD (G1314B). Assay selectivity including RHT peak purity was assessed using a diode-array detector (DAD, G1315B). Data acquisition and processing were carried out with Agilent ChemStation® software version B.04.03 SP1.

The HPLC column used was Grace Apollo C_{18}, 5µm particle size, 150mm × 4.6mm (Grace Davidson Discovery Science, Baulkham Hills, Australia). Sample temperature in the autosampler was maintained at 4°C to exclude potential thermal effects on the stability of the analytes. The column temperature was maintained at 50°C by a Waters® 1122/WTC-120 external column heater (Waters Australia Pty Ltd, Rydalmere, Australia).

The ratio between the organic and aqueous phase was varied in order to achieve a good separation within an analysis time of 10 minutes. The final mobile phase consisted of a volume-by-volume (v/v) ratio of 80% water and 20% ACN containing 0.1% TFA. The mobile phase was filtered through a 0.2µm hydrophilic nylon filter (Cat. # GNWP04700, Merck Millipore, Bayswater, Australia) to get rid of any particles. An isocratic mode was used for all the analysis at a mobile phase flow rate of 1.5mL per minute. Injection volume for all samples was 50µL, and detection of RHT was monitored at a wavelength of 214nm.

3.3.2 Forced Degradation Studies

Forced degradation studies were conducted according to published protocols to indicate the selectivity of the proposed method (ICH, 2000; Dandekar & Patravale, 2009; Raju *et al.*, 2012). A constant concentration of RHT (25µg/mL) was used for all degradation studies. For acid decomposition (hydrolysis) studies, an RHT solution was prepared in 2N HCl and incubated for 48 hrs at 37° and 60°C. For base hydrolysis studies, RHT solution was prepared in 0.5N NaOH and was incubated at 37°C for 48 hrs and 60°C for 4 hrs. Both the acid and alkaline samples were cooled to RT and neutralised before analysing by HPLC.

To assess the stability of RHT in water, RHT solution (25µg/mL) was prepared in water and incubated for 48 hrs at 37° and 60°C. Effect of oxidation was determined by incubating RHT for 48 hrs at 37° and 60°C in 30% H_2O_2.

All degraded product was analysed by HPLC, and RHT peak purity was evaluated using a diode-array detector by obtaining five UV spectra across the peak. The similarity among these five spectra was determined and reported using ChemStation® software to determine the peak purity. Co-elution of any degraded product along with the drug peak made it impure and demonstrated through dissimilar UV spectra. The software also reported whether the peak purity in each spectrum was within the automatically set threshold limit.

3.3.3 Method Validation

The developed HPLC method was fully validated with respect to selectivity, linearity, precision, accuracy, limit of detection (LOD) and limit of quantification (LOQ) consistent with the International Conference on Harmonisation (ICH) Guidelines for Validation of Analytical Procedures, Q2B (ICH, 1996) and the United States Pharmacopeia and National Formulary (USP 37-NF 32).

3.3.3.1 Selectivity

The forced degradation study samples (all) were used to assess the selectivity of the method (Section 3.3.2). Also, supernatants of both blank NPs (dual ligand NPs without any loaded drug) and RHT-loaded dual ligand NPs were diluted 200X in the mobile phase and injected into the HPLC to find out whether any interfering peaks elute near the drug peak. The matrix interference was also investigated in the similar fashion from (i) PBS medium from release study of dual ligand NPs without any loaded drug, and (ii) uptake/transport study buffer (HBSS-P) comprised of HBSS containing 10mM HEPES and 20mM glucose.

3.3.3.2 Linearity

The linearity of the developed method was assessed in two different solvents, one solvent used for RHT loading in the NPs and the other for the *in vitro* release study. *Firstly*, different concentrations of RHT solution (0.1 to 2mg/mL) were prepared into 0.3% vitamin E-TPGS from one stock solution (2mg/mL) in 0.3% vitamin E-TPGS. Each solution was diluted 200 times (50µL into 10mL) with mobile phase to obtain final RHT standard concentrations of 0.5, 1, 2, 3, 4, 5, 6, 7, 8, 9 and 10µg/mL. 50µL of these standards were injected to the HPLC, in duplicate. *Secondly*, another set of standards with the same concentration range was prepared by diluting an RHT stock solution in Milli-Q water (1mg/mL) with 10mM PBS (pH 7.4). Again, 50µL of these standards were injected to the HPLC in duplicate. Average peak area data was plotted against corresponding standard concentrations using Microsoft® Excel 2016 to construct the standard calibration curve. The linearity was established by calculating the R^2 value.

3.3.3.3 Precision

The precision of the proposed method was determined by injecting four RHT concentrations (1, 4, 6 and 10µg/mL) in both solvents six times into the HPLC. The RSD values were calculated for all concentrations.

3.3.3.4 Limit of Detection (LOD)

The LOD was determined as the drug concentration which produced signal three times greater than the baseline noise level. Two blank solvents, namely (a) 0.3% vitamin E-TPGS diluted 200 times in the mobile phase, and (b) 10mM PBS, pH 7.4, were injected six times to determine the average noise levels. Standard RHT solutions prepared in the mobile phase were analysed and calibration curves constructed by plotting average peak heights against the corresponding concentrations. The LOD was calculated by the following formula:

$$LOD = 3 \times \frac{Peak\ height\ of\ noise}{Slope\ of\ calibration\ curve\ constructed\ by\ peak\ height\ vs.\ conc}$$

3.3.3.5 Limit of Quantification (LOQ)

Using the same data, the LOQ was determined as ten times greater than the baseline noise level. The LOQ was calculated by the following formula:

$$LOQ = 10 \times \frac{Peak\ height\ of\ noise}{Slope\ of\ calibration\ curve\ constructed\ by\ peak\ height\ vs.\ conc}$$

3.3.3.6 Intra- and Inter-day Repeatability

Three standard concentrations of RHT (low, medium and high) within the calibration curve were selected for these experiments. For both solvents, the intra- and inter-day repeatability of the method was assessed by analysing 1, 5 and 10µg/mL RHT standards, in triplicate, at different time points in the same day and on two different days. The relative standard deviation (RSD) was calculated for each analysed concentration and compared with the nominal limit to evaluate the intra- and inter-day repeatability of the method.

3.3.3.7 Accuracy

The accuracy of the developed method was determined in two solvent mixtures to assess the interference of the NPs and solvents. *Firstly*, a batch of drug-free nanoparticle (blank-NP) was prepared, and the supernatant was collected during the last step of the preparation. The supernatant was then spiked with RHT to obtain a solution of RHT (2mg/mL). This stock solution was diluted with the same solvent to prepare five RHT solutions with concentrations of 0.1, 0.4, 0.8, 1.2 and 1.6mg/mL. These solutions were diluted 200 times with the mobile phase to obtain final drug concentrations of 0.5, 2, 4, 6, 8 and 10µg/mL and injected in the HPLC column in triplicate. This procedure mimics the method of sample preparation for RHT concentration determination in NPs supernatant.

Secondly, an *in vitro* release study of the blank-NPs was carried out at pH 7.4 in PBS. 3mL blank-NP suspension was taken in a dialysis tube (MWCO 12000), sealed and placed in a 60g amber glass jar containing 50mL pre-warmed PBS at 37°C. The setup was placed on an orbital shaker in the hot room (37°C) and horizontally shaken at 100 rpm. Release medium from outside the dialysis bag was collected after 24 hrs, spiked with RHT standard solution (200 µg/mL) prepared in Milli-Q water to get final RHT concentrations of 2, 4, 6, 8 and 10µg/mL and injected in the HPLC column in triplicate. The concentration of RHT in all samples was determined against RHT standards prepared in mobile phase.

The method accuracy was determined by calculating the percentage of measured concentration over the added concentration in each case.

3.4 Results and Discussion

3.4.1 Development and Optimisation of HPLC Method

The HPLC method for separation and quantification of RHT in PBS (pH 7.4) and NPs supernatant (containing 0.3% vitamin E-TPGS) was developed and validated. An appropriate combination of the column type, column temperature, mobile phase composition and flow rate, injection volume and detection system was optimised. The UV wavelength of 214nm was selected for the detection of the compound based on the UV spectrum of RHT. Although choosing a lower wavelength (209nm) produced a much stronger drug signal, higher background noise made this approach impractical. The initial mobile phase composition was selected upon considering published methods as well as the high pKa (8.85) of the RHT (Canney, 2005). An acidic condition (pH 2.6) was maintained to keep all RHT molecules positively charged (Figure 3.1). At this lower pH, the silane groups of the C_{18} column were also fully protonated, leading to weak interaction with RHT. Thus, a short elution time was expected.

A mobile phase composed of ACN and water (50:50 v/v) containing 0.1% TFA was selected initially at a flow rate of 1mL/min. However, RHT eluted along with the solvent front, suggesting the need reduce the organic phase ratio in the mobile phase. After a few trials, a ratio of 20:80 (v/v) for ACN: water was found to be optimum to produce the best peak shape and separation. The flow rate was increased to 1.5mL/min to reduce the retention time at 6.83 min. Arumugam *et al.* (2011a) also employed similar mobile phase composed of ACN and water (26:74 v/v) and acidic pH of 4.5 for the analysis of RHT.

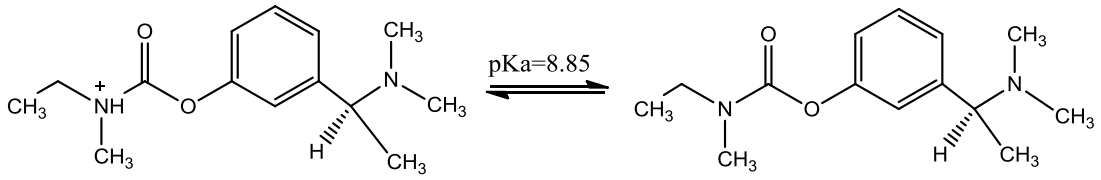

Figure 3.1. Ionisation of rivastigmine tartrate at different pH.

Optimum conditions for RHT analysis were as follows: compounds were separated using a Grace Apollo C_{18} column using a column temperature of 50°C to give a sharper peak shape, and the samples were kept at 4°C in the sample holder. The mobile phase composition was selected as 20% ACN:80% water containing 0.1% TFA (v/v). An isocratic condition was employed for all the analysis at a mobile phase flow rate of 1.5mL/min. A constant injection volume of 50µL was used for all the analysis. Figure 3.2 illustrates a typical RHT peak around 6.8 minutes eluted using the optimum conditions listed above.

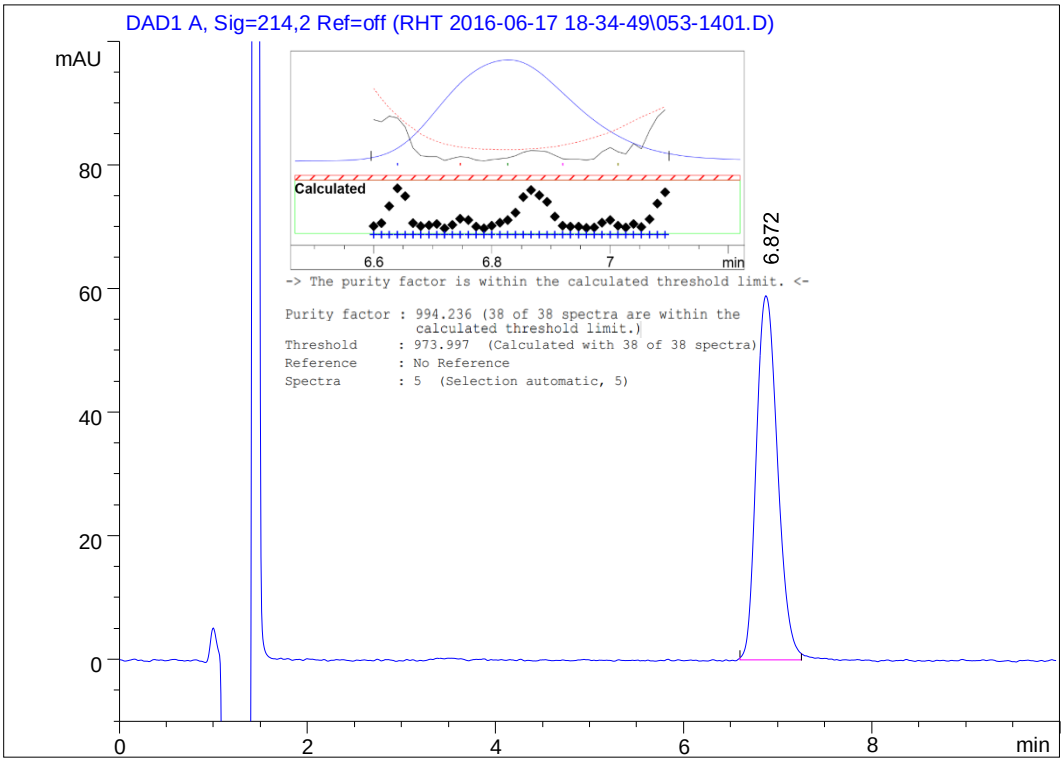

Figure 3.2. A typical chromatogram showing the peak of rivastigmine tartrate (RHT) in the mobile phase at a retention time of 6.9 minutes. Peak purity report is shown in the insert confirming that the RHT peak is pure and the purity factor is within the calculated threshold limit.

3.4.2 Forced Degradation of RHT

The main aim of the forced degradation studies of RHT was to assess the selectivity of the proposed analytical method. According to MSDS supplied by the manufacturer, RHT is chemically stable under normal conditions with known incompatibilities of strong acids, bases and oxidising agents. No light sensitivity data was found in the MSDS, however, literature reported that RHT is stable when exposed to light for at least ten days (Rao *et al.*, 2005). In our investigation, various stress conditions were employed to simulate any possible degradation that might occur during the NPs preparation and further experiments. RHT was subjected to hydrolysis (acidic, alkaline and neutral pH) and oxidation. The summarised observations (Table 3.2) conform with published literature (Rao *et al.*, 2005) where a similar degradation pattern for RHT was reported. The table shows that acidic conditions displayed less degradation effect on the drug at both 37° and 60°C. In contrast, RHT was found to be liable to basic condition, particularly at the elevated temperature. The drug demonstrated excellent stability against hydrolysis conditions at neutral pH under both test temperatures but, oxidised easily even at 37°C with complete degradation after incubation at 60°C for 48 hrs.

Table 3.2. Summary of findings of RHT forced degradation studies.

Forced degradation condition	**Temp. (°C)**	**Incubation duration**	**RHT Conc. (µg/mL)**		**Remaining percentage**
			Initial	**Final**	
Acid hydrolysis – RHT in 2N HCl	60	48 hrs	25.0	21.9	87.4
	37	48 hrs		24.5	97.8
Base hydrolysis – RHT in 0.5N NaOH	60	2 hrs		20.2	80.9
	37	48 hrs		7.4	29.7
Hydrolysis – RHT in Water	60	48 hrs		24.8	99.2
	37	48 hrs		24.9	99.7
Oxidation – RHT in 30% (w/v) H_2O_2	60	48 hrs		0.0	0.0
	37	48 hrs		19.9	79.6

Figure 3.3 and Figure 3.4 illustrate the HPLC spectra of RHT under various stress conditions. The peak purity analysis was conducted using the default settings of the ChemStation® software without any manual data entry. The software generated report indicated clearly if the RHT peaks are pure. The peak purity of degraded products was not checked because we were only interested in assessing the method's capability of resolving pure RHT peak. The objective of degradation study was fulfilled completely because RHT peak eluted well-separated from the degraded products (retention time <6 min) and was analysed to be a pure peak. Thus, the proposed method was sufficiently selective to be used with confidence for the quantification of RHT.

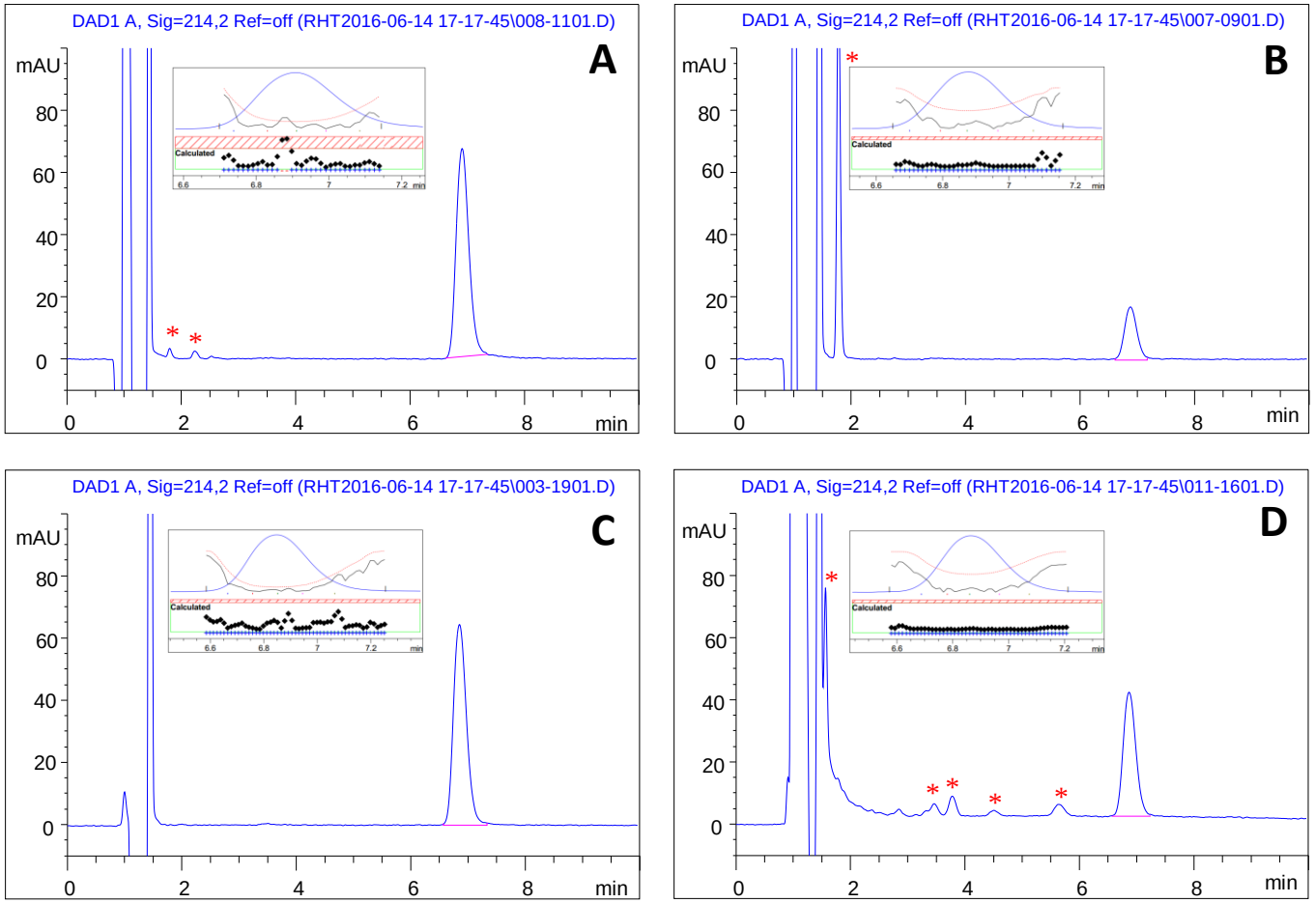

Figure 3.3. HPLC chromatogram of RHT under various stress conditions conducted at 37°C for 48 hr – (A) acid degradation, (B) alkali degradation, (C) hydrolysis, and (D) oxidation. Analysis of RHT was not interfered by the degradation products (*). Peak purity reports are shown in the inserts confirming that the RHT peaks are pure and the purity factors are within the calculated threshold limit.

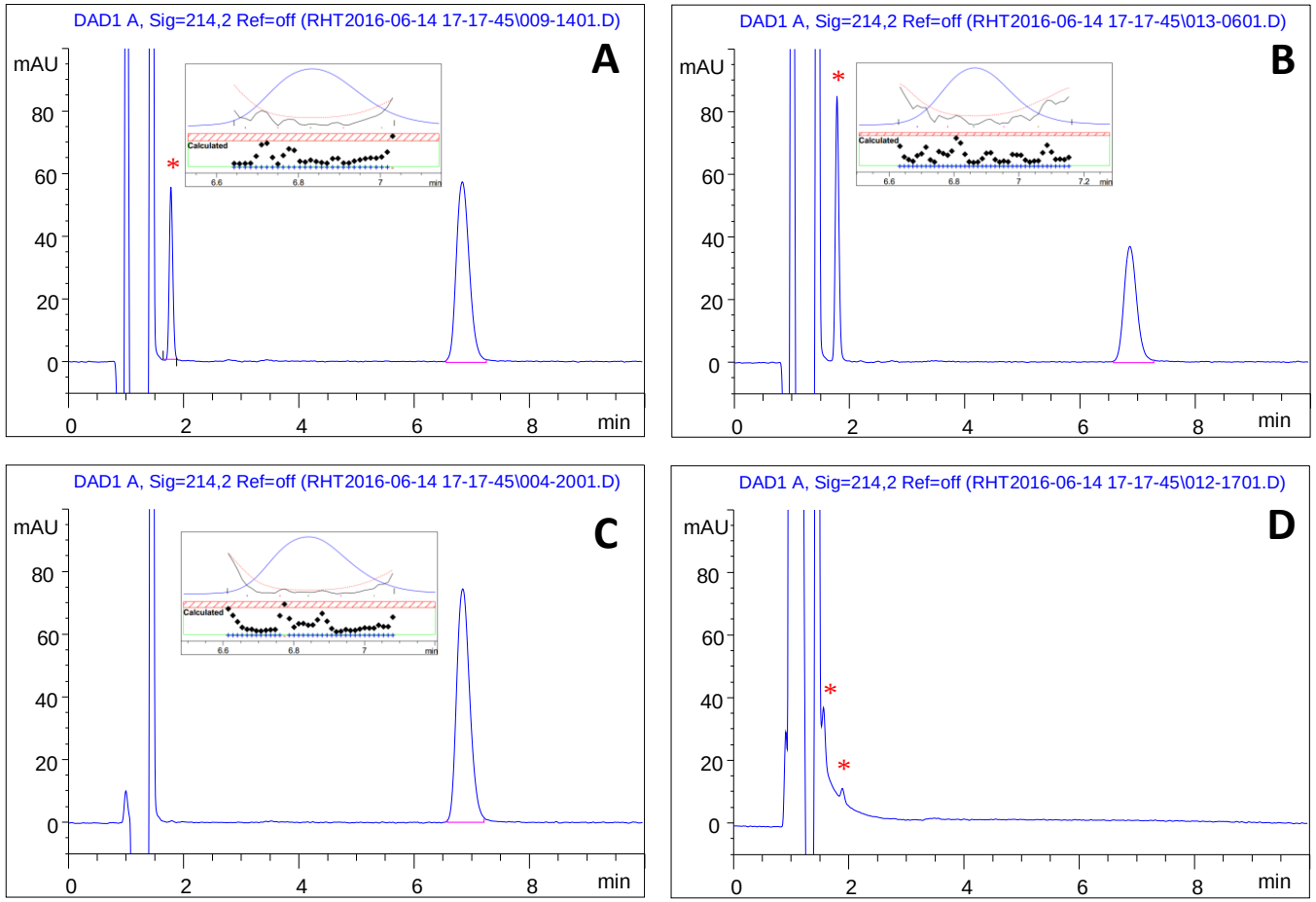

Figure 3.4. HPLC chromatogram of RHT under various stress conditions conducted at 60°C – (A) acid degradation for 48 hrs, (B) alkali degradation for 2 hrs, (C) hydrolysis for 48 hrs, and (D) oxidation for 48 hrs. Analysis of RHT was not interfered by the degradation products (*). Peak purity reports are shown in the inserts confirming that the RHT peaks are pure and the purity factors are within the calculated threshold limit.

3.4.3 Method Validation

3.4.3.1 Selectivity

The selectivity of any analytical method is the most important parameter that should be addressed during its validation. A selective analytical method ensures that it has the capability to generate "true results" that are free from matrix or medium interference. In case of the HPLC method, the analytical method must have the ability to separate the molecule(s) of interest from other interfering components and quantify it accurately and precisely. Selectivity of the method must be checked independently for each mixture/medium from which the drug is intended to be analysed. Along with the forced degradation study samples, we also investigated selectivity of the proposed RHT analytical method from three medium:

1) Supernatant of dual ligand NPs without any loaded drug (200X diluted in the mobile phase)

2) PBS medium from release study of dual ligand NPs without any loaded drug, and

3) Uptake/transport study medium (HBSS-P)

The HPLC spectra in Figure 3.5, 3.6 and 3.7 indicate that there was no peak around the RHT retention time (6.9 minutes) in any of the above medium illustrating that there was no matrix interference.

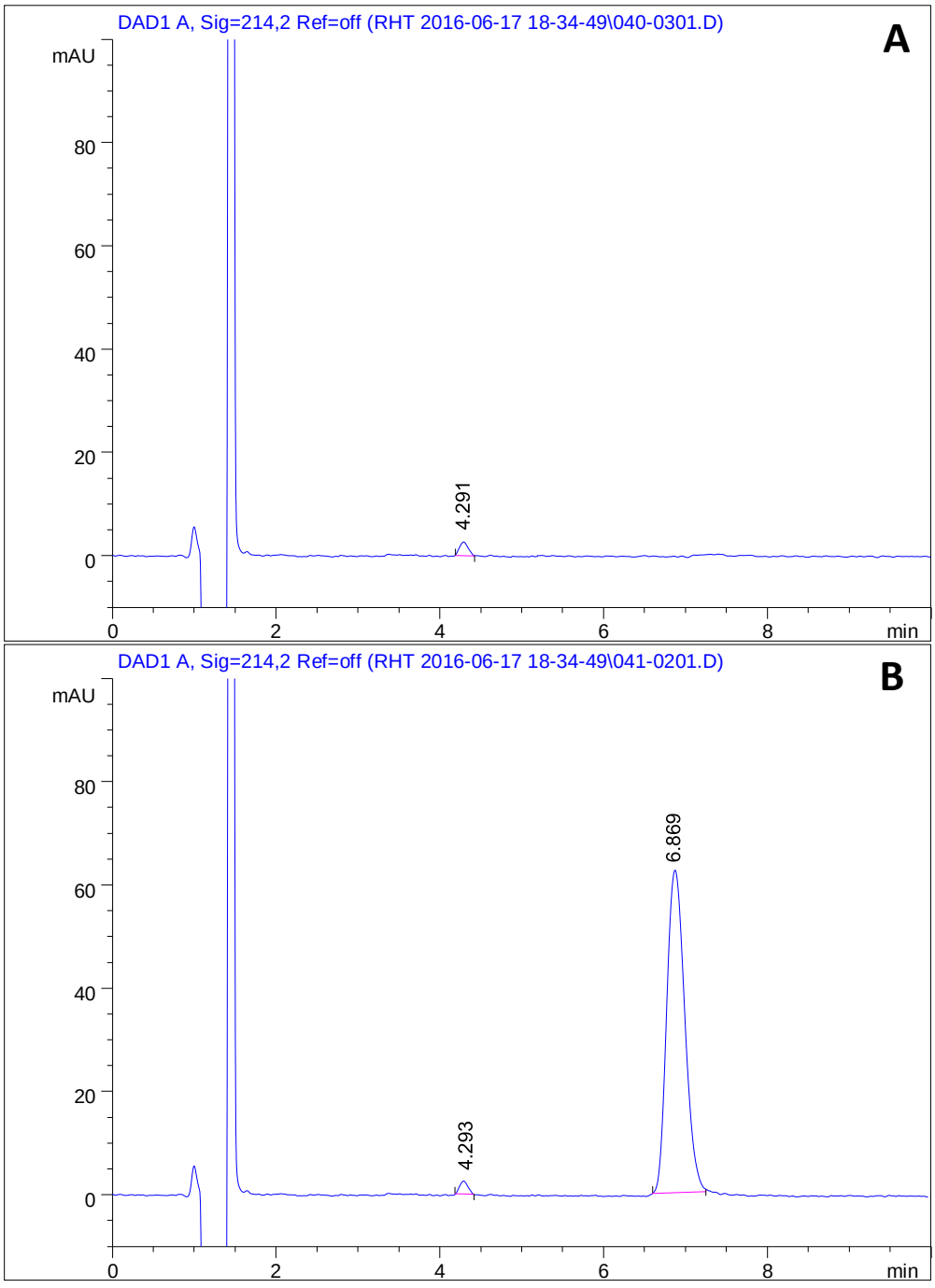

Figure 3.5. HPLC Chromatogram of supernatants of (A) dual ligand NPs without any loaded drug (200X diluted in the mobile phase), and (B) RHT-loaded dual ligand NPs (200X diluted in the mobile phase). No peak around the RHT retention time (6.9 minutes) is seen to illustrate that there is no matrix interference.

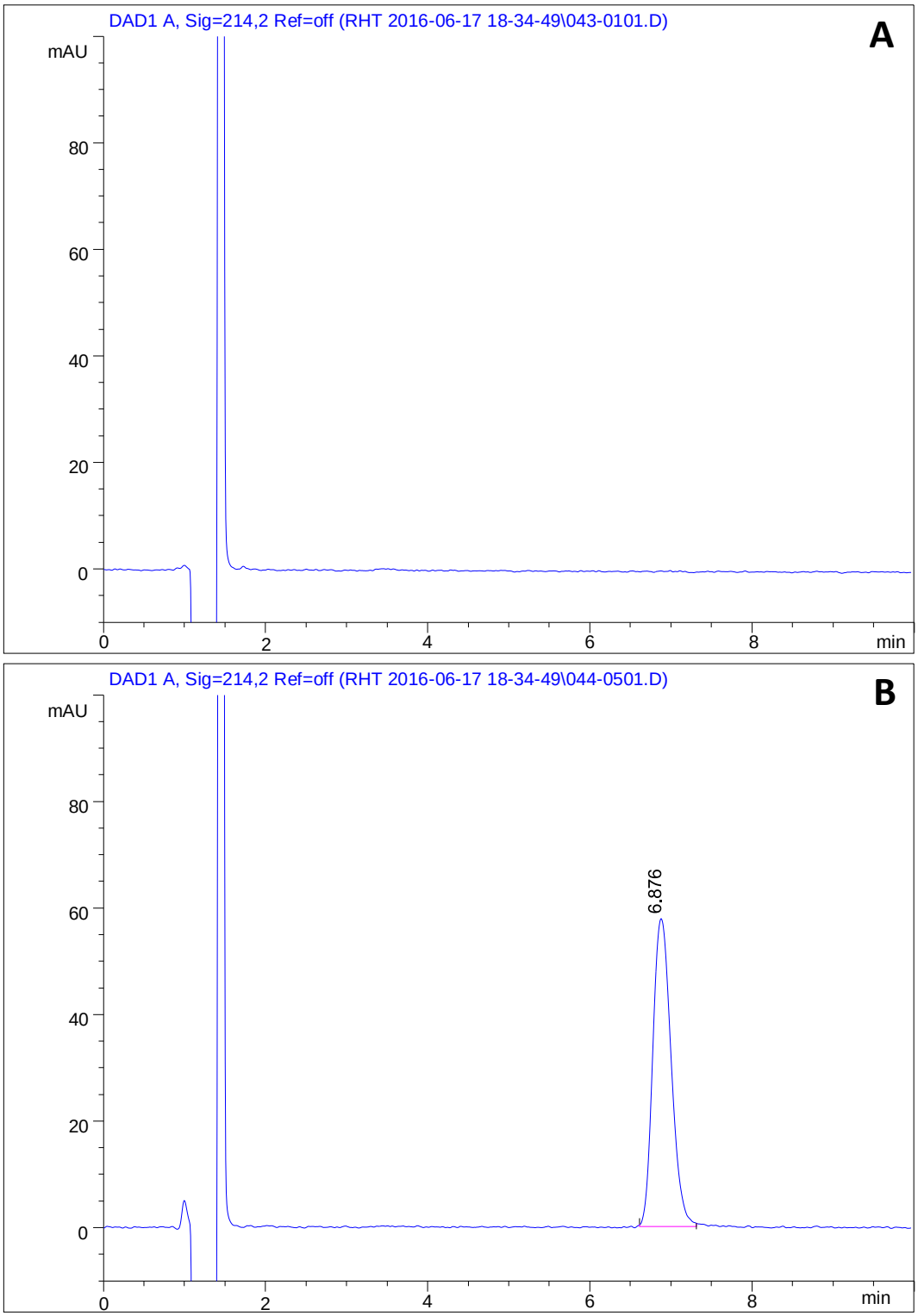

Figure 3.6. HPLC Chromatogram of PBS medium after 24 hours release study of (A) dual ligand NPs without any loaded drug , and (B) RHT-loaded dual ligand NPs. No peak around the RHT retention time (6.9 minutes) is seen to illustrate that there is no matrix interference.

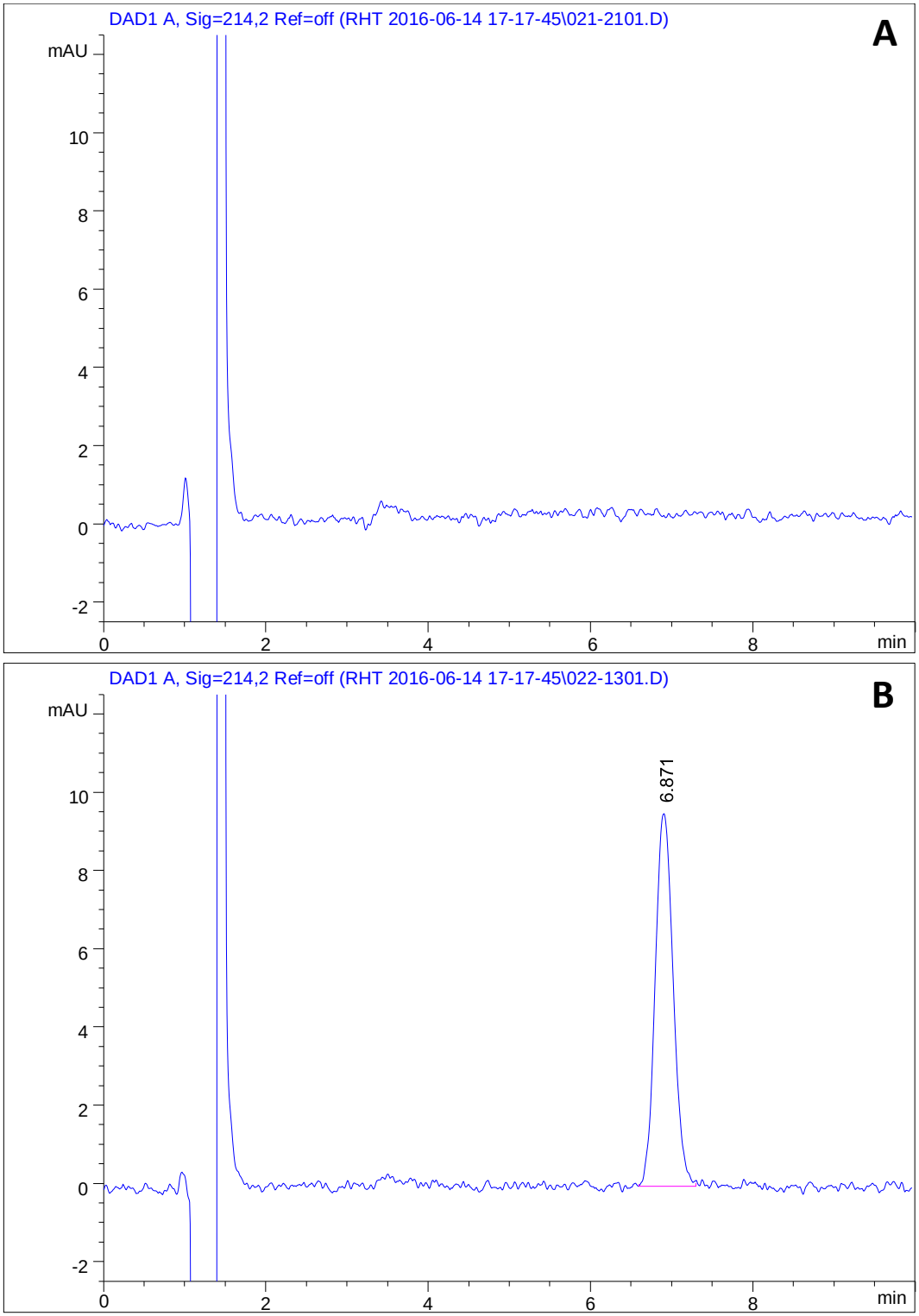

Figure 3.7. HPLC Chromatogram of (A) uptake/transport study medium (HBSS-P), and (B) released RHT in HBSS-P after 4 hours of transport study. No peak around the RHT retention time (6.9 minutes) is seen to illustrate that there is no matrix interference.

3.4.3.2 Linearity

The different concentrations of RHT in both solvents produced a linear response in the detector. For 50µL injections of RHT in vitamin E-TPGS (200 times diluted in the mobile phase), the regression plot demonstrated a nearly perfect linear relationship over the concentration range of 0.5-10µg/mL that covered the concentration encountered in the RHT loading analysis. The coefficient of variance was 0.9999. The same concentration ranges of RHT in PBS also demonstrated a good linear relationship with a coefficient of variance of 0.9998. The standard calibration curves are shown in Figure 3.8 and Figure 3.9.

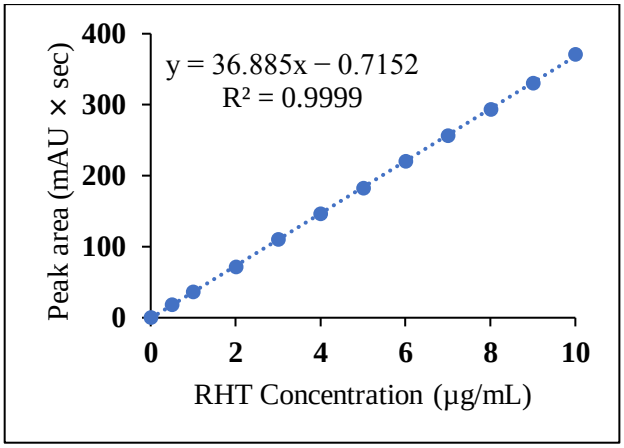

Figure 3.8. Calibration curve of RHT solution in vitamin E-TPGS diluted 200 times in the mobile phase.

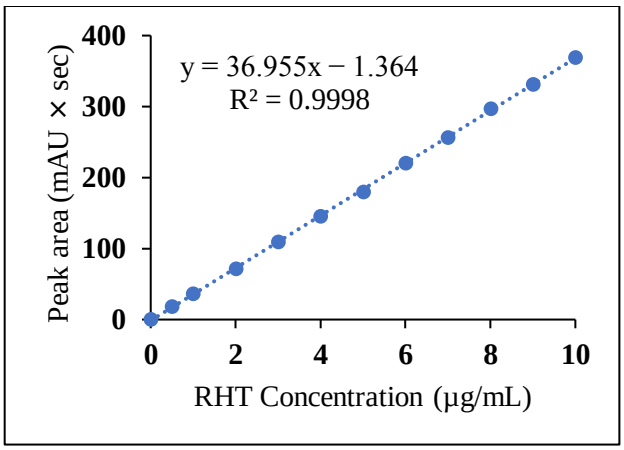

Figure 3.9. Calibration curve of RHT solution in 10mM PBS (pH 7.4).

3.4.3.3 Precision

The precision data of the developed method are tabulated in Table 3.3. For the first solvent system, the RSD values among six injections of RHT was 1.04%, 0.59%, 0.49% and 0.17%, respectively for 1, 4, 6 and 10µg/mL of RHT (Table 3.3 (a)). A similar trend was observed in the case of the second solvent system, where the coefficient of variation values was 1.28%, 0.67%, 0.28% and 0.19%, respectively for 1, 4, 6 and 10µg/mL of RHT (Table 3.3 (b)). All these precision values were below the nominally acceptable level of ≤ 2% (Swartz & Krull, 2012) and hence, the method was acceptable as a precise method. The data also indicated that at the low concentration range of RHT, the quantification error is relatively larger.

Table 3.3. The precision of the HPLC method for determination of RHT.

(a) RHT in 0.3% vitamin E-TPGS diluted 200 times in the mobile phase.

Injection number	RHT peak area (mAU × sec)			
	1µg/mL	4µg/mL	6µg/mL	10µg/mL
1	37.0	146.7	218.9	370.2
2	36.2	146.8	221.2	371.3
3	36.2	144.6	220.4	370.1
4	36.8	145.3	220.4	369.5
5	36.7	146.4	218.9	369.8
6	36.1	146.0	218.6	370.3
Average =	36.50	145.97	219.73	370.20
SD =	0.38	0.86	1.07	0.61
RSD =	1.04	0.59	0.49	0.17

(b) RHT in PBS.

Injection number	RHT peak area (mAU × sec)			
	1µg/mL	4µg/mL	6µg/mL	10µg/mL
1	36.1	146.7	221.1	369.9
2	35.8	146.2	220.9	368.5
3	35.7	144.2	220.6	369.1
4	36.2	145.6	221.9	370.2
5	36.9	145.4	220.1	369.6
6	36.6	146.8	221.3	368.5
Average =	36.22	145.82	220.98	369.30
SD =	0.46	0.97	0.61	0.72
RSD =	1.28	0.67	0.28	0.19

3.4.3.4 LOD and LOQ

The LOD of an analytical procedure is the lowest detectable amount of an analyte in a sample but not necessarily a quantifiable value. It was calculated as three times the average noise peak height divided by the slope of the calibration curve of the peak height. For the current method, the lowest possible concentration of RHT in both solvent systems that could be detected was determined as 60ng/mL.

The LOQ is the lowest amount of the drug in the sample that can be confidently quantified using the method. It was calculated as ten times of the average noise peak height divided by the slope of the calibration curve of the peak height. For the current method, the lowest possible concentration of RHT that could be quantified in both solvent system was determined as 201ng/mL. The LOD and LOQ data and calculation is summarised in Table 3.4 and Table 3.5.

Table 3.4. LOD and LOQ data with the calculation for RHT in 0.3% vitamin E-TPGS (200 times diluted in mobile phase).

Sample	**Noise (mAU)**	**Slope of calibration curve constructed by peak height *vs.* concentration**
Blank (0.3% vitamin E-TPGS diluted 200 times in mobile phase)	0.053 0.054 0.054 0.053 0.054 0.053	2.67
Average noise height	0.053	

LOD = 0.060 µg/mL
LOQ = 0.201 µg/mL

Table 3.5. LOD and LOQ data with the calculation for RHT in 10mM PBS (pH 7.4).

Sample	**Noise (mAU)**	**Slope of calibration curve constructed by peak height vs. concentration**
Blank (10mM PBS, pH 7.4)	0.053 0.054 0.053 0.055 0.053 0.053	2.66
Average noise height	0.054	

LOD = 0.060 µg/mL
LOQ = 0.201 µg/mL

3.4.3.5 Intra- and Inter-day Repeatability

In the intraday repeatability experiments, the RSD values were 0.69%, 0.92% and 0.49% for RHT in the first solvent and 0.73%, 0.65% and 0.35% for RHT in the second solvent for the RHT concentrations of 1, 5 and 10µg/mL, respectively. All values were within the acceptable limit of RSD ≤ 2% (Swartz & Krull, 2012).

In the inter-day repeatability experiments, the RSD among the repeats were calculated as 1.32%, 0.92% and 1.19% for the first solvent whereas in the second solvent the RSD values were 0.64%, 1.11% and 1.02% for the RHT concentrations of 1, 5 and 10µg/mL, respectively. All values were within the acceptable limit of RSD ≤ 2% (Swartz & Krull, 2012).

The intra- and inter-day repeatability data are shown in Table 3.6.

Table 3.6. Intra- and inter-day repeatability of RHT analysis in two solvents.

RHT concentration[a] (µg/mL)	**RHT in vitamin E-TPGS (200X diluted in mobile phase)**		**RHT in 10mM PBS (release media)**	
	Intra-day RSD[b]	**Inter-day RSD[c]**	**Intra-day RSD[b]**	**Inter-day RSD[c]**
1	0.69	1.32	0.73	0.64
5	0.92	0.92	0.65	1.11
10	0.49	1.19	0.35	1.02

[a]Each concentration was analysed in triplicate (n=3).
[b]The analyses were carried out at 0, 3 and 8 hrs on the same day and all data were included in the calculation.
[c]The analyses were carried out at day 1 and 2 and all data were included in the calculation.

3.4.3.6 Accuracy

The accuracy of a method demonstrates that the technique can accurately quantify the molecule(s) of interest in the presence of other possible interfering components such as excipients, reactions components, release chamber and medium. The accuracy of the proposed method was calculated as percentage recovery from the six concentrations covering the entire RHT concentration range within the calibration curve. The accuracy data with calculation is shown in Table 3.7 and Table 3.8. All the samples were successfully recovered with an accuracy of 100±2% which is within the acceptable range (Swartz & Krull, 2012).

Table 3.7. Accuracy data for RHT in 0.3% vitamin E-TPGS (200 times diluted in the mobile phase).

Prepared Concentration (µg/mL)	**Measured Concentration (µg/mL)**	**Recovery (%)**
0.50	0.49	98.0
2.00	1.99	99.5
4.00	3.96	99.0
6.00	5.97	99.5
8.00	8.03	100.4
10.00	9.99	99.9
	Mean ± SD =	99.4 ± 0.8

Table 3.8. Accuracy data for RHT in 10mM PBS (pH 7.4).

Prepared Concentration (µg/mL)	**Measured Concentration (µg/mL)**	**Recovery (%)**
0.50	0.49	98.4
2.00	2.01	100.5
4.00	4.04	101.0
6.00	5.95	99.2
8.00	7.98	99.8
10.00	9.99	99.9
	Mean ± SD =	99.8 ± 0.9

3.5 Conclusion

The HPLC method plays an important role in determining the NPs drug loading and drug release and generates data that will ultimately be helpful for the subsequent cellular and animal studies. In this chapter, a simple, reliable and fast HPLC method was developed and validated for RHT analysis during the RHT-loaded NPs preparation and *in vitro* drug release studies. The chromatographic separation was achieved using Grace C_{18} column maintained at 50°C. The isocratic mobile phase consisted of TFA containing ACN and water with a flow rate of 1.5mL/min. The method exhibited good linearity over the assayed concentration range and good intra- and inter-day precision. The developed HPLC method is accurate and selective for RHT analysis with good detection and quantification limits and is suitable for its intended use. This stability indicating analytical method can be adapted easily to analyse RHT from pharmaceutical finished products and biological matrices.

Chapter 4 Formulation Development and Characterisation

4.1 Introduction/Overview

RHT has demonstrated significant improvement of patient's cognitive and behavioural symptoms (Finkel, 2004; Grossberg, 2005; Shah *et al.*, 2015). Present RHT therapy is associated with severe cholinergic side effects because of the high and frequent dosing of the drug to compensate/counteract its (i) low bioavailability (36%), (ii) short half-life (one hour), and (iii) restricted entry into the brain due to its highly water soluble (80mg/mL) property (Tamai & Tsuji, 1996; Fazil *et al.*, 2012). Many approaches have been proposed to assist hydrophilic drugs to cross the BBB including physical and chemical modification of the BBB and use of targeted DDS such as liposomes and NPs. Each technique has its own benefit and limitations which are described in the Chapter 1, Section 1.3. However, polymeric NPs has unique advantage of being small in size and having the capability of being grafted with targeting ligand(s) or made of desired surface properties. Also, they can be made from biocompatible and biodegradable materials such as PLGA. Furthermore, NPs can be used for carrying both hydrophilic and lipophilic molecules and for controlled release of therapeutic molecules. Thus, RHT-loaded polymeric NPs with targeting ligand(s) can be a promising technique to improve the RHT treatment of AD (Joshi *et al.*, 2010; Shah *et al.*, 2015).

In this chapter, a novel dual ligand NPs formulation was developed and optimised as a platform technology for delivering drugs to the brain. RHT was selected as a model drug to test the formulation. The NPs were characterised by their morphology, particle size, size distribution, surface charge, EE and DL. Nano-sized particles with high RHT loading were successfully produced following optimisation of formulation factors. *In vitro* drug release of the formulations was performed and the data were analysed using kinetic models to understand the drug release mechanism. Also, two lipophilic tracers called 1,1'-dioctadecyl-3,3,3',3'-tetramethylindodicarbocyanine (DiD) and coumarin-6 were loaded independently in the optimised NPs systems for cellular investigations, which are described in further chapters.

4.2 Materials

EtAc (Cat. # E/0900/17) and DCM (Cat. # D/1856/17) were obtained from Thermo Fisher Scientific (Scoresby, Australia). RHT (Cat. # IC-CS-146-0-140108, 99.2%) was procured from Innochem Technology Co. Ltd. (Beijing, China). PBS (Cat. # P3813), vitamin E-TPGS (Cat. # 57668), coumarin-6 (Cat. # 442631, ≥ 98%), Pluronic® F127 (Cat. # P2443), PVA (Cat. # 360627), Resomer® RG 502H (acid terminated PLGA, Cat. # 719897, MW=7-17 kDa, PLA/PGA ratio of 50/50) and Resomer® RG 503H (acid terminated PLGA, Cat. # 719870, MW=24-38 kDa, PLA/PGA ratio of 50/50) were purchased from Sigma-Aldrich (Castle Hill, Australia). High MW PLGA (Purasorb® PDLG, MW=110 kDa) was purchased from Corbion Purac Biochem BV (Gorinchem, Netherlands). Low MW acid terminated PLGA (Cat. # B6013-1, intrinsic viscosity 0.19 dL/g, number-average MW ~3.5 kDa), with a 50/50 ratio (PLA/PGA) was supplied as LACTEL Absorbable Polymers (Durect Corporation, Birmingham, USA). 1,2-distearoyl-sn-glycero-3-phosphoethanolamine-N-[methoxy (polyethylene glycol)-5000] (DSPE-mPEG, Cat. # PG1-DS-5k) was obtained from Nanocs (Boston, USA). SA-ODA conjugate was synthesised (Chapter 2) from SA (Cat. # A2388) and ODA (Cat. # 305391), both of which were purchased from Sigma Aldrich (Castle Hill, Australia). DSPE-PEG-TAT conjugate was also synthesised (Chapter 2) from DSPE-PEG-NHS (Cat. # PG2-DSNS-2k) purchased from Nanocs (Boston, USA) and TAT peptide was custom-synthesised by GL Biochem Ltd (Shanghai, China). DiD (Cat. # D7757) was obtained from Life Technologies Australia Pty Ltd (Scoresby, Australia).

4.3 Methods

4.3.1 Preparation of PLGA NPs

The most important factor that determines the NPs preparation technique for a drug is the physicochemical properties of the drug itself, especially its hydro- and lipophilicity (Olivier, 2005; Lu *et al.*, 2014; Sharma *et al.*, 2016b). Our model drug, RHT, has both hydrophilic and lipophilic characters making it challenging to select the best NPs preparation method (Figiel & Sadowsky, 2008; Kurz *et al.*, 2009). To address the problem, two techniques were investigated for NPs preparation, namely solvent evaporation method, and double emulsion solvent evaporation method. In addition, post loading method was also investigated for RHT incorporation in NPs.

Briefly, in the solvent evaporation method, an O/W emulsion was prepared first with the organic phase containing polymer matrix and the drug. NPs was solidified by evaporation of the organic solvent. In the double emulsion solvent evaporation method, a primary W/O emulsion was prepared first where the water phase contained the drug. This was further emulsified in water containing stabiliser to obtain the final W/O/W emulsion. The organic solvent was then evaporated to produce NPs. In the post loading method, empty NPs were first prepared using O/W method. The NPs were then incubated with a concentrated drug solution at 37°C with agitation to facilitate migration/absorption of the drug into the empty NPs by the simple diffusion process.

Three types of NPs were prepared varying the number of grafted ligands on the NPs surface. The full composition of the NPs is given in Table 4.1.

Table 4.1. Formulation of different types of NPs according to ligand incorporation.

NPs type	**Formulation**			
	Core polymer (PLGA)	**PEGylated**	**Ligand 1 (SA)**	**Ligand 2 (TAT peptide)**
1	√	√	-	-
2	√	√	√	-
3	√	√	√	√

In the following sections, the PLGA NPs preparation methods are discussed in details:

4.3.1.1 NPs by Oil-in-Water (O/W) Method

The basis of this technique is to prepare a nano-emulsion of oil in water where the oil phase contains the drug. Mainly lipophilic agents are loaded into the NPs by this method (Vauthier & Bouchemal, 2009; Khadka *et al.*, 2014). The general procedure for preparation of NPs by O/W method is described here. Specific names and concentrations of the components in the final NPs preparation are discussed in the NPs optimisation sections (sections 4.3.2 and 4.4.1).

Firstly, a 4mL stabiliser solution (water phase) was placed in a 13mL test tube and 2mL organic solvent containing the ligands, DSPE-mPEG, PLGA and drug (oil phase) was added dropwise at a rate of about 0.5mL per minute to the stabiliser solution while it was under vortex. The vortexing was continued for an extra 15 seconds after the addition was completed. The content was sonicated using a 200-watt direct immersion probe sonicator (UP200S with an S7 sonotrode, Hielscher Ultrasonics GmbH, Teltow, Germany) on an ice bath for 2 minutes at 20% amplitude (40 watts) and 0.4 cycles per minute. The resulting emulsion (Figure 4.1, left) was then transferred completely by rinsing into a 500mL RBF and the organic solvent was evaporated under reduced pressure using a rotary evaporator (Büchi Rotavapor R-200, Flawil, Switzerland) at 50°C and rotation speed of 100 rpm. The suspension was centrifuged using an Avanti-JE centrifuge and JA-20 rotor (Beckman Coulter, Inc., Indianapolis, USA) at 17,000g speed for 30 minutes at 4°C and the sediment redispersed in Milli-Q water. The supernatant was used to determine the drug EE and DL while the NP suspension was stored at 4°C and all experiments were conducted within next 7 days. Prior to commencing any experiment, an aliquot from this NP suspension was further centrifuged using a Microfuge® 16 centrifuge (Beckman Coulter, Inc., Krefeld, Germany) at 16,000g for 5 minutes. The supernatant was analysed to determine the exact drug loading at the start of any studies that were conducted after resuspending the NPs in the medium as per individual protocol.

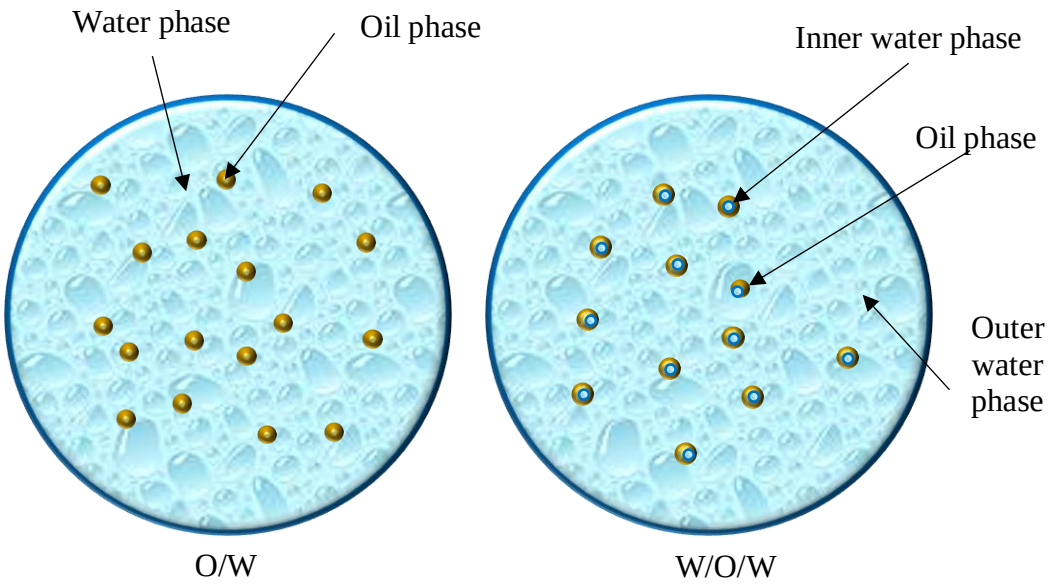

Figure 4.1. Illustration of O/W and W/O/W emulsion system.

4.3.1.2 NPs by Water-in-Oil-in-Water (W/O/W) Method

This method is comprised of three main steps – (a) preparation of a primary emulsion of water in oil where the water phase contains the drug, (b) preparation of the final emulsion (W/O/W) by further emulsifying the primary emulsion with water, and (c) evaporation of the organic solvent to form the NPs by solidification of emulsion droplet. Mainly hydrophilic agents are loaded into the NPs by this method (Vauthier & Bouchemal, 2009; Khadka *et al.*, 2014). Below is a general procedure for preparation of NPs by W/O/W method.

Firstly, a 3-mL solution of the ligands, DSPE-mPEG and PLGA dissolved in EtAc (oil phase) was transferred to a 13mL test tube under vortex. The aqueous phase (0.5mL) containing the drug (inner water phase) was added dropwise (~0.5mL min^{-1}) to the oil phase. Vortexing was continued for an extra 15 seconds after the addition was completed. The content was sonicated using a probe sonicator in an ice bath for 2 minutes at 20% amplitude (40 watts) and 0.4 cycles per minutes. The resulting primary emulsion was then transferred to a 20mL glass vial containing 15mL stabiliser solution (outer water phase) and immediately sonicated using the probe sonicator in an ice bath for 2 minutes at 60% amplitude (120 watts) and 0.4 cycles per minutes.

Final emulation (Figure 4.1, right) was transferred to 500mL RBF and the organic solvent was evaporated under reduced pressure using rotary evaporator at 50°C and rotation speed of 100 rpm. The suspension was centrifuged at 17,000g at 4°C for 30 min and the sediments were redispersed in Milli-Q water. The supernatant was used to determine the drug EE and DL while the NP suspension was stored at 4°C and all experiments were conducted within next 7 days. Prior to commencing any experiment, an aliquot from this NP suspension was further centrifuged using Microfuge® 16 centrifuge at 16,000g for 5 minutes. The supernatant was analysed to determine the exact drug loading at the start of any studies that were conducted after resuspending the NPs in the medium as per individual protocol.

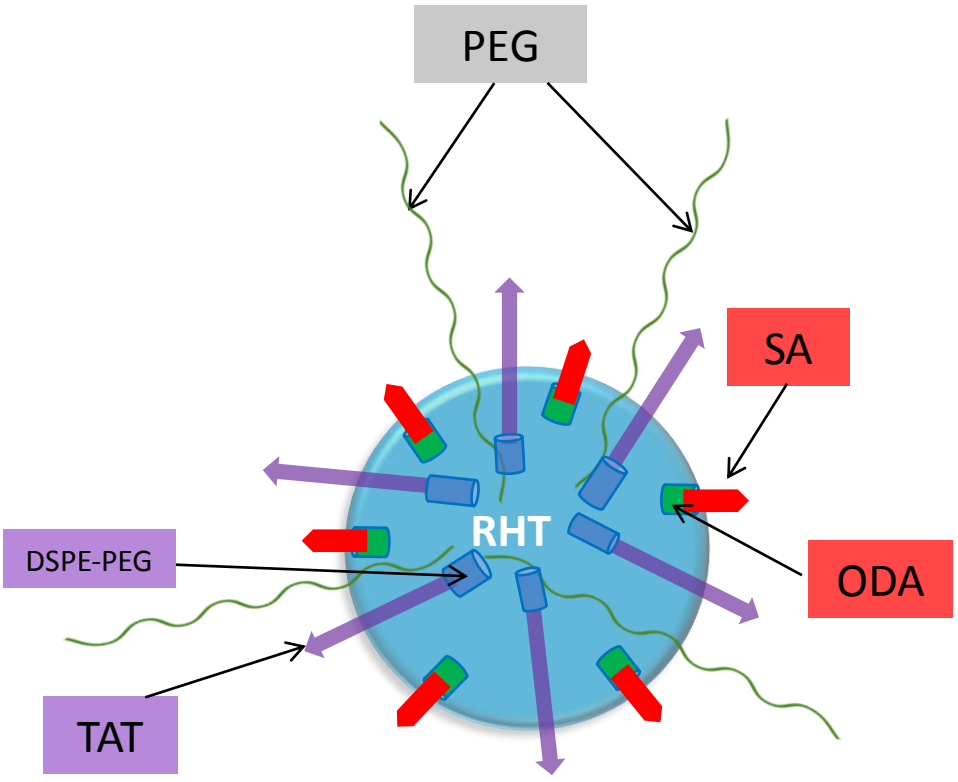

Figure 4.2. Illustration of RHT-loaded PEGylated NPs with dual ligands – (i) SA and (ii) TAT peptide.

4.3.1.3 NPs by Post Loading Method

Although not extensively used, the post loading method of NPs preparation is reported to be very promising (Wang *et al.*, 2011). This technique mainly uses the passive diffusion capability of the drug in the core polymer. As RHT possess both lipophilic and hydrophilic properties, the post loading technique was investigated.

Blank NPs was prepared using O/W method discussed above without any drug. After the solvent evaporation and centrifugation steps, the supernatant was replaced by the RHT solution (2mg drug in 4mL in water). After resuspending the blank NPs, the suspension was shaken on an Orbit Shaker (Model 3519, Lab-Line Instruments, Inc., Melrose Park, IL, USA) for 1 hour at 37°C. Then, the suspension was centrifuged at 17,000g speed for 30 min at 4°C and redispersed in Milli-Q water. The NP suspension was stored at 4°C and all experiments conducted within 7 days of preparation.

4.3.2 Optimisation of NPs formulation

The procedure for NPs formulation optimisation involved assessment of factors outlined in Table 4.2. In each case, the best setting was carried over for optimising the next factor. To minimize the cost, optimisation of NPs formulation was conducted without ligands and DSPE-mPEG. Only optimum PLGA formulation was then used for incorporation of dual ligands with DSPE-mPEG. The methods used for formulation are described in the following sections.

Table 4.2. Overview of the formulation factors examined.

Optimisation Step	Factors optimised						
	PLGA		Drug		Stabiliser type and conc. (% w/v)	Organic solvent	Preparation method
	MW (kDa)	Conc. (mg/mL)	Type	Amount (mg)			
Salt vs. free base (RHT vs. RV)			RHT, RV				
Organic solvent						DCM, EtAc	
Preparation method							O/W, W/O/W, modified W/O/W, post loading
PLGA MW	3.3, 7-17, 24-38, 110						
Stabiliser type & concentration					PVA - 0.6%, 1.0% Pluronic - 0.5%, 1.0% Vit E-TPGS - 0.3%, 1.0%		
PLGA conc.		10, 15, 20, 25, 30					
Drug polymer ratio				5, 10, 20, 30, 40			

RHT represents rivastigmine tartrate salt whereas RV represents the free rivastigmine base.

4.3.2.1 Effect of Rivastigmine Ionic Forms

The model drug was purchased as rivastigmine tartaric acid salt and a portion was converted into rivastigmine base (RV). Incorporation of both RV (6.25mg) and RHT (10mg) in PLGA NPs, using both O/W and W/O/W method (section 4.3.1.1 and 4.3.1.2), with Purasorb® PDLG as the core polymer and 0.6% (w/v) PVA as the stabiliser, was investigated. The particle size, polydispersity index (PDI) and % DL were compared to select the best combination.

Conversion of RHT salt to RV base

400mg RHT salt was dissolved in 10mL water and few drops of potassium carbonate solution (2M) added to the solution to raise the pH to above 10. The free RV base was extracted for 4-5 times with 5-10mL DCM every time until the aqueous phase was completely clear. Collected DCM was concentrated using rotary evaporation (50 rpm, 40°C, ~10 min) and transferred into two pre-weighed 4mL vials. The oily RV base was obtained after overnight removal of the residual solvent at 30°C under vacuum. ^{1}H NMR and HPLC were performed to confirm the identity and structural integrity of the drug.

4.3.2.2 Effect of Organic Solvent

Both DCM and EtAc have been used as organic solvents in the NPs preparation. We compared these two organic solvents in terms of their boiling points, solubility of RHT salt in the solvents and particle size of the prepared NPs. W/O/W method was used to prepare the NPs using 30mg Purasorb® PDLG as the core polymer, 10mg RHT salt as drug and 0.6% (w/v) PVA as stabiliser. The particle size, PDI and % DL were compared to determine the organic solvent of choice.

4.3.2.3 Effect of NPs Preparation Technique

The best preparation technique was determined by preparing NPs with O/W, W/O/W, modified W/O/W and post loading methods (Section 4.3.1). In the modified W/O/W method, stabiliser was included in both aqueous phases. EtAc was used as the organic phase, 30mg Purasorb® PDLG as the core polymer, 10mg RHT salt or 6.25mg RV base as drug and 0.6% (w/v) PVA as stabiliser. The particle size, PDI and % DL were compared to determine the preparation method of choice.

4.3.2.4 Effect of Polymer MW

The polymer MW and physical properties (like viscosity) vary with their chain length. In NPs preparation, PLGA with a wide range of MW has been used and reported (Costantino *et al.*, 2005; Joshi *et al.*, 2010; Tahara *et al.*, 2011; Tsai *et al.*, 2011; Averineni *et al.*, 2012). In our laboratory, four PLGA co-polymers were tested to determine the best polymer for our drug (see Table 4.3). All polymers had different MW but consisted of same ratio (50:50) of lactide and glycolide groups. The NPs were prepared by modified W/O/W method using EtAc as the organic solvent, 30mg PLGA (of various MW) as core polymer, 10mg RHT salt as drug and 0.6% (w/v) PVA as stabiliser. The particle size, PDI and % DL were compared to find out the optimal polymer MW.

Table 4.3. The different types of PLGA polymers used with their corresponding supplier, MW and terminal group.

Name of polymer	Supplier and address	MW	Terminal group
Durect® PLGA	Durect Corporation, Birmingham, USA	3.3 kDa	Acid terminated
Resomer® RG 502H	Sigma-Aldrich, Castle Hill, Australia	7-17 kDa	Acid terminated
Resomer® RG 503H	Sigma-Aldrich, Castle Hill, Australia	24-38 kDa	Acid terminated
Purasorb® PDLG	Corbion Purac Biochem BV, Gorinchem, Netherlands	110 kDa	Ester terminated

4.3.2.5 Effect of Stabiliser

PVA is a widely-used stabiliser in NPs preparation but must be removed very carefully from the formulation to minimise its toxic effects (Sahoo *et al.*, 2002). However, there is a minimum amount of PVA that has to remain in the formulation for maintaining NPs stability. To overcome this problem, an alternate stabiliser was sought: PVA, Pluronic® F127 and vitamin E-TPGS were tested. The NPs were prepared by modified W/O/W method using EtAc as the organic solvent, 30mg Resomer® RG 503H as core polymer, 10mg RHT salt as drug and two concentrations of PVA, Pluronic® F127 or vitamin E-TPGS as stabiliser. The particle size, PDI and % DL were compared to determine the optimal type and concentration of stabiliser.

4.3.2.6 Effect of Polymer Concentration

Polymer quantity also plays an important role in the NPs preparation technique, determining the particle size and drug loading capacity. To determine the optimum PLGA concentration, several batches of NPs were prepared by modified W/O/W method using EtAc as the organic solvent, Resomer® RG 503H (30, 45, 60, 75 or 90mg) as core polymer, 10mg RHT salt as drug and 0.3% vitamin E-TPGS as stabiliser. The particle size, PDI and % DL were compared to determine the best polymer concentration.

4.3.2.7 Effect of Drug Polymer Ratio

The amount of drug required to achieve optimum DL was determined by making several batches of NPs with different amount of drug while keeping all other parameters constant. Briefly, NPs were prepared by modified W/O/W method using EtAc as the organic solvent, 60mg Resomer® RG 503H as core polymer, RHT salt (5, 10, 20, 30 or 40mg) as drug and 0.3% (w/v) vitamin E-TPGS as stabiliser. The particle size, PDI and % DL were compared to determine the best drug polymer ratio.

4.3.2.8 Effect of Sonication Settings

The primary emulsion (W/O) was prepared into a 13mL test tube following a published method (McCall & Sirianni, 2013). The minimum power of the available probe sonicator (40 watts) was used to avoid loss of content by excessive agitation. The cycle setting was kept at 0.4 cycles/min to avoid unnecessary heat production. The sonication time was optimised by studying the effect of sonication time on primary emulsion formation, and checking the stability of both the emulsion and drug over 30 minutes.

A similar exercise was conducted to determine the sonication time for preparation of the secondary emulsion (W/O/W). However, because this step was carried out in a 20-mL glass vial, it was assumed that it would require higher wattage setting to deliver enough power to sonicate the mixture homogeneously. So, the cycle setting and time of sonication were kept identical as the previous step for method simplicity and power was gradually raised from 40 to 160 watts. The optimised power setting was selected by observing the final emulsion stability for 30 minutes.

4.3.3 Preparation of Dual Ligand PLGA NPs

Two ligands (SA-ODA and DSPE-PEG-TAT) and the PEG chain (DSPE-mPEG) were incorporated in the optimised NPs system to prepare PEGylated dual ligand PLGA NPs. The AD model drug, RHT as well as two lipophilic fluorescent tracers (DiD or coumarin-6) were incorporated independently. The preparation methods are briefly discussed here:

4.3.3.1 Preparation of PEGylated Dual Ligand RHT-loaded NPs

The PEGylated dual ligand RHT-loaded NPs was prepared using modified double emulsion solvent evaporation method comprising of three main steps - (i) preparation of a primary emulsion of water in oil where water phase contains RHT, (ii) preparation of the final emulsion (W/O/W) by further emulsifying the primary emulsion with water containing stabiliser, and (iii) evaporation of the organic solvent to form the NPs by solidification of emulsion droplet. The procedure below was followed for the NPs preparation-

- 4mg SA-ODA was dissolved in 150µL ethanol (100% v/v) whereas 4mg DSPE-PEG-TAT and 4mg DSPE-mPEG were dissolved in 150µL chloroform. These two solutions were rinsed and mixed with 3mL EtAc. Finally, 50mg PLGA (Resomer® 503H) was dissolved in it to obtain the complete organic phase.
- 30mg RHT was dissolved in 0.5mL 0.3% (w/w) vitamin E-TPGS solution to obtain the inner aqueous phase.
- The organic phase containing the ligands, DSPE-mPEG and PLGA was transferred to a 13mL test tube under high vortex. The inner aqueous phase containing the drug was added dropwise (~0.5mL min^{-1}) to the oil phase.
- Vortexing was continued for an extra 15 seconds after the addition was completed. The content was sonicated using a probe sonicator in an ice bath for two minutes at 20% amplitude (40 watts) and 0.4 cycles per minutes.
- The resulting primary emulsion was then transferred to a 20mL glass vial containing 15mL 0.3% (w/w) vitamin E-TPGS solution (outer aqueous phase) and immediately sonicated using the probe sonicator in an ice bath for two minutes at 60% amplitude (120 watts) and 0.4 cycles per minutes.

- Final emulation was transferred to 500mL RBF and the organic solvent was evaporated under reduced pressure using rotary evaporator at 50°C and rotation speed of 100 rpm.
- The suspension was centrifuged at 17,000g at 4°C for 30 min and the sediments were redispersed in 5mL Milli-Q water. The supernatant was used to determine the drug EE and DL while the NP suspension was stored at 4°C and all experiments were conducted within next 7 days.
- Immediately before commencing any experiment, the NP suspension was centrifuged again using Microfuge® 16 at 16,000g for 5 minutes to remove the supernatant and NP pellets were re-dispersed in the experimental medium. The exact drug loading in the NPs was re-calculated after analysing RHT in the supernatant.

4.3.3.2 Preparation of PEGylated Dual Ligand Dye-loaded NPs

The PEGylated dual ligand DiD or coumarin-6-loaded NPs was prepared using single emulsion solvent evaporation method comprising of two main steps - (i) preparation of an emulsion of oil in water where oil phase contains the dye, and (ii) evaporation of the organic solvent to form the NPs by solidification of emulsion droplet. The procedure below was followed for the NPs preparation-

- 0.2 mg DiD and 2mg SA-ODA was dissolved in 75µL ethanol (100% v/v) whereas 2mg DSPE-PEG-TAT and 2mg DSPE-mPEG were dissolved in 75µL chloroform. These two solutions were rinsed and mixed with 2mL EtAc. Finally, 35mg PLGA (Resomer® 503H) was dissolved in it to obtain the complete organic phase.
- In case of coumarin-6-loaded NPs, 0.2mg coumarin-6 was used in place of DiD and was dissolved directly in EtAc after dissolving both ligands, DSPE-mPEG and PLGA.
- 4mL 0.3% (w/w) vitamin E-TPGS solution (aqueous phase) was placed in a 13mL test tube and the organic phase containing the ligands, DSPE-mPEG, PLGA and the dye was added dropwise at a rate of about 0.5mL per minute to the stabiliser solution while it was under high vortex.

- The vortexing was continued for an extra 15 seconds after the addition was completed. The content was sonicated using a 200-watt direct immersion probe sonicator on an ice bath for 2 minutes at 20% amplitude (40 watts) and 0.4 cycles per minute.
- The resulting emulsion was then transferred completely by rinsing into a 500mL RBF and the organic solvent was evaporated under reduced pressure using a rotary evaporator at 50°C and rotation speed of 100 rpm.
- The suspension was centrifuged at 17,000g speed for 30 minutes at 4°C and the sediment redispersed in 5mL Milli-Q water. The supernatant was used to determine the drug EE and DL while the NP suspension was stored at 4°C and all experiments were conducted within next 7 days.
- Prior to commencing any experiment, a 1mL aliquot from this NP suspension was further centrifuged using a Microfuge® 16 centrifuge (Beckman Coulter, Inc., Krefeld, Germany) at 16,000g for 5 minutes. The supernatant was analysed to determine the exact drug loading at the start of any studies that were conducted after resuspending the NPs in the medium as per individual protocol.

4.3.4 Characterisation of PLGA NPs

The final drug-loaded PEGylated dual ligand NPs were characterised by evaluating their morphology, particle size and zeta potential, drug entrapment and loading efficiency, Differential Scanning Calorimetry (DSC) analysis and their *in vitro* release properties. The following sections describe the details of conditions under which experiments were conducted.

4.3.4.1 Freeze Drying of NPs

The RHT-loaded dual ligand PEGylated PLGA NP suspension was frozen at −80°C for a minimum of 30 minutes in a 20mL glass vial. The freeze dryer was turned on and kept running for immediate transfer of the sample. To avoid melting of the frozen content, a vial cap was promptly replaced by a small piece of aluminium foil and secured using a rubber band. A few moisture escape holes were pierced on the foil with a needle, and the vial was placed in the drying chamber of the freeze dryer. The sample was dried for 48 hrs and the final dry NPs was sealed properly and stored at −20°C for the FESEM and DSC analysis (McCall & Sirianni, 2013).

4.3.4.2 Morphology of NPs

The morphological evaluation of NPs was performed using FESEM (Zeiss, Neon 40EsB, Oberkochen, Germany). Freeze dried NPs were placed on metallic stubs with double-sided carbon tape, air-blown to remove the excess powder, and coated with approximately 3nm platinum by a sputter coater (Cressington Sputter Coater 208HR, Cressington Scientific Instrument Ltd., Watford, England) using the attached high resolution thickness controller (Cressington MTM-20, Cressington Scientific Instrument Ltd., Watford, England) before the morphological analysis.

4.3.4.3 Particle Size and Zeta Potential Analysis

The NP suspensions were diluted with Milli-Q water to 0.5mg/mL and transferred into disposable folded capillary cell (DTS1070, Malvern Instruments, Malvern, Worcestershire, UK) for both zeta potential, particle size and size distribution analysis. Samples were analysed in triplicate by using a Malvern Zetasizer Nano ZS (Malvern Instruments, Malvern, Worcestershire, UK).

4.3.4.4 Evaluation of EE and DL

The amount of drug entrapped in the NPs was calculated by the difference between the total amount of drug added to the NPs formulation and the amount of free drug remaining in the aqueous supernatant. During NPs preparation, a 50µL supernatant was collected after the centrifugation step, diluted to 10mL with mobile phase (200 times dilution) and the amount of free RHT was determined by HPLC method, whereas the amount of DiD and coumarin-6 were analysed using an EnSpire® 2300 multimode plate reader (PerkinElmer corporation, Wellesley, USA). DL and EE were calculated using the following equations:

$$\text{DL}\ (\%) = \left(\frac{\text{Amount of drug added} - \text{amount of free drug}}{\text{Weight of NP}\ \dagger}\right) \times 100$$

$$\text{EE}\ (\%) = \left(\frac{\text{Amount of drug added} - \text{amount of free drug}}{\text{Amount of drug added}}\right) \times 100$$

†Weight of the NPs was calculated as sum of the weights of drug, core polymer, ligands and DSPE-mPEG present in the corresponding formulation.

4.3.4.5 Differential Scanning Calorimetry Analysis

DSC thermograms of RHT, PLGA, a physical mixture of RHT and PLGA and freeze dried RHT-loaded PLGA NPs were obtained using a DSC8000 (Perkin-Elmer corporation, Wellesley, USA). Approximately 5 mg of each sample was weighed on the bottom aluminium pan, the top pan was added and hermetically sealed using a DSC sample pan hand crimper. DSC thermogram was recorded while heating the pan over a heating range of 50-200°C at 50°C/min temperature increment rate under a nitrogen purge. An empty hermetically sealed aluminium pan was used as the reference. Data were collected and analysed by the Pyris® software version R10.1.

4.3.4.6 *In vitro* Release of Rivastigmine from NPs

The *in vitro* release profile of RHT-loaded NPs was carried out at pH 7.4 in PBS under a sink condition. 3mL RHT-loaded NP suspension containing 1mg RHT (calculated from drug loading data) was placed in a standard RC dialysis tube, MWCO of 12 kDa (Spectra/por®-Spectrum Labs. Inc., Rancho Dominguez, CA, USA). This dialysis tube was sealed with dialysis tubing closures (Spectra/Por® Closures) and placed in a 60g glass jar containing 50mL pre-warmed PBS at 37°C. The jar was placed on an Orbit Shaker in the hot room (37°C) and horizontally shaken at 100 rpm. 1mL sample was withdrawn at 0, 15, 30 and 45 min, 1h, 1.5h, 2h, 3h, 4h, 8h and 24h. The jar was replenished with an equal volume of fresh PBS. The amount of RHT released in the release medium (PBS) was analysed by HPLC method. Drug diffusion from RHT solution was evaluated using the same protocol. All drug release study was conducted in triplicate.

To understand the drug release mechanism from the NPs, the release data was fitted in four kinetics models namely zero order, first order, Higuchi model and Korsmeyer-Peppas model (Higuchi, 1963; Korsmeyer *et al.*, 1983; Fu & Kao, 2010). For the different models, obtained release data were plotted as follows-

- zero order: cumulative % drug release *vs.* time,
- first order: log cumulative % drug remaining *vs.* time,
- Higuchi's model: cumulative % drug released *vs.* square root of time,
- Korsmeyer-Peppas model: log cumulative % drug released *vs.* log time.

4.3.5 Stability of Dual Ligand PEGylated PLGA NPs

Blank-NPs and RHT-loaded PLGA NPs without any ligand (NP-0L), with SA ligand (NP-1L), and with double ligands (NP-2L) in Milli-Q water were stored at 4°C for seven days to assess their stability. After every 24 hrs, the NPs size and zeta potential were measured using Malvern Zetasizer. Also, during storage at 4°C, the leached amount of RHT, DiD and coumarin-6 from their NPs was investigated for seven days. Moreover, as the release study was conducted with PBS at 37°C, the HPLC spectra obtained at 24 hrs time point was observed for any degradation product to ensure that RHT was stable in the buffer at 37°C for at least 24 hrs.

4.4 Results and Discussion

4.4.1 Optimisation of NPs Formulation

RHT is a highly water soluble tartaric acid salt form of rivastigmine and has 8.0% w/v aqueous solubility at 20°C, whereas free RV base has only 0.2% w/v aqueous solubility. The O/W method is preferable for NPs preparation due to relatively smaller size of the final NPs (McClements, 2015), therefore RHT was chemically converted into RV to be used in O/W method. Conversion of RHT to RV was successful and the product yield was approximately 99% (w/w). The physical characteristics of the product matched with the Material Safety Data Sheet (MSDS) specifications (viscous, yellow liquid). ^{1}H NMR spectra (Figure 4.3 and Figure 4.4) confirmed the absence of the tartaric acid and the structural integrity of the RV base.

Preliminary trials were conducted using O/W method incorporating both RV base and RHT salt as the drug, however, neither RV or RHT could achieve satisfactory drug loading. The possible reason was probably the hydrophilicity of the drug that has also been reported by other researchers (Vrignaud *et al.*, 2011; Arpicco *et al.*, 2016). Although RV is a free base it has a solubility of about 2.04mg/mL (0.2% w/v) in the aqueous phase, which promotes drug escape resulting in very low drug loading (~0.1%). The W/O/W method using RV base also did not improve drug loading. A higher drug loading (~0.4%) was achieved with RHT, therefore, this highly water-soluble salt form (which was dissolved in the inner aqueous phase) was selected in conjunction with the W/O/W method for NPs preparation.

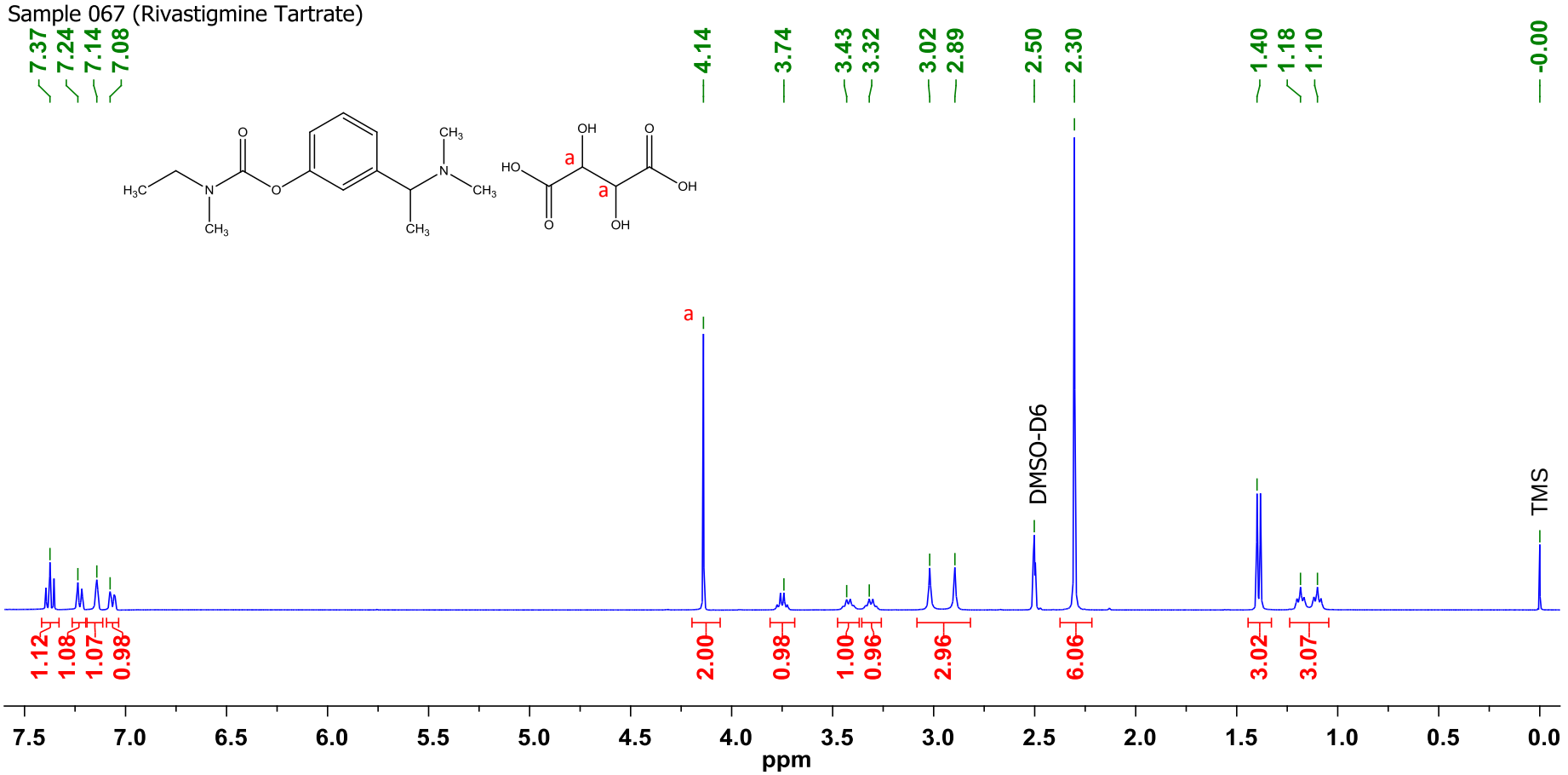

Figure 4.3. ^{1}H NMR spectra of rivastigmine tartrate salt illustrating presence of the tartrate molecule. The singlet peak at 4.14 ppm can be assigned to the two identical protons in the tartrate molecule (denoted by **a**).

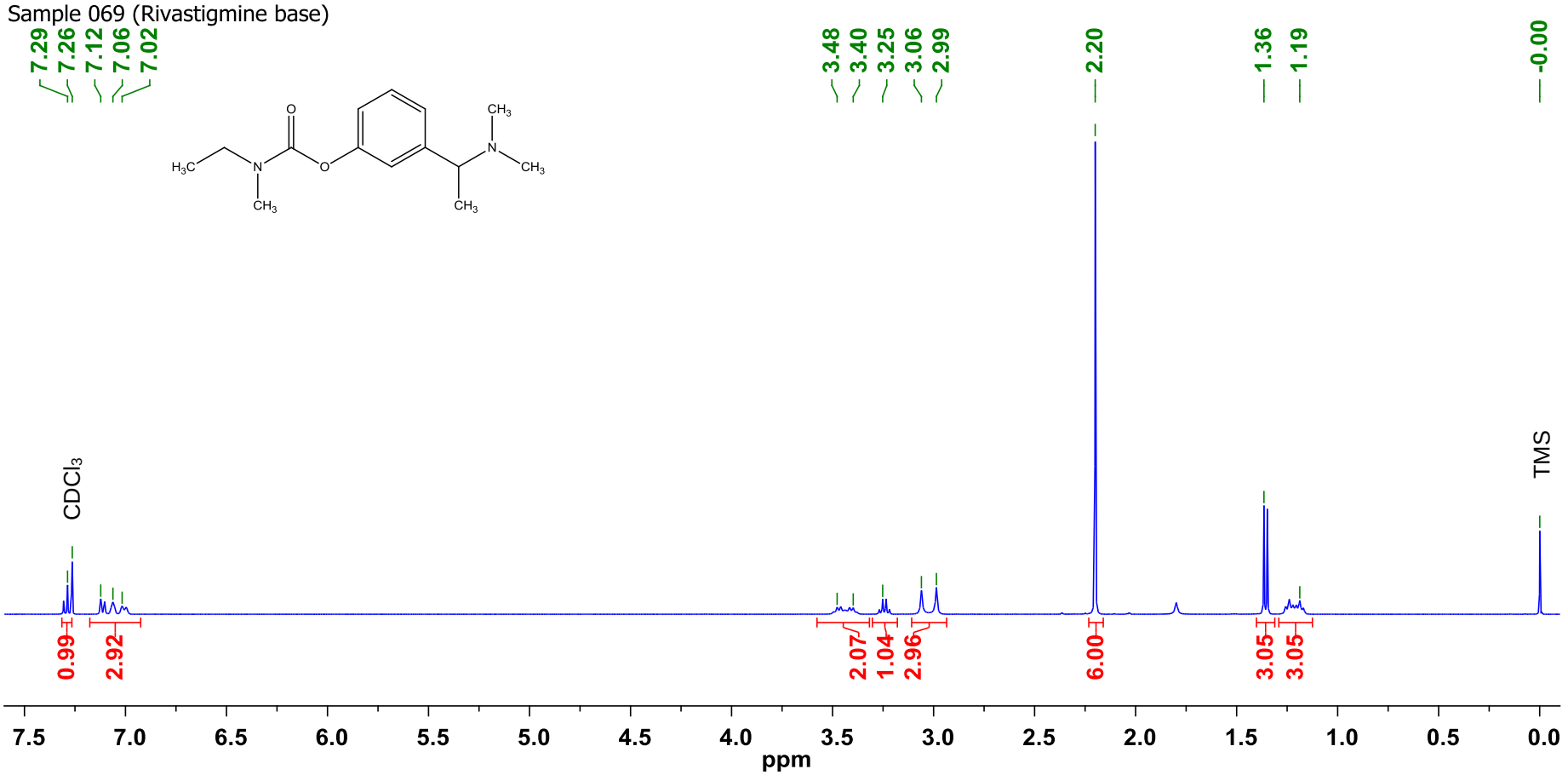

Figure 4.4. ^{1}H NMR spectra of rivastigmine base illustrating absence of the tartrate peak at 4.14ppm confirming conversion of the rivastigmine salt into free base.

For the solvent evaporation method, the low boiling point of DCM (39.6°C) favours its wide use as the organic solvent system, as it is easy to remove at low temperature with or without vacuum. EtAc has a higher boiling point (77.1°C) compared to DCM and needs approximately 50°C under reduced pressure to remove it during NPs preparation procedure. Consequently, DCM is a popular choice for the preparation of PLGA NPs and has been widely used (Astete & Sabliov, 2006; McCall & Sirianni, 2013). However, we found that using the same method and settings, swapping EtAc with DCM produced smaller particle size. This phenomenon has been reported previously, with the explanation that EtAc is miscible with water to some extent, resulting in a reduced surface tension of the polymer droplet in the primary emulsion, producing smaller NPs (McCall & Sirianni, 2013).

Subsequent experiments revealed that RHT has very low solubility in EtAc (0.2% w/v) compared to that in DCM, which is higher than 10% (w/v). The principle of the W/O/W method is to keep the drug of interest in the inner aqueous phase. Thus, the lower the solubility of the drug in the organic phase, the higher the chance that it will stay in the inner aqueous phase rather than diffuse to the outer aqueous phase. Considering these factors, EtAc was selected as the organic phase of the choice for NPs preparations.

Among all NPs preparation techniques under investigation, the post drug loading with RV produced NPs with most consistent size and % DL, with minimum batch-to-batch variation (Table 4.4). This is attributed to the simple method (mixing only) used in post-loading the drug onto naked NPs. However, the % DL of the NPs produced by post drug loading technique was too low to be considered as the optimal technique for future batch production. The O/W method, as expected and reported elsewhere (Lee *et al.*, 2000; Rosca *et al.*, 2004), was not able to entrap a satisfactory amount of drug in the NPs. The % DL in the W/O/W was approximately four times higher than that achieved by the O/W technique, however, it was still not deemed to be optimal formulation. In the modified W/O/W method, after adding the stabiliser (0.6% w/v PVA) in the inner aqueous phase, the % DL increased to about 0.8% and hence the addition of a stabiliser was chosen to be included in the technique for the future trials.

Table 4.4. Effect of preparation techniques on particle size and DL of the NPs.

Preparation technique	Drug	Particle size ± SD (nm) (n=3)	% DL ± SD (n=3)
O/W	RHT	151.9±8.2	0.1±0.03
W/O/W	RHT	166.3±6.1	0.4±0.1
*Modified W/O/W	RHT	160.1±11.6	0.8±0.1
Post drug loading	RHT	148.1±2.1	0.2±0.1
Post drug loading	RV	146.4±1.7	0.1±0.03

**a stabiliser was included with the inner aqueous phase.*
All NPs were prepared from Purasorb® PDLG; EtAc was used as the organic phase, RHT or RV (as per the table) was incorporated as the model drug and 0.6% (w/w) PVA solution was used as the stabiliser.

After finalising the ionic form of the drug, organic solvent and NPs preparation technique, optimisation of PLGA MW was undertaken. Although the ratio between the lactide and glycolide groups was the same (50:50) in the four PLGA co-polymers tested, their MW were significantly different which affected the drug loading (Table 4.5). PLGA with MW 3.3 kDa entrapped minimum amount of drug despite using the modified W/O/W method. Resomer® RG 502H achieved 1.3% drug loading, whereas, Resomer® RG 503H produced NPs with the highest drug loading of 1.5%. The high MW Purasorb® PDLG (110 kDa) produced NPs with inferior drug loading compared to the Resomer® RG 503H, hence the later was selected as the polymer of choice.

The relationship between the PLGA MW and the drug loading efficiency was reviewed previously by others. The authors concluded that usually under the same experimental conditions, higher MW PLGA polymers are generally capable of producing larger particles with higher drug loading (Dinarvand *et al.*, 2011). Our experiment results followed this pattern for the first three MW. We speculate that the higher viscosity exerted by the high MW (110kDa) PLGA polymer delayed the organic solvent removal evident by the longer time taken in the rotary evaporator. Therefore, the escape of the drug molecule to the outer aqueous phase was facilitated, as has been reported earlier (Mittal *et al.*, 2007).

Table 4.5. Effect of PLGA MW on particle size and DL of the PLGA NPs.

PLGA Polymer type (MW)	Particle size ± SD (nm) (n=3)	% DL ± SD (n=3)
Durect® PLGA (3.3 kDa)	80.3±3.4	0.4±0.1
Resomer® RG 502H (7-17 kDa)	91.4±4.2	1.3±0.2
Resomer® RG 503H (24-38 kDa)	102.6±7.1	1.5±0.1
Purasorb® PDLG (110 kDa)	160.1±11.6	0.8±0.1

All NPs were prepared using modified W/O/W method; EtAc was used as the organic phase and RHT was incorporated as the model drug and 0.6% (w/w) PVA solution was used as the stabiliser.

During the stabiliser optimisation step, we found that the physical properties and % DL of the NPs produced with PVA, Pluronic F127 and vitamin E-TPGS as the stabiliser, were similar at both high and low concentrations (Table 4.6). However, vitamin E-TPGS has some properties that can provide an advantage over the other two stabilisers under investigation. It is not only an effective and biocompatible form of vitamin E to prevent vitamin E shortage, but can also enhance the oral absorption of vitamin E, which is of benefit in the management of AD (Grundman, 2000; Mu & Feng, 2002; Morris *et al.*, 2015; Boccardi *et al.*, 2016). Therefore, unlike other stabilisers, vitamin E-TPGS does not need to be removed completely at the end of the NPs production, saving extra steps and time. Some researchers have reported NPs preparation using 0.6% (w/v) or higher of vitamin E-TPGS as a stabiliser (Sun *et al.*, 2014b; Al-Quadeib *et al.*, 2015), but our experiments did not show any significant improvement in NPs properties when compared to NPs made using 0.3% (w/v) concentration. This concentration, therefore, was selected for further NPs development.

Table 4.6. Effect of stabilisers on particle size and DL of the PLGA NPs.

Stabiliser	Conc. (w/v)	Particle size ± SD (nm) (n=3)	% DL ± SD (n=3)
PVA	0.6%	102.6±7.1	1.5±0.1
	1.0%	109.1±3.4	1.4±0.1
Pluronic® F127	0.5%	100.6±6.5	1.3±0.1
	1.0%	99.1±5.6	1.4±0.2
Vitamin E-TPGS	0.3%	96.3±2.1	1.4±0.1
	1.0%	94.3±2.6	1.4±0.1

All NPs were prepared from Resomer® RG 503H polymer using modified W/O/W method; EtAc was used as the organic phase and RHT was incorporated as the model drug.

In the next optimisation step, when polymer concentration was raised to 20mg/mL (*i.e.* 60mg), NPs with 2.1% DL was produced while other properties remained satisfactory (Table 4.7). Lowering the PLGA concentration resulted in smaller particle size, but also substantially reduced the drug loading capacity, making the DDS impractical. An increment of the PLGA concentration up to 30mg/mL did not significantly increase the DL capacity ($p > 0.05$). Moreover, the average particle size exceeded the target size of 200nm and the final NP suspension was too viscous to handle comfortably. Increasing the PLGA concentration also raised the viscosity of the organic phase, which in turn resisted the reduction of the size of oil droplets, thereby producing larger NPs (Zweers *et al.*, 2003; Sharma *et al.*, 2016b).

After determining the best solvent, drug molecular form, preparation technique, type and amount of the polymer and stabiliser, final experiments were carried out to find the appropriate polymer:drug ratio (*i.e.*, theoretical drug loading or TDL) for the NPs preparation. Higher TDL was found to elevate the NPs drug loading to a certain level, after that the loading became almost constant (Table 4.8). Thus, a 30mg drug was selected for addition to the inner aqueous phase at the beginning of the NPs preparation procedure. Although the EE is low, considering that RHT is a highly water soluble drug, 3% drug loading was considered as satisfactory. Encapsulation of a hydrophilic moiety into a hydrophobic matrix is known to be a challenging task with 1-3% DL reported previously (Govender *et al.*, 1999; Chen *et al.*, 2008a).

Table 4.7. Effect of PLGA concentrations on particle size and DL of the NPs.

PLGA in Organic phase (3mL)		**Particle size ± SD (nm)**	**% DL ± SD**
Conc. (mg/mL)	**Amount (mg)**	**(n=3)**	**(n=3)**
10	30	96.3±2.1	1.4±0.1
15	45	123.9±3.3	1.7±0.2
20	60	159.9±6.7	2.1±0.2
25	75	186.4±5.4	2.2±0.1
30	90	210.6±6.1	2.3±0.2

All NPs were prepared from Resomer® RG 503H polymer using modified W/O/W method; EtAc was used as the organic phase, RHT was incorporated as the model drug and 0.3% (w/w) vitamin E-TPGS solution was used as the stabiliser.

Table 4.8. Effect of TDL on EE, DL, particle size and zeta potential of the PLGA NPs (n=3).

PLGA (mg)	RHT (mg)	TDL (%)	EE ± SD (%)	DL ± SD (%)†	Particle size ± SD (nm)†	Zeta potential ± SD (mV)†
60	5	7.7	8.4±0.1	0.73±0.1	135.3±3.2	-31.3±1.0
	10	14.3	12.8±0.2	2.1±0.2	159.9±6.7	-26.1±3.5
	20	25.0	8.4±0.1	2.7±0.1	157.4±4.3	-29.2±3.6
	30	33.3	6.1±0.1	3.0±0.1	148.2±7.1	-26.7±2.7
	40	40.0	4.9±0.2	3.1±0.1	145.1±5.1	-28.8±4.2

†The value reported here is the mean of three measurements.
All NPs were prepared from Resomer® RG 503H polymer using modified W/O/W method; EtAc was used as the organic phase, RHT was incorporated as the model drug and 0.3% (w/w) vitamin E-TPGS solution was used as the stabiliser.

Sonication power and time had to be optimised with the change in each parameter, because any alteration of stabiliser type and amount and/or polymer type and concentration influenced the stability of the emulsion (both primary and secondary). With the optimised amount of PLGA and drug, it was found that a 2-minute sonication at 40 watts power and 0.4 cycles per minutes produced a primary emulsion that was stable for at least 10 minutes, which was sufficient to carry out the next step. This lower sonication power also helped to retain the contents within the 13mL test tube that was used for the primary emulsion preparation. A higher power produced a stable emulsion in a lesser amount of time but resulted in the loss of contents as a fine mist during the NPs preparation. Other researchers also used the lower sonication power for NPs preparation and it was also reported that higher sonication power and/or longer sonication time may even result in larger particle size due to droplet coalescence (Kaltsa *et al.*, 2014; Amin *et al.*, 2016; Lee & Cho, 2017).

The secondary emulsion was prepared in a relatively larger (20mL) container demanding more power. Keeping the cycles and time similar to the previous step, the sonication power was increased to determine the optimum level of 120 watts. These sonication settings ensured that the secondary emulsion was stable for at least 30 minutes, which was sufficient time to carry out the solvent evaporation by rotary evaporation.

4.4.2 Preparation of Dual Ligand PLGA NPs

Once the PLGA NPs formulation was optimised, we incorporated the two ligands and DSPE-mPEG to prepare PEGylated dual ligand RHT-loaded PLGA NPs. Later, the lipophilic fluorescent dyes (DiD or coumarin-6) were also incorporated separately instead of RHT to prepare - (a) PEGylated dual ligand DiD-loaded PLGA NPs, and (b) PEGylated dual ligand coumarin-6-loaded PLGA NPs. The RHT-loaded PLGA NPs were used for physicochemical characterisation whereas the dye-loaded NPs were employed in cellular characterisation of this novel DDS. The drug loading in case of the fluorescent dyes was kept only 0.5% w/w intentionally because previous studies reported that higher drug loading (> 0.7% w/w) results in fluorescence quenching and thus, should be avoided (Wagh *et al.*, 2012).

The main challenge of formulating the dual ligand NPs was the solubility issue of the ligands and PEG chain in our chosen organic solvent. Our optimised NPs formulation used EtAc as the organic phase, in which, neither of the ligands (SA-ODA and DSPE-PEG-TAT) nor the DSPE-mPEG demonstrated sufficient solubility. That is why, we decided to use co-solvents to incorporate them into our formulation. SA-ODA was dissolved in ethanol whereas DSPE-PEG-TAT and DSPE-mPEG were made into solution using chloroform. Fortunately, both ethanol and chloroform are readily miscible with each other as well as with EtAc making this formulation approach possible. The order of solvent/solute addition seemed to be crucial because clear solution was obtained only when pure EtAc was mixed with ligand containing co-solvents. On the contrary, EtAc containing PLGA were unable to produce clear solution when mixed with ethanol (containing SA-ODA) and chloroform (containing DSPE-PEG-TAT and DSPE-mPEG). So, it was decided to add the PLGA at the final step of organic phase preparation process.

The particle size, PDI, zeta potential and drug loading values of the optimised PEGylated PLGA NPs formulation (blank, loaded with RHT, DiD or coumarin-6) with or without ligands are summarised in Table 4.9.

Table 4.9. Summary of particle size, PDI, zeta potential and drug loading values of blank and drug loaded optimised PLGA NPs formulation with or without ligands (n=3).

Sl No.	Loaded drug	Preparation method	PEGylated	Ligand 1 (TAT peptide)	Ligand 2 (SA)	Particle size ± SD (nm)†	PDI ± SD†	Zeta potential ± SD (mV)†	DL ± SD (%)†
1	None	W/O/W	Yes	Yes	Yes	176.3±5.9	0.13±0.02	-23.8±3.2	N/A
2	RHT	W/O/W	Yes	-	-	128.3±3.4	0.13±0.03	-26.4±1.3	2.9±0.1
3	RHT	W/O/W	Yes	-	Yes	134.9±6.7	0.12±0.01	-28.3±2.3	2.8±0.2
4	RHT	W/O/W	Yes	Yes	Yes	139.5±3.9	0.13±0.03	-24.3±2.5	3.0±0.1
5	None	O/W	Yes	Yes	Yes	134.3±3.2	0.09±0.03	-25.4±1.2	N/A
6	DiD	O/W	Yes	-	-	110.2±5.8	0.16±0.02	-24.9±3.6	0.44±0.2
7	DiD	O/W	Yes	-	Yes	115.6±2.9	0.13±0.02	-27.6±2.5	0.46±0.2
8	DiD	O/W	Yes	Yes	Yes	120.2±3.7	0.12±0.01	-21.6±2.6	0.44±0.3
9	Coumarin-6	O/W	Yes	-	-	116.1±4.6	0.09±0.03	-23.4±1.9	0.48±0.1
10	Coumarin-6	O/W	Yes	-	Yes	114.9±6.4	0.12±0.03	-22.4±2.9	0.47±0.2
11	Coumarin-6	O/W	Yes	Yes	Yes	122.5±3.9	0.14±0.01	-22.8±3.4	0.46±0.1

† The value reported here is the mean of three measurements.
All NPs were prepared from Resomer® RG 503H polymer using EtAc as the organic solvent and 0.3% (w/w) vitamin E-TPGS solution as the stabiliser.

4.4.3 Characterisation of NPs Formulation

4.4.3.1 Morphology of NPs

FESEM images (Figure 4.5) were captured at a very low voltage (3kV) because at higher power, the particles started to deform/melt very quickly under the beam. Images of the RHT loaded PLGA NPs without any ligand confirmed that they were smooth, spherical, and mostly below 200nm, like previously reported images (Manoochehri *et al.*, 2013; Luo *et al.*, 2016).

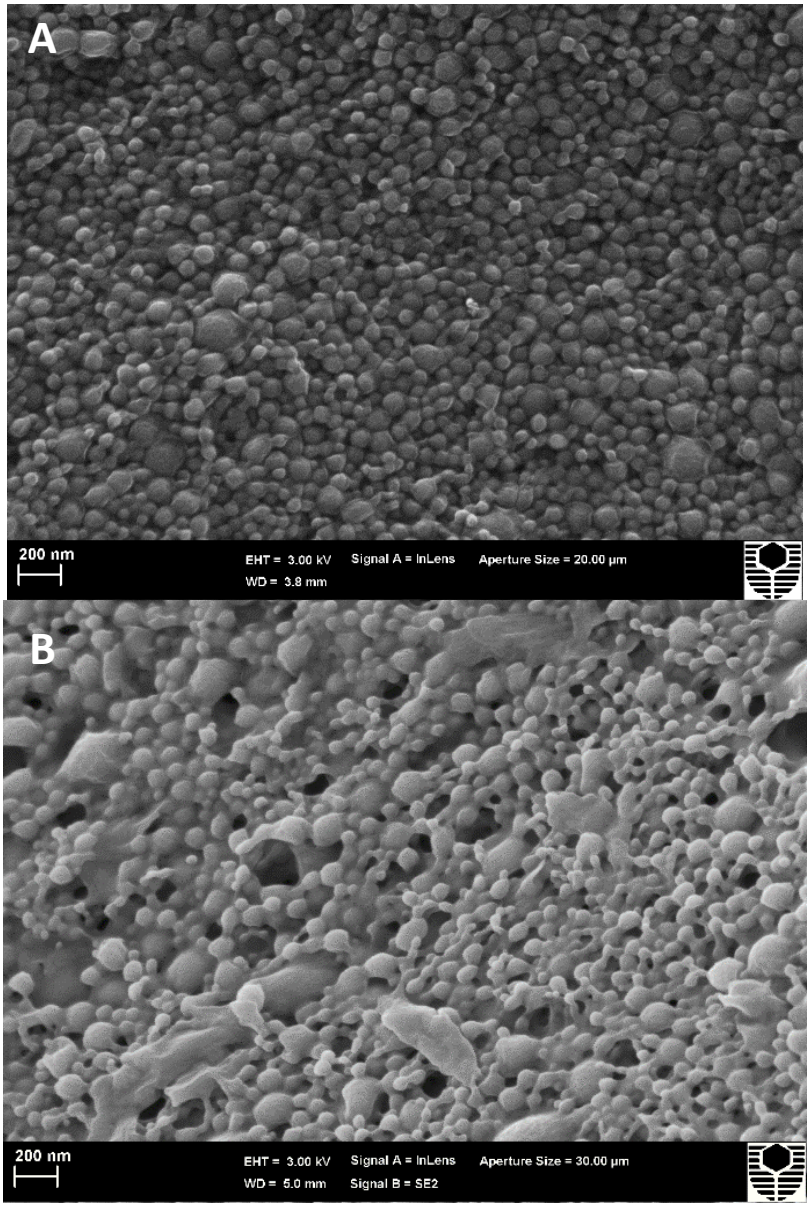

Figure 4.5. FESEM image of RHT loaded PEGylated PLGA NPs without any ligand (A) and with dual ligands (B).

However, under the same instrument setup, PLGA NPs with dual ligand showed distinct structural modifications, which suggests that the nature of the NPs surface had altered significantly due to the ligand attachments. It was also observed the deformation of dual ligand PLGA NPs occurred much quicker under the beam than that of naked PLGA NPs. This phenomenon is expected as the presence of ligands and their linkage would have modified the melting points of the core polymer, producing the irregular shape of NPs as a result of the melting process. Chen *et al.* (2011) also published their work illustrating FESEM images of PLGA NPs with ligands showing non-smooth and non-discrete particles.

Image analysis by ImageJ® software (Ver. 1.50i) confirmed that the particle size distribution is narrow (Figure 4.6) and matched the data obtained from the Malvern particle size analyser.

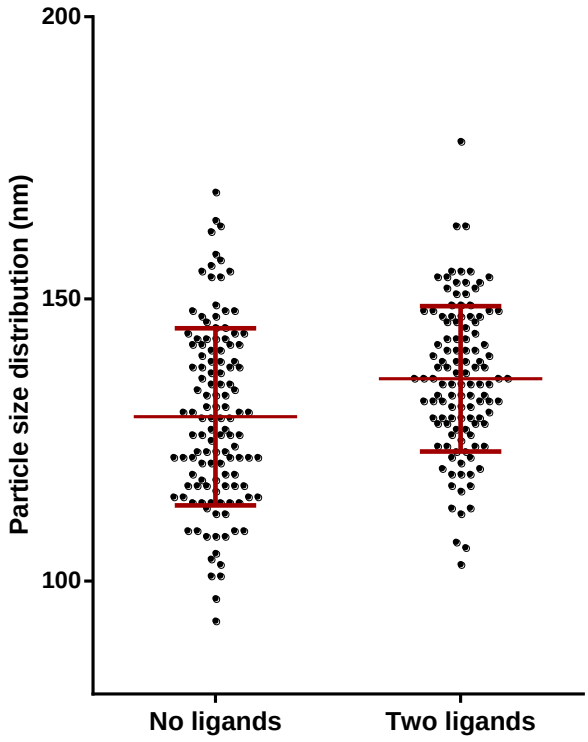

Figure 4.6. Particle size distribution of PLGA NPs.

4.4.3.2 Particle Size and Zeta Potential Analysis

The particle size and surface charge of the optimised NPs were satisfactory (section 4.4.1). The PDI of all NPs batches was below 0.2, which indicates a narrow particle size distribution. Figure 4.7 shows typical particle size distribution and surface charge spectra of RHT-loaded NPs generated by the Malvern Zetasizer. The particle size, PDI, zeta potential and drug loading values from different optimisation trials of PLGA NPs are summarised in **Error! Reference source not found.** in the Appendix IV.

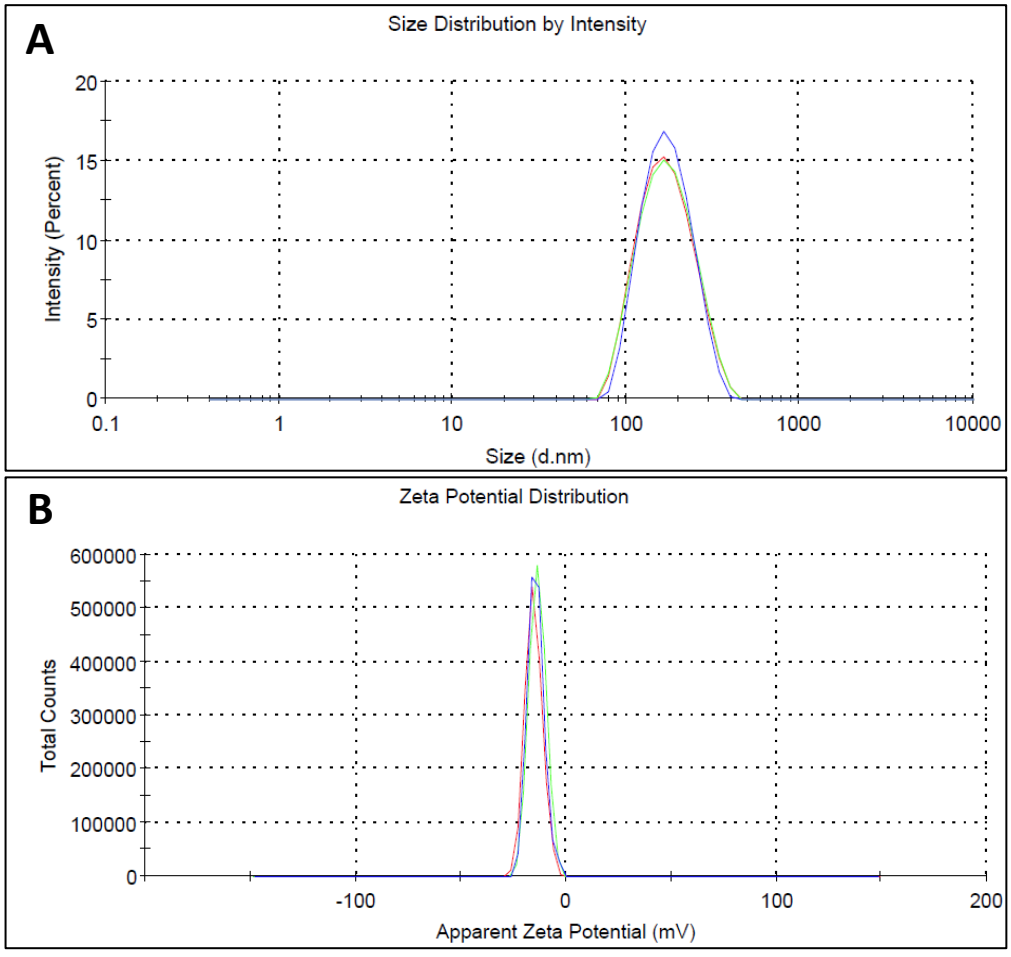

Figure 4.7. Illustration of typical particle size distribution (A) and surface charge (B) of RHT-loaded NPs.

4.4.3.3 Differential Scanning Calorimetry Analysis

Figure 4.8 illustrates the DSC thermogram of RHT, PLGA, RHT and PLGA physical mixture, and RHT loaded PLGA NPs. It can be observed that RHT has an endothermic glass transition temperature around 125°C. PLGA did not melt within the experimental temperature range as evident by the straight line which is expected for an amorphous polymer. In the physical mixture thermogram, a peak is observed at 120°C corresponding to the RHT melting point peak in its crystalline form. This peak is absent in PLGA NPs thermogram suggesting that the drug was no longer in a crystalline state, rather it was embedded in the PLGA matrix in an amorphous state. Manoochehri *et al.* (2013) also reported a similar thermogram confirming that the drug is in the matrix and not adsorbed on the particle surface.

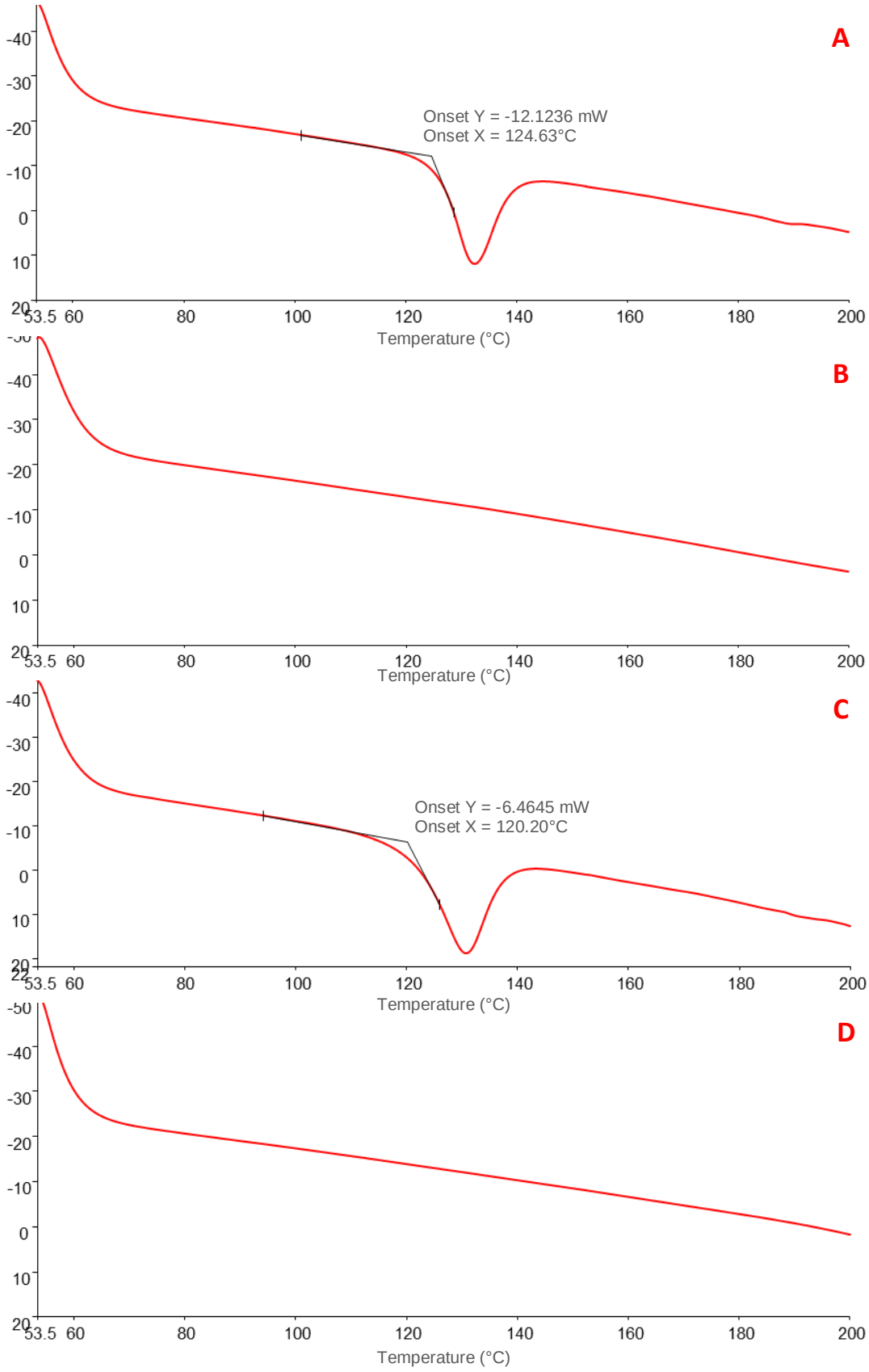

Figure 4.8. DSC thermograms of RHT (A), PLGA (B), RHT and PLGA physical mixture (C), and RHT loaded PLGA NPs (D).

4.4.3.4 *In vitro* Drug Release from NPs

Almost 50% of the encapsulated drug released from the NPs over 24 hrs (Figure 4.9). The grafting of the ligands had minimal effect on the release profile. After 24 hrs, the graph did not attain the plateau level indicating that the particles were capable of releasing more drug and can be utilised for controlled release of RHT. Other researchers also found similar release pattern for their PLGA NPs (Chen *et al.*, 2011; Fazil *et al.*, 2012). There was a small amount of burst release in the first one hour (<10%) that may act clinically as 'loading dose'. This low initial RHT release from the NPs ensures that most of the loaded drug will rely on the carrier system to cross the BBB. The *in vitro* drug release mechanism was determined using kinetics models. The developed DDS provided sustained RHT release and close to ideal drug release profile has been obtained. As expected, drug release from all NPs demonstrated best fit to the Higuchi model (Figure 4.10 and Table 4.10). It can be postulated that the release of RHT from PLGA NPs (non-swellable and non-erodible drug) occurred via permeation through pores in the matrix as well as a diffusion-governed release (Higuchi, 1963). This corresponds with published *in vitro* release data for lupeol and 2-Methoxyestradiol from PLGA NPs, which also fitted well to the Higuchi model (Cháirez-Ramírez *et al.*, 2015; Pillai *et al.*, 2017). For drug release pattern from all the NPs, R^2 values near unity were also observed for the Korsmeyer-Peppas model indicating that drug release may have occurred through a combination of swelling of polymer matrix and diffusion of the drug. This may have occurred due to the presence of PEG in the polymer matrix. The nanocarriers showed a non-Fickian release profile with slope exponent values higher that 0.5 (Table 4.10).

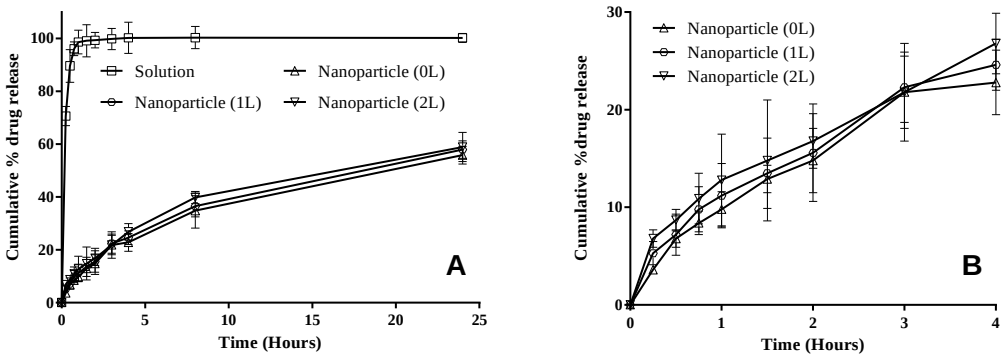

Figure 4.9. RHT release from the solution and PEGylated PLGA NPs without any ligand (0L), single-ligand (1L) and dual ligands (2L) over a 24 hrs period (A) and over first 4 hrs period (B). Error bars represent SD of three measurements.

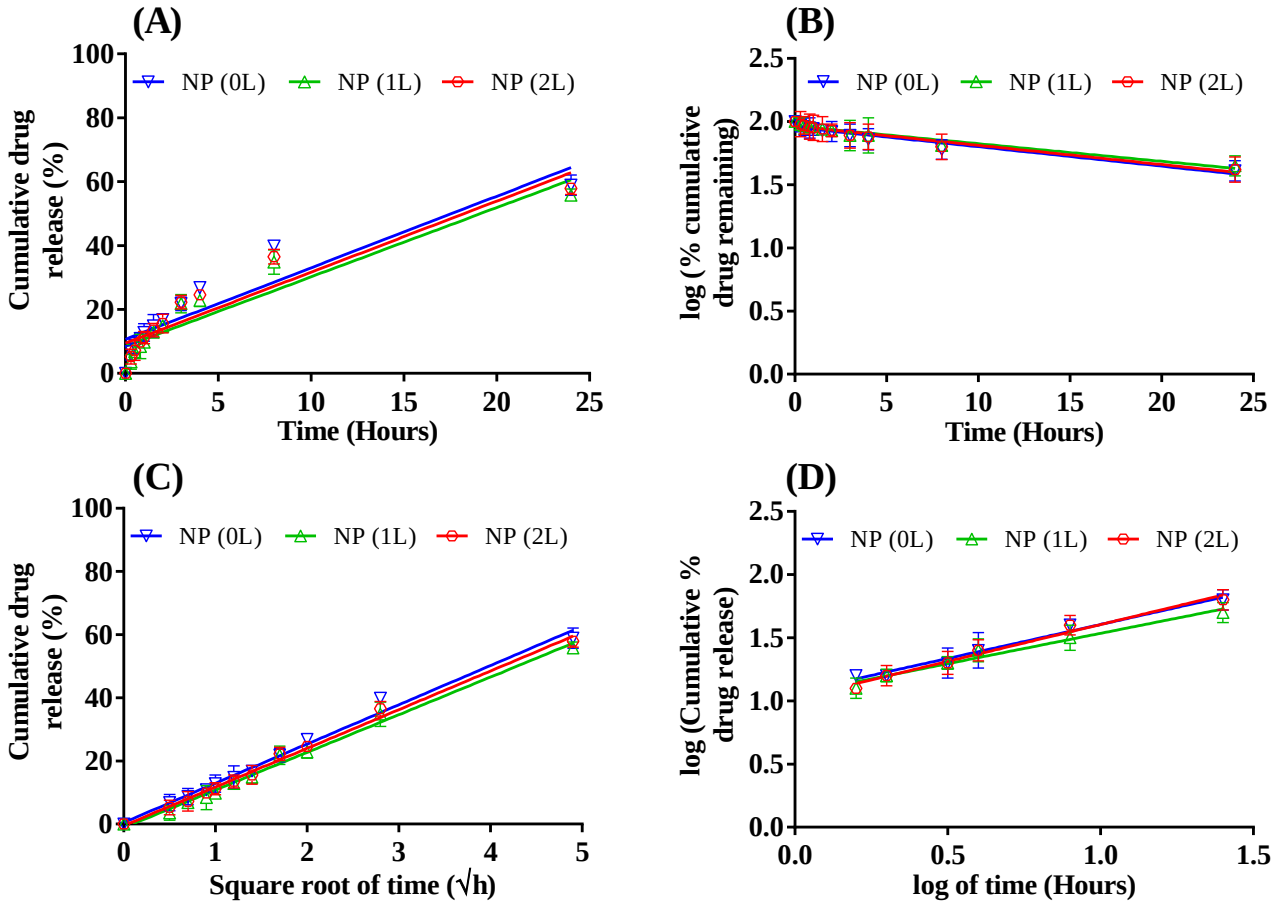

Figure 4.10. Drug release fitted to (A) zero-order, (B) first-order, (C) Higuchi model and (D) Korsmeyer-Peppas model. Error bars represent SD of three measurements.

Table 4.10. *In vitro* drug release from rivastigmine solution and rivastigmine loaded PLGA NPs formulations.

Formulation	Zero order		First Order		Higuchi model		Korsemeyer peppas model			Release type
	R^2	K_0	R^2	K_1	R^2	K_H	R^2	K_K	n	
Solution	0.0776	1.198	0.9982	-1.834	0.2459	11.057	-	-	-	-
NPs (0L)	0.8667	2.241	0.9400	-0.01541	0.9889	12.43	0.9804	0.5385	0.54	Non-Fickian
NPs (1L)	0.8843	2.169	0.9441	-0.01399	0.9916	11.93	0.9710	0.4821	0.48	Non-Fickian
NPs (2L)	0.8842	2.225	0.9532	-0.01523	0.9935	12.25	0.9801	0.5846	0.58	Non-Fickian

where, R^2 is the regression coefficient, K_0 is the zero-order release rate constant, K_1 is the first order release rate constant, K_H is the Higuchi rate constant, K_K is the cube root law release constant and n is the slope exponent.

4.4.4 Stability of RHT-loaded PLGA NPs

In the stability study of the NPs, only small variations in size and zeta potential was observed over the 7 days (Figure 4.11 and Figure 4.12). There was no significant difference was found for these data ($p > 0.05$). This indicated that the developed NPs systems were stable for at least 7 days at 4°C and all results generated by experiments conducted within that period were valid.

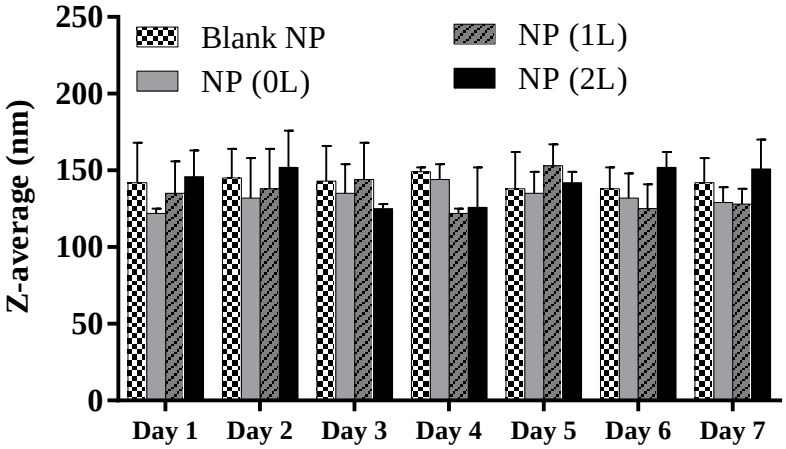

Figure 4.11. Effect of storage time (day 1 to 7) on particle size of blank NPs, RHT-loaded NPs without any ligand (NP-0L), with SA ligand (NP-1L) and with double ligands (NP-2L) in water. Experiment was conducted at 4°C. All data represent the mean ± SD (n = 3). No statistically significant differences have been found ($p > 0.05$).

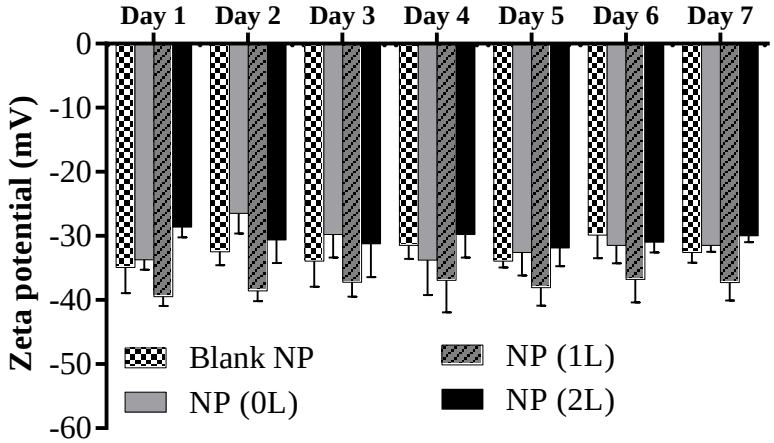

Figure 4.12. Effect of storage time (day 1 to 7) on surface charge of blank NPs, RHT-loaded NPs without any ligand (NP-0L), with SA ligand (NP-1L) and with double ligands (NP-2L) in water. Experiment was conducted at 4°C. All data represent the mean ± SD (n = 3). No statistically significant differences have been found ($p > 0.05$).

HPLC spectra from the release study (Figure 4.13) did not show any drug degradation, indicating that the drug is stable in PBS at 37°C for minimum 24 hrs.

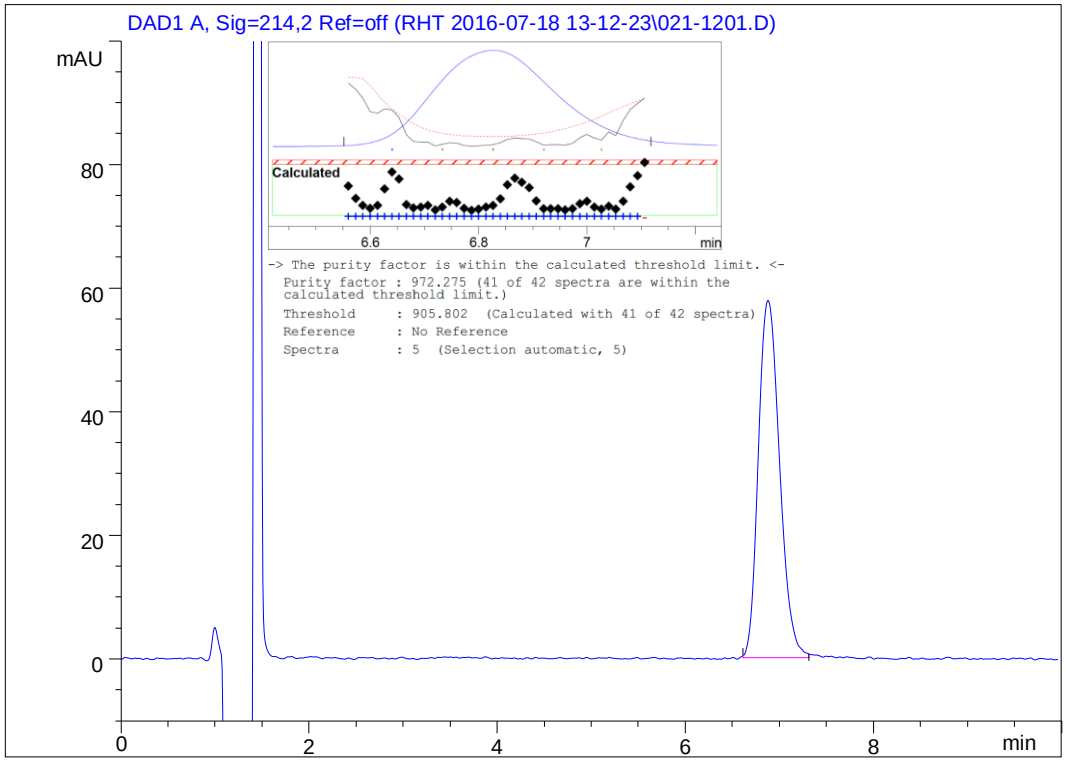

Figure 4.13. HPLC chromatogram of RHT after 24 hrs of release study showing that there is no degradation product present. Peak purity report is shown in the insert confirming that the RHT peak is pure and the purity factor is within the calculated threshold limit.

Leach study data are shown in Figure 4.14. As suspected, being a highly water soluble drug, RHT leached out of the dual ligand NPs systems about 5.5% over the 7 days' investigation. On the other hand, being a highly lipophilic molecule, only less than 0.5% w/w coumarin-6 was leached out of the NPs systems after 7 days. Previous researchers also have reported very negligible release of the encapsulated coumarin-6, only about 0.05% in 24 hrs (Alai & Lin, 2015) and only about 0.1% in 48 hrs (Davda & Labhasetwar, 2002). In similar fashion, only 0.16% w/w DiD was leached out of the dual ligand NPs formulations by the end of the experiment.

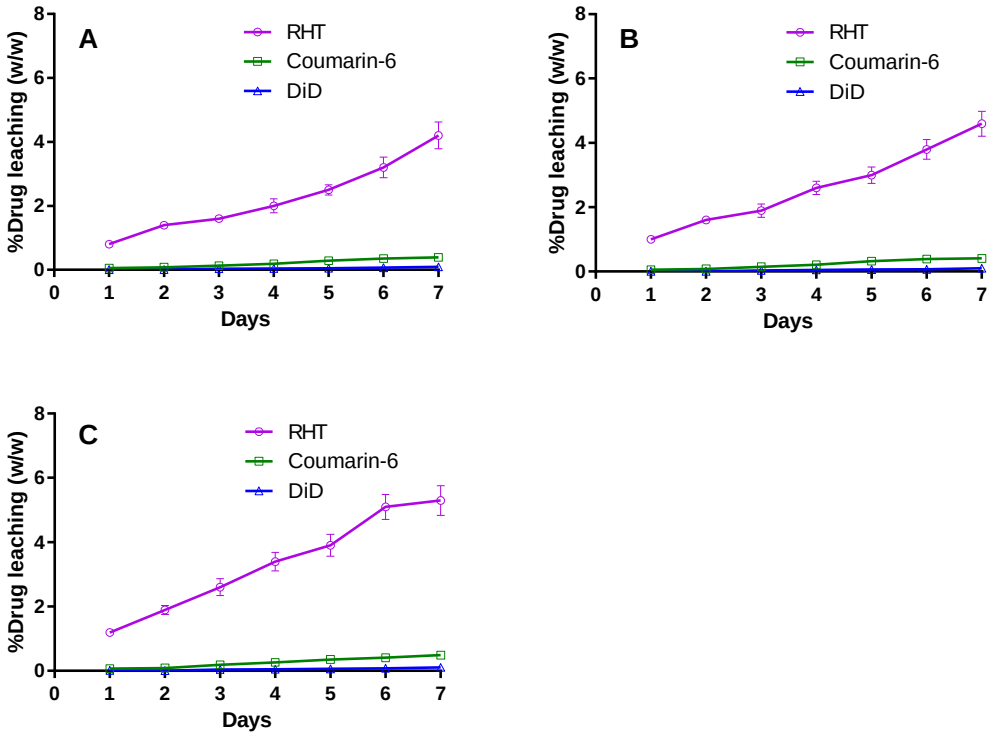

Figure 4.14. Percentage of drug leached from drug loaded PEGylated PLGA NPs without any ligand (A), with SA ligand (B), and with double ligands (C) over the period of 7 days when stored at 4°C. All data represent the mean ± SD (n = 3).

Although not very drastic changes were observed, the leaching of all three molecules were slightly lower in NPs with single ligand and lowest in case of the NPs without any ligand. The incorporation of the ligands might have introduced "channels" in the PLGA matrix that facilitated the drug leach. The drug release which was conducted at 37°C as opposed to 4°C of the stability study, also demonstrated the similar trend (Figure 4.9).

4.5 Conclusions

In this study, RHT-loaded PEGylated PLGA NPs with double ligands were prepared and optimised. Many formulation factors including the effect of type and concentration of PLGA, organic solvents, emulsion preparation techniques, type and concentration of stabilisers and energy setting during emulsification were investigated. Finally, a modified double emulsion solvent evaporation method was employed to load 3% RHT in the PLGA NPs with a particle size less than 200 nm. The resulting NPs were stable for at least seven days at 4°C with minimum alteration in particle size and zeta potential values. Drug leaching was also low in case of RHT, and nearly zero in case of DiD and coumarin-6 loaded NPs. The study demonstrated that *in vitro* release of RHT from the developed NPs system mainly followed Higuchi model kinetics. A sustained release of drug from the PLGA NPs was observed during the *in vitro* release study for 24 hrs. These results indicated that compared to RHT solution, PLGA NPs could be beneficial in sustaining RHT release for a prolonged period. Incorporation of the brain targeting ligands had minimum effect on drug release. The *in vitro* characterisation of various NPs indicated that the optimal formulation of NPs should be prepared with Resomer® RG 503H polymer, RHT and EtAc by W/O/W method incorporating vitamin E-TPGS as a stabiliser in both inner and outer aqueous phases. These NPs were selected for further investigation by cell culture work.

Chapter 5 Cellular Characterisation of Nanoparticles

5.1 Introduction/Overview

The novel PLGA NPs formulation grafted with dual ligands was developed and optimised to increase brain uptake and residence time of RHT. These PEGylated NPs were designed to administer through IV route. To exert the desired therapeutic effect, the NPs must cross the BBB and release the loaded drug. The efficiency of nanoparticulate DDS for CNS application depends on many factors including their ability to cross the BBB which involves internalisation into the endothelial cells and release of the drug into the brain parenchyma (Tosi *et al.*, 2010; Upadhyay, 2014a; Wei *et al.*, 2014).

Cellular uptake efficiency not only determines drug transport and the pharmacological efficacy of the drug but also influences the toxicity of the drug loaded NPs. For this reason, it is mandatory to study how various parameters like type of ligand, particle concentration, incubation temperature and time. affect the cellular uptake of the NPs. *In vitro* cellular study is a well-accepted preliminary screening tool for developing drug delivery platform technologies. It is preferable to perform experiments on the cells prior to animal studies which are somewhat slow, highly laborious and usually incur more expense. Depending on the route of administration and the target organ, various cell lines have been reported for studying *in vitro* cellular uptake of NPs (Gao *et al.*, 2016; Dadras *et al.*, 2017; Saneja *et al.*, 2017). The hCMEC/D3 cells, which originates from the human cerebral microvascular endothelium have been widely used for cell uptake experiment for CNS-targeted NPs. The hCMEC/D3 cell line represents an excellent *in vitro* alternative of the human BBB and forms a contact-inhibited monolayer on collagen type I or type IV (Weksler *et al.*, 2013). They are stable, easily grown and maintain a normal BBB phenotype containing endothelial markers - CD34, CD31, CD40, CD105, CD144 (VE-cadherin) and von Willebrand factor (Weksler *et al.*, 2013). Therefore, at present, the hCMEC/D3 cell line is commonly used as an *in vitro* model for assessing brain-targeted NPs uptake by the BBB (Georgieva *et al.*, 2011; Gregori *et al.*, 2016).

In addition to cell uptake, transport through barrier endothelial cells into underlying tissue is also important to characterise DDS and many *in vitro* cell models have been reported for the cellular transport studies of NPs (Chithrani *et al.*, 2010; Sharma *et al.*, 2014). It would be ideal to use either a primary or an immortalised cell line which is human CNS origin for this study. Primary human brain cells, however, are usually not the first choice because of the ethical issues and for their poor capability of TJ formation when cultured. Endothelial cells from other sources like rat, bovine, porcine are difficult to isolate and culture (Patabendige *et al.*, 2013a; He *et al.*, 2014). A few researchers used immortalised human endothelial cell lines (such as hCMEC/D3) for their cellular transport experiments. However, the reported low TEER values of their model indicated that an alternative cell line capable of producing high TEER would be more suitable for the NPs transport study (Vu *et al.*, 2009; Weksler *et al.*, 2013). TEER represents the ionic conductance across the BBB and is the most frequently used parameter to evaluate BBB integrity or TJ functionality (Srinivasan *et al.*, 2015). The human epithelial colorectal adenocarcinoma (Caco-2) cells are well known for their ability to produce very high TEER due to the formation of TJ when cultured in a monolayer for 21-25 days (Hughes & Crowe, 2010; Crowe & Keelan, 2012). This cell line offers an effective *in vitro* alternative to the human BBB. Although, it takes comparatively longer culture time than other cell lines to differentiate, Caco-2 cell line has demonstrated TEER value more than 300Ω.cm^2 compared to 30-50Ω.cm^2 reported for hCMEC/D3 (Weksler *et al.*, 2013) despite the fact that *in vivo* conditions demonstrate TEER values exceeding 1000Ω.cm^2 (Eigenmann *et al.*, 2013; Senarathna *et al.*, 2016). Also, Caco-2 cell line demonstrated expression of TJ proteins like claudin-1, occludin, and zonula occluden-1 (ZO-1) which is similar to that found in human BBB endothelial cells (Li *et al.*, 2004).

In this chapter, the novel nanoparticulate drug delivery system was evaluated through cellular characterisation on two well-established human origin cell lines. The hCMEC/D3 and Caco-2 cell lines were employed to investigate cellular uptake (both quantitative and qualitative) and transport via a tight cell monolayer.

5.2 Materials

Paraformaldehyde (PFA, Cat. # P6148, ≥94.0%), Hanks' balanced salt solution (HBSS, Cat. # H6648), high glucose Dulbecco's modified Eagle's medium (DMEM, Cat. # D5671), 4-(2-Hydroxyethyl)piperazine-1-ethanesulfonic acid (HEPES, Cat. # H3375, ≥99.5%), penicillin-streptomycin (Cat. # P4333), 4′,6-Diamidino-2-phenylindole dihydrochloride (DAPI, Cat. # D9542, ≥98.0%), fluorescein isothiocyanate labelled Phalloidin (Phalloidin-FITC, Cat. # P5282), L-ascorbic acid (Cat. # A4544, ≥98.0%), rat tail Collagen type I solution (Cat. # C3867), trypan blue (Cat. # T6146), Triton X-100 (Cat. # T8787), radio-immune precipitation assay buffer (RIPA buffer, Cat. # R0278), methyl thiazolyldiphenyl-tetrazolium bromide (MTT, Cat. # M2128, ≥98%), hydrocortisone (Cat. # 54090, ≥97.0%) and bovine serum albumin (BSA, Cat. # A2153, >96%) were purchased from Sigma-Aldrich (Castle Hill, Australia). DiD (Cat. # D7757), Pierce 660nm protein assay reagent (Cat. # 22660), MEM vitamin solution (Cat. # 11120-052), MEM non-essential amino acids solution (NEAA, Cat. # 11140-050) GlutaMAX supplement (Cat. # 35050-061), goat serum (Cat. # 16210-072), basic fibroblast growth factor (bFGF, Cat. # PHG0026) and TrypLE express enzyme (Cat. # 12604-021) were obtained from Life Technologies Australia Pty Ltd (Scoresby, Australia). Endothelial basal medium-2 (EBM-2, Cat. # 00190860) was purchased from Lonza Australia Pty Ltd (Mt Waverley, Australia). HyClone PBS (Cat. # SH30256.02) were procured from GE Healthcare Australia Pty. Ltd. (Parramatta, Australia). D-glucose anhydrous (Cat. # 783) and DMSO (Cat. # 2225) were obtained from Ajax Finechem (Taren Point, Australia). Anti-occludin primary antibody (Cat. # ab31721) and goat anti-rabbit IgG H&L secondary antibody coupled with Alexa Fluor® 488 (Cat. # ab150077) were sourced from Abcam plc. (Melbourne, Australia). Vectashield® antifade mounting medium (Cat. # H-1000) was purchased from Vector Laboratories, Inc. (Burlingame, USA). Foetal bovine serum (FBS, Cat. # FBS-001-AU) was obtained from SerANA (WA) Pty Ltd (Bunbury, Australia). Distilled water was purified from tap water by Hydro-Check Systems (Model no. 414R, Hydro-Check Systems, Inc., Carlsbad, USA) and further sterilised by autoclave at 121°C for 1 hr.

5.3 Methods

5.3.1 Cell Cultures

Caco-2 cell line was procured from the American Type Culture Collection (ATCC, Rockville, USA). hCMEC/D3 cell line was a gift from the Institut Cochin (INSERM, Paris, France). The culture details for both the cell lines are presented in Table 5.1. Cell growth, morphology and confluency were regularly monitored with a Nikon inverted microscope (Eclipse TS100, Nikon Instruments Inc., Tokyo, Japan) and images were captured with the help of the attached Nikon digital sight camera head (DS-Fi2) and controller (DS-L3). Mycoplasma were routinely tested for in the facility by genomic PCR from cells cultured in an antibiotic-free medium. Sample preparation for the mycoplasma testing is given in Appendix V.

Table 5.1. The hCMEC/D3 and Caco-2 cell culture details.

		hCMEC/D3	**Caco-2**
Cell type		Human cerebral microvascular endothelial	Human epithelial colorectal adenocarcinoma cells
Origin		Institut Cochin, INSERM, Paris, France	ATCC
Passage number		29-33	81-91
Culturing flasks (medium volume)		Corning T25 (3-5mL) Corning T75 (12-15mL)	
Culturing plates	Cytotoxicity	Nunc 96-well polystyrene plate	
	Uptake study	Nunc 24-well polystyrene plate	
	Transport study	Nunc 24-well polystyrene plate + Transwell insert	
Confocal Microscopy		Glass slides and coverslips (22mm), Ibidi micro-dish (35mm)	
Culture Medium		EBM-2	DMEM
Serum		10% (v/v) FBS - heat-inactivated at 56°C for 30 minutes before use	
Supplements		1% (v/v) P/S 1.4µM Hydrocortisone 5µg.mL^{-1} ascorbic acid 10mM HEPES 2ng.mL^{-1} bFGF - aliquots were stored at −20°C and added extemporaneously in the culture medium	1% (v/v) P/S 1% (v/v) vitamin mix 1% (v/v) NEAA 1% (v/v) glutamax
Coating of flasks/plates		Rat collagen type I	None

Both the cells were initially cultured into T25 and then into T75 cell culture flask when a large number of cells were necessary for experiments. For better cell adhesion, the hCMEC/D3 cells were seeded into flasks that were pre-coated with collagen.

5.3.1.1 Preparation of Working Collagen Solutions

Rat tail collagen type I was received as a sterile solution at a concentration of 4mg/mL in acetic acid. According to the manufacturer's instruction, its surface coverage is 6-10 μg/cm^2. So, the rat collagen was diluted 30-50 fold in sterile water and appropriate concentration and volume to cover the culture surface was added to containers (*e.g.*, 150μL for 24-well, 2mL for T25, 6mL for T75) and incubated at 37°C for at least 1 hour. The containers were washed three times with PBS to remove the free collagen and acetic acid. The PBS was aspirated and the coated flasks/plates were dried overnight under UV light inside a biosafety cabinet. Multiple flasks were collagen-coated at once and kept securely in their original package at RT maintaining their sterility for future usage.

5.3.1.2 Cell Passaging

The cell monolayer confluency instead of a fixed incubation time was used for determining the appropriate time for cell passaging. Thus, after reaching about 80-90% cell confluency for both hCMEC/D3 and Caco-2 cells, they were passaged to seed into appropriate plates for experiments and/or flasks for maintenance. The procedure followed is given below:

- Cells were washed twice with calcium and magnesium free PBS, trypsinized with TrypLE Express (1mL per T25 flask and 3mL per T75 flask) and incubated for 5-10 minutes at 37°C until most of the cells were rounded up and detached from the bottom of the flasks (visualised under a microscope).
- Medium containing FBS (twice the volume of the TrypLE Express) was added to deactivate the effect of TrypLE Express.
- The cell suspension was then centrifuged at 335g for 7 minutes using an Allegra X-12 centrifuge (Beckman Coulter, Inc., Brea, USA), the supernatant was discarded and the cell pellet was resuspended in fresh media.

- The number of viable cells was counted using haemocytometer by trypan blue exclusion method. 10µL of cell suspension and 10µL of Trypan Blue solution (0.4% w/v) were mixed well and 10µL sample was carefully loaded to haemocytometer for microscopic examination. Cells without staining were considered to be viable because trypan blue dye can only diffuse through the cell wall of dead cells.
- For maintaining the stock, cells were split at a ratio of 1:3 to 1:10 depending on the experimental schedule. A lower splitting ratio was used when a large number of cells were needed within a short period and vice versa. Approximately 10,000 to 40,000 cells/cm^2 of the cell culture flask were seeded in all experiments.
- Cells were cultured in appropriate medium (Table 5.1) at 37°C, 5% CO_2 and 95% humidified air.

5.3.1.3 Cryopreservation and Resurrection of Cells

A sterile freezing medium containing 95% FBS and 5% filter-sterilised DMSO as cryopreservant was prepared. For cryopreservation, in the final step during passaging procedure cells were resuspended in the freezing medium instead of regular medium. The suspension was then transferred into 1.8mL cryopreservation vials (Greiner bio-one, Kremsmünster, Austria) and placed in a −80°C freezer to allow controlled cooling of the vials down to −80°C. Cells were stored at −80°C if needed to be revived within next 1-4 months. For long term preservation, after being exposed to −80°C overnight, the vials were transferred into the liquid nitrogen tank.

To resurrect, the cryovials were removed from the −80°C freezer or liquid nitrogen tank and placed into a water bath (37°C) to thaw the cell suspension (~1 min). The melted cell suspension was immediately diluted into pre-warmed cell medium in a 15mL falcon tube and was centrifuged at 335g for 7 minutes to get rid of the toxic DMSO. The cell pellet was then resuspended in pre-warmed cell medium (3.5mL) and transferred in a T25 flask. The flask was incubated at 37°C temperature with 5% CO_2 in humidified atmosphere in a cell culture incubator and culture medium was replaced twice a week until the cells were ready for passaging.

5.3.2 Leaching of NPs in Culture and Assay Media

Before commencing any cellular studies, the leaching of RHT, DiD and coumarin-6 from NPs were investigated in the appropriate medium for a period of time to cover the relevant experiment durations (Table 5.2). Briefly, the transport buffer (HBSS-P) was prepared comprised of HBSS containing 10mM HEPES and 20mM glucose. Medium pH was adjusted to 7.4 using 5M NaOH. All types of NPs included in the Table 5.2 were investigated in triplicate. 2mL of the NP suspension in appropriate medium was placed in tightly closed vials and incubated for 6 hrs or 24 hrs as per Table 5.2. At the end of the incubation, the vials were removed, contents were centrifuged at 16,000g for 5 minutes. The supernatants were discarded rather than analysed because they demonstrated a high fluorescence background reading probably due to the presence of phenol red in the media. The NP pellets were dissolved in 1mL ACN and the DiD content was determined by fluorescence intensity measurement using an EnSpire® 2300 multimode plate reader (PerkinElmer corporation, Wellesley, USA) at excitation/emission wavelength of 644/664nm. The RHT content was determined using the validated HPLC method. The drug leaching was calculated indirectly by subtracting the values obtained via the above experiments from the values obtained by dissolving and analysing the same amount of fresh NPs.

Table 5.2. Leach study design for NPs showing the suspending medium, incubation time and the corresponding experiments' information. All studies were conducted at 37°C temperature with 5% CO_2 in humidified atmosphere in a cell culture incubator.

NPs type	Suspending Media	Incubation time	Experiments to cover	
			Name	Time
DiD-loaded NPs: i) without any ligand, ii) with only sialic acid (SA) ligand and iii) with both SA and TAT ligands	HBSS-P	6h	Uptake study Transport study	3h 3h
DiD-loaded NPs with both SA and TAT ligands	DMEM*	24h	Cytotoxicity study	24h
RHT-loaded NPs with both SA and TAT ligands	DMEM*	24h	Cytotoxicity study	24h
DiD-loaded NPs with both SA and TAT ligands	EBM-2*	24h	Cytotoxicity study	24h
RHT-loaded NPs with both SA and TAT ligands	EBM-2*	24h	Cytotoxicity study	24h

**See Table 5.1 for complete medium composition.*

5.3.3 Evaluation of Cytotoxicity

Different concentrations of DiD and RHT solutions, as well as DiD and RHT-loaded NP suspensions, were tested for cytotoxicity in both hCMEC/D3 and Caco-2 cell lines, at two time points (6 hrs and 24 hrs). All experimental concentrations were selected to cover the whole ranges of concentrations used in the NPs uptake and transport studies according to the literature (Degim *et al.*, 2010; Mutlu *et al.*, 2011; García-González *et al.*, 2016). A well-established MTT assay (Averineni *et al.*, 2012; Dwyer *et al.*, 2012) was employed and below is the test procedure followed:

- MTT was dissolved in PBS (pH 7.4) to obtain a stock concentration of 5mg/mL, which was 0.2µm filter-sterilized into a sterile container and wrapped with aluminium foil for light protection. See Appendix VI for detailed procedures.
- The cytotoxicity assay was initiated by seeding the cells in Nunc 96-well plates (Cat. # 167008, Thermo Fisher Scientific, Scoresby, Australia) at various seeding densities as discussed further in following sections.
- At an appropriate stage of growth in the 96-well plates, the cell medium was replaced with 200µL of appropriate prewarmed medium containing different concentrations of drug solutions or NP suspensions. For statistical validity, at least four wells were treated with each concentration of drug or NPs.
- At predetermined times (6 hrs or 24 hrs) with NPs or drug solutions, 20µL of MTT stock solution was added to the cells in culture, attaining a final MTT concentration of 0.45mg/mL, and further incubated for 3 hrs. During this time, MTT was reduced to form purple MTT formazan crystal in living cells.
- After 3h, the medium in each well was aspirated and replaced with 100µL DMSO followed by 10 minutes shaking on a Ratek platform mixer (OM6, Ratek Instruments Pty Ltd, Boronia, Australia) at 50 rpm at RT to completely dissolve the MTT formazan crystal and cell membranes.
- The quantity of formed MTT formazan crystal by the cells which is directly proportional to the number of viable cells was measured by recording absorbance at 570nm using the multimode plate reader.
- Simultaneously, wells containing NPs only without cells were used as the blank. These blank data were subtracted from each corresponding sample data to obtain the net absorbance data.

- Positive control where the cells were treated with medium only as well as negative control where the cells were treated with 2% DMSO, were also maintained always to ensure the validity of the generated data. Assays where the negative control did not demonstrate a 0% cell viability were considered as invalid.
- Percent of cell viability was calculated from the following equation:

$$\%\ Cell\ viability\ = \frac{Sample\ net\ absorbance}{Positive\ control\ net\ absorbance} \times 100\%$$

5.3.3.1 Cytotoxicity in hCMEC/D3 Cells

RHT-loaded NPs, DiD-loaded NPs, empty NPs, RHT solution and DiD solution were tested for cytotoxicity in hCMEC/D3 cells using MTT assay. All the NPs tested were PEGylated PLGA NPs containing SA and TAT ligands with or without RHT or the lipophilic tracer, DiD. The hCMEC/D3 is a fast-growing cell line, therefore, only 2000 cells per well were seeded in 96-well plates and incubated at 37°C temperature with 5% CO_2 in humidified atmosphere in a cell culture incubator using the medium described in Table 5.1. Different concentrations of drug solutions and NP suspensions were prepared in the culture media. Cell medium was replaced with 200µL of the prewarmed drug solutions or NP suspensions (in quadruplicate) after 24 hrs of seeding when the cells were about 50-60% confluent. MTT assay was performed after 6 hrs or 24 hrs using separate plates. The experiments were replicated with a later passage of the cell line and unpaired t-test was performed using the two sets of quadruplicate results. If the first two data sets were statistically different ($p < 0.05$), then another replicate was carried out.

5.3.3.2 Cytotoxicity in Caco-2 Cells

As per above, three types of NPs and two solutions were tested for cytotoxicity in Caco-2 cells using the MTT assay. The Caco-2 cell line is relatively slow growing, therefore, 5000 cells per well were seeded in 96-well plates and incubated at 37°C temperature with 5% CO_2 in humidified atmosphere in a cell culture incubator using the medium described in Table 5.1. After three days, which was enough time for the Caco-2 cells to undergo at least a full set of division, the culture medium was replaced by 200µL of the prewarmed different concentrations of the drug solutions or NP suspensions. MTT assay was performed as per the hCMEC/D3 cell line.

5.3.4 Evaluation of NPs Cellular Uptake by hCMEC/D3 Cells

Two types of study were carried out to assess the effect of different variabilities including NPs ligands, incubation temperature, incubation time and particle concentrations. on the cellular uptake of the NPs. They are – (a) the quantitative assays, which were performed using a plate reading spectrophotometer to determine the accurate amount of NPs uptake by the cells, and (b) the qualitative assay, using confocal laser scanning microscopy (CLSM) which were used for visual confirmation of the uptake phenomenon and to confirm the NPs internalisation and localisation.

5.3.4.1 Quantitative Analysis of NPs Cellular Uptake

The quantitative assay was conducted by determining the amount of NPs uptake per mg of cell protein using the procedure below (Kooijmans *et al.*, 2012):

- The cells were seeded onto a Nunc 24-well plate (Cat. # 142475, Thermo Fisher Scientific, Scoresby, Australia) coated with type-1 rat tail collagen which was prepared as per method in Section 5.3.1.1 at a density of 15,000 cells/cm^2 with EBM-2 medium with appropriate supplements (Table 5.1).
- The medium was replaced twice a week and cells were maintained at 37°C, 5% CO_2 and 95% humidified air until they become nearly confluent (3-4 days).
- The medium was removed and cells were rinsed twice with 500µL of pre-warmed HBSS-P. The cells were incubated for 30 min in HBSS-P at 37°C for equilibration.
- After 30 min, the HBSS-P was replaced with 550µL of HBSS-P containing DiD solution or DiD-loaded PEGylated NPs as per Table 5.3 at a NPs concentration of 100µg/mL.
- Immediately after application, 50µL of NP suspension was removed from the wells so that the initial NPs concentration can be determined.
- After a predetermined incubation time, the medium was aspirated (and analysed) and cells were washed quickly three times with ice-cold PBS to remove excess NPs.

- 100µL RIPA buffer was added to each well and shaken on platform mixer for 10 minutes to solubilize the cells and NPs (Eigenmann *et al.*, 2013).
- The plate was centrifuged for 5 minutes at 3200g and the supernatant was used for analysis of both cell protein and DiD content.
- *Protein analysis*: 10µL supernatant was placed in a 96-well plate and 150µL Pierce™ 660nm Protein Assay Reagent was added. The plate was incubated for 5 minutes at RT and absorbance was determined at 660nm using the plate reader. Simultaneously, with each protein analysis, BSA standards were placed on the same plate along with the samples, treated and analysed similarly to obtain a calibration curve. The cell protein quantity in each well was determined.
- *NPs analysis*: 50µL supernatant was placed in a white opaque 96-well microplate (OptiPlate-96, PerkinElmer corporation, Wellesley, USA) and the fluorescence intensity was measured at excitation/emission wavelength of 644/664nm using the plate reader. Simultaneously, with each NPs analysis, a set of cell-containing wells were treated similarly to the test wells without exposing to the samples. Different known concentrations of DiD-loaded NPs were added just before the RIPA buffer addition. These were analysed similarly to the samples to obtain a calibration curve. The NPs uptake in each well was determined.
- For each type of NPs or at each time point, the microgram of NPs uptake per mg of cell protein was calculated.

Table 5.3. Cell uptake study design for NPs showing incubation temperature and time for the NPs under investigation. NP1 had both SA and TAT ligands, NP2 had only SA ligand and NP3 was prepared without any ligand.

Temperature of incubation	**Time of incubation (hour)**		
	1	**2**	**3**
37°C	NP1	NP1	NP1
	-	NP2	-
	-	NP3	-
4°C	-	NP1	-

Note: NPs concentration of 100µg/mL was used in all these studies.

5.3.4.2 Qualitative Analysis of NPs Cellular Uptake by CLSM

This study was carried out to assess the internalisation and localisation of NPs in hCMEC/D3 cells. The cells were incubated with Phalloidin-FITC solution (1.67µg/mL) to stain their actin filaments whereas the cell nucleus was stained with DAPI solution (1.0µg/mL). Both solution preparation procedures are briefly described here:

Phalloidin-FITC Working Solution

The supplied 0.1mg Phalloidin-FITC was dissolved in methanol to obtain a concentration of 0.5mg/mL. This stock solution was aliquoted and stored at −20°C protected from light. A diluted working solution of Phalloidin-FITC in PBS at a ratio of 1:300 (stock solution: PBS) was prepared prior to the application.

DAPI Working Solution

1mg DAPI powder was dissolved in sterile water to obtain a concentration of 1.0mg/mL. This stock solution was aliquoted and stored at −20°C protected from light. A diluted working solution in PBS (1/1000) was prepared prior to the application.

Both DiD- and coumarin-6-loaded NPs were used in these experiments. Also, both conventional methods for sample preparation, namely on the glass coverslip and in the Ibidi® micro-dish were conducted for assessing image quality. They are briefly described here:

Immunostaining Procedure for Cells Grown on Coverslip

- Only 5000 cells/cm^2 were seeded on the ethanol-sterilized glass coverslips (ProSciTech, Cat. # G408, Dia-22mm) placed in a 6-well plate. Experiments were commenced when the cells were well-settled and only 30-40% confluent.
- The medium was removed, cells were rinsed twice and equilibrated with HBSS-P for 30 min at 37°C.
- 1mL pre-warmed DiD-loaded NP suspended in HBSS-P (100µg/mL) was placed in each well and incubated for 1 hour. In the case of coumarin-6-loaded NPs, a lower NPs concentration (50 µg/mL) and shorter incubation period (15 min) was used because a higher concentration and longer incubation period produced oversaturated images.

- The medium was removed and cells were rinsed twice with 2mL of ice-cold PBS quickly. The quick washes ensured that the cells retained their original morphology and did not deform/shrink due to the absence of essential nutrients and ions.
- 2mL of warm (37°C) 4% PFA in PBS was added, incubated for 15 min at RT in the dark and washed twice with 2mL PBS each time.
- 2mL of cold (4°C) 0.1% Triton X-100/PBS was added and incubate for exactly three minutes to permeabilize the cells. Longer treatment time caused the Phalloidin-FITC to stain the nucleus also.
- Cells were rinsed twice with 2mL PBS, the coverslip was removed carefully and place in a new dry well. Precaution was taken to keep the slides always wet.
- 200µL Phalloidin-FITC working solution was added on each coverslip and incubated for 30 minutes at RT.
- Cells were washed three times with PBS for five minutes each time (total 15 minutes) with 2mL of PBS per well each time to remove unbound Phalloidin-FITC.
- DAPI working solution was added (2mL) and incubated for 5 minutes and rinsed with 2mL PBS.
- 8µL of mounting medium (Vectashield®) was placed on a clean microscope slide (SPGE90, Hurst Scientific Pty Ltd, Canning Vale, Australia).
- The coverslip containing cells was removed from the well and mounted on the slide facing the surface with cells upside down so that the cells touch the mounting medium avoiding any air bubble.
- The slide was left in open (but in dark) to evaporate the excess moisture for 4-5 hrs and then transparent nail polish was used to completely seal the coverslip to avoid further moisture loss.
- After the nail polish was completely dried, the prepared slides were stored at 4°C and image was taken with a Nikon A1 Confocal Laser Microscope (Nikon Instruments Inc., Tokyo, Japan).

Immunostaining procedure for cells grown in Ibidi® micro-dish

- In 35mm Ibidi® micro-dish (Petri dish with #1.5 coverslip, ibidi/DKSH/81156, Ibidi, DKSH Australia Pty. Ltd., Hallam, Australia) 5000 cells/cm^2 were seeded. Experiments were commenced when the cells were approximately 30-40% confluent.
- Cells were rinsed twice and equilibrated with HBSS-P for 30 min at 37°C followed by an incubation period of 15 minutes with 1mL pre-warmed coumarin-6-loaded NPs (50 µg/mL).
- NP suspension was removed and the cells were rinsed twice with 2mL ice-cold PBS quickly.
- 2mL of warm (37°C) 4% PFA in PBS was added, incubated for 15 min at RT in the dark and washed twice with 2mL PBS each time.
- DAPI working solution was added (2mL) and incubated for 30 minutes, rinsed with PBS and finally added 2mL PBS.
- Images were taken with the Nikon A1 confocal laser microscope.
- Three images per samples were analysed by ImageJ® software ver. 1.50i for comparing fluorescence intensity of the internalised NPs.

5.3.5 Evaluation of NPs Transport Across BBB Model

5.3.5.1 Development of an *in Vitro* BBB Model

Human colonic adenocarcinoma cell line (Caco-2) within passage numbers 81 to 91 was used for these experiments following the published methods (Degim *et al.*, 2010; Hughes & Crowe, 2010). The human cerebral microvascular endothelial cell line (hCMEC/D3) was also considered based on reports from other laboratories that have used it as a BBB model (Weksler *et al.*, 2013; Ma *et al.*, 2014). For both cell lines, to stabilise the cell phenotype, after reviving the cells from liquid nitrogen, they were cultured for at least two passages before being seeded on the 0.6 cm^2 Millicell cell culture polycarbonate Transwell inserts (Cat. # PITP01250, Merck Millipore, Bayswater, Australia) placed in 24-well plates (Figure 5.1).

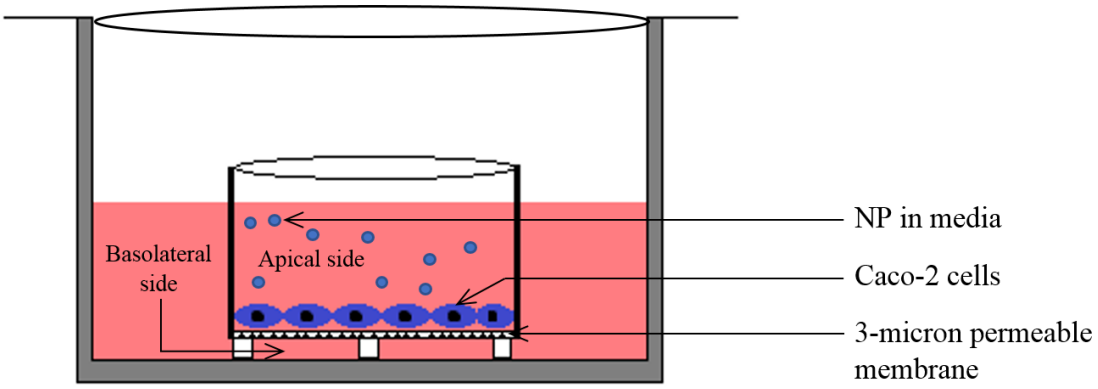

Figure 5.1. Diagram of an *in vitro* BBB model.

The inserts were coated with rat tail collagen type I as per section 5.3.1.1 prior to seed the hCMEC/D3 cells. Both cells were grown in a 37°C incubator with 5% CO_2 in "growth medium" (see Table 5.1) onto Millipore filter inserts in 24-well plates. Caco-2 cells were seeded at a concentration of 65,000 cells per cm^2, equivalent to 39,000 cells per insert, whereas, seeding concentrations for hCMEC/D3 cells were 50,000 cells/cm^2, equivalent to 30,000 cells per insert as per literature and the supplier recommendation (Poller *et al.*, 2008; Senarathna *et al.*, 2016). The medium was replaced twice a week. See Appendix VII for routine medium replacement procedure. Inserts with TEER value $\geq$ 250 $\Omega.cm^2$ were used for transport studies. To allow full maturation of the cells monolayer, the transport study across the Caco-2 cell monolayers was carried out in between 21-25 days post seeding (Senarathna *et al.*, 2016).

5.3.5.2 Characterisation of the *in Vitro* BBB Model

Three types of characterisation methods were used to ensure that the cell monolayers used for the NPs transport study were intact and formed TJ which did not permit NPs permeation via passive diffusion. These methods were – A) Electrical resistance measurement, B) Sucrose permeability assay and C) Confocal microscopy assay.

Electrical Resistance Measurement

TEER measurement has been used widely as a preliminary screening tool for developing and characterising *in vitro* BBB model (Srinivasan *et al.*, 2015). TEER measurements were performed using an EVOM meter and the ethanol-sterilized ENDOHM 12 chamber (World Precision Instruments, Sarasota, USA) every day from day 1 to day 6 for hCMEC/D3 and twice a week from day 5 to day 32 for Caco-2 cells after seeding.

Sucrose Permeability Assay

Sucrose is well-known for having a very low apparent permeability coefficient (P_{app}) across the BBB due to the presence of TJ and hence, it is widely accepted and used as a paracellular permeability marker (Witt *et al.*, 2008). Although the presence of the invertase or sucrase enzyme in Caco-2 cells could hydrolyse some sucrose (Zhou *et al.*, 1998), this would have minimum impact on the purpose of this assay because this assay was one of the three methods employed for BBB characterisation. The sucrose permeability via BBB solely depends on the barrier tightness because (a) sucrose is hydrophilic, so cannot use lipid channel to pass through, and (b) it is not a substrate for any receptor-mediated endocytosis (Franke *et al.*, 1999).

The hCMEC/D3 cells did not demonstrate satisfactory TEER across the monolayer, possibly caused by incomplete TJ formation. A similar phenomenon was also observed by other researchers who found that the hCMEC/D3 cells, when grown on the transwell inserts, showed poor expression of TJ protein, ZO-1 and Claudin-5 leading to low TEER (Biemans *et al.*, 2017). Hence, only Caco-2 cells were subjected to the permeability assay. The cells were seeded on the insert and incubated according to the section 5.3.5.1. On day 7, 14, 21 and 28 days, both sides of three inserts were washed with pre-warmed permeability assay buffer (pH 7.4) named HBSS-F (HBSS containing 10% FBS). 0.3mL HBSS-F was added into each insert and 0.6mL was added to each well and the plate was equilibrated for 30 min at 37°C. The buffer was aspirated and 0.3mL sucrose solution (500 µg/mL) in the buffer was added to the apical side of each insert. 0.6mL buffer was added to each well and the plate was incubated at 37°C. After 30, 60, 90, 120 and 180 min, 120µL samples from the basolateral receptor compartment of the well was collected into 2mL HPLC amber vials and replaced with equal volume of pre-warmed fresh HBSS-F buffer.

At the conclusion of the study, 120µL sample was also taken from apical donor chamber to determine remaining level of the sucrose. The concentration of sucrose was determined by an HPLC method. Briefly, an Agilent 1200 system (Agilent Technologies Australia, Mulgrave) was employed for the separation and detection of the sucrose. The instrument consisted of a degasser (G1379B), binary pump (G1312A), autosampler (G1329A) with thermo-control unit (G1330B), thermostat controlled column compartment (G1316A) and refractive index detector (G1362A). The HPLC column used was Grace Apollo (Grace Davidson Discovery Science, Baulkham Hills, Australia) C_{18}, 5µm particle size, 150mm × 4.6mm. An isocratic mobile phase containing water and ACN at a ratio of 95:5 was used as the mobile phase used at a flow rate of 1mL/min. Acquired data were processed by Agilent ChemStation®, B.04.03 SP1 software. A set of sucrose standards in HBSS-F was analysed under the same sample treatment protocol and used to calculate the sucrose concentration in the receiver chamber. The P_{app} of sucrose was calculated using the equation:

$$P_{app} = \frac{dQ}{dt} \times \frac{1}{60} \times \frac{1}{A} \times \frac{1}{C_0}$$

where dQ/dt is the permeability rate (µg/min) which is the slope of the linear region of the curve constructed by plotting cumulative amount of sucrose in basolateral chamber against time (t), A is the surface area of the membrane (cm^2), and C_0 is the initial concentration in the donor chamber (µg/mL).

Confocal Laser Scanning Microscopy (CLSM) Assay

The purpose of CLSM assay was to visually detect the presence of occludin in the *in vitro* BBB cell model. It is a well-known fact that the three major TJ proteins are claudin, occludin, and junction adhesion molecules (Lee *et al.*, 2017). We planned to investigate at least two of the proteins, however, considering the resource constrain, occludin detection by CLSM was performed only. Louzao *et al.* (2015) also presented confocal microscopic images of the occudin protein only as an TJ integrity evidence.

A primary polyclonal rabbit anti-occludin antibody and a secondary goat anti-rabbit IgG-Alexa Fluor® 488 antibody were used in this exercise. The secondary antibody contains a bright, green-fluorescent dye (Alexa Fluor® 488) (Figure 5.2). Thus, when treated with both antibodies, the TJ Occludin protein was visible under a fluorescent microscope at the green channel (Ex/Em 488/525nm). Both hCMEC/D3 and Caco-2 cells were microscopically examined for the presence of the TJ protein (occludin). 35mm Ibidi® micro-dish were used to grown both cells in a 37°C incubator with 5% CO_2 in "growth medium" (see Table 5.1) which was replaced twice a week. Stock primary and secondary antibody concentrations were 1µg/µL and 2 µg/µL, respectively. Antibody aliquot and storage protocol is included in Appendix VIII.

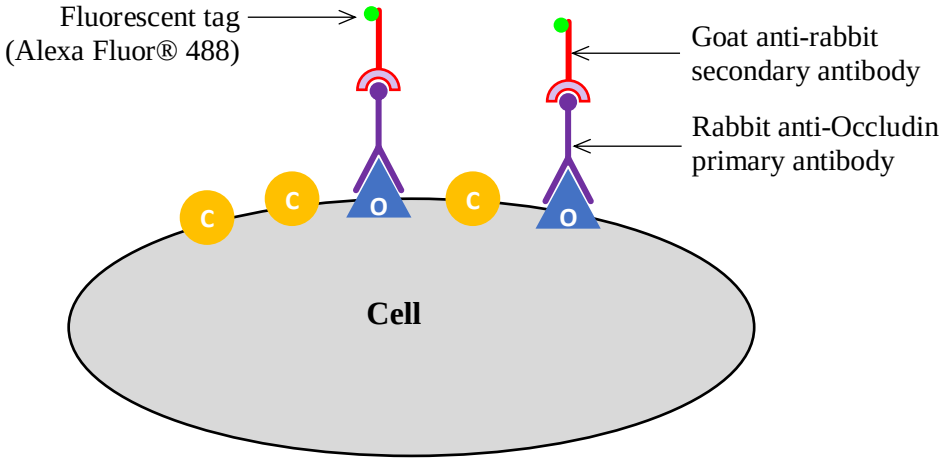

Figure 5.2. A simple illustration of immunostaining principle.

Caco-2 cells were seeded at a concentration of 65,000 cells per cm^2, whereas, seeding concentrations for hCMEC/D3 cells were 50,000 cells/cm^2 as per literature and the supplier recommendation (Poller *et al.*, 2008; Senarathna *et al.*, 2016). The day of the experiment was selected based on the highest TEER value found in previous experiments which was day 3 and day 21 for hCMEC/D3 and Caco-2 cells, respectively. The immunostaining protocol was supplied by the antibody supplier and was optimised as follows:

- The medium was removed and cells were rinsed twice with 2mL of ice-cold PBS quickly. The quick washes ensured that the cells retained their original morphology and did not deform/shrink due to the absence of essential nutrients and ions.
- To fix the cells, 2mL of warm (37°C) 4% PFA in PBS was added, incubated for 15 min at RT in the dark and washed twice with 2mL PBS each time.
- 2mL of cold (4°C) 0.1% Triton X-100/PBS was added and incubate for exactly three minutes to permeabilize the cells.
- Cells were rinsed twice with 2mL PBS, 2mL blocking solution (10% goat serum and 1% BSA in PBS) was added, and incubated at RT for 1 hour (or, overnight at 4°C).
- The primary antibody was centrifuged at 16000g for 5 minutes to obtain the clear supernatant. Only clear solution was used for the experiments.
- The blocking solution was removed, 400µL primary antibody (1:100 diluted in blocking solution) was added and incubated at RT for 1 hour.
- Cells were washed three times with PBS for five minutes each time (total 15 minutes) with 2mL of PBS per well each time to remove unbound primary antibody.
- The secondary antibody was also centrifuged at 16000g for 5 minutes and only the supernatant was used for the next step.
- 400µL secondary antibody (1:200 diluted in blocking solution) was added and incubated at RT for 1 hour in the dark.
- Cells were washed three times with PBS for five minutes each time (total 15 minutes) with 2mL of PBS per well each time.

- DAPI working solution (Section 5.3.4.2) was added (2mL), incubated for 5 minutes at RT, rinsed with 2mL PBS and added 2mL PBS in the micro-dish.
- The micro-dish was observed under the Nikon confocal microscope and images were taken.

5.3.5.3 Determination of NPs Transport Across the BBB Model

Caco-2 cell monolayers on the transwell inserts having initial TEER values of more than 250 $\Omega.cm^2$ were selected for these experiments. Both sides of the insert were washed with pre-warmed HBSS-P. For equilibration, 0.3 and 0.6mL HBSS-P was added to the apical and basolateral side of the insert, respectively. The plate was incubated for 30 min at 37°C in the incubator. Medium from both sides of the insert was aspirated and 0.3mL DiD solution (0.5µg/mL) or DiD-loaded NP suspension (100µg/mL) or RHT-loaded NP suspension (100µg/mL) in HBSS-P was added to the apical side of each insert. 0.6mL HBSS-P was added to the basolateral side of the insert and the plate was placed in the incubator.

After 30, 60, 90, 120 and 180 min, 120µL samples from the basolateral receptor compartment of the well was collected into 2mL HPLC amber vials and replaced with equal volume of pre-warmed fresh buffer. At the end of the study, 120µL sample was also taken from apical donor chamber to determine remaining level of the drug. TEER was measured immediately after completing the experiments to determine the barrier integrity during the experiments.

600µL ACN was added to each sample vial (*i.e.*, HPLC vials) and vortex for 10 minutes to dissolve the NPs. 100µL solution was then transferred to white opaque 96-well microplate and the fluorescence intensity of DiD was measured at excitation/emission wavelength of 644/664nm using the plate reader. The RHT concentration was analysed by validated HPLC method.

5.4 Results and Discussion

5.4.1 Cell Cultures

All cell culture experiments were conducted in a physical containment level 2 (PC2) cell culture laboratory with the highest possible quality of the media, cell-line, cell culture consumables and personal hygiene. The results presented in this chapter were generated from mycoplasma negative cell lines which were regularly checked by the facility researcher. Figure 5.3 and Figure 5.4 illustrates the mycoplasma negative results of the both cell lines used.

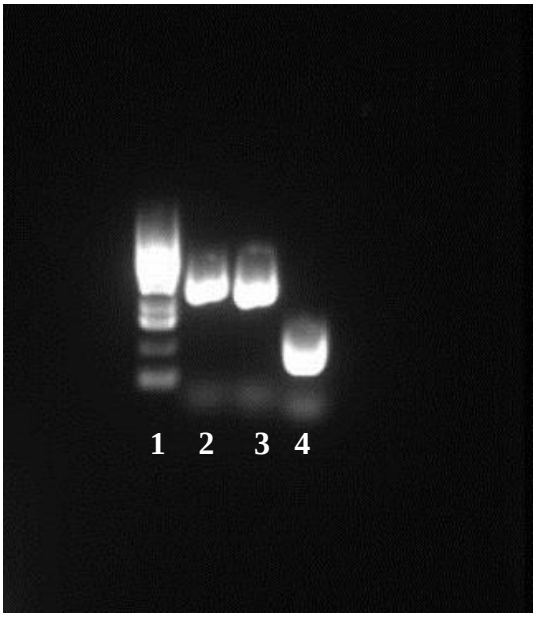

Figure 5.3. PCR gel image of hCMEC/D3 mycoplasma negative result. 1st lane (left): 100 base-pair (bp) ladder, 2nd lane: hCMEC/D3 cells, 3rd lane: negative control, 4th lane: positive control. The upper band of 500bp is an internal positive control showing that PCR reaction has worked; the lower band of 250bp is mycoplasma positive band.

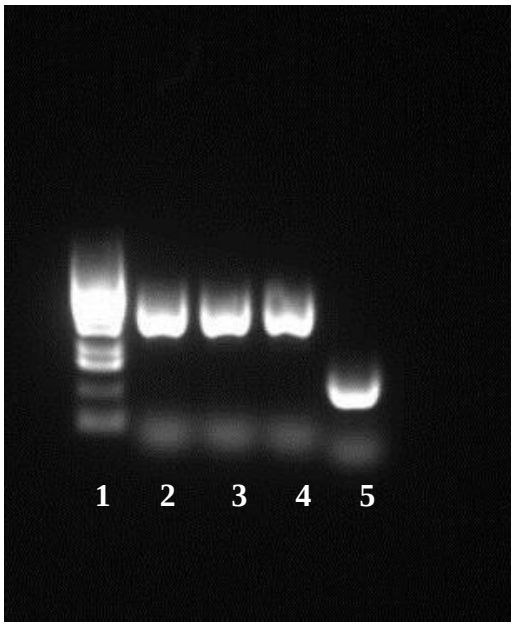

Figure 5.4. PCR gel image of Caco-2 mycoplasma negative result. 1st lane (left): 100 bp ladder, 2nd lane: Caco-2 cells, 3rd lane: LS174T (from another researcher), 4th lane: negative control, 5th lane: positive control. The upper band of 500bp is an internal positive control showing that PCR reaction has worked, the lower band of 250bp is mycoplasma positive band.

5.4.2 Evaluation of Cytotoxicity

A series of experiments were conducted to determine the toxicity level of drug and NPs in both hCMEC/D3 and Caco-2 cell lines. The important purpose of this study was to determine what should be the working concentrations of the NPs for the uptake and transport studies which were non-toxic to the cells. The NPs concentration used in the cell uptake and transport study was 100µg/mL because this concentration is considered to be maximum for various cellular studies by other researchers (Qi *et al.*, 2005; Vangara *et al.*, 2013; Sun *et al.*, 2014a; Chen & Li, 2015). We assessed the cytotoxicity of the NPs up to the concentration of 200µg/mL and due to the 3% RHT loading in NPs (Chapter 4), this was equivalent to 15µM or 6µg/mL RHT as our upper limit for the cytotoxicity studies. The cytotoxicity data of individual NPs, drug and lipophilic tracers at different concentrations are presented in Figure 5.5, Figure 5.6 and Figure 5.7.

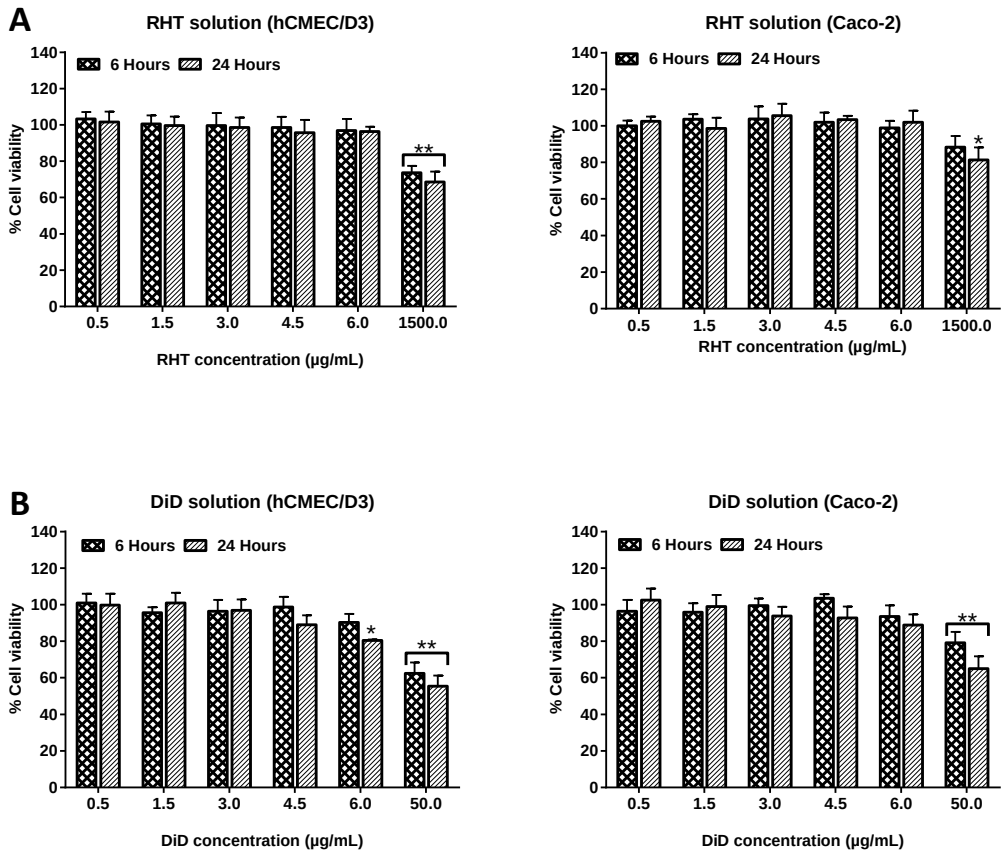

Figure 5.5. Effect of 6 hrs and 24 hrs exposure to different concentrations of RHT (A) and DiD (B) on hCMEC/D3 (left) and Caco-2 (right) cell survival (% of control). 1500 µg/mL RHT and 50µg/mL DiD solution as positive controls showed that the MTT assay worked. The cell viability of the untreated cells was taken as 100%. Statistically significant reduction in cell viability compared to untreated cells are shown with: (*) where the $p < 0.05$ and (**) where the $p < 0.01$. All data are presented as mean ± SEM (n=8).

From Figure 5.5, it can be noticed that the concentrations of 1.5mg/mL for RHT and 50µg/mL for DiD solution resulted in significant reduction of cell viability. These higher drug concentrations were selected based on what reported in the literature (Goldblum *et al.*, 2002) and confirmed by our trials. Although they were much higher than that were used in our other experiments, this was done to prove that the cells do respond to the drug at a high concentration. The cytotoxicity demonstrated by RHT in Caco-2, MDCK, Vero and Chang cells has been reported earlier (Goldblum *et al.*, 2002; Degim *et al.*, 2010; Mutlu *et al.*, 2011) and some cells were more than 80% viable at RHT concentration as high as 50 mg/mL. Our finding about the RHT cytotoxicity agrees with these published results.

In the case of the DiD solution, the cell viability in both the cell lines was significantly lower than the control at 50µg/mL DiD concentration. This toxicity may not reflect the true toxicity of the DiD because the DiD stock solution (1mg/mL) was prepared in ethanol as per manufacturer instruction and then diluted to 0.5µg/mL using the culture medium. The solvent (ethanol) may have contributed to the cytotoxicity (Wang *et al.*, 2014b).

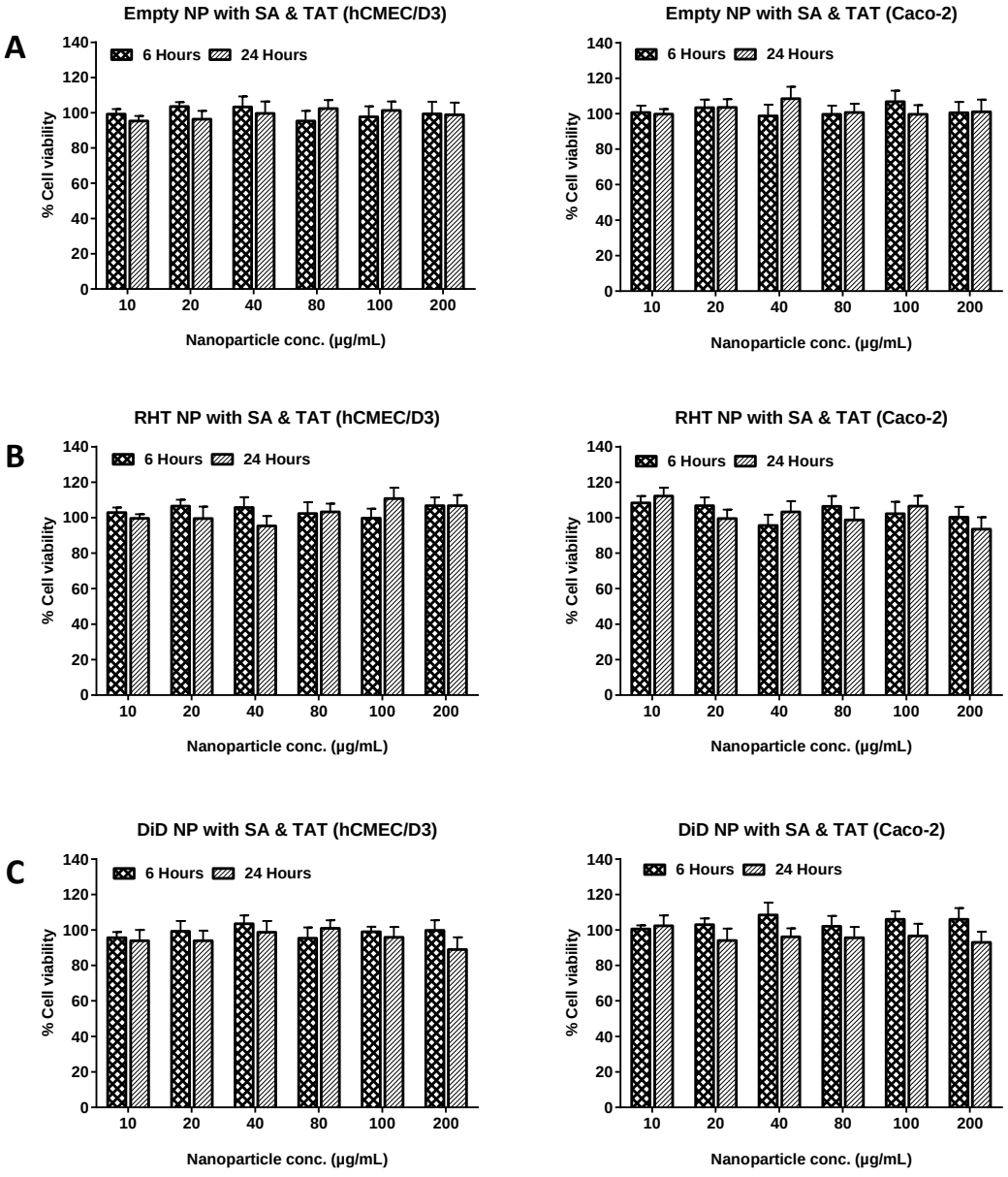

Figure 5.6. Effect of 6 hrs and 24 hrs exposure of different concentrations of blank NPs (A), RHT-loaded NPs (B) and DiD-loaded NPs (C) on hCMEC/D3 (left) and Caco-2 (right) cell survival (% of control). No statistically significant differences were observed even at the highest NPs concentration. All data are presented as mean ± SEM (n=8).

The Figure 5.6 illustrates that the NPs concentration used in the studies (100 µg/mL) was safe and none of the NPs types at any concentration significantly altered the cell viability when compared to the control group ($p > 0.05$). Other researchers also found that unless the NPs encapsulates cytotoxic drugs (like doxorubicin), cytotoxicity of PEGylated PLGA NPs is insignificant (Heidarian *et al.*, 2015; Cao *et al.*, 2016).

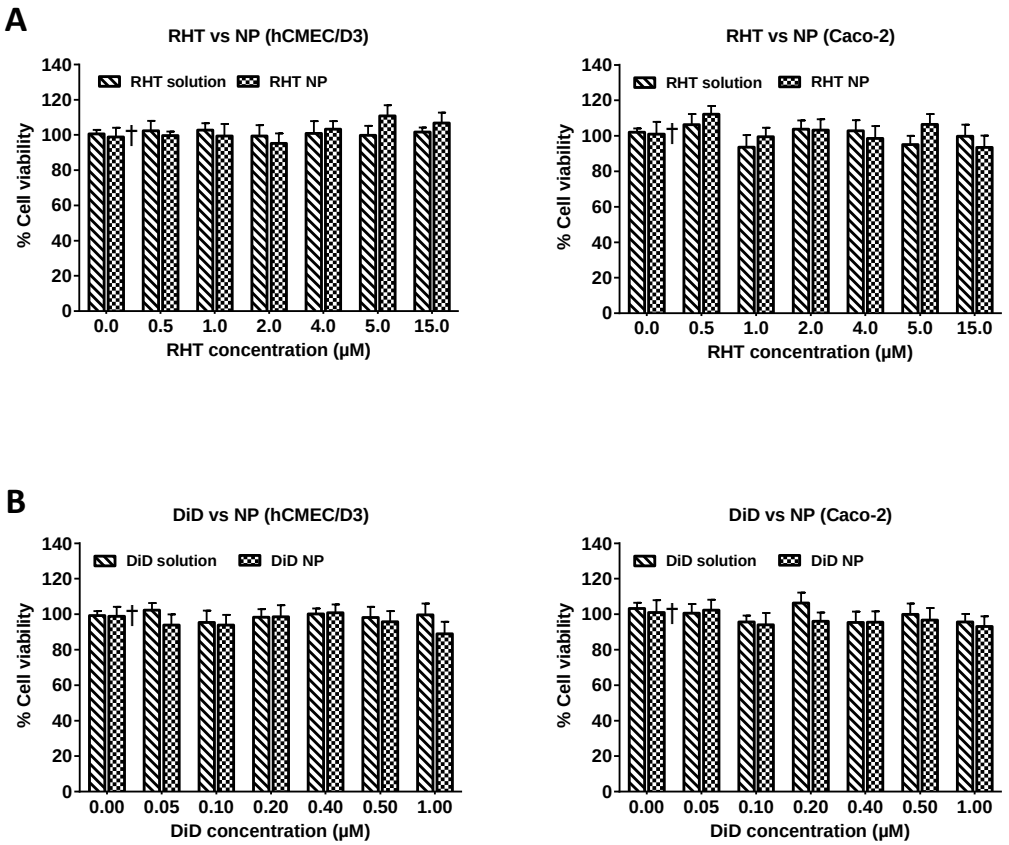

Figure 5.7. Comparative cytotoxicity effect after 24 hrs exposure of RHT-loaded NPs (A) and DiD-loaded NPs (B) with different RHT or DiD concentrations on hCMEC/D3 (left) and Caco-2 (right) cells (% of control). All data are presented as mean ± SEM (n=8). † - the concentration of NPs, in this case, is 200 µg/mL representing the highest NPs concentration associated with 15µM RHT or 1µM DiD.

Also, Figure 5.8 shows that the cell morphology of both cell lines remains almost identical before and after the NPs treatment. This visual data support the cell viability data, further confirming that the NPs and drug under experiment were safe to the cells at least up to the experimental concentrations of 100µg/mL NPs loaded with 3% RHT or 0.5% DiD.

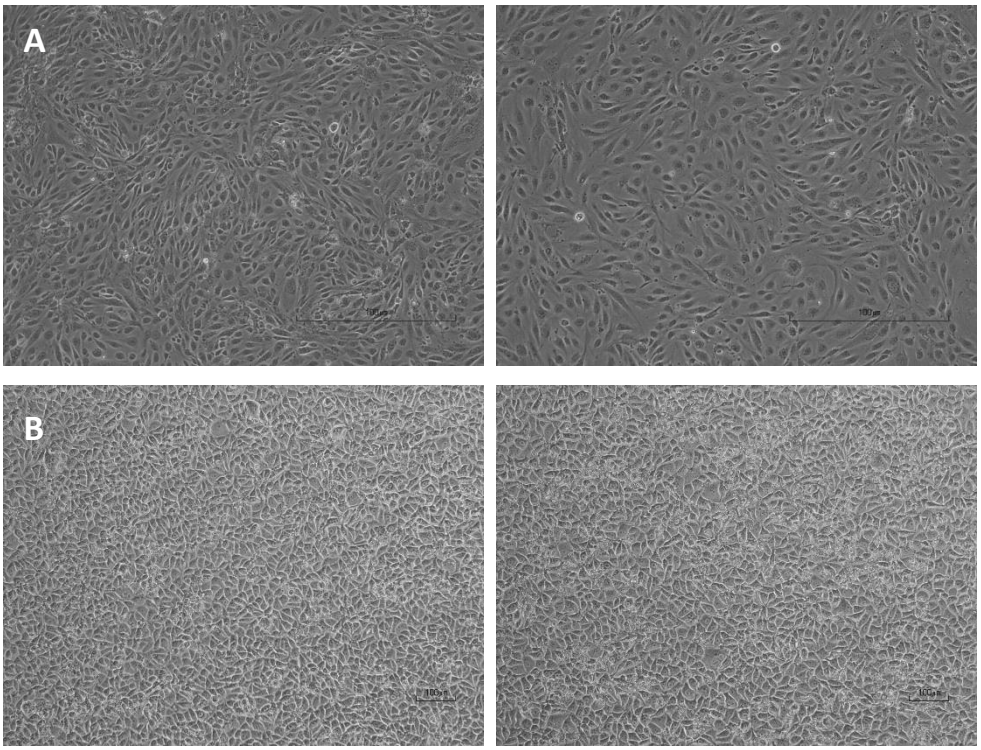

Figure 5.8. hCMEC/D3 (A) and Caco-2 (B) cell morphology before (left) and after (right) 24 hrs exposure of 100µg/mL PEGylated RHT NPs with dual targeting ligands.

5.4.3 Evaluation of NPs Cellular Uptake by hCMEC/D3 Cells

The cellular uptake study is widely used for assessing NPs formulations during the nanoparticulate drug delivery system development. The study was conducted to find out the effect of the ligand attachment, the level of uptake in cells and uptake mechanisms. A highly fluorescent lipophilic tracer (DiD) was loaded in different types of NPs and were used for the studies. This far-red lipophilic, photostable and fluorescent dye possess unique property of being weakly fluorescent in water but highly fluorescent in a lipid environment. According to the manufacturer, DiD binds with the phospholipid cell membrane when applied to the cells as a solution. Thus, it has been used for cellular and tissue tracking (Sutton *et al.*, 2008; Lassailly *et al.*, 2010; Seabold *et al.*, 2010). DiD-loaded lipid NPs has been used for improved *in vivo* fluorescence imaging in mouse (Texier *et al.*, 2009). The cellular uptake study results are presented in the following sections:

5.4.3.1 Quantitative Investigation

The DiD quantification was carried out by measuring its fluorescence intensity of the samples and concentrations were calculated from the calibration curve (Figure 5.9).

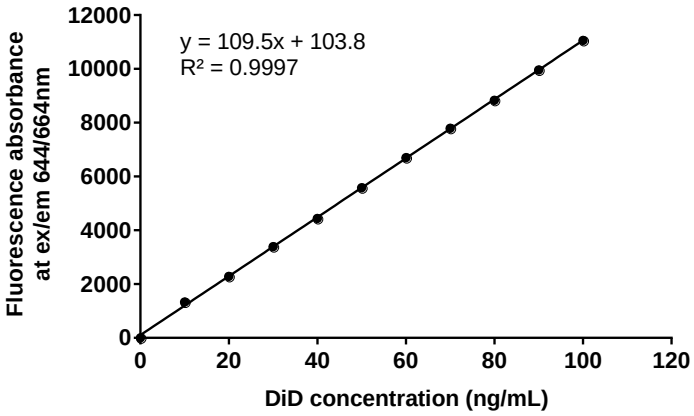

Figure 5.9. Calibration curve of DiD in RIPA buffer.

Effects of NPs Surface modification

The PLGA NPs without any ligand has been reported to get taken up by the endothelial cells (Lee *et al.*, 2015). The probable mechanism of NPs uptake depicted by the authors is endocytosis, but, lack of ligand incorporation makes the drug delivery less interactive with cells. Surface-modified NPs with site-specific ligands has demonstrated higher uptake. Saneja *et al.* (2017) showed that cellular uptake of hyaluronic acid (HA) conjugated PLGA NPs in the target MiaPaca-2 cancer cell line was increased almost three-fold compared to the non-HA conjugated NPs. Also, Yan *et al.* (2013) reported a 4.5-fold increase in NPs uptake in Caco-2 cells using TAT peptide as a surface ligand. In our study, the PLGA NPs conjugated with both TAT peptide and SA demonstrated superior cell uptake, which is about 3.4-fold compared to the NPs with single ligand and 3-fold compared to the NPs without any ligand (Figure 5.10). This indicates that the TAT peptide facilitated the uptake of the NPs which was consistent with that reported by other researchers (Krol *et al.*, 2013; Malhotra *et al.*, 2013; Sharma *et al.*, 2016a). Tosi *et al.* (2010) employed BBB-penetrating peptide (similopioid peptide) as BBB targeting ligand for increasing NPs brain uptake whereas SA was used as a brain parenchyma targeting ligand to enhance the NPs brain residual time. It was found that incorporation of SA on the NPs surface did not facilitate NPs brain uptake rather only helped the NPs to remain inside the brain for a longer time that ultimately resulted in enhanced pharmacological activity in the rats (Tosi *et al.*, 2010). In our study, also, SA did not influence the cell uptake efficiency of TAT peptide. A future *in vivo* study is needed to prove the effectiveness of SA ligand.

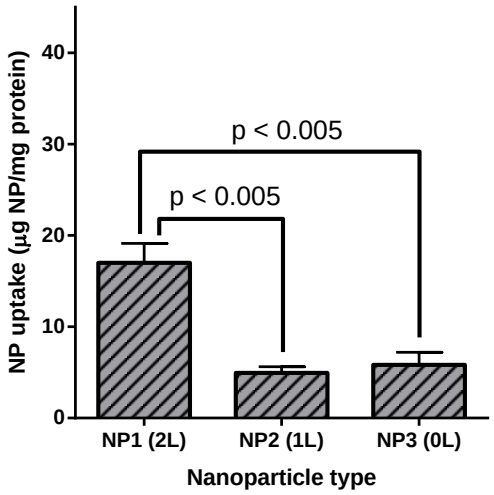

Figure 5.10. Effect of surface modification on the uptake of PEGylated PLGA NPs by hCMEC/D3 cells.NP1 had both SA and TAT ligands, NP2 had only SA ligand and NP3 was prepared without any ligand. All data are presented as mean ± SD (n=3).

Effects of Particle Concentration

The increment of the NPs concentrations showed a continuous increase in the cellular uptake in a nearly linear fashion until it attained plateau at very high NPs concentration (2.5mg/mL). This suggests that passive diffusion was unlikely to be the mechanism here for the NPs cellular uptake where the rate and amount of particle transport only depend on the particle concentration. The probable NPs uptake mechanism in this context could be either receptor-mediated transcytosis (RMT) or adsorptive-mediated transcytosis (AMT) (Chen & Liu, 2012). Both of them are energy dependent NPs uptake mechanisms which are saturable.

Other researchers also reported that small NPs (~250 nm) generally undergo energy-dependent cellular uptake that can be saturated at higher particle concentration (Win & Feng, 2005; Chaudhari *et al.*, 2012; Zaki & Hafez, 2012). Tahara *et al.* (2009) performed a detailed investigation on the cellular uptake of PLGA NPs in human lung adenocarcinoma A549 cells. Their study revealed that despite the particle size difference, almost all types of the PLGA based NPs demonstrated a saturation level (182µg NP/mg protein) at a concentration of 1.0mg/mL. Interestingly, our cellular uptake finding agrees with their data in a reasonable manner, especially, the amount of NPs uptake per mg of cell protein data. Of course, the numbers do not match because of the different setup (cell line and NPs formulation), however, our data agree with the pattern of the uptake shown by the team.

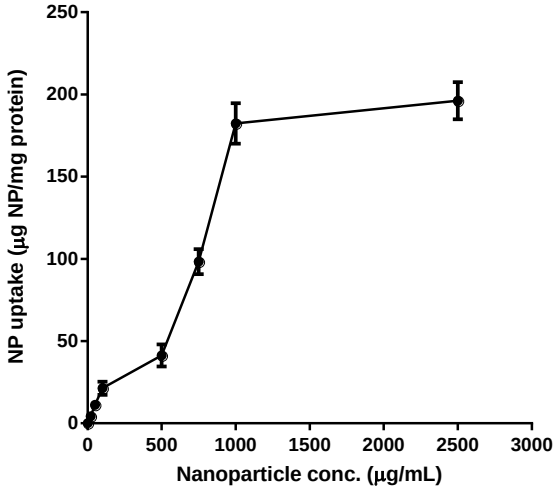

Figure 5.11. Effect of particle concentration on the uptake of PEGylated dual ligand PLGA NPs by hCMEC/D3 cells at 37°C in 2 hours. All data are presented as mean ± SD (n=3).

Effects of Exposure Time

This study demonstrated an interesting outcome – the cellular uptake was almost same for the first two hours of the study, however, showed a hike at the 3-hour period (Figure 5.12). This suggests that on top of the first mechanism, there might be another uptake mechanism present which was triggered lately to facilitate NPs uptake in greater extent. The study was conducted only for three hours because the assay medium (HBSS-P) lacked serum and other growth factors vital for the longer-term cell viability hence did not allow us to continue the experiments beyond a few hours.

This finding agrees with published data by Mao *et al.* (2010) who assessed the ability of TAT peptide-mediated cellular uptake of SiO_2 NPs. The authors conducted the study for 24 hrs and from their cellular uptake data, an obvious sharp rise in the NPs uptake was observed at four hours' post treatment.

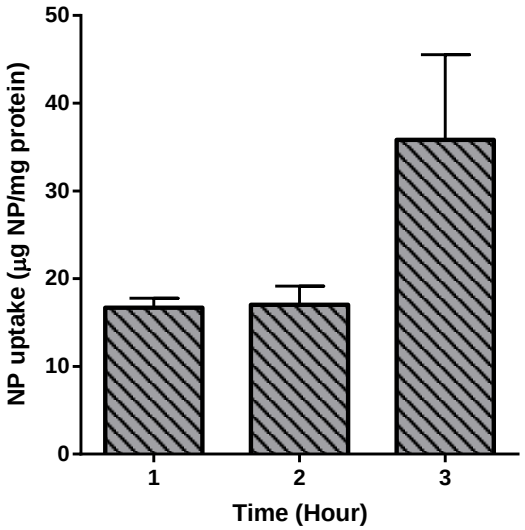

Figure 5.12. Effect of exposure time on the uptake of PEGylated dual ligand PLGA NPs by hCMEC/D3 cells. All data are presented as mean ± SD (n=3).

Effects of temperature

To find out the effect of temperature on the NPs uptake in the cell, the uptake study was conducted at both 4° and 37°C. Generally, at low temperature (4°C), cell metabolism is reduced leading to a reduction in energy-dependent uptake. On the other hand, when incubated at 37°C, the cells remain metabolically active and the uptake takes place in a usual manner. In our study, at 4°C, the NPs uptake was reduced significantly (2.5-fold) suggesting that the uptake mechanism was to certain extent energy dependent (Figure 5.13), not passive diffusion by nature.

Other researchers have carried out the investigation to depict the effect of time, temperature, particle size and concentration on the cellular uptake of their particulate formulations (Desai *et al.*, 1997; Win & Feng, 2005; Kulkarni & Feng, 2013; Sims *et al.*, 2016). Apart from the experimental reports, both theoretical (Zhang *et al.*, 2009) and computer simulation (Decuzzi & Ferrari, 2007) research has been published claiming to predict the cellular uptake behaviour of NPs. The common findings are - (a) the particles with smaller diameter demonstrated (100-200 nm) greater uptake compared to the larger diameter particles, (b) the particle uptake increases up to a certain time until it reaches the plateau level, (c) at lower temperature, the cellular uptake reduces significantly (2-3 fold), and (d) cellular uptake increases in a linear fashion with particle concentration, reaching a steady state at very high particle concentration. Our findings agree with all the above, however, we have only smaller sized NPs, so the investigation regarding the particle size was not carried out.

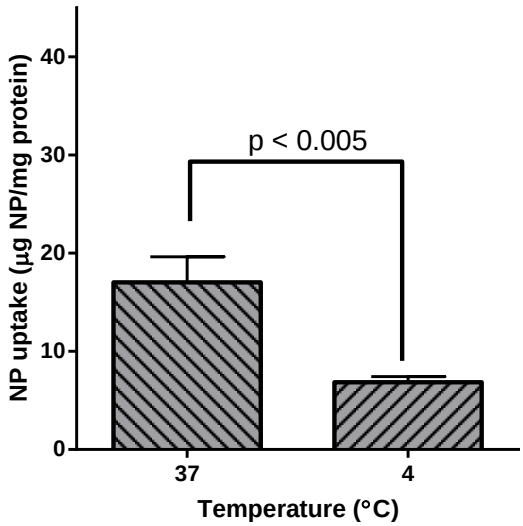

Figure 5.13. Effect of incubation temperature on the uptake of PEGylated dual ligand PLGA NPs by hCMEC/D3 cells. All data are presented as mean ± SD (n=3).

5.4.3.2 Qualitative Investigation

The uptake of DiD-loaded PEGylated PLGA NPs with double targeting ligands by hCMEC/D3 cells was qualitatively evaluated by the confocal microscopy. CLMS is a powerful technique that also allows capturing cross-section image of cells and provides valuable information on the particle localisation. It can provide selective optical sectioning, high resolution and in depth imaging of cellular microstructures without the need to physically section the sample. Labelling the cell actin fibres with Phalloidin-FITC and nuclei with DAPI resulted in the extracellular membrane, nuclei as well as the fluorescence red dye (DiD) loaded NPs being visualised. Our CLSM studies demonstrated that the DiD-loaded NPs were internalised rather than attached to the cell surface (Figure 5.14).

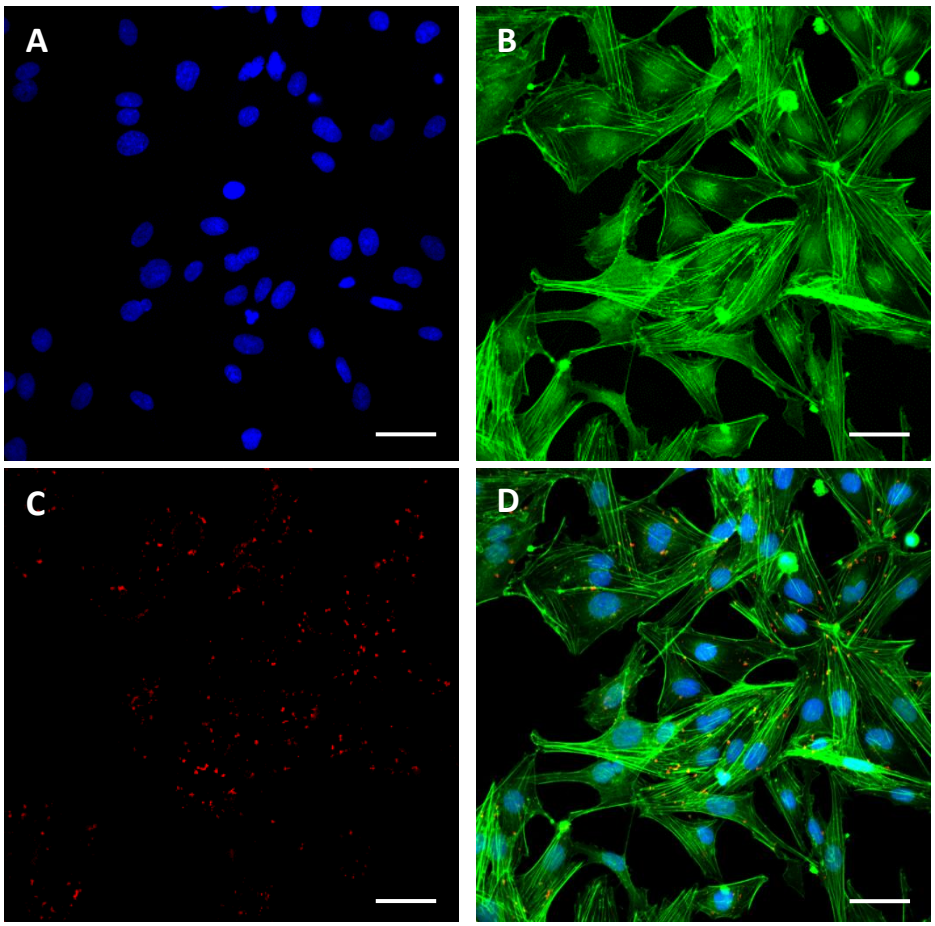

Figure 5.14. CLSM image of hCMEC/D3 cells after 1-hour incubation with DiD-loaded PEGylated PLGA NPs with double targeting ligands at 37ºC showing a perinuclear accumulation of particles. Nuclei stained with DAPI (A), actin filaments stained by Phalloidin-FITC (B), DiD-loaded PEGylated dual ligand NPs (C) and merged image (D). The scale bars correspond to 20 μm.

The red DiD-loaded NPs in preliminary experiments were found to be very dim and were difficult to distinguish under CLSM in contrast to the expectation. To overcome this limitation, coumarin-6-loaded NPs was decided to use. This fluorescent dye solution has been reported to show extremely low Caco-2 cellular uptake even after two hours' incubation at 37°C suggesting that cellular uptake of coumarin-6 solution is practically nil (Zhang *et al.*, 2016). Thus, the uptake of green coumarin-6-loaded PEGylated PLGA NPs with double targeting ligands by the same hCMEC/D3 cells was also qualitatively evaluated by confocal microscopy. However, staining of cell actin filaments could not be performed because the only available actin filament probe was Phalloidin-FITC which displays the same green fluorescence as the NPs thereby masking the particle detection. Figure 5.15 shows that the green scattered NPs were internalised and accumulated mostly around the cell nuclei when 50 µg/mL particles were incubated with the hCMEC/D3 cells at 37°C for 15 minutes. Similar observation was reported by other researchers who conducted their study with HeLa cells and coumarin-6-loaded PLGA NPs with CPP as a surface ligand (Steinbach *et al.*, 2016).

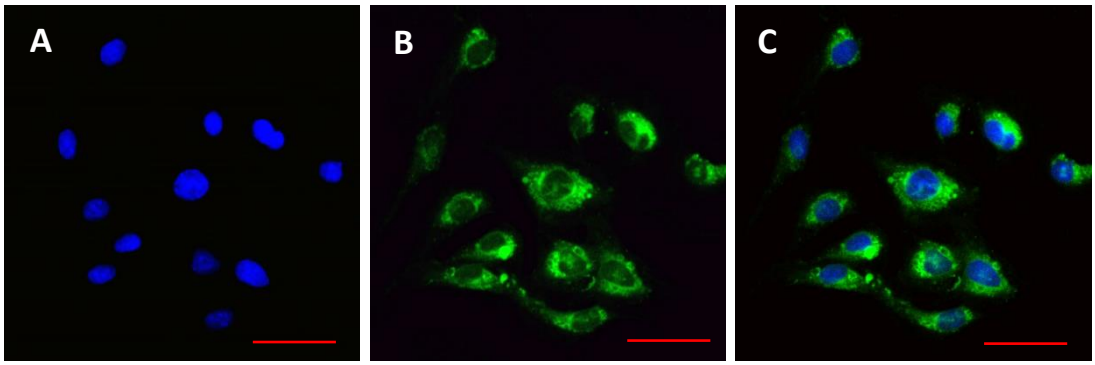

Figure 5.15. CLSM image of hCMEC/D3 cells after 15-minute incubation with coumarin-6-loaded PEGylated PLGA NPs with double targeting ligands at 37ºC showing a perinuclear accumulation of particles. Blue channel (A) obtained by DAPI filter, green channel (B) obtained by FITC filter and colour overlay (C) images are provided. The scale bars correspond to 20 µm.

The effect of ligand attachment on coumarin-6-loaded dual ligand PLGA NPs as well as the incubation temperature was investigated next. All NPs under investigation were incubated for 15 minutes at a particle concentration of 50 µg/mL. The coumarin-6 loaded NPs with and without ligands were incubated at 37°C to compare the effect of the ligand attachment. Also, the coumarin-6 loaded NPs with dual ligands were incubated at 4°C to compare the effect of the incubation temperature. The dual ligand NPs without any loaded dye was employed as the control to ensure that the green fluorescence generated by the samples were true representations of the internalised coumarin loaded NPs rather than autofluorescence from cell culture surface. Figure5.16-A clearly shows that neither the cells nor the culture dish produced any visible autofluorescence. Figure5.16-B and C illustrate a distribution of green coumarin-6 NPs within hCMEC/D3 cells. These images indicate that NPs internalisation within the cells may be governed by more than one process, such as endocytosis and passive diffusion (via a transcellular pathway) of extremely small NPs (Montenegro *et al.*, 2012).

The low temperature inhibits active transport mechanisms while maintaining the cellular ability to transport NPs via passive diffusion, therefore, it may reveal the transport mechanisms. An obvious enhancement of intracellular distribution of the PLGA NPs at 37°C in comparison to 4°C is noticed from Figure 5.16-C and D. This suggested that the main mechanism of NPs uptake by the hCMEC/D3 cells was endocytosis, an energy consuming process; with some image analysis using ImageJ® software revealed that NPs with double ligand incubated at 37°C was internalised 6.1-fold than the NPs without any ligand and 4.5-fold higher than the dual ligand NPs incubated at 4°C. Although this results did not perfectly match with our quantitative data (Section 5.4.3.1), which said that the increase was 3- and 2.5-fold, respectively, the trends are similar. There were many variabilities present in image capturing and analysis those might result in this variation in the results.

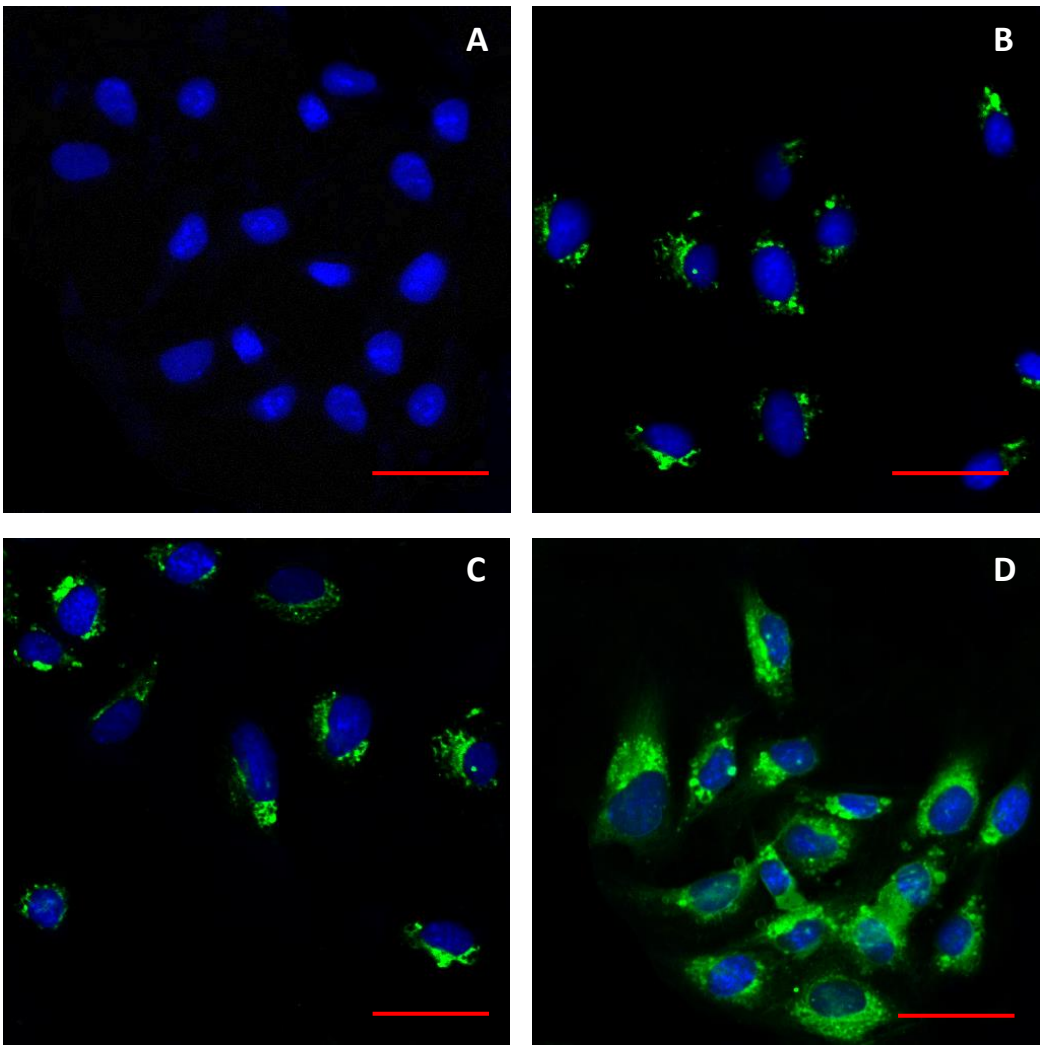

Figure 5.16. CLSM image of hCMEC/D3 cells after 15-minute incubation with PLGA NPs with different surface ligand and incubation temperature showing a comparative perinuclear accumulation of NPs. All are merged image of nuclei stained with DAPI (blue) and coumarin-6-loaded NPs (green). The scale bars correspond to 20 μm.
(A) control, PEGylated PLGA NPs with double targeting ligands without coumarin-6 at 37ºC,
(B) coumarin-6-loaded PEGylated PLGA NPs without any ligand at 37ºC,
(C) coumarin-6-loaded PEGylated PLGA NPs with dual targeting ligands at 4°C,
(D) coumarin-6-loaded PEGylated PLGA NPs with dual targeting ligands at 37ºC.

Optical sectioning

Three-dimensional Z-stack projection of optical sections (Figure 5.17 and Figure 5.18) illustrate that the NPs have travelled into the cell and gathered near the nucleus rather than just physically adhering to the cell surface. The DiD-loaded NPs are shown after splitting the channels to clearly locate the DiD NPs which were not fluorescent enough to be visualised once they were superimposed with other channels.

Coumarin-6 loaded NPs can be clearly seen and increasing concentration in the mid-section of the cells proves that the NPs were actually inside the cells. Many groups have recently used this modern technique to confirm the NPs internalisation (Cartiera *et al.*, 2009; Solovieva *et al.*, 2016).

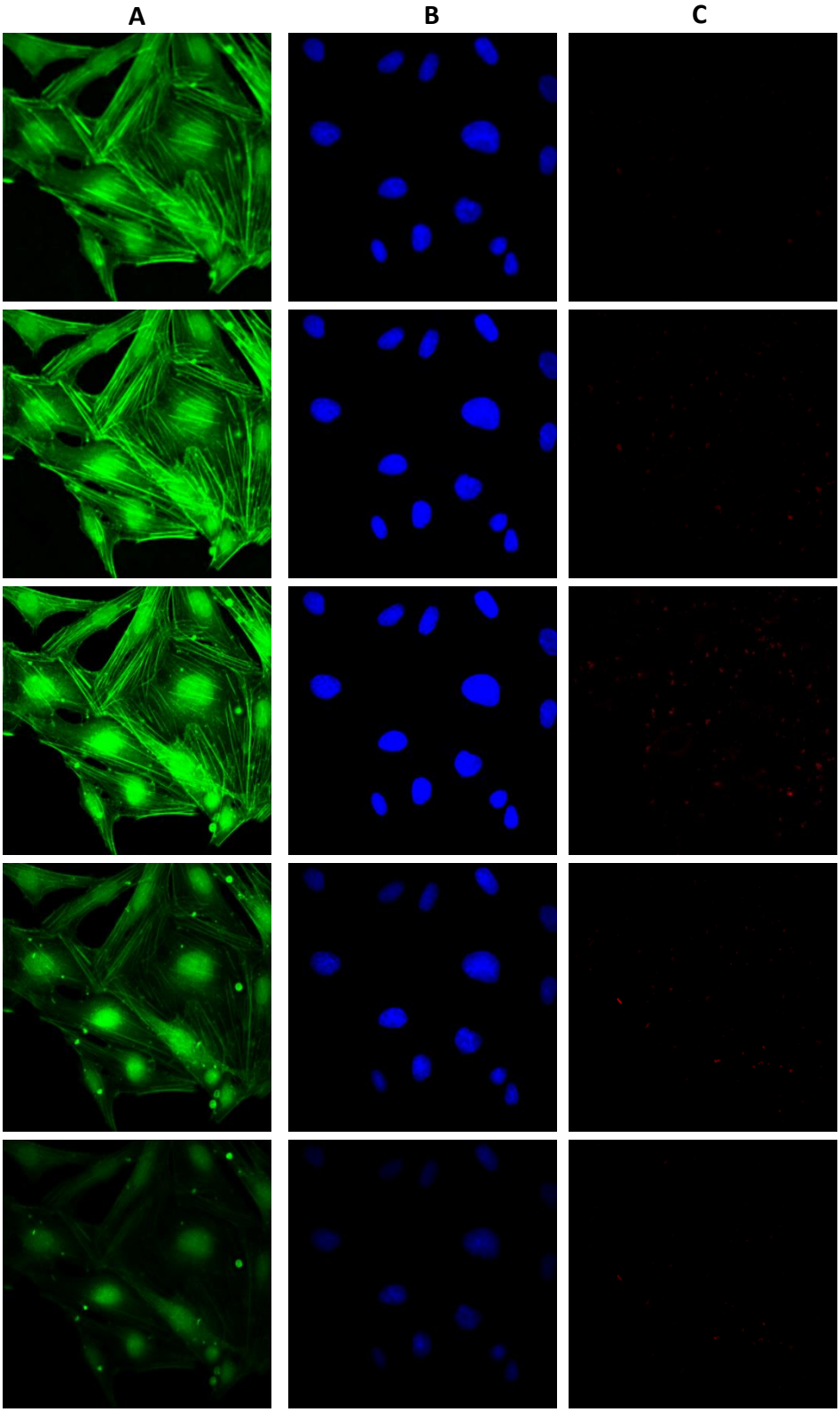

Figure 5.17. Intracellular distribution of DiD loaded PEGylated PLGA NPs with double targeting ligands in hCMEC/D3 after incubation for 2 hrs at 37°C as observed by CLSM.Five images of optical sections taken in the vertical axis at intervals of 1.3 µm from the apical surface confirming the internalisation of particles. Actin filaments stained by Phalloidin-FITC (A), nuclei stained with DAPI (B) and DiD-loaded NPs (C). Magnification = 400x.

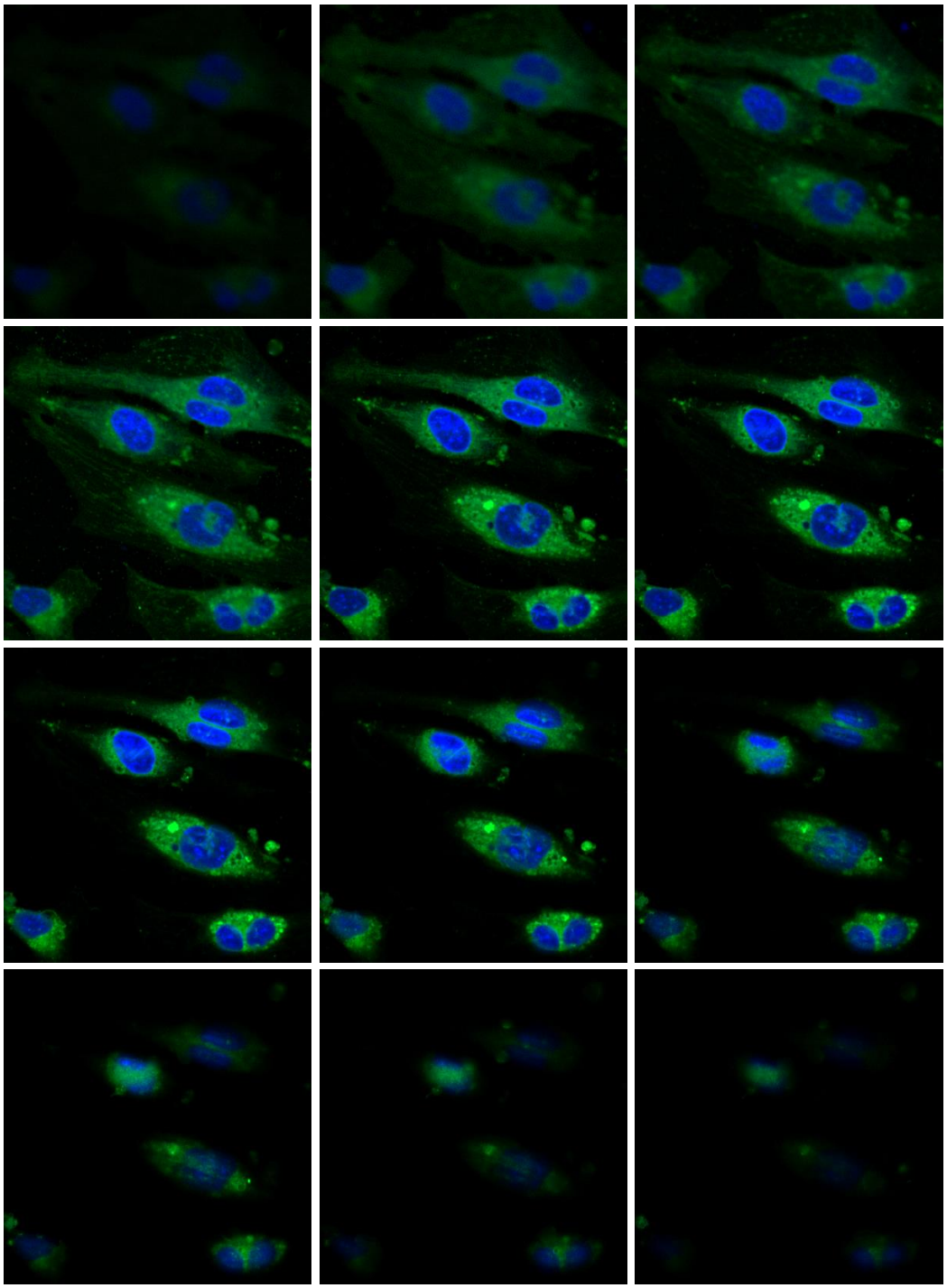

Figure 5.18. Intracellular distribution of coumarin-6-loaded PEGylated PLGA NPs with double targeting ligands in hCMEC/D3cells after incubation for 1 hr at 37ºC as observed by CLSM.Twelve superimposed images of optical sections taken in the vertical axis at intervals of 0.6µm from the apical surface (left to right; top to bottom, depths 0, 0.6, 1.2, 1.8, 2.4, 3, 3.6, 4.2, 4.8, 5.4, 6 and 6.6µm from apical surface) confirming the internalisation of green particles. Nucleus is stained with DAPI (blue). Magnification = 600x.

5.4.4 Evaluation of NPs Transport Across BBB Model

To evaluate how efficiently the NPs cross through the BBB, a suitable BBB model needed to be established and characterised. Different analyses were employed to ensure that the cell monolayers mimic the tightness of the BBB. *Secondly*, three types of NPs along with the positive and negative controls were assessed for their capabilities to travel through the BBB model.

5.4.4.1 Development and Characterisation of *in Vitro* BBB Model

Electrical Resistance Measurement

The TEER across the cell monolayers was measured as the preliminary assessment of the tightness of the *in vitro* BBB models. The study windows were selected as per the literature. Therefore, (a) the TEER of hCMEC/D3 cell monolayer was checked after every 24 hrs post-seeding up to six days because researchers reported that the highest TEER demonstrated by this cell line was around day 5-6 after they seeded the cells on inserts (Weksler *et al.*, 2013), and (b) the TEER of Caco-2 cell monolayer was checked twice a week post-seeding up to 32 days because the transport studies with this cell line were conducted previously within 21-25 days after the cell seeding (Crowe & Keelan, 2012; Senarathna *et al.*, 2016). Our study outcome (Figure 5.19) clearly shows that hCMEC/D3 did not possess high enough barrier tightness to be used as a BBB model. The cell growth cycle of hCMEC/D3 cells was investigated by Urich *et al.* (2012) who reported that freshly plated hCMEC/D3 cells attain confluency within 2-3 days and then reach a plateau level with little further changes that persists for several days. The researchers also observed cell overgrowth on the transwell filters after 7 days of post confluency. This agrees with our data where the hCMEC/D3 cells monolayer attained the highest TEER value (~15 $\Omega.cm^2$) at day 3 post-seeding which was much lesser than that the physiological TEER and hence was not considered for employing as BBB model for our study.

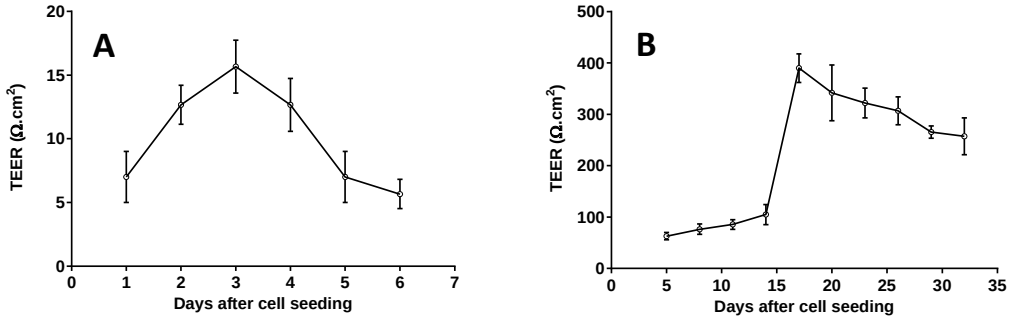

Figure 5.19. TEER of hCMEC/D3 cell monolayer over 6-days post seeding (A) and that of Caco-2 cell monolayer over 32-days post seeding (B). All data are presented as mean ± SD (n=3).

On the contrary, the Caco-2 cell monolayers demonstrated their maximum TEER value (~400 $\Omega.cm^2$) on day 17 after cell seeding and although gradually decreased, they retained the high TEER value (>300 $\Omega.cm^2$) at least for a week. Caco-2 cells have been used to estimate BBB permeability for nanocarriers due to the high TEER produced by the cell monolayer as well as the presence of the TJ proteins (Li *et al.*, 2004; Degim *et al.*, 2010; Senarathna *et al.*, 2016). However, other researchers suggested that Caco-2 cell monolayers are not an appropriate *in vitro* BBB model because linear correlations between *in vivo* and *in vitro* permeability data for Caco-2 BBB *in vitro* models has been lacking (Lundquist *et al.*, 2002; Garberg *et al.*, 2005). Nevertheless, due to our limited resource and time constraint, we employed Caco-2 cell monolayer as the *in vitro* BBB model assessing the transport of our NPs formulations on the basis that having TJ was a primary factor of consideration, and this cell line at least met that criteria.

Sucrose Permeability Assay

This study was carried out for Caco-2 cell monolayer to confirm the functionality of TJ in our *in vitro* BBB model. The sucrose flux in Caco-2 and other *in vitro* BBB models has been validated previously (Bowman *et al.*, 1983; Franke *et al.*, 1999), therefore, allowing comparison of our data with that reported to our model. In our study, we found that the ability of sucrose to penetrate through the Caco-2 cell monolayer reduced in a pattern in agreement with that of its TEER values. Thus, the lower permeability of the Caco-2 cell layer to sucrose was in correlation to high electrical resistance across the monolayer, reflecting the formation of TJ. Figure 5.20 illustrates that on the day 21 after seeding, the sucrose P_{app} across the cell monolayer was the lowest (2.89×10^{-6} cm/s) that suggested that TJ was at its peak and usage of Caco-2 cell monolayer around this day was scientifically valid.

The P_{app} of sucrose was determined to be 0.12×10^{-6} cm/s for the rat brain capillary (Levin, 1980). Our calculated P_{app} value was only 24 times higher than that of the reported *in vivo* human value and almost equal or lower than the values reported by many other research groups, such as 1.0×10^{-6} cm/s in porcine brain capillary endothelial cell monolayer (Franke *et al.*, 1999), 20.4×10^{-6} cm/s in bovine brain microvessel endothelial cell monolayer (Audus & Borchardt, 1986), 2.4×10^{-6} cm/s in Caco-2 cell monolayer (Hakkarainen *et al.*, 2010) and 10.5×10^{-6} cm/s in coculture of bovine brain capillary endothelial cell and astrocytes monolayer (Dehouck *et al.*, 1992). Hence, Caco-2 cell monolayer was deemed to be appropriate representation of the BBB in terms of TJ function and is suitable for the NPs transport study.

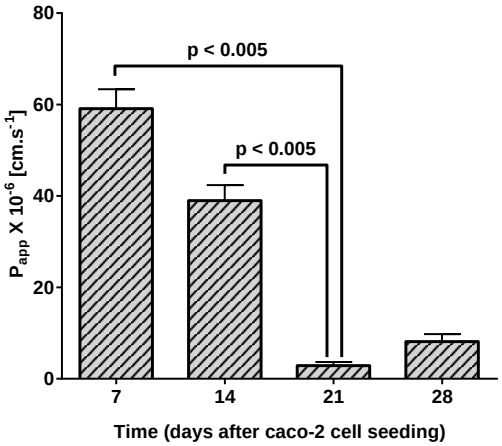

Figure 5.20. The decrement of P_{app} of sucrose (mean ± SD) over four weeks' period through Caco-2 cell monolayer on inserts indicating TJ formation around three weeks post seeding (n=3).

Confocal Microscopy Assay

The presence of one of the major TJ proteins (Occludin) was visually confirmed by immunostaining with primary and secondary antibodies. Images were taken for hCMEC/D3 and Caco-2 cell monolayers on day 3 and 21, respectively. The occludin protein was absent in between the adjacent hCMEC/D3 cells (Figure 5.21), while the Caco-2 cells demonstrated the clear presence of occludin (Figure 5.22) suggesting TJ formation among the adjacent cells as reported by Louzao *et al.* (2015).

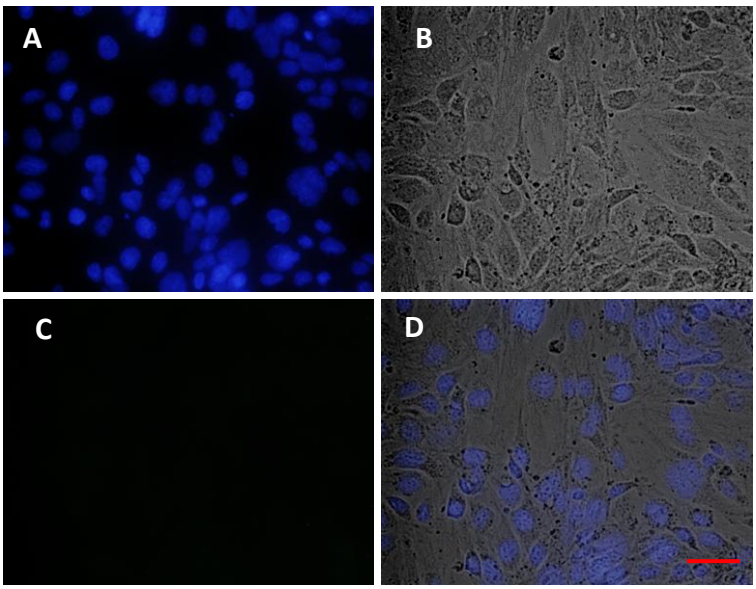

Figure 5.21. Immunofluorescence images of three days old hCMEC/D3 confluent monolayer showing the absence of TJ protein, occludin. Images of nuclei stained with DAPI (A), cell monolayer in bright-field (B), occludin stained with FITC (C) and merged image (D). The scale bar corresponds to 20 μm.

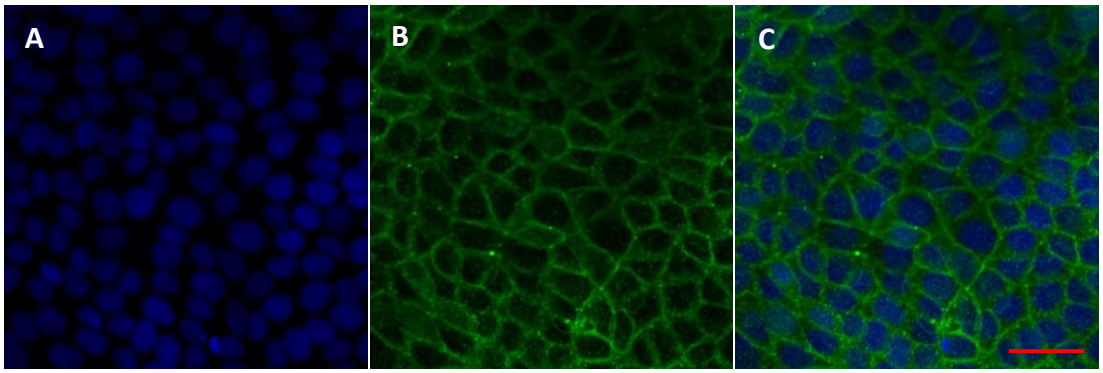

Figure 5.22. Confocal microscopy images of Caco-2 cell monolayer after 21-days post seeding. Image showing the DAPI stained nucleus (A), presence of well-structured FITC-stained TJ protein, occludin (B), and the superimposed image (C). The scale bar corresponds to 20 μm.

5.4.4.2 NPs Transport Across BBB Model

After establishing the *in vitro* BBB model, transport study of various types of NPs and DiD solution was conducted. Usage of phenol and FBS free HBSS-P medium for the study allowed us to use simple plate reader in fluorescence mode to analyse the DiD concentration in transport study samples. The fluorescence response of the DiD standard solutions as found to be linear up to 80ng/mL concentration in HBSS-P (Figure 5.23). The equation generated by the software was used to calculate the concentration of DiD throughout the experiments. The DiD standards were analysed every time the samples were analysed to nullify the variability of the analysis and calibration curve was constructed for the calculation purpose. However, we could not conduct the transport study more than three hours because of the lack of essential nutrients in the HBSS-P medium crucial for long-term survival of the cells.

As Figure 5.24 shows, approximately 21% of the total amount of the NPs with double ligands (NP1) was transported through the cell monolayer over the 3-hours period which was statistically significant (1.2 fold, $p < 0.05$) compared to the RHT solution. When compared to the transport of DiD solutions (1.7%), with that of the NP1, the statistical difference was remarkable (12.6-fold, $p < 0.001$) and very promising. Similar outcomes have been reported by several researchers who also employed TAT peptide as BBB targeting ligand for their nanocarriers (Rao *et al.*, 2008; Qin *et al.*, 2011a; Qin *et al.*, 2011b; Sharma *et al.*, 2013; Yan *et al.*, 2013; Sharma *et al.*, 2014).

NP2 (single ligand NP) and NP3 (zero ligand NP) did not show statistically significant difference against NP1 (dual ligand NP) and RHT solution, suggesting that SA alone as the ligand did not assist the NPs transportation process.

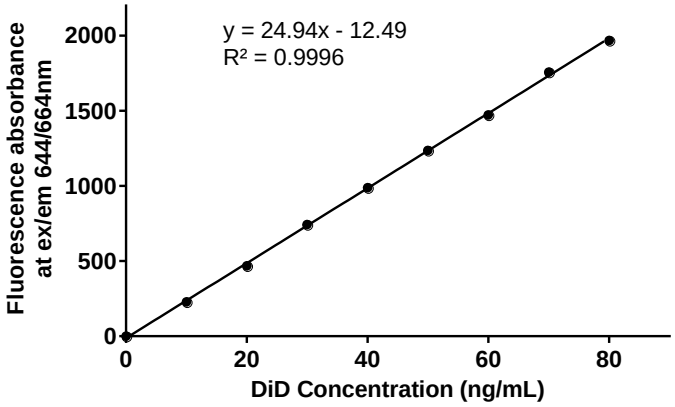

Figure 5.23. DiD calibration curve in HBSS-P.

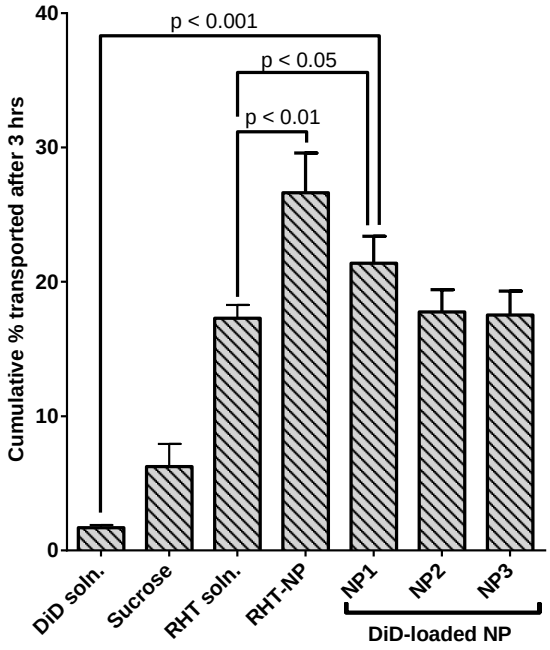

Figure 5.24. Comparison among different formulations showing cumulative percent transported through Caco-2 TJ after three hours of transport study. NP1 had both SA and TAT ligands, NP2 had only SA ligand and NP3 was prepared without any ligand. All data are presented as mean ± SD (n=3).

Figure 5.25 shows comparative cumulative percent transport of RHT, DiD and sucrose solutions as well as three types of DiD-loaded NPs. The cumulative percent transport of the RHT solution through Caco-2 cell monolayer was surprisingly high, however, agrees with the literature where the authors reported about 60% cumulative RHT transport in 24 hrs through the Caco-2 TJ (Degim *et al.*, 2010). Although the differences in cumulative percent transported among the three types of NPs were not significant ($p > 0.05$) compared to the RHT solution, huge elevation can be seen compared to that of the DiD solution and sucrose. There was no significant difference in TEER readings at the end of each experiment from the initial values suggesting the presence of an intact cell monolayer during the experiment.

Figure 5.25 also shows that the transport of RHT is about to attain the plateau level by the end of three hours' experiment, whereas, transport of the dual ligand NPs was still increasing. Most probably the cellular transport mechanism for RHT was saturated at that point. This hypothesis can further be emphasised with the fact that the RHT-loaded NPs demonstrated the highest cumulative percent transport among the DiD-loaded NPs and RHT solution. When compared to RHT-loaded NPs demonstrated 1.5-fold higher transport of the drug when compared with the RHT solution ($p < 0.01$). We postulate that there were two separate mechanism present for transporting NPs and RHT. Some amount of RHT must had leached from the RHT-loaded NPs due to the hydrophilic nature of the drug and contributed to the higher transport value of the NPs systems.

It might be questioned that the leaching can also contributed to DiD-loaded NPs, that can misleadingly raise their percent transport value. This argument is obsolete because we always centrifuged the NP suspension prior to commencing the experiment to get rid of any DiD that might had already leached out due to storage. We also found that the leaching from this highly lipophilic DiD-loaded NPs was only 0.16% w/w of the total loaded DiD (Section 4.4.4). Therefore, the cumulative transport values of each NPs can only be contributed by the NPs themselves.

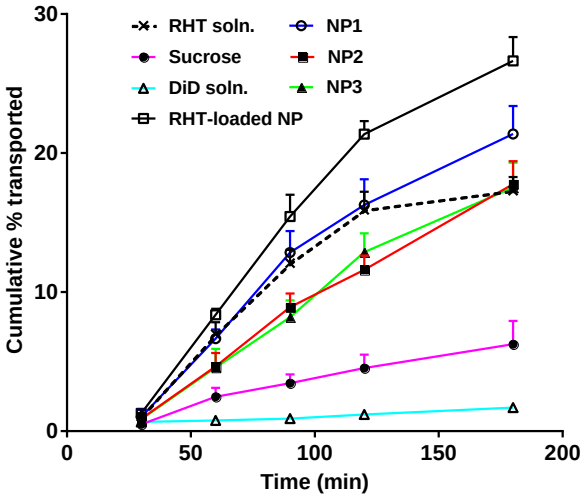

Figure 5.25. Transport experiments of RHT solution, RHT-loaded NPs, three types of DiD-loaded NPs, sucrose solution and DiD solution illustrating their cumulative percent transport through Caco-2 cell monolayer as *in vitro* BBB model over 180 minutes. NP1 had both SA and TAT ligands, NP2 had only SA ligand and NP3 was prepared without any ligand. All data are presented as mean ± SD (n=3).

The P_{app} values were calculated from Figure 5.25 and presented in Table 5.4. The values signify the rate of penetration of the compound of interest or NPs. The lower P_{app} values for sucrose ensure that during the experiments the barrier integrity was not compromised and they were still intact (Patabendige *et al.*, 2013a; Patabendige *et al.*, 2013b). On the other hand, the highest P_{app} value exerted by the RHT-loaded NPs indicates that the PEGylated dual ligand PLGA NPs system could be a promising tool for drug delivery.

Table 5.4. P_{app} of DiD solution, sucrose solution, RHT solution, RHT-loaded NPs and three types of DiD-loaded NPs under experiments. NP1 had both SA and TAT ligands, NP2 had only SA ligand and NP3 was prepared without any ligand.

Sample	dQ/dt		$P_{app} \times 10^{-6}$ (cm/sec)	
	Calculated by slope	Calculated by final point	Calculated by slope	Calculated by final point
DiD soln.	0.002	0.003	0.6	0.8
Sucrose	0.011	0.010	3.1	2.9
RHT soln.	0.050	0.029	13.8	8.0
RHT NP	0.067	0.044	18.7	12.3
NP1	0.052	0.036	14.4	9.9
NP2	0.034	0.030	9.3	8.2
NP3	0.040	0.029	11.0	8.1

5.5 General Summary

In this work, we used human brain cell line (hCMEC/D3) for NPs uptake studies. According to the results, endocytosis process might be responsible for the uptake of PLGA NPs by hCMEC/D3 cells. This human brain cells took up the PLGA NPs via a cellular mechanism that was saturable and temperature dependent. The rate of cellular uptake of NPs was mainly affected by the surface attached ligand, temperature and particle concentration. NPs whose surface was modified with TAT peptide showed the highest uptake. NPs with only SA as the ligand or without any ligand showed much lesser cellular uptake.

A similar trend was observed with the transport studies. NPs with dual ligands showed promising transport of the DiD lipophilic tracer whose cellular transport as a solution is very poor. Even transport of NPs with single and no ligand was also significantly higher than DiD solution. This dual ligand NPs system also stood out by demonstrating superior transport of RHT-loaded NPs. The human intestinal cell line (Caco-2) cultured on inserts as an *in vitro* BBB model was used for NPs transport studies. The three methods to investigate the BBB model (TEER measurement, sucrose permeability analysis and immunostaining for known TJ protein) provided enough evidence to confirm about the tightness of the model barrier which can represent TJ of the BBB. The quality control benchmark for permeability assay was set at a TEER of 250 $\Omega.cm^2$ and P_{app} of sucrose of 6×10^{-6} cm per sec. All the inserts under experiments achieved these targets. This BBB model retained the BBB features and proved to be a suitable substitute of *in vivo* BBB for PLGA NPs transport studies.

Toxicity effect of all the experimental solutions and NP suspensions were evaluated on corresponding cell lines using MTT assay and all formulations were found to have an insignificant effect on cell viability at the experimental concentrations. PLGA NPs surface modified with dual ligands thus may be employed as a drug delivery system for bioactive molecules, especially which show poor BBB penetration.

5.6 Conclusions

Based on our experiments, we concluded that dual ligand PLGA NPs is a novel, promising and biocompatible brain DDS with acceptable toxicity. This DDS provides an effective technique for brain delivery of any bioactive compound with the purpose of bioavailability enhancement.

Chapter 6 Summary, Future Research Scope and Conclusions

6.1 General Summary

In this research study, RHT-loaded PEG-PLGA NPs were developed with dual targeting ligands using double emulsion solvent evaporation technique. The resultant nanoparticles were of small particle size (<200nm), with a hydrophilic moiety (PEG) on the NPs surface to maximise their escaping capability from the physiological RES upon IV administration; with TAT peptide as 1st ligand grafted onto the NPs surface for targeting BBB to enhance brain penetration capability of NP; with SA as a second ligand incorporated into the NPs for interacting with the brain parenchyma after the NPs entered the brain to enhance the NPs residence time inside the brain. Both ligands were conjugated with lipophilic molecules so that they can be easily incorporated in the nanoparticles during their formulation with the core lipophilic polymer (PLGA). The TAT peptide was coupled with DSPE-PEG chain whereas the SA was with ODA. The conjugated DSPE-PEG-TAT product was characterised both quantitatively and qualitatively by RP-HPLC and MALTI-TOF-MS, respectively. The SA-ODA conjugate was also characterised by NMR and FT-IT analysis, respectively. Analyses confirmed the successful chemical conjugation of both.

PLGA NPs with dual targeting ligands for brain delivery system has been published by other researchers. However, there is no nanoparticulate DDS reported, as yet, that uses SA and TAT peptide together as targeting ligands for any drug. It is the first time, as far as the author is aware, such a novel NPs formulation was developed for RHT.

Several formulation factors were optimised to obtain NPs with desired particle size, zeta potential and drug loading. PLGA molecular weight and concentration, RHT ionic form, organic solvent composition, NPs preparation method, stabiliser type and concentration, as well as energy input during the emulsion preparation, were found to have critical role determining the desired NPs properties. After optimisation, the RHT loading of NPs has been improved from 0.1 to final 3% w/w while particle size controlled within 200nm. The optimised PEGylated dual ligand PLGA NPs was then loaded with RHT, the model AD drug in this project.

The physicochemical properties of NPs system were evaluated *in vitro* by assessing their particle size, zeta potential and drug loading and release, in addition to the morphology using FESEM. Release study showed that about 50% drug was released from the NPs within first 24 hours, suggesting that the NPs system are well capable of releasing the matrix-entrapped drug in a controlled manner. The developed NPs system was stable for at least 7 days at 4°C without any significant alteration in particle size and surface charge as well as the level of drug leaching.

A stability indicating HPLC analysis method was developed, optimised and fully validated for the quantification of RHT. This method was used throughout the project for determining the RHT stability and loading efficiency in the NPs, to analyse RHT release from the NPs in the release studies and to analyse RHT in the culture medium. RHT was found to be stable at neutral and acidic pH, however, showed degradation at basic pH, especially at elevated temperature. The developed HPLC method is capable of separating RHT from all other impurities, excipients, degradation products of RHT and medium making it a basic bench method for future modification for analysis of *in vivo* biological samples in future NPs evaluation.

Finally, an extensive cellular characterisation of the optimised NPs system was carried out to assess cellular response of the developed NPs in terms of cytotoxicity, cellular uptake and transport under the influence of targeting ligands. Drug leach from the NPs was assessed in appropriate assay medium simulating similar experimental conditions as like the cellular experiments. The cytotoxicity study was carried out in both human endothelial cell line (hCMEC/D3) and human colorectal cell line (Caco-2). The cellular uptake and cellular transport studies were conducted in hCMEC/D3 and Caco-2 cell lines, respectively. Drug leaching from the NPs in the assay medium was found to be negligible. The NPs system was found to have no significant detectable cytotoxic effect in both cell lines up to 200µg/mL concentration. The cellular uptake study revealed that the TAT peptide significantly enhanced the NPs uptake by an energy dependent process. Two independent model lipophilic tracers were loaded into the NPs system for the visualisation purpose. Confocal microscopy images confirmed the findings of the cellular uptake study and proved that the majority of NPs were, in fact, internalised instead of attached on the cell surface, possibly via energy-dependent endocytosis mechanism.

The transport study showed that a much higher amount and rate of drug transport was achieved by using the developed dual ligand NPs system in comparison to single ligand NPs or NPs without any ligand. Compared to the NPs system without any ligand, the dual ligand NPs system was found to transport higher amount of drug, however, it was not statistically significant. Overall, from this cellular studies, it can be concluded that the developed dual ligand NPs system was a safe and effective transporter of bioactive molecules into the brain across BBB. The results of this project also demonstrate that the platform NPs technology developed can be easily customised to load not only RHT but also other types of biomolecules for drug targeting/delivery into the CNS.

6.2 Limitations of the Study and Future Work

This research study was performed to investigate the feasibility and potential of dual ligand polymeric NPs to deliver a model drug (RHT) across the BBB. During this project, a few challenges were encountered and resolved. However, there are still some remained. For instance, drug loading and entrapment efficiency. Despite of many attempts, the drug entrapment efficiency was very low (6.1%) which may result a cost-ineffective process due to loss of high amount of drug during the formulation process. Incorporating a hydrophilic drug molecule into a hydrophobic matrix is always challenging issue which is yet to be addressed properly. Instead of using the PLGA by its own, a combination of the polymer with a compatible hydrophilic polymer may produce a better RHT entrapment. The drug loading was also relatively poor (3%) which needs to be improved. We speculate the reasons behind this low drug loading was the very high solubility of RHT in water (80mg/mL) as well as its solubility in the organic solvent EtAc (2mg/mL) used for NPs formulation. These factors facilitated RHT diffusion from the inner aqueous phase into the outer aqueous phase across the organic layer during the emulsion preparation step resulting in a low RHT amount in NPs.

The cellular uptake investigations could be carried out with depleted ATP level within hCMEC/D3 cells by treatment with sodium azide. This could further confirm the energy dependency of the NPs uptake process. In addition, a neuron cell line could not be included due to its unavailability at the time and the current cell lines did not permit us to investigate the effect of the SA ligand on cellular uptake and transport. The ultimate effect of both targeting ligands also has to be evaluated using an animal model especially when it is known that SA receptors are present in several organs other than brain parenchyma (liver, kidney, and lung). An increased accumulation of SA-covered NPs in those SA-receptor enriched organs has been reported by other workers (Tosi *et al.*, 2010). Therefore, we propose the future studies should include:

- A further optimisation of formulation process to increase EE,
- An uptake study using neurone cell line to assess the effect of SA ligand,
- Uptake study of RHT solution, coumarin-6, DiD solution and RHT-loaded NPs,
- Longer hours in transport study to see if the differences between the NPs and RHT even greater,
- Cellular uptake study of Caco-2 cells to see if it is similar to that of hCMEC/D3 and does this correlate to the transport study, and
- An *in vivo* biodistribution study of NPs with and without ligands in an animal model to confirm the effect of dual targeting ligand NPs.

6.3 Conclusions

This study highlights the potential of dual ligand PLGA NPs as a simple and effective particulate delivery system for delivery of bioactive molecule across the BBB. The research in this thesis highlighted the importance of various factors for the development of targeted DDS. This includes reaction optimisation for ligand conjugate synthesis, NPs formulation optimisation and evaluation of pharmaceutical factors such as EE, DL, release profile. The targeting capability of the TAT peptide was confirmed and the superior cellular uptake and transport of the drug loaded optimised dual ligand formulation by the human cell lines proved the potential use of TAT peptide as a BBB targeting agent for NPs system. Further in-depth cellular studies along with *in vivo* study are required to make final conclusion on the real potential of the developed NPs system as a truly targeted brain DDS.

Reference

Al-Quadeib, B. T., Radwan, M. A., Siller, L., Horrocks, B., & Wright, M. C. (2015). Stealth Amphotericin B nanoparticles for oral drug delivery: In vitro optimization. *Saudi Pharmaceutical Journal, 23*(3), 290-302.

Alai, M., & Lin, W. J. (2015). Application of nanoparticles for oral delivery of acid-labile lansoprazole in the treatment of gastric ulcer: in vitro and in vivo evaluations. *International Journal of Nanomedicine, 10*, 4029-4041.

Alexis, F., Pridgen, E., Molnar, L. K., & Farokhzad, O. C. (2008). Factors Affecting the Clearance and Biodistribution of Polymeric Nanoparticles. *Molecular Pharmaceutics, 5*(4), 505-515.

Amass, W., Amass, A., & Tighe, B. (1998). A review of biodegradable polymers: uses, current developments in the synthesis and characterization of biodegradable polyesters, blends of biodegradable polymers and recent advances in biodegradation studies. *Polymer International, 47*(2), 89-144.

Amin, M. L., Kim, D., & Kim, S. (2016). Development of hematin conjugated PLGA nanoparticle for selective cancer targeting. *European Journal of Pharmaceutical Sciences, 91*, 138-143.

Amini, H., & Ahmadiani, A. (2010). High-Performance Liquid Chromatographic Determination of Rivastigmine in Human Plasma for Application in Pharmacokinetic Studies. *Iranian Journal of Pharmaceutical Research, 9*(2), 115-121.

Anand, R., Gill, K. D., & Mahdi, A. A. (2013). Therapeutics of Alzheimer's disease: Past, present and future. *Neuropharmacology, 76 Pt A*, 27-50.

Antoniou, M., Gunasekera, G., & Wong, P. C. M. (2013). Foreign language training as cognitive therapy for age-related cognitive decline: A hypothesis for future research. *Neuroscience and Biobehavioral Reviews, 37*(10 Pt 2), 2689-2698.

Ariga, T. (2017). The Pathogenic Role of Ganglioside Metabolism in Alzheimer's Disease-Cholinergic Neuron-Specific Gangliosides and Neurogenesis. *Molecular Neurobiology, 54*(1), 623-638.

Arpicco, S., Battaglia, L., Brusa, P., Cavalli, R., Chirio, D., Dosio, F., . . . Ceruti, M. (2016). Recent studies on the delivery of hydrophilic drugs in nanoparticulate systems. *Journal of Drug Delivery Science and Technology, 32, Part B*, 298-312.

Arumugam, K., Chamallamudi, M., Mallayasamy, S., Mullangi, R., Ganesan, S., Jamadar, L., . . . Udupa, N. (2011a). High performance liquid chromatographic fluorescence detection method for the quantification of rivastigmine in rat plasma and brain: application to preclinical pharmacokinetic studies in rats. *Journal of Young Pharmacists, 3*(4), 315-321.

Arumugam, K., Chamallamudi, M. R., Gilibili, R. R., Mullangi, R., Ganesan, S., Kar, S. S., . . . Udupa, N. (2011b). Development and validation of a HPLC method for quantification of rivastigmine in rat urine and identification of a novel metabolite in urine by LC-MS/MS. *Biomedical Chromatography, 25*(3), 353-361.

Arumugam, K., Subramanian, G. S., Mallayasamy, S. R., Averineni, R. K., Reddy, M. S., & Udupa, N. (2008). A study of rivastigmine liposomes for delivery into the brain through intranasal route. *Acta pharmaceutica, 58*(3), 287-297.

Aryal, M., Vykhodtseva, N., Zhang, Y.-Z., & McDannold, N. (2015). Multiple sessions of liposomal doxorubicin delivery via focused ultrasound mediated blood–brain barrier disruption: A safety study. *Journal of Controlled Release, 204*, 60-69.

Astete, C. E., & Sabliov, C. M. (2006). Synthesis and characterization of PLGA nanoparticles. *Journal of Biomaterials Science, Polymer Edition, 17*(3), 247-289.

Attwood, D. (2013). Disperse systems. In M. E. Aulton (Ed.), *Aulton's Pharmaceutics: The Design and Manufacture of Medicines* (4 ed.). London, UK: Churchill Livingstone.

Audus, K. L., & Borchardt, R. T. (1986). Characteristics of the large neutral amino acid transport system of bovine brain microvessel endothelial cell monolayers. *Journal of Neurochemistry, 47*(2), 484-488.

Auffret, M., Le Jeune, F., Maurus, A., Drapier, S., Houvenaghel, J.-F., Robert, G. H., . . . Vérin, M. (2017). Apomorphine pump in advanced Parkinson's disease: Effects on motor and nonmotor symptoms with brain metabolism correlations. *Journal of the Neurological Sciences, 372*, 279-287.

Averineni, R., Shavi, G., Gurram, A., Deshpande, P., Arumugam, K., Maliyakkal, N., . . . Nayanabhirama, U. (2012). PLGA 50:50 nanoparticles of paclitaxel: Development, in vitro anti-tumor activity in BT-549 cells and in vivo evaluation. *Bulletin of Materials Science, 35*(3), 319-326.

Azad, T. D., Pan, J., Connolly, I. D., Remington, A., Wilson, C. M., & Grant, G. A. (2015). Therapeutic strategies to improve drug delivery across the blood-brain barrier. *Neurosurgical Focus, 38*(3), E9.

Azevedo, F. A. C., Carvalho, L. R. B., Grinberg, L. T., Farfel, J. M., Ferretti, R. E. L., Leite, R. E. P., . . . Herculano-Houzel, S. (2009). Equal numbers of neuronal and nonneuronal cells make the human brain an isometrically scaled-up primate brain. *The Journal of Comparative Neurology, 513*(5), 532-541.

Azimi, B., Nourpanah, P., Rabiee, M., & Arbab, S. (2014). Producing Gelatin Nanoparticles as Delivery System for Bovine Serum Albumin. *Iranian Biomedical Journal, 18*(1), 34-40.

Bachurin, S. O., Bovina, E. V., & Ustyugov, A. A. (2017). Drugs in Clinical Trials for Alzheimer's Disease: The Major Trends. *Medicinal Research Reviews*, doi: 10.1002/med.21434. [Epub ahead of print].

Badran, M. M., Mady, M. M., Ghannam, M. M., & Shakeel, F. (2017). Preparation and characterization of polymeric nanoparticles surface modified with chitosan for target treatment of colorectal cancer. *International Journal of Biological Macromolecules, 95*, 643-649.

Banerjee, J., Shi, Y., & Azevedo, H. S. (2016). In vitro blood–brain barrier models for drug research: state-of-the-art and new perspectives on reconstituting these models on artificial basement membrane platforms. *Drug Discovery Today, 21*(9), 1367-1386.

Banks, W. A. (2012). Drug delivery to the brain in Alzheimer's disease: Consideration of the blood–brain barrier. *Adv Drug Deliv Rev, 64*(7), 629-639.

Bassett, D. S., & Gazzaniga, M. S. (2011). Understanding complexity in the human brain. *Trends in Cognitive Sciences, 15*(5), 200-209.

Bhardwaj, V., Ankola, D., Gupta, S., Schneider, M., Lehr, C.-M., & Kumar, M. R. (2009). PLGA nanoparticles stabilized with cationic surfactant: safety studies and application in oral delivery of paclitaxel to treat chemical-induced breast cancer in rat. *Pharmaceutical Research, 26*(11), 2495-2503.

Bhatnagar, P., Pant, A. B., Shukla, Y., Panda, A., & Gupta, K. C. (2016). Hyaluronic acid grafted PLGA copolymer nanoparticles enhance the targeted delivery of Bromelain in Ehrlich's Ascites Carcinoma. *European Journal of Pharmaceutics and Biopharmaceutics, 105*, 176-192.

Bhatt, J., Subbaiah, G., Kambli, S., Shah, B., Nigam, S., Patel, M., . . . Yadav, G. (2007). A rapid and sensitive liquid chromatography-tandem mass spectrometry (LC-MS/MS) method for the estimation of rivastigmine in human plasma. *Journal of Chromatography B, 852*(1-2), 115-121.

Bhattacharjee, S. (2016). DLS and zeta potential – What they are and what they are not? *Journal of Controlled Release, 235*, 337-351.

Biemans, E., Jakel, L., de Waal, R. M. W., Kuiperij, H. B., & Verbeek, M. M. (2017). Limitations of the hCMEC/D3 cell line as a model for Abeta clearance by the human blood-brain barrier. *Journal of Neuroscience Research, 95*(7), 1513-1522.

Bilensoy, E. (2010). Cationic nanoparticles for cancer therapy. *Expert Opinion on Drug Delivery, 7*(7), 795-809.

Birks, J. S., Chong, L. Y., & Grimley Evans, J. (2015). Rivastigmine for Alzheimer's disease. *Cochrane Database of Systematic Reviews*(9), 1-198.

Boccardi, V., Baroni, M., Mangialasche, F., & Mecocci, P. (2016). Vitamin E family: Role in the pathogenesis and treatment of Alzheimer's disease. *Alzheimer's & Dementia: Translational Research & Clinical Interventions, 2*(3), 182-191.

Bondioli, L., Costantino, L., Ballestrazzi, A., Lucchesi, D., Boraschi, D., Pellati, F., . . . Vandelli, M. A. (2010). PLGA nanoparticles surface decorated with the sialic acid, N-acetylneuraminic acid. *Biomaterials, 31*(12), 3395-3403.

Bowman, P. D., Ennis, S. R., Rarey, K. E., Betz, A. L., & Goldstein, G. W. (1983). Brain microvessel endothelial cells in tissue culture: a model for study of blood-brain barrier permeability. *Annals of Neurology, 14*(4), 396-402.

Brar, S. K., & Verma, M. (2011). Measurement of nanoparticles by light-scattering techniques. *TrAC Trends in Analytical Chemistry, 30*(1), 4-17.

Brigger, I., Morizet, J., Laudani, L., Aubert, G., Appel, M., Velasco, V., . . . Vassal, G. (2004). Negative preclinical results with stealth nanospheres-encapsulated Doxorubicin in an orthotopic murine brain tumor model. *Journal of Controlled Release, 100*(1), 29-40.

Cai, Q., Wang, L., Deng, G., Liu, J., Chen, Q., & Chen, Z. (2016). Systemic delivery to central nervous system by engineered PLGA nanoparticles. *American Journal of Translational Research, 8*(2), 749-764.

Canney, D. J. (2005). Cholinomimetic drugs. In R. Hendrickson (Ed.), *Remington: The Science and Practice of Pharmacy* (21st ed., pp. 1397). Maryland, USA: Wolters Kluwer Health/Lippincott, Williams & Wilkins.

Cannon, J. R., & Greenamyre, J. T. (2011). The Role of Environmental Exposures in Neurodegeneration and Neurodegenerative Diseases. *Toxicological Sciences, 124*(2), 225-250.

Cao, L.-B., Zeng, S., & Zhao, W. (2016). Highly Stable PEGylated Poly(lactic-co-glycolic acid) (PLGA) Nanoparticles for the Effective Delivery of Docetaxel in Prostate Cancers. *Nanoscale Research Letters, 11*(1), 305.

Cartiera, M. S., Johnson, K. M., Rajendran, V., Caplan, M. J., & Saltzman, W. M. (2009). The Uptake and Intracellular Fate of PLGA Nanoparticles in Epithelial Cells. *Biomaterials, 30*(14), 2790-2798.

Causes of Death, Australia, 2015. (2016, 28/09/2016). [Accessed on: 03/Jan/2016] Retrieved from http://www.abs.gov.au/ausstats/abs@.nsf/Lookup/by%20Subject/3303.0~2015~Main%20Features~Australia's%20leading%20causes%20of%20death,%202015~3

Cháirez-Ramírez, M. H., Sánchez-Burgos, J. A., Gomes, C., Moreno-Jiménez, M. R., González-Laredo, R. F., Bernad-Bernad, M. J., . . . Rocha-Guzmán, N. E. (2015). Morphological and release characterization of nanoparticles formulated with poly (dl-lactide-co-glycolide) (PLGA) and lupeol: In vitro permeability and modulator effect on NF-κB in Caco-2 cell system stimulated with TNF-α. *Food and Chemical Toxicology, 85*, 2-9.

Chang, H.-H., Cheng, C.-L., Huang, P.-J., & Lin, S.-Y. (2014). Application of scanning electron microscopy and X-ray microanalysis: FE-SEM, ESEM-EDS, and EDS mapping for studying the characteristics of topographical microstructure and elemental mapping of human cardiac calcified deposition. *Analytical and Bioanalytical Chemistry, 406*(1), 359-366.

Chang, J., Jallouli, Y., Kroubi, M., Yuan, X. B., Feng, W., Kang, C. S., . . . Betbeder, D. (2009). Characterization of endocytosis of transferrin-coated PLGA nanoparticles by the blood-brain barrier. *International Journal of Pharmaceutics, 379*(2), 285-292.

Chaudhari, K. R., Kumar, A., Khandelwal, V. K. M., Ukawala, M., Manjappa, A. S., Mishra, A. K., . . . Murthy, R. S. R. (2012). Bone metastasis targeting: A novel approach to reach bone using Zoledronate anchored PLGA nanoparticle as carrier system loaded with Docetaxel. *Journal of Controlled Release, 158*(3), 470-478.

Chen, H., Zheng, Y., Tian, G., Tian, Y., Zeng, X., Liu, G., . . . Huang, L. (2011). Oral Delivery of DMAB-Modified Docetaxel-Loaded PLGA-TPGS Nanoparticles for Cancer Chemotherapy. *Nanoscale Research Letters, 6*(1), 4-4.

Chen, S., Yang, K., Tuguntaev, R. G., Mozhi, A., Zhang, J., Wang, P. C., & Liang, X.-J. (2016). Targeting tumor microenvironment with PEG-based amphiphilic nanoparticles to overcome chemoresistance. *Nanomedicine: Nanotechnology, Biology and Medicine, 12*(2), 269-286.

Chen, Y., & Li, T. (2015). Cellular Uptake Mechanism of Paclitaxel Nanocrystals Determined by Confocal Imaging and Kinetic Measurement. *The AAPS Journal, 17*(5), 1126-1134.

Chen, Y., & Liu, L. (2012). Modern methods for delivery of drugs across the blood–brain barrier. *Adv Drug Deliv Rev, 64*(7), 640-665.

Chen, Y., Siddalingappa, B., Chan, P. H. H., & Benson, H. A. E. (2008a). Development of a chitosan-based nanoparticle formulation for delivery of a hydrophilic hexapeptide, dalargin. *Peptide Science, 90*(5), 663-670.

Chen, Y., Wang, F., & Benson, H. A. (2008b). Effect of formulation factors on incorporation of the hydrophilic peptide dalargin into PLGA and mPEG-PLGA nanoparticles. *Biopolymers, 90*(5), 644-650.

Chen, Y. C., Hsieh, W. Y., Lee, W. F., & Zeng, D. T. (2013). Effects of surface modification of PLGA-PEG-PLGA nanoparticles on loperamide delivery efficiency across the blood-brain barrier. *Journal of Biomaterials Applications, 27*(7), 909-922.

Cheng, J., Teply, B. A., Sherifi, I., Sung, J., Luther, G., Gu, F. X., . . . Farokhzad, O. C. (2007). Formulation of functionalized PLGA–PEG nanoparticles for in vivo targeted drug delivery. *Biomaterials, 28*(5), 869-876.

Cheng, L., Jin, C., Lv, W., Ding, Q., & Han, X. (2011). Developing a Highly Stable PLGA-mPEG Nanoparticle Loaded with Cisplatin for Chemotherapy of Ovarian Cancer. *PloS One, 6*(9), e25433.

Cherian, J., & Gohil, K. (2015). Cautious Optimism for Growth In Alzheimer's Disease Treatments. *Pharmacy and Therapeutics, 40*(4), 288-289.

Chithrani, D. B., Dunne, M., Stewart, J., Allen, C., & Jaffray, D. A. (2010). Cellular uptake and transport of gold nanoparticles incorporated in a liposomal carrier. *Nanomedicine: Nanotechnology, Biology and Medicine, 6*(1), 161-169.

Chowdhury, S., Schatte, G., & Kraatz, H.-B. (2006). Rational Design of Bioorganometallic Foldamers: A Potential Model for Parallel β-Helical Peptides. *Angewandte Chemie International Edition, 45*(41), 6882-6884.

Ciappellano, S. G., Tedesco, E., Venturini, M., & Benetti, F. (2016). In vitro toxicity assessment of oral nanocarriers. *Adv Drug Deliv Rev, 106, Part B*, 381-401.

Cook, A. B., Barbey, R., Burns, J. A., & Perrier, S. (2016). Hyperbranched Polymers with High Degrees of Branching and Low Dispersity Values: Pushing the Limits of Thiol–Yne Chemistry. *Macromolecules, 49*(4), 1296-1304.

Costantino, L., Gandolfi, F., Tosi, G., Rivasi, F., Vandelli, M. A., & Forni, F. (2005). Peptide-derivatized biodegradable nanoparticles able to cross the blood–brain barrier. *Journal of Controlled Release, 108*(1), 84-96.

Crowe, A., & Keelan, J. A. (2012). Development of a model for functional studies of ABCG2 (breast cancer resistance protein) efflux employing a standard BeWo clone (B24). *ASSAY and Drug Development Technologies, 10*(5), 476-484.

Cui, Y., Xu, Q., Chow, P. K., Wang, D., & Wang, C. H. (2013). Transferrin-conjugated magnetic silica PLGA nanoparticles loaded with doxorubicin and paclitaxel for brain glioma treatment. *Biomaterials, 34*(33), 8511-8520.

Dadras, P., Atyabi, F., Irani, S., Ma'mani, L., Foroumadi, A., Mirzaie, Z. H., . . . Dinarvand, R. (2017). Formulation and evaluation of targeted nanoparticles for breast cancer theranostic system. *European Journal of Pharmaceutical Sciences, 97*, 47-54.

Dandekar, P. P., & Patravale, V. B. (2009). Development and Validation of a Stability-Indicating LC Method for Curcumin. *Chromatographia, 69*(9), 871-877.

Danhier, F., Ansorena, E., Silva, J. M., Coco, R., Le Breton, A., & Préat, V. (2012). PLGA-based nanoparticles: An overview of biomedical applications. *Journal of Controlled Release, 161*(2), 505-522.

Davda, J., & Labhasetwar, V. (2002). Characterization of nanoparticle uptake by endothelial cells. *International Journal of Pharmaceutics, 233*(1–2), 51-59.

de Andrade, D. F., Zuglianello, C., Pohlmann, A. R., Guterres, S. S., & Beck, R. C. R. (2015). Assessing the In Vitro Drug Release from Lipid-Core Nanocapsules: a New Strategy Combining Dialysis Sac and a Continuous-Flow System. *AAPS PharmSciTech, 16*(6), 1409-1417.

De Jong, W. H., & Borm, P. J. A. (2008). Drug delivery and nanoparticles: Applications and hazards. *International Journal of Nanomedicine, 3*(2), 133-149.

Decuzzi, P., & Ferrari, M. (2007). The role of specific and non-specific interactions in receptor-mediated endocytosis of nanoparticles. *Biomaterials, 28*(18), 2915-2922.

Degim, Z., Mutlu, N. B., Yilmaz, S., Essiz, D., & Nacar, A. (2010). Investigation of liposome formulation effects on rivastigmine transport through human colonic adenocarcinoma cell line (CACO-2). *Pharmazie, 65*(1), 32-40.

Dehouck, M. P., Jolliet-Riant, P., Bree, F., Fruchart, J. C., Cecchelli, R., & Tillement, J. P. (1992). Drug transfer across the blood-brain barrier: correlation between in vitro and in vivo models. *Journal of Neurochemistry, 58*(5), 1790-1797.

Desai, M. P., Labhasetwar, V., Walter, E., Levy, R. J., & Amidon, G. L. (1997). The Mechanism of Uptake of Biodegradable Microparticles in Caco-2 Cells Is Size Dependent. *Pharmaceutical Research, 14*(11), 1568-1573.

Dinarvand, R., Sepehri, N., Manoochehri, S., Rouhani, H., & Atyabi, F. (2011). Polylactide-co-glycolide nanoparticles for controlled delivery of anticancer agents. *International Journal of Nanomedicine, 6*, 877-895.

Dong, Y., & Feng, S. S. (2006). Nanoparticles of poly(D,L-lactide)/methoxy poly(ethylene glycol)-poly(D,L-lactide) blends for controlled release of paclitaxel. *J Biomed Mater Res A, 78*(1), 12-19.

Doolittle, E., Peiris, P. M., Doron, G., Goldberg, A., Tucci, S., Rao, S., . . . Karathanasis, E. (2015). Spatiotemporal Targeting of a Dual-Ligand Nanoparticle to Cancer Metastasis. *ACS Nano, 9*(8), 8012-8021.

Duncan, R., & Gaspar, R. (2011). Nanomedicine(s) under the Microscope. *Molecular Pharmaceutics, 8*(6), 2101-2141.

Dwyer, J., Hebda, J. K., Le Guelte, A., Galan-Moya, E.-M., Smith, S. S., Azzi, S., . . . Gavard, J. (2012). Glioblastoma Cell-Secreted Interleukin-8 Induces Brain Endothelial Cell Permeability via CXCR2. *PloS One, 7*(9), e45562.

Ehrlich, P. (1902). Immunology and cancer research. *Collected papers of Paul Ehrlich*, 442.

Ehrlich, P. (1906). *Uber die Beziehungen von chemische Constitution, Vertheilung, und pharmakologisher Wirkung. Collected Studies in Immunity. Repr. and Trans.* New York: John Wiley & Sons.

Eigenmann, D. E., Xue, G., Kim, K. S., Moses, A. V., Hamburger, M., & Oufir, M. (2013). Comparative study of four immortalized human brain capillary endothelial cell lines, hCMEC/D3, hBMEC, TY10, and BB19, and optimization of culture conditions, for an in vitro blood–brain barrier model for drug permeability studies. *Fluids and Barriers of the CNS, 10*(1), 1-17.

El-Hammadi, M. M., Delgado, Á. V., Melguizo, C., Prados, J. C., & Arias, J. L. (2017). Folic acid-decorated and PEGylated PLGA nanoparticles for improving the antitumour activity of 5-fluorouracil. *International Journal of Pharmaceutics, 516*(1–2), 61-70.

Enz, A., Chappuis, A., & Dattler, A. (2004). A simple, rapid and sensitive method for simultaneous determination of rivastigmine and its major metabolite NAP 226-90 in rat brain and plasma by reversed-phase liquid chromatography coupled to electrospray ionization mass spectrometry. *Biomedical Chromatography, 18*(3), 160-166.

Erdo, F., Denes, L., & de Lange, E. (2017). Age-associated physiological and pathological changes at the blood-brain barrier: A review. *Journal of Cerebral Blood Flow and Metabolism, 37*(1), 4-24.

Escalona-Rayo, O., Fuentes-Vázquez, P., Leyva-Gómez, G., Cisneros, B., Villalobos, R., Magaña, J. J., & Quintanar-Guerrero, D. (2017). Nanoparticulate strategies for the treatment of polyglutamine diseases by halting the protein aggregation process. *Drug Development and Industrial Pharmacy*, 1-21.

Fang, Z., Chen, S., Qin, J., Chen, B., Ni, G., Chen, Z., . . . Wu, C. (2016). Pluronic P85-coated poly (butylcyanoacrylate) nanoparticles overcome phenytoin resistance in P-glycoprotein overexpressing rats with lithium-pilocarpine-induced chronic temporal lobe epilepsy. *Biomaterials, 97*, 110-121.

Farlow, M. R., Grossberg, G. T., Sadowsky, C. H., Meng, X., & Velting, D. M. (2015). A 24-week, open-label extension study to investigate the long-term safety, tolerability, and efficacy of 13.3 mg/24 h rivastigmine patch in patients with severe Alzheimer disease. *Alzheimer Disease and Associated Disorders, 29*(2), 110-116.

Fazil, M., Md, S., Haque, S., Kumar, M., Baboota, S., Sahni, J. k., & Ali, J. (2012). Development and evaluation of rivastigmine loaded chitosan nanoparticles for brain targeting. *European Journal of Pharmaceutical Sciences, 47*(1), 6-15.

Feng, S.-S., & Chien, S. (2003). Chemotherapeutic engineering: Application and further development of chemical engineering principles for chemotherapy of cancer and other diseases. *Chemical Engineering Science, 58*(18), 4087-4114.

Feng, S. S. (2006). New-concept chemotherapy by nanoparticles of biodegradable polymers: where are we now? *Nanomedicine (Lond), 1*(3), 297-309.

Feng, S. S., Mu, L., Win, K. Y., & Huang, G. (2004). Nanoparticles of biodegradable polymers for clinical administration of paclitaxel. *Current Medicinal Chemistry, 11*(4), 413-424.

Field, L. D., Sternhell, S., & Kalman, J. R. (2013). *Organic Structures from Spectra* (5 ed.). West Sussex, UK: John Wiley & Sons.

Figiel, G., & Sadowsky, C. (2008). A systematic review of the effectiveness of rivastigmine for the treatment of behavioral disturbances in dementia and other neurological disorders. *Current Medical Research and Opinion, 24*(1), 157-166.

Finkel, S. I. (2004). Effects of rivastigmine on behavioral and psychological symptoms of dementia in Alzheimer's disease. *Clinical Therapeutics, 26*(7), 980-990.

Fong, J. W., Nazareno, J. P., Pearson, J. E., & Maulding, H. V. (1986). Evaluation of biodegradable microspheres prepared by a solvent evaporation process using sodium oleate as emulsifier. *Journal of Controlled Release, 3*(1), 119-130.

Fonte, P., Soares, S., Costa, A., Andrade, J. C., Seabra, V., Reis, S., & Sarmento, B. (2012). Effect of cryoprotectants on the porosity and stability of insulin-loaded PLGA nanoparticles after freeze-drying. *Biomatter, 2*(4), 329-339.

Frank, S., Testa, C. M., Stamler, D., Kayson, E., Davis, C., Edmondson, M. C., . . . Christopher, E. (2016). Effect of Deutetrabenazine on Chorea Among Patients With Huntington Disease: A Randomized Clinical Trial. *Journal of the American Medical Association, 316*(1), 40-50.

Franke, H., Galla, H.-J., & Beuckmann, C. T. (1999). An improved low-permeability in vitro-model of the blood–brain barrier: transport studies on retinoids, sucrose, haloperidol, caffeine and mannitol. *Brain Research, 818*(1), 65-71.

Frankfort, S. V., Ouwehand, M., van Maanen, M. J., Rosing, H., Tulner, L. R., & Beijnen, J. H. (2006). A simple and sensitive assay for the quantitative analysis of rivastigmine and its metabolite NAP 226-90 in human EDTA plasma using coupled liquid chromatography and tandem mass spectrometry. *Rapid Communications in Mass Spectrometry, 20*(22), 3330-3336.

Fu, Y., & Kao, W. J. (2010). Drug Release Kinetics and Transport Mechanisms of Non-degradable and Degradable Polymeric Delivery Systems. *Expert Opinion on Drug Delivery, 7*(4), 429-444.

Gao, H. (2016a). Perspectives on Dual Targeting Delivery Systems for Brain Tumors. *Journal of Neuroimmune Pharmacology, 12*, 6-16.

Gao, H. (2016b). Progress and perspectives on targeting nanoparticles for brain drug delivery. *Acta Pharmaceutica Sinica B, 6*(4), 268-286.

Gao, H., Pang, Z., & Jiang, X. (2013). Targeted delivery of nano-therapeutics for major disorders of the central nervous system. *Pharmaceutical Research, 30*(10), 2485-2498.

Gao, S., Tian, H., Xing, Z., Zhang, D., Guo, Y., Guo, Z., . . . Chen, X. (2016). A non-viral suicide gene delivery system traversing the blood brain barrier for non-invasive glioma targeting treatment. *Journal of Controlled Release, 243*, 357-369.

Garberg, P., Ball, M., Borg, N., Cecchelli, R., Fenart, L., Hurst, R. D., . . . Österberg, T. (2005). In vitro models for the blood–brain barrier. *Toxicology in Vitro, 19*(3), 299-334.

García-González, L., Yépez-Mulía, L., & Ganem, A. (2016). Effect of β-cyclodextrin on the internalization of nanoparticles into intestine epithelial cells. *European Journal of Pharmaceutical Sciences, 81*, 113-118.

Garg, T., Bhandari, S., Rath, G., & Goyal, A. K. (2015). Current strategies for targeted delivery of bio-active drug molecules in the treatment of brain tumor. *Journal of Drug Targeting, 23*(10), 865-887.

Geng, X., Wang, X., Xie, J., Zhang, X., Wang, X., Hou, Y., . . . Wang, M. (2016). Effect of l-DOPA on local field potential relationship between the pedunculopontine nucleus and primary motor cortex in a rat model of Parkinson's disease. *Behavioural Brain Research, 315*, 1-9.

Georgieva, J. V., Kalicharan, D., Couraud, P.-O., Romero, I. A., Weksler, B., Hoekstra, D., & Zuhorn, I. S. (2011). Surface Characteristics of Nanoparticles Determine Their Intracellular Fate in and Processing by Human Blood-Brain Barrier Endothelial Cells In Vitro. *Molecular Therapy, 19*(2), 318-325.

Ghaffarian, R., & Muro, S. (2013). Models and methods to evaluate transport of drug delivery systems across cellular barriers. *Journal of Visualized Experiments: JoVE*(80), 50638.

Goldblum, D., Gygax, M., Bohnke, M., & Garweg, J. G. (2002). In vitro toxicity of rivastigmine and donepezil in cells of epithelial origin. *Ophthalmic Research, 34*(2), 97-103.

Goldmann, E. E. (1913). *Vitalfärbung am Zentralnervensystem: Beitrag zur Physio-Pathologie des Plexus chorioideus und der Hirnhäute*: Königl. Akademie der Wissenschaften.

Gonzalez-Mariscal, L., Posadas, Y., Miranda, J., Uc, P. Y., Ortega-Olvera, J. M., & Hernandez, S. (2016). Strategies that Target Tight Junctions for Enhanced Drug Delivery. *Current Pharmaceutical Design, 22*(35), 5313-5346.

Govender, T., Stolnik, S., Garnett, M. C., Illum, L., & Davis, S. S. (1999). PLGA nanoparticles prepared by nanoprecipitation: drug loading and release studies of a water soluble drug. *Journal of Controlled Release, 57*(2), 171-185.

Greene, C., & Campbell, M. (2016). Tight junction modulation of the blood brain barrier: CNS delivery of small molecules. *Tissue Barriers, 4*(1), e1138017.

Greenwald, R. B., Zhao, H., Xia, J., & Martinez, A. (2003). Poly(ethylene glycol) transport forms of vancomycin: a long-lived continuous release delivery system. *Journal of Medicinal Chemistry, 46*(23), 5021-5030.

Gregori, M., Taylor, M., Salvati, E., Re, F., Mancini, S., Balducci, C., . . . Allsop, D. (2016). Retro-inverso peptide inhibitor nanoparticles as potent inhibitors of aggregation of the Alzheimer's Aβ peptide. *Nanomedicine: Nanotechnology, Biology and Medicine, 13*, 723-732.

Greig, N. H., Utsuki, T., Ingram, D. K., Wang, Y., Pepeu, G., Scali, C., . . . Lahiri, D. K. (2005). Selective butyrylcholinesterase inhibition elevates brain acetylcholine, augments learning and lowers Alzheimer β-amyloid peptide in rodent. *Proceedings*

of the National Academy of Sciences of the United States of America, 102(47), 17213-17218.

Grossberg, G. T. (2003). Cholinesterase Inhibitors for the Treatment of Alzheimer's Disease:: Getting On and Staying On. *Current Therapeutic Research, Clinical and Experimental, 64*(4), 216-235.

Grossberg, G. T. (2005). Effect of rivastigmine in the treatment of behavioral disturbances associated with dementia: review of neuropsychiatric impairment in Alzheimer's disease. *Current Medical Research and Opinion, 21*(10), 1631-1639.

Grundman, M. (2000). Vitamin E and Alzheimer disease: the basis for additional clinical trials. *The American journal of clinical nutrition, 71*(2), 630s-636s.

Guo, F., Guo, D., Zhang, W., Yan, Q., Yang, Y., Hong, W., & Yang, G. (2017). Preparation of curcumin-loaded PCL-PEG-PCL triblock copolymeric nanoparticles by a microchannel technology. *European Journal of Pharmaceutical Sciences, 99*, 328-336.

Gupta, R., & Mohanty, S. (2017). Nanoparticle formulation having ability to control the release of protein for drug delivery application. *Materials Science and Engineering: C, 70, Part 1*, 327-333.

Hakkarainen, J. J., Jalkanen, A. J., Kaariainen, T. M., Keski-Rahkonen, P., Venalainen, T., Hokkanen, J., . . . Forsberg, M. M. (2010). Comparison of in vitro cell models in predicting in vivo brain entry of drugs. *International Journal of Pharmaceutics, 402*(1-2), 27-36.

Hau, P., Fabel, K., Baumgart, U., Rummele, P., Grauer, O., Bock, A., . . . Bogdahn, U. (2004). Pegylated liposomal doxorubicin-efficacy in patients with recurrent high-grade glioma. *Cancer, 100*(6), 1199-1207.

Havrdova, M., Polakova, K., Skopalik, J., Vujtek, M., Mokdad, A., Homolkova, M., . . . Zboril, R. (2014). Field emission scanning electron microscopy (FE-SEM) as an approach for nanoparticle detection inside cells. *Micron, 67*, 149-154.

He, Y., Yao, Y., Tsirka, S. E., & Cao, Y. (2014). Cell-Culture Models of the Blood–Brain Barrier. *Stroke, 45*(8), 2514-2526.

Heidarian, S., Derakhshandeh, K., Adibi, H., & Hosseinzadeh, L. (2015). Active targeted nanoparticles: Preparation, physicochemical characterization and in vitro cytotoxicity effect. *Research in Pharmaceutical Sciences, 10*(3), 241-251.

Herculano-Houzel, S. (2009). The human brain in numbers: a linearly scaled-up primate brain. *Frontiers in Human Neuroscience, 3*(31), 1-11.

Hervé, F., Ghinea, N., & Scherrmann, J. M. (2008). CNS delivery via adsorptive transcytosis. *AAPS Journal, 10*(3), 455-472.

Higuchi, T. (1963). Mechanism of sustained-action medication. Theoretical analysis of rate of release of solid drugs dispersed in solid matrices. *Journal of Pharmaceutical Sciences, 52*(12), 1145-1149.

Hiorth, Y. H. (2016). *Falls in Parkinson's disease* (Doctoal thesis), University of Stavanger, Norway. Retrieved from https://brage.bibsys.no/xmlui/handle/11250/2428786

Hossain, M., Jhee, S. S., Shiovitz, T., McDonald, C., Sedek, G., Pommier, F., & Cutler, N. R. (2002). Estimation of the absolute bioavailability of rivastigmine in patients with mild to moderate dementia of the Alzheimer's type. *Clinical Pharmacokinetics, 41*(3), 225-234.

Hovanessian, A. G., Soundaramourty, C., El Khoury, D., Nondier, I., Svab, J., & Krust, B. (2010). Surface expressed nucleolin is constantly induced in tumor cells to mediate calcium-dependent ligand internalization. *PloS One, 5*(12), e15787.

Hu, J., Fu, S., Peng, Q., Han, Y., Xie, J., Zan, N., . . . Fan, J. (2017). Paclitaxel-loaded polymeric nanoparticles combined with chronomodulated chemotherapy on lung cancer: In vitro and in vivo evaluation. *International Journal of Pharmaceutics, 516*(1–2), 313-322.

Huang, J., Zhang, H., Yu, Y., Chen, Y., Wang, D., Zhang, G., . . . Zhong, Y. (2014). Biodegradable self-assembled nanoparticles of poly (d,l-lactide-co-

glycolide)/hyaluronic acid block copolymers for target delivery of docetaxel to breast cancer. *Biomaterials, 35*(1), 550-566.

Hughes, J., & Crowe, A. (2010). Inhibition of P-glycoprotein-mediated efflux of digoxin and its metabolites by macrolide antibiotics. *Journal of Pharmacological Sciences, 113*(4), 315-324.

Hurelbrink, C. B., & Lewis, S. J. G. (2011). Pathological considerations in the treatment of Parkinson's disease: More than just a wiring diagram. *Clinical Neurology and Neurosurgery, 113*(1), 1-6.

Ibrahim, M. M., Abd-Elgawad, A. E. H., Soliman, O. A. E., & Jablonski, M. M. (2013). Nanoparticle-based topical ophthalmic formulations for sustained celecoxib release. *Journal of Pharmaceutical Sciences, 102*(3), 1036-1053.

ICH. (1996). *Q2B Validation of Analytical Procedures: Methodology*. [Accessed on: 04 Jan 2017] Retrieved from http://www.fda.gov/downloads/Drugs/GuidanceComplianceRegulatoryInformation/Guidances/UCM073384.pdf.

ICH. (2000). *Stability testing of new drug substances and products (Q1AR)*. [Accessed on: 04 Jan 2017] Retrieved from http://www.ich.org/products/guidelines/quality/quality-single/article/stability-testing-of-new-drug-substances-and-products.html.

Iwata, H., Matsuda, S., Mitsuhashi, K., Itoh, E., & Ikada, Y. (1998). A novel surgical glue composed of gelatin and N-hydroxysuccinimide activated poly(L-glutamic acid):: Part 1. Synthesis of activated poly(L-glutamic acid) and its gelation with gelatin. *Biomaterials, 19*(20), 1869-1876.

Jain, S., Mishra, V., Singh, P., Dubey, P. K., Saraf, D. K., & Vyas, S. P. (2003). RGD-anchored magnetic liposomes for monocytes/neutrophils-mediated brain targeting. *International Journal of Pharmaceutics, 261*(1–2), 43-55.

James, R., Manoukian, O. S., & Kumbar, S. G. (2016). Poly(lactic acid) for delivery of bioactive macromolecules. *Adv Drug Deliv Rev, 107*, 277-288.

Jaruszewski, K. M., Ramakrishnan, S., Poduslo, J. F., & Kandimalla, K. K. (2012). Chitosan enhances the stability and targeting of immuno-nanovehicles to cerebro-vascular deposits of Alzheimer's disease amyloid protein. *Nanomedicine: Nanotechnology, Biology, and Medicine, 8*(2), 250-260.

Jenkins, S. I., Weinberg, D., al-Shakli, A. F., Fernandes, A. R., Yiu, H. H. P., Telling, N. D., . . . Chari, D. M. (2016). 'Stealth' nanoparticles evade neural immune cells but also evade major brain cell populations: Implications for PEG-based neurotherapeutics. *Journal of Controlled Release, 224*, 136-145.

Jones, A. R., & Shusta, E. V. (2007). Blood-Brain Barrier Transport of Therapeutics via Receptor-Mediation. *Pharmaceutical Research, 24*(9), 1759-1771.

Joseph, E., & Saha, R. N. (2017). Investigations on pharmacokinetics and biodistribution of polymeric and solid lipid nanoparticulate systems of atypical antipsychotic drug: effect of material used and surface modification. *Drug Development and Industrial Pharmacy*, 1-12.

Joshi, S. A., Chavhan, S. S., & Sawant, K. K. (2010). Rivastigmine-loaded PLGA and PBCA nanoparticles: Preparation, optimization, characterization, in vitro and pharmacodynamic studies. *European Journal of Pharmaceutics and Biopharmaceutics, 76*(2), 189-199.

Kabanov, A. V., Batrakova, E. V., & Alakhov, V. Y. (2002). Pluronic block copolymers for overcoming drug resistance in cancer. *Adv Drug Deliv Rev, 54*(5), 759-779.

Kaltsa, O., Gatsi, I., Yanniotis, S., & Mandala, I. (2014). Influence of Ultrasonication Parameters on Physical Characteristics of Olive Oil Model Emulsions Containing Xanthan. *Food and Bioprocess Technology, 7*(7), 2038-2049.

Karthik, A., Subramanian, G. S., Surulivelrajan, M., Ranjithkumar, A., & Kamat, S. B. (2008). Fluorimetric determination of rivastigmine in rat plasma by a reverse phase--high performance liquid chromatographic method. Application to a pharmacokinetic study. *Arzneimittel-Forschung, 58*(5), 205-210.

Karve, S., Werner, M. E., Cummings, N. D., Sukumar, R., Wang, E. C., Zhang, Y.-A., & Wang, A. Z. (2011). Formulation of Diblock Polymeric Nanoparticles through Nanoprecipitation Technique. *Journal of Visualized Experiments : JoVE*(55), 3398.

Kaur, P., Garg, T., Rath, G., & Goyal, A. K. (2016). In situ nasal gel drug delivery: A novel approach for brain targeting through the mucosal membrane. *Artificial Cells, Nanomedicine, and Biotechnology, 44*(4), 1167-1176.

Khachaturian, Z. S., Petersen, R. C., Snyder, P. J., Khachaturian, A. S., Aisen, P., de Leon, M., . . . Bain, L. J. (2011). Developing a global strategy to prevent Alzheimer's disease: Leon Thal Symposium 2010. *Alzheimer's & Dementia, 7*(2), 127-132.

Khadka, P., Ro, J., Kim, H., Kim, I., Kim, J. T., Kim, H., . . . Lee, J. (2014). Pharmaceutical particle technologies: An approach to improve drug solubility, dissolution and bioavailability. *Asian Journal of Pharmaceutical Sciences, 9*(6), 304-316.

Khanam, H., Ali, A., Asif, M., & Shamsuzzaman. (2016). Neurodegenerative diseases linked to misfolded proteins and their therapeutic approaches: A review. *European Journal of Medicinal Chemistry, 124*, 1121-1141.

Khare, V., Kour, S., Alam, N., Dubey, R. D., Saneja, A., Koul, M., . . . Gupta, P. N. (2014). Synthesis, characterization and mechanistic-insight into the anti-proliferative potential of PLGA-gemcitabine conjugate. *International Journal of Pharmaceutics, 470*(1–2), 51-62.

Kibria, G., Hatakeyama, H., Ohga, N., Hida, K., & Harashima, H. (2011). Dual-ligand modification of PEGylated liposomes shows better cell selectivity and efficient gene delivery. *Journal of Controlled Release, 153*(2), 141-148.

Kim, S. Y., Choi, E.-S., Lee, H.-J., Moon, C., & Kim, E. (2015). Transthyretin as a new transporter of nanoparticles for receptor-mediated transcytosis in rat brain microvessels. *Colloids and Surfaces B: Biointerfaces, 136*, 989-996.

Klang, V., Valenta, C., & Matsko, N. B. (2013). Electron microscopy of pharmaceutical systems. *Micron, 44*, 45-74.

Konan, Y. N., Gurny, R., & Allémann, E. (2002). Preparation and characterization of sterile and freeze-dried sub-200 nm nanoparticles. *International Journal of Pharmaceutics, 233*(1–2), 239-252.

Kooijmans, S. A. A., Senyschyn, D., Mezhiselvam, M. M., Morizzi, J., Charman, S. A., Weksler, B., . . . Nicolazzo, J. A. (2012). The Involvement of a Na+- and Cl−-Dependent Transporter in the Brain Uptake of Amantadine and Rimantadine. *Molecular Pharmaceutics, 9*(4), 883-893.

Korsmeyer, R. W., Gurny, R., Doelker, E., Buri, P., & Peppas, N. A. (1983). Mechanisms of solute release from porous hydrophilic polymers. *International Journal of Pharmaceutics, 15*(1), 25-35.

Kovacic, P., & Somanathan, R. (2012). Redox Processes in Neurodegenerative Disease Involving Reactive Oxygen Species. *Current Neuropharmacology, 10*(4), 289-302.

Kratz, F. (2008). Albumin as a drug carrier: design of prodrugs, drug conjugates and nanoparticles. *Journal of Controlled Release, 132*.

Kreuter, J. (2013). Mechanism of polymeric nanoparticle-based drug transport across the blood-brain barrier (BBB). *Journal of Microencapsulation, 30*(1), 49-54.

Kreuter, J. (2014). Drug delivery to the central nervous system by polymeric nanoparticles: What do we know? *Adv Drug Deliv Rev, 71*, 2-14.

Krol, S., Macrez, R., Docagne, F., Defer, G., Laurent, S., Rahman, M., . . . Mahmoudi, M. (2013). Therapeutic benefits from nanoparticles: The potential significance of nanoscience in diseases with compromise to the blood brain barrier. *Chemical Reviews, 113*(3), 1877-1903.

Kulkarni, S. A., & Feng, S.-S. (2013). Effects of Particle Size and Surface Modification on Cellular Uptake and Biodistribution of Polymeric Nanoparticles for Drug Delivery. *Pharmaceutical Research, 30*(10), 2512-2522.

Kumar, A., Singh, A., & Ekavali. (2015). A review on Alzheimer's disease pathophysiology and its management: an update. *Pharmacological Reports, 67*(2), 195-203.

Kuo, Y.-C., & Chen, Y.-C. (2015). Targeting delivery of etoposide to inhibit the growth of human glioblastoma multiforme using lactoferrin- and folic acid-grafted poly(lactide-co-glycolide) nanoparticles. *International Journal of Pharmaceutics, 479*(1), 138-149.

Kuo, Y.-C., & Yu, H.-W. (2011). Transport of saquinavir across human brain-microvascular endothelial cells by poly (lactide-co-glycolide) nanoparticles with surface poly-(γ-glutamic acid). *International Journal of Pharmaceutics, 416*(1), 365-375.

Kurz, A., Farlow, M., & Lefèvre, G. (2009). Pharmacokinetics of a novel transdermal rivastigmine patch for the treatment of Alzheimer's disease: a review. *International Journal of Clinical Practice, 63*(5), 799-805.

Langiu, M., Dadparvar, M., Kreuter, J., & Ruonala, M. O. (2014). Human Serum Albumin-Based Nanoparticle-Mediated In Vitro Gene Delivery. *PloS One, 9*(9), e107603.

Larsen, M. T., Kuhlmann, M., Hvam, M. L., & Howard, K. A. (2016). Albumin-based drug delivery: harnessing nature to cure disease. *Molecular and Cellular Therapies, 4*(1), 3.

Lassailly, F., Griessinger, E., & Bonnet, D. (2010). "Microenvironmental contaminations" induced by fluorescent lipophilic dyes used for noninvasive in vitro and in vivo cell tracking. *Blood, 115*(26), 5347-5354.

Lee, J.-H., Park, T. G., & Choi, H.-K. (2000). Effect of formulation and processing variables on the characteristics of microspheres for water-soluble drugs prepared by w/o/o double emulsion solvent diffusion method. *International Journal of Pharmaceutics, 196*(1), 75-83.

Lee, J.-M., Park, J.-M., Song, M. K., Oh, Y. J., Kim, C.-J., & Kim, Y.-J. (2017). The ameliorative effects of exercise on cognitive impairment and white matter injury from blood-brain barrier disruption induced by chronic cerebral hypoperfusion in adolescent rats. *Neuroscience Letters, 638*, 83-89.

Lee, L., Hossain, M., Wang, Y., & Sedek, G. (2004). Absorption of rivastigmine from different regions of the gastrointestinal tract in humans. *Journal of Clinical Pharmacology, 44*(6), 599-604.

Lee, S. S., Lee, Y. B., & Oh, I. J. (2015). Cellular uptake of poly(dl-lactide-co-glycolide) nanoparticles: effects of drugs and surface characteristics of nanoparticles. *Journal of Pharmaceutical Investigation, 45*(7), 659-667.

Lee, S. Y., & Cho, H.-J. (2017). Dopamine-conjugated poly(lactic-co-glycolic acid) nanoparticles for protein delivery to macrophages. *Journal of Colloid and Interface Science, 490*, 391-400.

Levin, V. A. (1980). Relationship of octanol/water partition coefficient and molecular weight to rat brain capillary permeability. *Journal of Medicinal Chemistry, 23*(6), 682-684.

Li, C.-p., Zheng, L.-j., Mao, M., Rao, G.-w., & Shan, W.-g. (2011). HPLC determination of rivastigmine hydrogen tartrate capsules. *Chinese Journal of Pharmaceutical Analysis, 31*(6), 1123-1125.

Li, N., Lewis, P., Samuelson, D., Liboni, K., & Neu, J. (2004). Glutamine regulates Caco-2 cell tight junction proteins. *American Journal of Physiology - Gastrointestinal and Liver Physiology, 287*(3), G726.

Liang, H., Friedman, J. M., & Nacharaju, P. (2017). Fabrication of biodegradable PEG–PLA nanospheres for solubility, stabilization, and delivery of curcumin. *Artificial Cells, Nanomedicine, and Biotechnology, 45*(2), 297-304.

Lingineni, K., Belekar, V., Tangadpalliwar, S. R., & Garg, P. (2017). The role of multidrug resistance protein (MRP-1) as an active efflux transporter on blood–brain barrier (BBB) permeability. *Molecular Diversity*, 1-11.

Liu, J., Wei, T., Zhao, J., Huang, Y., Deng, H., Kumar, A., . . . Liang, X.-J. (2016a). Multifunctional aptamer-based nanoparticles for targeted drug delivery to circumvent cancer resistance. *Biomaterials, 91*, 44-56.

Liu, P., Yu, H., Sun, Y., Zhu, M., & Duan, Y. (2012). A mPEG-PLGA-b-PLL copolymer carrier for adriamycin and siRNA delivery. *Biomaterials, 33*(17), 4403-4412.

Liu, Y., An, S., Li, J., Kuang, Y., He, X., Guo, Y., . . . Jiang, C. (2016b). Brain-targeted co-delivery of therapeutic gene and peptide by multifunctional nanoparticles in Alzheimer's disease mice. *Biomaterials, 80*, 33-45.

Lobenberg, R., & Kreuter, J. (1996). Macrophage targeting of azidothymidine: a promising strategy for AIDS therapy. *AIDS Research and Human Retroviruses, 12*(18), 1709-1715.

Louzao, M. C., Fernandez, D. A., Abal, P., Fraga, M., Vilarino, N., Vieytes, M. R., & Botana, L. M. (2015). Diarrhetic effect of okadaic acid could be related with its neuronal action: Changes in neuropeptide Y. *Toxicology Letters, 237*(2), 151-160.

Lu, C.-T., Zhao, Y.-Z., Wong, H. L., Cai, J., Peng, L., & Tian, X.-Q. (2014). Current approaches to enhance CNS delivery of drugs across the brain barriers. *International Journal of Nanomedicine, 9*, 2241-2257.

Lu, X.-Y., Wu, D.-C., Li, Z.-J., & Chen, G.-Q. (2011). Chapter 7 - Polymer Nanoparticles. In V. Antonio (Ed.), *Progress in Molecular Biology and Translational Science* (1 ed., Vol. 104, pp. 299-323). Cambridge, USA: Academic Press.

Lundquist, S., Renftel, M., Brillault, J., Fenart, L., Cecchelli, R., & Dehouck, M.-P. (2002). Prediction of Drug Transport Through the Blood-Brain Barrier in Vivo: A Comparison Between Two in Vitro Cell Models. *Pharmaceutical Research, 19*(7), 976-981.

Luo, L., Zheng, S., Huang, Y., Qin, T., Xing, J., Niu, Y., . . . Wang, D. (2016). Preparation and characterization of Chinese yam polysaccharide PLGA nanoparticles and their immunological activity. *International Journal of Pharmaceutics, 511*(1), 140-150.

Ma, S., Liu, X., Xu, Q., & Zhang, X. (2014). Transport of ginkgolides with different lipophilicities based on an hCMEC/D3 cell monolayer as a blood–brain barrier cell model. *Life Sciences, 114*(2), 93-101.

Mahapatro, A., & Singh, D. K. (2011). Biodegradable nanoparticles are excellent vehicle for site directed in-vivo delivery of drugs and vaccines. *Journal of Nanobiotechnology, 9*, 55-55.

Mainardes, R. M., & Evangelista, R. C. (2005). PLGA nanoparticles containing praziquantel: effect of formulation variables on size distribution. *International Journal of Pharmaceutics, 290*(1-2), 137-144.

Maletinska, L., Blakely, E. A., Bjornstad, K. A., Deen, D. F., Knoff, L. J., & Forte, T. M. (2000). Human glioblastoma cell lines: levels of low-density lipoprotein receptor and low-density lipoprotein receptor-related protein. *Cancer Research, 60*(8), 2300-2303.

Malhotra, M., Tomaro-Duchesneau, C., & Prakash, S. (2013). Synthesis of TAT peptide-tagged PEGylated chitosan nanoparticles for siRNA delivery targeting neurodegenerative diseases. *Biomaterials, 34*(4), 1270-1280.

Manoochehri, S., Darvishi, B., Kamalinia, G., Amini, M., Fallah, M., Ostad, S. N., . . . Dinarvand, R. (2013). Surface modification of PLGA nanoparticles via human serum albumin conjugation for controlled delivery of docetaxel. *DARU Journal of Pharmaceutical Sciences, 21*(1), 58.

Mao, Z., Wan, L., Hu, L., Ma, L., & Gao, C. (2010). Tat peptide mediated cellular uptake of SiO2 submicron particles. *Colloids and Surfaces B: Biointerfaces, 75*(2), 432-440.

Margus, H., Padari, K., & Pooga, M. (2012). Cell-penetrating peptides as versatile vehicles for oligonucleotide delivery. *Molecular Therapy, 20*(3), 525-533.

Martinez, M. N. (2011). Factors Influencing the Use and Interpretation of Animal Models in the Development of Parenteral Drug Delivery Systems. *The AAPS Journal, 13*(4), 632-649.

McCall, R. L., & Sirianni, R. W. (2013). PLGA nanoparticles formed by single- or double-emulsion with vitamin E-TPGS. *Journal of Visualized Experiments : JoVE*(82), 51015.

McClements, D. J. (2015). Encapsulation, protection, and release of hydrophilic active components: Potential and limitations of colloidal delivery systems. *Advances in Colloid and Interface Science, 219*, 27-53.

Miao, D., Jiang, M., Liu, Z., Gu, G., Hu, Q., Kang, T., . . . Chen, J. (2014). Co-administration of Dual-Targeting Nanoparticles with Penetration Enhancement Peptide for Antiglioblastoma Therapy. *Molecular Pharmaceutics, 11*(1), 90-101.

Milletti, F. (2012). Cell-penetrating peptides: classes, origin, and current landscape. *Drug Discovery Today, 17*(15–16), 850-860.

Misra, A., Ganesh, S., Shahiwala, A., & Shah, S. P. (2003). Drug delivery to the central nervous system: a review. *Journal of Pharmacy & Pharmaceutical Sciences, 6*(2), 252-273.

Misra, R., Acharya, S., Dilnawaz, F., & Sahoo, S. K. (2009). Sustained antibacterial activity of doxycycline-loaded poly(D,L-lactide-co-glycolide) and poly(epsilon-caprolactone) nanoparticles. *Nanomedicine (Lond), 4*(5), 519-530.

Mittal, G., Sahana, D. K., Bhardwaj, V., & Ravi Kumar, M. N. V. (2007). Estradiol loaded PLGA nanoparticles for oral administration: Effect of polymer molecular weight and copolymer composition on release behavior in vitro and in vivo. *Journal of Controlled Release, 119*(1), 77-85.

Mogoşanu, G. D., Grumezescu, A. M., Bejenaru, C., & Bejenaru, L. E. (2016). Polymeric protective agents for nanoparticles in drug delivery and targeting. *International Journal of Pharmaceutics, 510*(2), 419-429.

Montalbetti, C. A. G. N., & Falque, V. (2005). Amide bond formation and peptide coupling. *Tetrahedron, 61*(46), 10827-10852.

Montenegro, L., Trapani, A., Latrofa, A., & Puglisi, G. (2012). In vitro evaluation on a model of blood brain barrier of idebenone-loaded solid lipid nanoparticles. *Journal of Nanoscience and Nanotechnology, 12*(1), 330-337.

Morris, M. C., Schneider, J. A., Li, H., Tangney, C. C., Nag, S., Bennett, D. A., . . . Barnes, L. L. (2015). Brain tocopherols related to Alzheimer's disease neuropathology in humans. *Alzheimer's & Dementia, 11*(1), 32-39.

Mu, L., & Feng, S. S. (2002). Vitamin E TPGS used as emulsifier in the solvent evaporation/extraction technique for fabrication of polymeric nanospheres for controlled release of paclitaxel (Taxol®). *Journal of Controlled Release, 80*(1–3), 129-144.

Mu, L., & Feng, S. S. (2003). A novel controlled release formulation for the anticancer drug paclitaxel (Taxol®): PLGA nanoparticles containing vitamin E TPGS. *Journal of Controlled Release, 86*(1), 33-48.

Murakami, H., Kobayashi, M., Takeuchi, H., & Kawashima, Y. (1999). Preparation of poly (DL-lactide-co-glycolide) nanoparticles by modified spontaneous emulsification solvent diffusion method. *International Journal of Pharmaceutics, 187*(2), 143-152.

Mutlu, N. B., Değim, Z., Yılmaz, Ş., Eşsiz, D., & Nacar, A. (2011). New perspective for the treatment of Alzheimer diseases: Liposomal rivastigmine formulations. *Drug Development and Industrial Pharmacy, 37*(7), 775-789.

Nagpal, K., Singh, S. K., & Mishra, D. N. (2013). Optimization of brain targeted chitosan nanoparticles of Rivastigmine for improved efficacy and safety. *International Journal of Biological Macromolecules, 59*, 72-83.

Nair, M., Jayant, R. D., Kaushik, A., & Sagar, V. (2016). Getting into the brain: Potential of nanotechnology in the management of NeuroAIDS. *Adv Drug Deliv Rev, 103*, 202-217.

Navarro, S. M., Morgan, T. W., Astete, C. E., Stout, R. W., Coulon, D., Mottram, P., & Sabliov, C. M. (2016). Biodistribution and toxicity of orally administered poly (lactic-co-glycolic) acid nanoparticles to F344 rats for 21 days. *Nanomedicine (Lond), 11*(13), 1653-1669.

Niwa, T., Takeuchi, H., Hino, T., Kunou, N., & Kawashima, Y. (1993). Preparations of biodegradable nanospheres of water-soluble and insoluble drugs with D, L-lactide/glycolide copolymer by a novel spontaneous emulsification solvent diffusion method, and the drug release behavior. *Journal of Controlled Release, 25*(1), 89-98.

Norakankorn, C., Pan, Q., Rempel, G. L., & Kiatkamjornwong, S. (2007). Synthesis of Poly(methyl methacrylate) Nanoparticles Initiated by 2,2′-Azoisobutyronitrile via

Differential Microemulsion Polymerization. *Macromolecular Rapid Communications, 28*(9), 1029-1033.
Oberoi, R. K., Parrish, K. E., Sio, T. T., Mittapalli, R. K., Elmquist, W. F., & Sarkaria, J. N. (2016). Strategies to improve delivery of anticancer drugs across the blood-brain barrier to treat glioblastoma. *Neuro-Oncology, 18*(1), 27-36.
Oldendorf, W. H., Hyman, S., Braun, L., & Oldendorf, S. Z. (1972). Blood-brain barrier: penetration of morphine, codeine, heroin, and methadone after carotid injection. *Science, 178*(4064), 984-986.
Olivier, J.-C. (2005). Drug transport to brain with targeted nanoparticles. *NeuroRx, 2*(1), 108-119.
Owens, D. E., 3rd, & Peppas, N. A. (2006). Opsonization, biodistribution, and pharmacokinetics of polymeric nanoparticles. *International Journal of Pharmaceutics, 307*(1), 93-102.
Özcan, İ., Azizoğlu, E., Şenyiğit, T., Özyazıcı, M., & Özer, Ö. (2013). Comparison of PLGA and lecithin/chitosan nanoparticles for dermal targeting of betamethasone valerate. *Journal of Drug Targeting, 21*(6), 542-550.
Pagar, K. P., Sardar, S. M., & Vavia, P. R. (2014). Novel L-lactide-depsipeptide polymeric carrier for enhanced brain uptake of rivastigmine in treatment of Alzheimer's disease. *Journal of Biomedical Nanotechnology, 10*(3), 415-426.
Pang, L., Zhang, C., Qin, J., Han, L., Li, R., Hong, C., . . . Wang, J. (2017). A novel strategy to achieve effective drug delivery: exploit cells as carrier combined with nanoparticles. *Drug Delivery, 24*(1), 83-91.
Papadia, K., Markoutsa, E., & Antimisiaris, S. G. (2016). How do the physicochemical properties of nanoliposomes affect their interactions with the hCMEC/D3 cellular model of the BBB? *International Journal of Pharmaceutics, 509*(1–2), 431-438.
Pardridge, W. M. (1998). CNS drug design based on principles of blood-brain barrier transport. *Journal of Neurochemistry, 70*(5), 1781-1792.
Pardridge, W. M. (2005a). The blood-brain barrier: bottleneck in brain drug development. *NeuroRx, 2*(1), 3-14.
Pardridge, W. M. (2005b). Drug and gene targeting to the brain via blood–brain barrier receptor-mediated transport systems. *International Congress Series, 1277*, 49-62.
Pardridge, W. M. (2007). Drug Targeting to the Brain. *Pharmaceutical Research, 24*(9), 1733-1744.
Park, K. E., Noh, Y.-W., Kim, A., & Lim, Y. T. (2017). Hyaluronic acid-coated nanoparticles for targeted photodynamic therapy of cancer guided by near-infrared and MR imaging. *Carbohydrate Polymers, 157*, 476-483.
Patabendige, A., Skinner, R. A., & Abbott, N. J. (2013a). Establishment of a simplified in vitro porcine blood–brain barrier model with high transendothelial electrical resistance. *Brain Research, 1521*, 1-15.
Patabendige, A., Skinner, R. A., Morgan, L., & Joan Abbott, N. (2013b). A detailed method for preparation of a functional and flexible blood–brain barrier model using porcine brain endothelial cells. *Brain Research, 1521*, 16-30.
Patel, H. K., Gajbhiye, V., Kesharwani, P., & Jain, N. K. (2016). Ligand anchored poly(propyleneimine) dendrimers for brain targeting: Comparative in vitro and in vivo assessment. *Journal of Colloid and Interface Science, 482*, 142-150.
Patel, M. M., & Patel, B. M. (2017). Crossing the Blood–Brain Barrier: Recent Advances in Drug Delivery to the Brain. *CNS Drugs, 31*(2), 109-133.
Patil, Y., Toti, U., Khdair, A., Ma, L., & Panyam, J. (2009). Single-Step Surface Functionalization of Polymeric Nanoparticles for Targeted Drug Delivery. *Biomaterials, 30*(5), 859-866.
Patravale, V., Dandekar, P., & Jain, R. (2012). 4 - Nanotoxicology: evaluating toxicity potential of drug-nanoparticles *Nanoparticulate Drug Delivery* (pp. 123-155). Sawston, Cambridge: Woodhead Publishing.
Pawley, J. (1997). The development of field-emission scanning electron microscopy for imaging biological surfaces. *Scanning, 19*(5), 324-336.

Peng, S., Zou, L., Liu, W., Li, Z., Liu, W., Hu, X., . . . Liu, C. (2017). Hybrid liposomes composed of amphiphilic chitosan and phospholipid: Preparation, stability and bioavailability as a carrier for curcumin. *Carbohydrate Polymers, 156*, 322-332.

Pillai, G. J., Paul-Prasanth, B., Nair, S. V., & Menon, D. (2017). Influence of surface passivation of 2-Methoxyestradiol loaded PLGA nanoparticles on cellular interactions, pharmacokinetics and tumour accumulation. *Colloids and Surfaces B: Biointerfaces, 150*, 242-249.

Pohanka, M. (2014). Inhibitors of Acetylcholinesterase and Butyrylcholinesterase Meet Immunity. *International Journal of Molecular Sciences, 15*(6), 9809-9825.

Poller, B., Gutmann, H., Krähenbühl, S., Weksler, B., Romero, I., Couraud, P.-O., . . . Huwyler, J. (2008). The human brain endothelial cell line hCMEC/D3 as a human blood-brain barrier model for drug transport studies. *Journal of Neurochemistry, 107*(5), 1358-1368.

Pommier, F., & Frigola, R. (2003). Quantitative determination of rivastigmine and its major metabolite in human plasma by liquid chromatography with atmospheric pressure chemical ionization tandem mass spectrometry. *Journal of Chromatography B, 784*(2), 301-313.

Postek, M. T., Vladár, A. E., Villarrubia, J. S., & Muto, A. (2016). Comparison of Electron imaging modes for dimensional measurements in the scanning electron microscope. *Microscopy and Microanalysis*, 1-10.

Pulicherla, K. K., & Verma, M. K. (2015). Targeting Therapeutics Across the Blood Brain Barrier (BBB), Prerequisite Towards Thrombolytic Therapy for Cerebrovascular Disorders—an Overview and Advancements. *AAPS PharmSciTech, 16*(2), 223-233.

Qi, L.-F., Xu, Z.-R., Li, Y., Jiang, X., & Han, X.-Y. (2005). In vitro effects of chitosan nanoparticles on proliferation of human gastric carcinoma cell line MGC803 cells. *World Journal of Gastroenterology : WJG, 11*(33), 5136-5141.

Qin, Y., Chen, H., Yuan, W., Kuai, R., Zhang, Q., Xie, F., . . . He, Q. (2011a). Liposome formulated with TAT-modified cholesterol for enhancing the brain delivery. *International Journal of Pharmaceutics, 419*(1–2), 85-95.

Qin, Y., Chen, H., Zhang, Q., Wang, X., Yuan, W., Kuai, R., . . . He, Q. (2011b). Liposome formulated with TAT-modified cholesterol for improving brain delivery and therapeutic efficacy on brain glioma in animals. *International Journal of Pharmaceutics, 420*(2), 304-312.

Queiroz, L. H., Jr., Queiroz, D. P., Dhooghe, L., Ferreira, A. G., & Giraudeau, P. (2012). Real-time separation of natural products by ultrafast 2D NMR coupled to on-line HPLC. *Analyst, 137*(10), 2357-2361.

Raju, T. S., Kalyanaraman, L., Reddy, V. V., & Swamy, P. Y. (2012). Development and validation of an UPLC method for the rapid separation of positional isomers and potential impurities of rivastigmine hydrogen tartrate in drug substance and drug product. *Journal of Liquid Chromatography & Related Technologies, 35*(7), 896-911.

Rao, B. M., Srinivasu, M. K., Kumar, K. P., Bhradwaj, N., Ravi, R., Mohakhud, P. K., . . . Kumar, P. R. (2005). A stability indicating LC method for Rivastigmine hydrogen tartrate. *Journal of Pharmaceutical and Biomedical Analysis, 37*(1), 57-63.

Rao, K. S., Reddy, M. K., Horning, J. L., & Labhasetwar, V. (2008). TAT-conjugated nanoparticles for the CNS delivery of anti-HIV drugs. *Biomaterials, 29*(33), 4429-4438.

Rassu, G., Soddu, E., Posadino, A. M., Pintus, G., Sarmento, B., Giunchedi, P., & Gavini, E. (2017). Nose-to-brain delivery of BACE1 siRNA loaded in solid lipid nanoparticles for Alzheimer's therapy. *Colloids and Surfaces B: Biointerfaces, 152*, 296-301.

Raucher, D., & Ryu, J. S. (2015). Cell-penetrating peptides: strategies for anticancer treatment. *Trends in Molecular Medicine, 21*(9), 560-570.

Rautio, J., Laine, K., Gynther, M., & Savolainen, J. (2008). Prodrug Approaches for CNS Delivery. *The AAPS Journal, 10*(1), 92-102.

Reiman, E. M. (2017). Alzheimer disease in 2016: Putting AD treatments and biomarkers to the test. *Nature reviews. Neurology, 13*(2), 74-76.

Rosca, I. D., Watari, F., & Uo, M. (2004). Microparticle formation and its mechanism in single and double emulsion solvent evaporation. *Journal of Controlled Release, 99*(2), 271-280.

Roy, B., & Dwivedi, Y. (2017). Understanding epigenetic architecture of suicide neurobiology: A critical perspective. *Neuroscience and Biobehavioral Reviews, 72*, 10-27.

Sah, E., & Sah, H. (2015). Recent Trends in Preparation of Poly(lactide-co-glycolide) Nanoparticles by Mixing Polymeric Organic Solution with Antisolvent. *Journal of Nanomaterials, 2015*, 22.

Sahana, D. K., Mittal, G., Bhardwaj, V., & Kumar, M. N. (2008). PLGA nanoparticles for oral delivery of hydrophobic drugs: influence of organic solvent on nanoparticle formation and release behavior in vitro and in vivo using estradiol as a model drug. *Journal of Pharmaceutical Sciences, 97*(4), 1530-1542.

Sahoo, S. K., Panyam, J., Prabha, S., & Labhasetwar, V. (2002). Residual polyvinyl alcohol associated with poly (D,L-lactide-co-glycolide) nanoparticles affects their physical properties and cellular uptake. *Journal of Controlled Release, 82*(1), 105-114.

Salvalaio, M., Rigon, L., Belletti, D., D'Avanzo, F., Pederzoli, F., Ruozi, B., . . . Tosi, G. (2016). Targeted Polymeric Nanoparticles for Brain Delivery of High Molecular Weight Molecules in Lysosomal Storage Disorders. *PloS One, 11*(5), e0156452.

Sanders, L. M., Kent, J. S., McRae, G. I., Vickery, B. H., Tice, T. R., & Lewis, D. H. (1984). Controlled release of a luteinizing hormone-releasing hormone analogue from poly(d,l-lactide-co-glycolide) microspheres. *Journal of Pharmaceutical Sciences, 73*(9), 1294-1297.

Saneja, A., Nayak, D., Srinivas, M., Kumar, A., Khare, V., Katoch, A., . . . Gupta, P. N. (2017). Development and mechanistic insight into enhanced cytotoxic potential of hyaluronic acid conjugated nanoparticles in CD44 overexpressing cancer cells. *European Journal of Pharmaceutical Sciences, 97*, 79-91.

Schakenraad, J. M., Oosterbaan, J. A., Nieuwenhuis, P., Molenaar, I., Olijslager, J., Potman, W., . . . Feijen, J. (1988). Biodegradable hollow fibres for the controlled release of drugs. *Biomaterials, 9*(1), 116-120.

Schnyder, A., & Huwyler, J. (2005). Drug Transport to Brain with Targeted Liposomes. *NeuroRx, 2*(1), 99-107.

Seabold, G. K., Daunais, J. B., Rau, A., Grant, K. A., & Alvarez, V. A. (2010). DiOLISTIC labeling of neurons from rodent and non-human primate brain slices. *Journal of visualized experiments : JoVE*(41), 2081.

Seidlitz, A., Nagel, S., Semmling, B., Grabow, N., Martin, H., Senz, V., . . . Weitschies, W. (2011). Examination of drug release and distribution from drug-eluting stents with a vessel-simulating flow-through cell. *European Journal of Pharmaceutics and Biopharmaceutics, 78*(1), 36-48.

Senarathna, S. M. D. K. G., Page-Sharp, M., & Crowe, A. (2016). The Interactions of P-Glycoprotein with Antimalarial Drugs, Including Substrate Affinity, Inhibition and Regulation. *PloS One, 11*(4), e0152677.

Sha, Y., Deng, C., Liu, Z., Huang, T., Yang, B., & Duan, G. (2004). Headspace solid-phase microextraction and capillary gas chromatographic-mass spectrometric determination of rivastigmine in canine plasma samples. *Journal of Chromatography B, 806*(2), 271-276.

Shah, B., Khunt, D., Bhatt, H., Misra, M., & Padh, H. (2015). Application of quality by design approach for intranasal delivery of rivastigmine loaded solid lipid nanoparticles: Effect on formulation and characterization parameters. *European Journal of Pharmaceutical Sciences, 78*, 54-66.

Sharma, G., Lakkadwala, S., Modgil, A., & Singh, J. (2016a). The role of cell-penetrating peptide and transferrin on enhanced delivery of drug to brain. *International Journal of Molecular Sciences, 17*(6), 1-18.

Sharma, G., Modgil, A., Layek, B., Arora, K., Sun, C., Law, B., & Singh, J. (2013). Cell penetrating peptide tethered bi-ligand liposomes for delivery to brain in vivo: Biodistribution and transfection. *Journal of Controlled Release, 167*(1), 1-10.

Sharma, G., Modgil, A., Zhong, T., Sun, C., & Singh, J. (2014). Influence of Short-Chain Cell-Penetrating Peptides on Transport of Doxorubicin Encapsulating Receptor-Targeted Liposomes Across Brain Endothelial Barrier. *Pharmaceutical Research, 31*(5), 1194-1209.

Sharma, N., Madan, P., & Lin, S. (2016b). Effect of process and formulation variables on the preparation of parenteral paclitaxel-loaded biodegradable polymeric nanoparticles: A co-surfactant study. *Asian Journal of Pharmaceutical Sciences, 11*(3), 404-416.

She, Z., Zhang, T., Wang, X., Li, X., Song, Y., Cheng, X., . . . Deng, Y. (2014). The anticancer efficacy of pixantrone-loaded liposomes decorated with sialic acid–octadecylamine conjugate. *Biomaterials, 35*(19), 5216-5225.

Silva, R., Vilas-Boas, V., Carmo, H., Dinis-Oliveira, R. J., Carvalho, F., de Lourdes Bastos, M., & Remião, F. (2015). Modulation of P-glycoprotein efflux pump: induction and activation as a therapeutic strategy. *Pharmacology and Therapeutics, 149*, 1-123.

Sims, L. B., Curtis, L. T., Frieboes, H. B., & Steinbach-Rankins, J. M. (2016). Enhanced uptake and transport of PLGA-modified nanoparticles in cervical cancer. *Journal of Nanobiotechnology, 14*, 33.

Singh, R., & Lillard, J. W. (2009). Nanoparticle-based targeted drug delivery. *Experimental and Molecular Pathology, 86*(3), 215-223.

Sinko, P. J. (2011). *Martin's Physical Pharmacy and Pharmaceutical Sciences: Physical Chemical and Biopharmaceutical Principles in the Pharmaceutical Sciences* (6 ed.). Philadelphia, USA: Lippincott Williams & Wilkins.

Sivak, L., Subr, V., Tomala, J., Rihova, B., Strohalm, J., Etrych, T., & Kovar, M. (2017). Overcoming multidrug resistance via simultaneous delivery of cytostatic drug and P-glycoprotein inhibitor to cancer cells by HPMA copolymer conjugate. *Biomaterials, 115*, 65-80.

Solovieva, A. O., Vorotnikov, Y. A., Trifonova, K. E., Efremova, O. A., Krasilnikova, A. A., Brylev, K. A., . . . Shestopalov, M. A. (2016). Cellular internalisation, bioimaging and dark and photodynamic cytotoxicity of silica nanoparticles doped by {Mo6I8}4+ metal clusters. *Journal of Materials Chemistry B, 4*(28), 4839-4846.

Son, G. M., Kim, H. Y., Ryu, J. H., Chu, C. W., Kang, D. H., Park, S. B., & Jeong, Y. I. (2014). Self-assembled polymeric micelles based on hyaluronic acid-g-poly(D,L-lactide-co-glycolide) copolymer for tumor targeting. *International Journal of Molecular Sciences, 15*(9), 16057-16068.

Srinivasan, B., Kolli, A. R., Esch, M. B., Abaci, H. E., Shuler, M. L., & Hickman, J. J. (2015). TEER measurement techniques for in vitro barrier model systems. *Journal of Laboratory Automation, 20*(2), 107-126.

Steinbach, J. M., Seo, Y.-E., & Saltzman, W. M. (2016). Cell penetrating peptide-modified poly(lactic-co-glycolic acid) nanoparticles with enhanced cell internalization. *Acta Biomaterialia, 30*, 49-61.

Story, M. R. (2016). *Cost-Effectiveness of Psychotherapy and Dementia: A Comparison by Treatment Modality and Healthcare Provider.* (Masters thesis), Brigham Young University, USA. Retrieved from http://hdl.lib.byu.edu/1877/etd8760

Sulheim, E., Baghirov, H., von Haartman, E., Bøe, A., Åslund, A. K. O., Mørch, Y., & Davies, d. L. C. (2016). Cellular uptake and intracellular degradation of poly(alkyl cyanoacrylate) nanoparticles. *Journal of Nanobiotechnology, 14*(1), 1-14.

Sulochana, S. P., Sharma, K., Mullangi, R., & Sukumaran, S. K. (2014). Review of the validated HPLC and LC-MS/MS methods for determination of drugs used in clinical practice for Alzheimer's disease. *Biomedical Chromatography, 28*(11), 1431-1490.

Sun, W., Qu, D., Ma, Y., Chen, Y., Liu, C., & Zhou, J. (2014a). Enhanced stability and antibacterial efficacy of a traditional Chinese medicine-mediated silver nanoparticle delivery system. *International Journal of Nanomedicine, 9*, 5491-5502.

Sun, Y., Yu, B., Wang, G., Wu, Y., Zhang, X., Chen, Y., . . . Xu, S. (2014b). Enhanced antitumor efficacy of vitamin E TPGS-emulsified PLGA nanoparticles for delivery of paclitaxel. *Colloids and Surfaces B: Biointerfaces, 123*, 716-723.

Sutton, E. J., Henning, T. D., Pichler, B. J., Bremer, C., & Daldrup-Link, H. E. (2008). Cell tracking with optical imaging. *European Radiology, 18*(10), 2021-2032.

Swartz, M. E., & Krull, I. S. (2012). Chapter 4: Method Validation Basics *Handbook of Analytical Validation* (pp. 61-80). Boca Raton, Florida, USA: CRC Press.

Swerdlow, R. H. (2007). Is aging part of Alzheimer's disease, or is Alzheimer's disease part of aging? *Neurobiology of Aging, 28*(10), 1465-1480.

Tahara, K., Miyazaki, Y., Kawashima, Y., Kreuter, J., & Yamamoto, H. (2011). Brain targeting with surface-modified poly(d,l-lactic-co-glycolic acid) nanoparticles delivered via carotid artery administration. *European Journal of Pharmaceutics and Biopharmaceutics, 77*(1), 84-88.

Tahara, K., Sakai, T., Yamamoto, H., Takeuchi, H., Hirashima, N., & Kawashima, Y. (2009). Improved cellular uptake of chitosan-modified PLGA nanospheres by A549 cells. *International Journal of Pharmaceutics, 382*(1–2), 198-204.

Tamai, I., & Tsuji, A. (1996). Drug delivery through the blood-brain barrier. *Adv Drug Deliv Rev, 19*(3), 401-424.

Tan, L. K., & Patsiga, R. A. (1977). A Study of the Fluorescence Analysis of Primary Amines in Nonaqueous Solutions. *Analytical Letters, 10*(6), 437-449.

Tan, S. B., Williams, A. F., & Kelly, D. (2013). Effectiveness of multidisciplinary interventions to improve the quality of life for people with Parkinson's disease: A systematic review. *International Journal of Nursing Studies, 51*(1), 166-174.

Tehrani, S. F., Bernrad, F., Leclair, G., L'écuyer, M.-A., Prat, A., Hildgen, P., & Roullin, V. G. (2016). *PEG-PLGA nanoparticles: investigation of BBB translocation according to PEG chain length using a primary endothelial cell permeability model.* Paper presented at the 10th World Biomaterials Congress, Montréal, Canada.

Texier, I., Goutayer, M., Da Silva, A., Guyon, L., Djaker, N., Josserand, V., . . . Vinet, F. (2009). Cyanine-loaded lipid nanoparticles for improved in vivo fluorescence imaging. *Journal of Biomedical Optics, 14*(5), 054005.

Timbie, K. F., Mead, B. P., & Price, R. J. (2015). Drug and gene delivery across the blood–brain barrier with focused ultrasound. *Journal of Controlled Release, 219*, 61-75.

Tong, H.-I., Kang, W., Shi, Y., Zhou, G., & Lu, Y. (2016). Physiological function and inflamed-brain migration of mouse monocyte-derived macrophages following cellular uptake of superparamagnetic iron oxide nanoparticles—Implication of macrophage-based drug delivery into the central nervous system. *International Journal of Pharmaceutics, 505*(1–2), 271-282.

Tosi, G., Vergoni, A. V., Ruozi, B., Bondioli, L., Badiali, L., Rivasi, F., . . . Vandelli, M. A. (2010). Sialic acid and glycopeptides conjugated PLGA nanoparticles for central nervous system targeting: In vivo pharmacological evidence and biodistribution. *Journal of Controlled Release, 145*(1), 49-57.

Tosi, G., Vilella, A., Chhabra, R., Schmeisser, M. J., Boeckers, T. M., Ruozi, B., . . . Grabrucker, A. M. (2014). Insight on the fate of CNS-targeted nanoparticles. Part II: Intercellular neuronal cell-to-cell transport. *Journal of Controlled Release, 177*, 96-107.

Tournier, N., Goutal, S., Auvity, S., Traxl, A., Mairinger, S., Wanek, T., . . . Langer, O. (2017). Strategies to Inhibit ABCB1- and ABCG2-Mediated Efflux Transport of Erlotinib at the Blood-Brain Barrier: A PET Study on Nonhuman Primates. *Journal of Nuclear Medicine, 58*(1), 117-122.

Tsai, Y.-M., Chien, C.-F., Lin, L.-C., & Tsai, T.-H. (2011). Curcumin and its nano-formulation: The kinetics of tissue distribution and blood–brain barrier penetration. *International Journal of Pharmaceutics, 416*(1), 331-338.

Upadhyay, R. K. (2014a). Drug Delivery Systems, CNS Protection, and the Blood Brain Barrier. *BioMed Research International, 2014*, 869269.

Upadhyay, R. K. (2014b). Transendothelial Transport and Its Role in Therapeutics. *International Scholarly Research Notices, 2014*, 309404.

Urich, E., Lazic, S. E., Molnos, J., Wells, I., & Freskgård, P.-O. (2012). Transcriptional Profiling of Human Brain Endothelial Cells Reveals Key Properties Crucial for Predictive in vitro Blood-Brain Barrier Models. *PloS One, 7*(5), e38149.

USP-NF. (2014). Chapter <1225> Validation of Compendial Procedures *The United States Pharmacopeia 37 / National Formulary 32*. Rockville, MD, 2006: The United States Pharmacopeia Convention, Inc.

Valente, J. F. A., Gaspar, V. M., Antunes, B. P., Countinho, P., & Correia, I. J. (2013). Microencapsulated chitosan–dextran sulfate nanoparticles for controled delivery of bioactive molecules and cells in bone regeneration. *Polymer, 54*(1), 5-15.

Vangara, K. K., Liu, J. L., & Palakurthi, S. (2013). Hyaluronic Acid-decorated PLGA-PEG Nanoparticles for Targeted Delivery of SN-38 to Ovarian Cancer. *Anticancer Research, 33*(6), 2425-2434.

Vauthier, C., & Bouchemal, K. (2009). Methods for the Preparation and Manufacture of Polymeric Nanoparticles. *Pharmaceutical Research, 26*(5), 1025-1058.

Vermeiren, Y., & De Deyn, P. P. (2017). Targeting the norepinephrinergic system in Parkinson's disease and related disorders: The locus coeruleus story. *Neurochemistry International, 102*, 22-32.

Vogel, B. E., Lee, S. J., Hildebrand, A., Craig, W., Pierschbacher, M. D., Wong-Staal, F., & Ruoslahti, E. (1993). A novel integrin specificity exemplified by binding of the alpha v beta 5 integrin to the basic domain of the HIV Tat protein and vitronectin. *The Journal of Cell Biology, 121*(2), 461-468.

Vrignaud, S., Benoit, J.-P., & Saulnier, P. (2011). Strategies for the nanoencapsulation of hydrophilic molecules in polymer-based nanoparticles. *Biomaterials, 32*(33), 8593-8604.

Vu, K., Weksler, B., Romero, I., Couraud, P. O., & Gelli, A. (2009). Immortalized human brain endothelial cell line HCMEC/D3 as a model of the blood-brain barrier facilitates in vitro studies of central nervous system infection by Cryptococcus neoformans. *Eukaryotic Cell, 8*(11), 1803-1807.

Wagh, A., Qian, S. Y., & Law, B. (2012). Development of biocompatible polymeric nanoparticles for in vivo NIR and FRET imaging. *Bioconjugate Chemistry, 23*(5), 981-992.

Wang, B., Lv, L., Wang, Z., Zhao, Y., Wu, L., Fang, X., . . . Xin, H. (2014a). Nanoparticles functionalized with Pep-1 as potential glioma targeting delivery system via interleukin 13 receptor alpha2-mediated endocytosis. *Biomaterials, 35*(22), 5897-5907.

Wang, D., Fu, J., Shi, Y., Peng, D., Yuan, L., He, B., . . . Zhang, Q. (2016). The modulation of tumor vessel permeability by thalidomide and its impacts on different types of targeted drug delivery systems in a sarcoma mouse model. *Journal of Controlled Release, 238*, 186-196.

Wang, D., & Wu, L.-P. (2017). Nanomaterials for delivery of nucleic acid to the central nervous system (CNS). *Materials Science and Engineering: C, 70, Part 2*, 1039-1046.

Wang, S., Fan, W., Kim, G., Hah, H. J., Lee, Y. E., Kopelman, R., . . . Pandey, R. K. (2011). Novel methods to incorporate photosensitizers into nanocarriers for cancer treatment by photodynamic therapy. *Lasers in Surgery and Medicine, 43*(7), 686-695.

Wang, Y., Tong, J., Chang, B., Wang, B., Zhang, D., & Wang, B. (2014b). Effects of alcohol on intestinal epithelial barrier permeability and expression of tight junction-associated proteins. *Molecular Medicine Reports, 9*(6), 2352-2356.

Watson, D. G. (2005). Chapter 12: High-Pressure Liquid Chromatography *Pharmaceutical Analysis: A Textbook for Pharmacy Students and Pharmaceutical Chemists* (2nd ed., pp. 267-314). Edinburgh, UK: Churchill Livingstone.

Wei, X., Chen, X., Ying, M., & Lu, W. (2014). Brain tumor-targeted drug delivery strategies. *Acta Pharmaceutica Sinica B, 4*(3), 193-201.

Weiss, N., Miller, F., Cazaubon, S., & Couraud, P.-O. (2009). The blood-brain barrier in brain homeostasis and neurological diseases. *Biochimica et Biophysica Acta (BBA) - Biomembranes, 1788*(4), 842-857.

Weksler, B., Romero, I. A., & Couraud, P.-O. (2013). The hCMEC/D3 cell line as a model of the human blood brain barrier. *Fluids Barriers CNS, 10*(1), 1-10.

Wibroe, P. P., Ahmadvand, D., Oghabian, M. A., Yaghmur, A., & Moghimi, S. M. (2016). An integrated assessment of morphology, size, and complement activation of the PEGylated liposomal doxorubicin products Doxil®, Caelyx®, DOXOrubicin, and SinaDoxosome. *Journal of Controlled Release, 221*, 1-8.

Wicki, A., Witzigmann, D., Balasubramanian, V., & Huwyler, J. (2015). Nanomedicine in cancer therapy: challenges, opportunities, and clinical applications. *Journal of Controlled Release, 200*, 138-157.

Williams, R. J., & Spencer, J. P. E. (2012). Flavonoids, cognition, and dementia: Actions, mechanisms, and potential therapeutic utility for Alzheimer disease. *Free Radical Biology and Medicine, 52*(1), 35-45.

Wilson, B., Samanta, M. K., Santhi, K., Kumar, K. P. S., Paramakrishnan, N., & Suresh, B. (2008). Poly(n-butylcyanoacrylate) nanoparticles coated with polysorbate 80 for the targeted delivery of rivastigmine into the brain to treat Alzheimer's disease. *Brain Research, 1200*, 159-168.

Wimo, A., Guerchet, M., Ali, G.-C., Wu, Y.-T., Prina, A. M., Winblad, B., . . . Prince, M. (2017). The worldwide costs of dementia 2015 and comparisons with 2010. *Alzheimer's & Dementia, 13*(1), 1-7.

Win, K. Y., & Feng, S.-S. (2005). Effects of particle size and surface coating on cellular uptake of polymeric nanoparticles for oral delivery of anticancer drugs. *Biomaterials, 26*(15), 2713-2722.

Win, K. Y., & Feng, S. S. (2006). In vitro and in vivo studies on vitamin E TPGS-emulsified poly(D,L-lactic-co-glycolic acid) nanoparticles for paclitaxel formulation. *Biomaterials, 27*(10), 2285-2291.

Winblad, B., Amouyel, P., Andrieu, S., Ballard, C., Brayne, C., Brodaty, H., . . . Zetterberg, H. (2016). Defeating Alzheimer's disease and other dementias: a priority for European science and society. *The Lancet Neurology, 15*(5), 455-532.

Witt, K. A., & Davis, T. P. (2006). CNS drug delivery: Opioid peptides and the blood-brain barrier. *The AAPS Journal, 8*(1), E76-E88.

Witt, K. A., Gillespie, T. J., Huber, J. D., Egleton, R. D., & Davis, T. P. (2001). Peptide drug modifications to enhance bioavailability and blood-brain barrier permeability. *Peptides, 22*(12), 2329-2343.

Witt, K. A., Mark, K. S., Sandoval, K. E., & Davis, T. P. (2008). Reoxygenation stress on blood-brain barrier paracellular permeability and edema in the rat. *Microvascular Research, 75*(1), 91-96.

Wohlfart, S., Khalansky, A. S., Gelperina, S., Maksimenko, O., Bernreuther, C., Glatzel, M., & Kreuter, J. (2011). Efficient chemotherapy of rat glioblastoma using doxorubicin-loaded PLGA nanoparticles with different stabilizers. *PloS One, 6*(5), e19121.

Xie, X., Yang, Y., Lin, W., Liu, H., Liu, H., Yang, Y., . . . Deng, J. (2015). Cell-penetrating peptide-siRNA conjugate loaded YSA-modified nanobubbles for ultrasound triggered siRNA delivery. *Colloids and Surfaces B: Biointerfaces, 136*, 641-650.

Xu, R. (2015). Light scattering: A review of particle characterization applications. *Particuology, 18*, 11-21.

Yaghmur, A., & Glatter, O. (2009). Characterization and potential applications of nanostructured aqueous dispersions. *Advances in Colloid and Interface Science, 147–148*, 333-342.

Yan, L., Wang, H., Jiang, Y., Liu, J., Wang, Z., Yang, Y., . . . Huang, Y. (2013). Cell-penetrating peptide-modified PLGA nanoparticles for enhanced nose-to-brain macromolecular delivery. *Macromolecular Research, 21*(4), 435-441.

Yang, B., Ren, B. X., & Tang, F. R. (2017). Prenatal irradiation–induced brain neuropathology and cognitive impairment. *Brain and Development, 39*(1), 10-22.

Yang, Z.-Z., Zhang, Y.-Q., Wang, Z.-Z., Wu, K., Lou, J.-N., & Qi, X.-R. (2013). Enhanced brain distribution and pharmacodynamics of rivastigmine by liposomes following intranasal administration. *International Journal of Pharmaceutics, 452*(1–2), 344-354.

Yin, T., Yang, L., Liu, Y., Zhou, X., Sun, J., & Liu, J. (2015). Sialic acid (SA)-modified selenium nanoparticles coated with a high blood–brain barrier permeability peptide-B6 peptide for potential use in Alzheimer's disease. *Acta Biomaterialia, 25*, 172-183.

Zaki, N. M., & Hafez, M. M. (2012). Enhanced Antibacterial Effect of Ceftriaxone Sodium-Loaded Chitosan Nanoparticles Against Intracellular Salmonella typhimurium. *AAPS PharmSciTech, 13*(2), 411-421.

Zemek, F., Drtinova, L., Nepovimova, E., Sepsova, V., Korabecny, J., Klimes, J., & Kuca, K. (2014). Outcomes of Alzheimer's disease therapy with acetylcholinesterase inhibitors and memantine. *Expert Opinion on Drug Safety, 13*(6), 759-774.

Zhan, C., & Lu, W. (2012). The blood-brain/tumor barriers: challenges and chances for malignant gliomas targeted drug delivery. *Current Pharmaceutical Biotechnology, 13*(12), 2380-2387.

Zhang, C., Wan, X., Zheng, X., Shao, X., Liu, Q., Zhang, Q., & Qian, Y. (2014). Dual-functional nanoparticles targeting amyloid plaques in the brains of Alzheimer's disease mice. *Biomaterials, 35*(1), 456-465.

Zhang, H., Yang, X., Zhao, L., Jiao, Y., Liu, J., & Zhai, G. (2016). In vitro and in vivo study of Baicalin-loaded mixed micelles for oral delivery. *Drug Delivery, 23*(6), 1933-1939.

Zhang, S., Li, J., Lykotrafitis, G., Bao, G., & Suresh, S. (2009). Size-Dependent Endocytosis of Nanoparticles. *Advanced materials (Deerfield Beach, Fla.), 21*, 419-424.

Zhang, Z., Tongchusak, S., Mizukami, Y., Kang, Y. J., Ioji, T., Touma, M., . . . Sasada, T. (2011). Induction of anti-tumor cytotoxic T cell responses through PLGA-nanoparticle mediated antigen delivery. *Biomaterials, 32*(14), 3666-3678.

Zhou, J., Wu, K., Fernandes, C. L., Cheng, A. L., & Finch, P. W. (1998). Keratinocyte growth factor down-regulates expression of the sucrase-isomaltase gene in Caco-2 intestinal epithelial cells. *The Journal of Biological Chemistry, 273*(50), 33367-33373.

Zhou, Z., Badkas, A., Stevenson, M., Lee, J. Y., & Leung, Y. K. (2015). Herceptin conjugated PLGA-PHis-PEG pH sensitive nanoparticles for targeted and controlled drug delivery. *International Journal of Pharmaceutics, 487*(1-2), 81-90.

Zlokovic, B. V. (2008). New therapeutic targets in the neurovascular pathway in Alzheimer's disease. *Neurotherapeutics, 5*(3), 409-414.

Zweers, M. L. T., Grijpma, D. W., Engbers, G. H. M., & Feijen, J. (2003). The preparation of monodisperse biodegradable polyester nanoparticles with a controlled size. *Journal of Biomedical Materials Research Part B: Applied Biomaterials, 66B*(2), 559-566.

Every reasonable effort has been made to acknowledge the owners of copyright material. I would be pleased to hear from any copyright owner who has been omitted or incorrectly acknowledged

Appendices

Appendix I: Approval from Publishers for Use of Figures

ELSEVIER LICENSE
TERMS AND CONDITIONS

Jan 29, 2017

This Agreement between Naz H Huda ("You") and Elsevier ("Elsevier") consists of your license details and the terms and conditions provided by Elsevier and Copyright Clearance Center.

License Number	4038210470337
License date	Jan 29, 2017
Licensed Content Publisher	Elsevier
Licensed Content Publication	Journal of Controlled Release
Licensed Content Title	Drug and gene delivery across the blood–brain barrier with focused ultrasound
Licensed Content Author	Kelsie F. Timbie, Brian P. Mead, Richard J. Price
Licensed Content Date	10 December 2015
Licensed Content Volume Number	219
Licensed Content Issue Number	n/a
Licensed Content Pages	15
Start Page	61
End Page	75
Type of Use	reuse in a thesis/dissertation
Portion	figures/tables/illustrations
Number of figures/tables/illustrations	1
Format	both print and electronic
Are you the author of this Elsevier article?	No

Will you be translating?	No
Order reference number	
Original figure numbers	Figure 1
Title of your thesis/dissertation	Development of a novel nanoparticulate carrier system for enhancement of bioactive molecule delivery into the brain
Expected completion date	Feb 2017
Estimated size (number of pages)	200
Elsevier VAT number	GB 494 6272 12
Requestor Location	Naz H Huda 118 Hill View Terrace Saint James, Western Australia 6102 Australia Attn: Naz H Huda
Total	0.00 AUD

ELSEVIER LICENSE
TERMS AND CONDITIONS

Feb 08, 2017

This Agreement between Naz H Huda ("You") and Elsevier ("Elsevier") consists of your license details and the terms and conditions provided by Elsevier and Copyright Clearance Center.

License Number	4044240585087
License date	Feb 08, 2017
Licensed Content Publisher	Elsevier
Licensed Content Publication	Advanced Drug Delivery Reviews
Licensed Content Title	Modern methods for delivery of drugs across the blood–brain barrier
Licensed Content Author	Yan Chen, Lihong Liu
Licensed Content Date	15 May 2012
Licensed Content Volume	64
Licensed Content Issue	7
Licensed Content Pages	26
Start Page	640
End Page	665
Type of Use	reuse in a thesis/dissertation
Portion	figures/tables/illustrations
Number of figures/tables/illustrations	1
Format	both print and electronic
Are you the author of this Elsevier article?	No
Will you be translating?	No
Order reference number	
Original figure numbers	Figure 2
Title of your thesis/dissertation	Development of a novel nanoparticulate carrier system for enhancement of bioactive molecule delivery into the brain
Expected completion date	Feb 2017
Estimated size (number of pages)	220
Elsevier VAT number	GB 494 6272 12

Requestor Location	Naz H Huda 118 Hill View Terrace Saint James, Western Australia 6102 Australia Attn: Naz H Huda
Total	0.00 AUD

ELSEVIER LICENSE
TERMS AND CONDITIONS

Jan 29, 2017

This Agreement between Naz H Huda ("You") and Elsevier ("Elsevier") consists of your license details and the terms and conditions provided by Elsevier and Copyright Clearance Center.

License Number	4038221478997
License date	Jan 29, 2017
Licensed Content Publisher	Elsevier
Licensed Content Publication	Journal of Controlled Release
Licensed Content Title	DLS and zeta potential – What they are and what they are not?
Licensed Content Author	Sourav Bhattacharjee
Licensed Content Date	10 August 2016
Licensed Content Volume Number	235
Licensed Content Issue Number	n/a
Licensed Content Pages	15
Start Page	337
End Page	351
Type of Use	reuse in a thesis/dissertation
Intended publisher of new work	other
Portion	figures/tables/illustrations
Number of figures/tables/illustrations	1
Format	both print and electronic
Are you the author of this Elsevier article?	No
Will you be translating?	No
Order reference number	
Original figure numbers	Figure 4
Title of your thesis/dissertation	Development of a novel nanoparticulate carrier system for enhancement of bioactive molecule delivery into the brain
Expected completion date	Feb 2017
Estimated size (number of pages)	200
Elsevier VAT number	GB 494 6272 12

Requestor Location	Naz H Huda 118 Hill View Terrace Saint James, Western Australia 6102 Australia Attn: Naz H Huda
Total	0.00 AUD

Terms and Conditions

INTRODUCTION

1. The publisher for this copyrighted material is Elsevier. By clicking "accept" in connection with completing this licensing transaction, you agree that the following terms and conditions apply to this transaction (along with the Billing and Payment terms and conditions established by Copyright Clearance Center, Inc. ("CCC"), at the time that you opened your Rightslink account and that are available at any time at http://myaccount.copyright.com).

GENERAL TERMS

2. Elsevier hereby grants you permission to reproduce the aforementioned material subject to the terms and conditions indicated.
3. Acknowledgement: If any part of the material to be used (for example, figures) has appeared in our publication with credit or acknowledgement to another source, permission must also be sought from that source. If such permission is not obtained then that material may not be included in your publication/copies. Suitable acknowledgement to the source must be made, either as a footnote or in a reference list at the end of your publication, as follows:
"Reprinted from Publication title, Vol /edition number, Author(s), Title of article / title of chapter, Pages No., Copyright (Year), with permission from Elsevier [OR APPLICABLE SOCIETY COPYRIGHT OWNER]." Also Lancet special credit - "Reprinted from The Lancet, Vol. number, Author(s), Title of article, Pages No., Copyright (Year), with permission from Elsevier."
4. Reproduction of this material is confined to the purpose and/or media for which permission is hereby given.
5. Altering/Modifying Material: Not Permitted. However figures and illustrations may be altered/adapted minimally to serve your work. Any other abbreviations, additions, deletions and/or any other alterations shall be made only with prior written authorization of Elsevier Ltd. (Please contact Elsevier at permissions@elsevier.com). No modifications can be made to any Lancet figures/tables and they must be reproduced in full.
6. If the permission fee for the requested use of our material is waived in this instance, please be advised that your future requests for Elsevier materials may attract a fee.
7. Reservation of Rights: Publisher reserves all rights not specifically granted in the combination of (i) the license details provided by you and accepted in the course of this licensing transaction, (ii) these terms and conditions and (iii) CCC's Billing and Payment terms and conditions.
8. License Contingent Upon Payment: While you may exercise the rights licensed immediately upon issuance of the license at the end of the licensing process for the transaction, provided that you have disclosed complete and accurate details of your proposed use, no license is finally effective unless and until full payment is received from you (either by publisher or by CCC) as provided in CCC's Billing and Payment terms and conditions. If full payment is not received on a timely basis, then any license preliminarily granted shall be deemed automatically

revoked and shall be void as if never granted. Further, in the event that you breach any of these terms and conditions or any of CCC's Billing and Payment terms and conditions, the license is automatically revoked and shall be void as if never granted. Use of materials as described in a revoked license, as well as any use of the materials beyond the scope of an unrevoked license, may constitute copyright infringement and publisher reserves the right to take any and all action to protect its copyright in the materials.
9. Warranties: Publisher makes no representations or warranties with respect to the licensed material.
10. Indemnity: You hereby indemnify and agree to hold harmless publisher and CCC, and their respective officers, directors, employees and agents, from and against any and all claims arising out of your use of the licensed material other than as specifically authorized pursuant to this license.
11. No Transfer of License: This license is personal to you and may not be sublicensed, assigned, or transferred by you to any other person without publisher's written permission.
12. No Amendment Except in Writing: This license may not be amended except in a writing signed by both parties (or, in the case of publisher, by CCC on publisher's behalf).
13. Objection to Contrary Terms: Publisher hereby objects to any terms contained in any purchase order, acknowledgment, check endorsement or other writing prepared by you, which terms are inconsistent with these terms and conditions or CCC's Billing and Payment terms and conditions. These terms and conditions, together with CCC's Billing and Payment terms and conditions (which are incorporated herein), comprise the entire agreement between you and publisher (and CCC) concerning this licensing transaction. In the event of any conflict between your obligations established by these terms and conditions and those established by CCC's Billing and Payment terms and conditions, these terms and conditions shall control.
14. Revocation: Elsevier or Copyright Clearance Center may deny the permissions described in this License at their sole discretion, for any reason or no reason, with a full refund payable to you. Notice of such denial will be made using the contact information provided by you. Failure to receive such notice will not alter or invalidate the denial. In no event will Elsevier or Copyright Clearance Center be responsible or liable for any costs, expenses or damage incurred by you as a result of a denial of your permission request, other than a refund of the amount(s) paid by you to Elsevier and/or Copyright Clearance Center for denied permissions.

LIMITED LICENSE

The following terms and conditions apply only to specific license types:
15. **Translation**: This permission is granted for non-exclusive world **English** rights only unless your license was granted for translation rights. If you licensed translation rights you may only translate this content into the languages you requested. A professional translator must perform all translations and reproduce the content word for word preserving the integrity of the article.
16. **Posting licensed content on any Website**: The following terms and conditions apply as follows: Licensing material from an Elsevier journal: All content posted to the web site must maintain the copyright information line on the bottom of each image; A hyper-text must be included to the Homepage of the journal from which you are licensing at http://www.sciencedirect.com/science/journal/xxxxx or the Elsevier homepage

for books at http://www.elsevier.com; Central Storage: This license does not include permission for a scanned version of the material to be stored in a central repository such as that provided by Heron/XanEdu.
Licensing material from an Elsevier book: A hyper-text link must be included to the Elsevier homepage at http://www.elsevier.com . All content posted to the web site must maintain the copyright information line on the bottom of each image.

Posting licensed content on Electronic reserve: In addition to the above the following clauses are applicable: The web site must be password-protected and made available only to bona fide students registered on a relevant course. This permission is granted for 1 year only. You may obtain a new license for future website posting.
17. **For journal authors:** the following clauses are applicable in addition to the above:
Preprints:
A preprint is an author's own write-up of research results and analysis, it has not been peer-reviewed, nor has it had any other value added to it by a publisher (such as formatting, copyright, technical enhancement etc.).
Authors can share their preprints anywhere at any time. Preprints should not be added to or enhanced in any way in order to appear more like, or to substitute for, the final versions of articles however authors can update their preprints on arXiv or RePEc with their Accepted Author Manuscript (see below).
If accepted for publication, we encourage authors to link from the preprint to their formal publication via its DOI. Millions of researchers have access to the formal publications on ScienceDirect, and so links will help users to find, access, cite and use the best available version. Please note that Cell Press, The Lancet and some society-owned have different preprint policies. Information on these policies is available on the journal homepage.
Accepted Author Manuscripts: An accepted author manuscript is the manuscript of an article that has been accepted for publication and which typically includes author-incorporated changes suggested during submission, peer review and editor-author communications.
Authors can share their accepted author manuscript:

- immediately
    - via their non-commercial person homepage or blog
    - by updating a preprint in arXiv or RePEc with the accepted manuscript
    - via their research institute or institutional repository for internal institutional uses or as part of an invitation-only research collaboration work-group
    - directly by providing copies to their students or to research collaborators for their personal use
    - for private scholarly sharing as part of an invitation-only work group on commercial sites with which Elsevier has an agreement
- after the embargo period
    - via non-commercial hosting platforms such as their institutional repository
    - via commercial sites with which Elsevier has an agreement

In all cases accepted manuscripts should:

- link to the formal publication via its DOI
- bear a CC-BY-NC-ND license - this is easy to do
- if aggregated with other manuscripts, for example in a repository or other site, be shared in alignment with our hosting policy not be added to or enhanced in any way to appear more like, or to substitute for, the published journal article.

Published journal article (JPA): A published journal article (PJA) is the definitive final record of published research that appears or will appear in the journal and embodies all value-adding publishing activities including peer review co-ordination, copy-editing, formatting, (if relevant) pagination and online enrichment.

Policies for sharing publishing journal articles differ for subscription and gold open access articles:

Subscription Articles: If you are an author, please share a link to your article rather than the full-text. Millions of researchers have access to the formal publications on ScienceDirect, and so links will help your users to find, access, cite, and use the best available version.

Theses and dissertations which contain embedded PJAs as part of the formal submission can be posted publicly by the awarding institution with DOI links back to the formal publications on ScienceDirect.

If you are affiliated with a library that subscribes to ScienceDirect you have additional private sharing rights for others' research accessed under that agreement. This includes use for classroom teaching and internal training at the institution (including use in course packs and courseware programs), and inclusion of the article for grant funding purposes.

Gold Open Access Articles: May be shared according to the author-selected end-user license and should contain a CrossMark logo, the end user license, and a DOI link to the formal publication on ScienceDirect.

Please refer to Elsevier's posting policy for further information.

18. **For book authors the following clauses are applicable in addition to the above:** Authors are permitted to place a brief summary of their work online only. You are not allowed to download and post the published electronic version of your chapter, nor may you scan the printed edition to create an electronic version. **Posting to a repository:** Authors are permitted to post a summary of their chapter only in their institution's repository.

19. **Thesis/Dissertation**: If your license is for use in a thesis/dissertation your thesis may be submitted to your institution in either print or electronic form. Should your thesis be published commercially, please reapply for permission. These requirements include permission for the Library and Archives of Canada to supply single copies, on demand, of the complete thesis and include permission for Proquest/UMI to supply single copies, on demand, of the complete thesis. Should your thesis be published commercially, please reapply for permission. Theses and dissertations which contain embedded PJAs as part of the formal submission can be posted publicly by the awarding institution with DOI links back to the formal publications on ScienceDirect.

Elsevier Open Access Terms and Conditions

Posting or linking by commercial companies for use by customers of those companies.

20. **Other Conditions**:

v1.9

Questions? customercare@copyright.com or +1-855-239-3415 (toll free in the US) or +1-978-646-2777.

Appendix II: Yield Calculation (SA-ODA)

The theoretical yield was calculated by multiplying the number of moles of the rate limiting compound (ODA) and the MW of the conjugate (SA-ODA):

The number of moles of ODA used = 0.0538 mmole

MW of SA-ODA = MW of SA + MW of ODA – MW of H_2O
= (309.27 + 269.51 – 18.02) g/mole or mg/mmole
= 560.76 mg/mmole

Theoretical yield = Number of moles of ODA × MW of SA-ODA
= 0.0538 × 560.76
= 30.17 mg

Final Product weight = 29.59 mg

$$The\ actual\ product\ yield(\%w/w) = \frac{Final\ product\ weight}{Theoretical\ yield\ (weight)} \times 100$$

$$= \frac{29.59}{30.17} \times 100$$

$$= 98.1\%$$

Appendix III: Yield Calculation (DSPE-PEG-TAT)

The theoretical yield was calculated by multiplying the number of moles of the rate limiting compound (TAT peptide) and the MW of the conjugate (DSPE-PEG-TAT):

The number of moles of TAT peptide used = 0.041 mmole

MW of DSPE-PEG-TAT = MW of TAT + MW of DSPE-PEG-NHS – MW of NHS
= (1340 + 2000 – 115) g/mole or mg/mmole
= 3225 mg/mmole

Theoretical yield = Number of moles of TAT peptide × MW of DSPE-PEG-TAT
= 0.041 × 3225
= 132.2 mg

Final Product weight = 110.1 mg

$$The\ actual\ product\ yield(\%w/w) = \frac{Final\ product\ weight}{Theoretical\ yield\ (weight)} \times 100$$

$$= \frac{110.2}{132.2} \times 100$$

$$= 83.3\%$$

Appendix IV: Summary of PLGA NPs formulation optimisation trials.

Table 6.1. Summary of particle size, PDI, zeta potential and DL values from different optimisation trials of PLGA NPs (n=3).

Optimisation step	Prep. method	PLGA NPs formulation				Particle size ± SD (nm)†	PDI ± SD†	Zeta pot. ± SD (mV)†	% DL ± SD†
		Drug (amount)	Org. phase	Polymer (MW, amount)	Stabiliser (conc.)				
Salt vs. base (RHT vs. RV)	O/W	RHT (10mg)	DCM	Purasorb® PDLG (110kDa, 30mg)	PVA (0.6% w/v)	176.2±	0.12±0.02	-25.6±6.5	0.09±0.01
	W/O/W	RHT (10mg)				212.1±5.9	0.19±0.03	-29.5±2.9	0.36±0.02
	O/W	RV (6.25mg)				185.7±	0.17±0.03	-24.9±5.9	0.08±0.01
	W/O/W	RV (6.25mg)				197.2±	0.12±0.03	-26.4±3.9	0.09±0.02
Organic solvent	W/O/W	RHT (10mg)	DCM	Purasorb® PDLG (110kDa, 30mg)	PVA (0.6% w/v)	212.1±5.9	0.19±0.03	-29.5±2.9	0.36±.02
			EtAc			166.3±6.1	0.15±0.02	-31.2±1.6	0.43±0.1
Preparation technique	O/W	RHT (10mg)	EtAc	Purasorb® PDLG (110kDa, 30mg)	PVA (0.6% w/v)	151.9±8.2	0.18±0.03	-34.2±3.1	0.1±0.03
	W/O/W	RHT (10mg)				166.3±6.1	0.15±0.02	-31.2±1.6	0.4±0.1
	Modified W/O/W	RHT (10mg)				160.1±11.6	0.13±0.03	-25.9±2.6	0.8±0.1
	Post loading	RHT (10mg)				148.1±2.1	0.08±0.01	-22.2±3.4	0.2±0.1
		RV (6.25mg)				146.4±1.7	0.07±0.01	-28.1±2.6	0.1±0.03
PLGA MW	Modified W/O/W	RHT (10mg)	EtAc	Durect® PLGA (3.3 kDa, 30mg)	PVA (0.6% w/v)	80.3±3.4	0.17±0.03	-29.1±2.5	0.4±0.1
				Resomer® RG 502H (7-17 kDa, 30mg)		91.4±4.2	0.19±0.02	-31.2±1.9	1.3±0.2
				Resomer® RG 503H (24-38 kDa, 30mg)		102.6±7.1	0.15±0.01	-24.6±3.2	1.5±0.1
				Purasorb® PDLG (110 kDa, 30mg)		160.1±11.6	0.13±0.03	-25.9±2.6	0.8±0.1

† The value reported here is the mean of three measurements.

Table continued

Optimisation step	Prep. method	PLGA NPs formulation				Particle size ± SD (nm)†	PDI ± SD†	Zeta pot. ± SD (mV)†	% DL ± SD†
		Drug (amount)	Org. phase	Polymer (MW, amount)	Stabiliser (conc.)				
Stabiliser type & conc.	Modified W/O/W	RHT (10mg)	EtAc	Resomer® RG 503H (24-38 kDa, 30mg)	PVA (0.6% w/v)	102.6±7.1	0.15±0.01	-24.6±3.2	1.5±0.1
					PVA (1.0% w/v)	109.1±3.4	0.16±0.04	-23.4±1.9	1.4±0.1
					Pluronic® F127 (0.5% w/v)	100.6±6.5	0.11±0.02	-28.3±3.2	1.3±0.1
					Pluronic® F127 (1.0% w/v)	99.1±5.6	0.09±0.01	-27.1±1.6	1.4±0.2
					Vitamin E-TPGS (0.3% w/v)	96.3±2.1	0.15±0.02	-33.2±2.6	1.4±0.1
					Vitamin E-TPGS (1.0% w/v)	94.3±2.6	0.13±0.03	-30.2±2.9	1.4±0.1
PLGA conc.	Modified W/O/W	RHT (10mg)	EtAc	Resomer® RG 503H (24-38 kDa, 30mg)	Vitamin E-TPGS (0.3% w/v)	96.3±2.1	0.15±0.02	-33.2±2.6	1.4±0.1
				Resomer® RG 503H (24-38 kDa, 45mg)		123.9±3.3	0.08±0.03	-28.6±3.9	1.7±0.2
				Resomer® RG 503H (24-38 kDa, 60mg)		159.9±6.7	0.16±0.04	-26.1±3.5	2.1±0.2
				Resomer® RG 503H (24-38 kDa, 75mg)		186.4±5.4	0.15±0.01	-34.7±2.3	2.2±0.1
				Resomer® RG 503H (24-38 kDa, 90mg)		210.6±6.1	0.09±0.03	-30.6±2.6	2.3±0.2
Drug polymer ratio	Modified W/O/W	RHT (5mg)	EtAc	Resomer® RG 503H (24-38 kDa, 60mg)	Vitamin E-TPGS (0.3% w/v)	135.3±3.2	0.12±0.03	-31.3±1.0	0.73±0.1
		RHT (10mg)				159.9±6.7	0.16±0.04	-26.1±3.5	2.1±0.2
		RHT (20mg)				157.4±4.3	0.16±0.02	-29.2±3.6	2.7±0.1
		RHT (30mg)				148.2±7.1	0.12±0.04	-26.7±2.7	3.0±0.1
		RHT (40mg)				145.1±5.1	0.13±0.03	-28.8±4.2	3.1±0.1

† The value reported here is the mean of three measurements.

Appendix V: Sample Preparation for Mycoplasma Testing

Mycoplasmas can drastically alter cell DNA, RNA and protein synthesis as well as can compete with host cells for biosynthetic precursors, nutrients, amino acid and ATP. As a result, research results can be skewed and become non-reproducible. Although the proper aseptic technique was always employed in the laboratory work and antibiotic was always present in the medium to prevent bacterial infection, regular (three monthly) testing of all cell cultures was performed to ensure the absence of mycoplasma. The procedure followed was as below:

- Cells were cultured for two weeks without any antibiotics. The hCMEC/D3 cells grew fast so they were split as usual and continued growing in the medium without antibiotics.
- Samples were prepared when cells were 80-90% confluent.
- 100µL of cell conditioned medium was collected into 1.5mL Eppendorf tube and boiled for 5 min at 95°C using bench heat block. The sample was stored at 4°C and tested within one week.
- Cells were washed with PBS and removed by cell scraper into PBS. An aliquot was used for cell counting and the rest was centrifuged at 335g for 5 minutes at 4°C.
- Cells were resuspended in PBS and approximately 0.5-1.0 × 10^6 cells were placed into a 1.5mL Eppendorf tube.
- The tube was centrifuged at 2000g for 1 minute at 4°C, the supernatant was removed, the cell pellet was resuspended in 1mL PBS and centrifuged again.
- Finally, the supernatant was removed and the cell pellet was stored at 4°C for mycoplasma testing was carried out within one week.
- Optimised PCR-based technique was used for mycoplasma detection, which was performed by CHIRI facility researcher, Curtin University.

Appendix VI: MTT Solution Preparation and Storage

According to the manufacturer website - "Reconstituted MTT solution is stable for at least 6 months when stored frozen (−20°C). Storage of reconstituted MTT solution at 2-8°C for more than 2 weeks may cause decomposition and yield erroneous results." So, the following procedure was carried out in a biosafety cabinet (where applicable) always protecting the reagent from light:

- 100mg of MTT was weighed out in a 50mL glass beaker and dissolved in 20mL PBS (pH 7.4) on a magnetic stirrer to obtain a stock concentration of 5mg/mL.
- The MTT solution was filter-sterilized using 0.2µm syringe tip filter directly into 4mL sterile containers and wrapped with aluminium foil for light protection.
- The stock solution was stored, at 4°C for frequent usage within 7 days or at −20°C for long term storage (up to 3 months), in a light-protected container.

Appendix VII: Medium Replacement Procedure for Cell Inserts

Maintaining pressure above the cell monolayer on an insert is important for the integrity of the TJ (Ghaffarian & Muro, 2013). Therefore, along with the usual cell culture practice, following procedure was always implemented:

- The medium from the lower chamber was aspirated first,
- Then, the medium from the upper chamber was aspirated,
- The upper chamber was filled first and finally,
- The lower chamber was filled with medium.

Appendix VIII: Antibody Aliquot and Storage Protocol

For immunostaining procedure, a primary and a secondary antibody were used. The anti-occludin antibody was specific to TJ occludin protein. However, the primary antibodies available are not generally fluorescently tagged due to high cost as well as being less sensitive, hence the secondary antibody was used. This anti-rabbit secondary antibody containing green-fluorescent dye is capable of binding with the primary antibody making them visible under fluorescent microscope.

100µg primary antibody was received at 1µg/µL concentration (100µL stock solution). 500µg secondary antibody was received at 2 µg/µL concentration (250µL stock solution). Upon receiving the antibody, they were centrifuged at 10,000g for 20 seconds to collect solution that is trapped in the threads of the vial. To avoid repeated freeze-thaw cycles, they were aliquoted as 10µL into Eppendorf low-protein-binding microcentrifuge tubes and kept at −80°C. At time of the cell treatment, one vial was taken out, thawed, removed necessary volume and if the next experiment was within next 1-2 weeks, stored it at 4°C; otherwise, returned it at −80°C immediately after use.

It should be noted here that:

- Aliquots should be no smaller than 10 µL; the smaller the aliquot, the more the stock concentration is affected by evaporation and adsorption of the antibody onto the surface of the storage vial.
- Storing of diluted antibodies can lead to rapid degradation of antibodies and not recommended by the supplier.
- The freezer for storage the antibodies must not be of the frost-free variety. These cycles between freezing and thawing (to reduce frost build-up), must be avoided.
- For the same reason, antibody vials should be placed in an area of the freezer that has minimal temperature fluctuations, for instance towards the back rather than on a door shelf.

Appendix IX: List of Publications and Presentations

- Naz Hasan Huda, Heather A. E. Benson and Yan Chen (2017) Development and analysis of functionalized poly(lactide-co-glycolide) polymer for drug delivery. SOJ Pharmacy & Pharmaceutical Sciences (ISSN: 2374-6866) (Accepted)

- Naz Hasan Huda, Andrew Crowe, Heather A. E. Benson and Yan Chen (2017) Formulation development and cellular transport studies of a novel poly(lactide-co-glycolide) nanoparticulate carrier system (Under preparation)

- Naz Hasan Huda, Andrew Crowe, Pierre-Olivier Couraud, Ignacio Romero, Babette Weksler and Yan Chen (2017) Cytotoxicity and cellular uptake of a novel dual ligand poly(lactide-co-glycolide) nanoparticulate carrier system for brain drug delivery (Under preparation)

- Naz Hasan Huda, Heather A. E. Benson, Yan Chen (2017) CNS Drug Delivery: Challenge, Current Strategies and Future Scope (Under preparation)

- Naz Hasan Huda, H. A. E. Benson, and Y. Chen. Development of functionalized PLGA polymer for targeted nanoparticle delivery. Drug Delivery Australia (DDA) hosted by the Australian Chapter of the Controlled Release Society (AUS-CRS) on 19-20th November 2015 at the University of Queensland (Brisbane, Australia). (Poster)

- Naz Hasan Huda, H. A. E. Benson, A. Crowe and Y. Chen. Dual ligand nanoparticulate drug delivery system - formulation development, optimisation and its cellular response. DDA hosted by AUS-CRS on 27-28th October 2016 at the University of New South Wales (Sydney, Australia). (Poster)

- Naz Hasan Huda, Heather Benson, Andrew Crowe, Yan Chen. Synthesis and quantitative analysis of polymer conjugate poly(lactic-co-glycolic acid)-diaminobutane (PLGA-DAB). Mark Liveris Research Student Seminar hosted by the Faculty of Health Sciences at Curtin University on 11th November 2014. (Poster)

- Naz Hasan Huda, Heather A. E. Benson, Yan Chen. Development of functionalized PLGA polymer for targeted nanoparticle delivery. Mark Liveris Research Student Seminar hosted by the Faculty of Health Sciences at Curtin University on 3rd September 2015. (Oral presentation)